# UC San Diego

## UC San Diego Electronic Theses and Dissertations

### Title

Meltwater, Matrices, and Mattak: Ocean Observations in Kalaallit Nunaat's Changing Glacial Fjords

### Permalink

https://escholarship.org/uc/item/7kf2p0v2

### ISBN

9798186185321

### Author

Roth, Aurora

### Publication Date

2026-08-05

Peer reviewed|Thesis/dissertation

eScholarship.org Powered by the California Digital Library
University of California

UNIVERSITY OF CALIFORNIA SAN DIEGO

# Meltwater, Matrices, and Mattak: Ocean Observations in Kalaallit Nunaat's Changing Glacial Fjords

A dissertation submitted in partial satisfaction of the
requirements for the degree Doctor of Philosophy

in

Oceanography

by

Aurora Roth

Committee in charge:

Fiamma Straneo, Chair
Sarah Giddings, Co-Chair
Karen Kovaka
Matthew Mazloff

2026

Copyright

Aurora Roth, 2026

All rights reserved.

The dissertation of Aurora Roth is approved, and it is acceptable in quality and form for publication on microfilm and electronically.

University of California San Diego

2026

EPIGRAPH

"Science at its best, is an act of care.
Research can be both rigorous and relational...
like any relationship it needs time, trust, and tenderness.
Those who come here to study Greenland,
leave here learning something from Greenland."

**Mari Kleist**, Chair, Greenland Research Council

What a curious journey
everywhere they went
they examined the people
and took their clothes, sleds, and equipment

What a curious journey
and every island or fjord
promontory or mountain was named
to honor those back home

What a curious journey
and returning again
with maps of the country
and tales of the people they saw

When the curious journey had finished
and they had arrived back home
they became famous, earning medals and fame
for having explored a country where human being live and dwell

**Aqqaluk Lynge**, Excerpts from *Tupigusullutik angalapput (A Curious Journey)*

If I could fall into the sea
Then I would be a CTD
'Cause you know I'd do a thousand casts
If I could just see you, tonight.

**OSNAP 2022 Team**; sung to the tune of A Thousand Miles by Vanessa Carlton

TABLE OF CONTENTS

Dissertation Approval Page . . . . . iii

Epigraph . . . . . iv

Table of Contents . . . . . v

List of Figures . . . . . ix

List of Tables . . . . . xiv

Acknowledgements . . . . . xv

Vita . . . . . xxii

Abstract of the Dissertation . . . . . xxiii

Introduction . . . . . 1
0.1 Kalaallit Nunaat: Land of the People . . . . . 1
0.1.1 Glacial fjords are meeting places . . . . . 1
0.2 The Climate Change Context . . . . . 3
0.2.1 Warmer global temperatures are melting the Greenland Ice Sheet . . . . . 3
0.2.2 Meltwater impacts global ocean circulation . . . . . 4
0.2.3 Melting glaciers impact marine ecosystems . . . . . 5
0.3 Anatomy of a glacial fjord . . . . . 6
0.4 The key questions . . . . . 11
0.5 Thesis structure and contributions . . . . . 12
0.5.1 Mathematical foundations . . . . . 13
0.6 Kalaallit Nunaat Kalaallit Pigaat: Greenland belongs to Greenlanders . . . . . 13

Chapter 1 A dataset for multidisciplinary applications: thirteen years of ocean observations in Sermilik Fjord, Southeast Greenland . . . . . 17
1.1 Introduction . . . . . 17
1.2 Sermilik Fjord setting . . . . . 21
1.2.1 Glaciological context . . . . . 21
1.2.2 Regional ocean context . . . . . 22
1.2.3 Sermilik Fjord water masses . . . . . 22
1.2.4 Helheim Glacier ice mélange . . . . . 23
1.3 Data . . . . . 25
1.3.1 CTD data . . . . . 25
1.3.2 XCTD data . . . . . 27
1.3.3 Combining CTD and XCTD data . . . . . 29
1.3.4 Profile locations and timing . . . . . 29
1.4 Methods . . . . . 31

1.4.1 Profile selection for analysis . . . 31
1.4.2 Creating gridded data using objective mapping . . . 32
1.4.3 Choosing a background field . . . 37
1.4.4 Choosing appropriate parameters . . . 37
1.4.5 Calculating a climatology . . . 38
1.5 Results . . . 38
1.5.1 Objective mapping performance . . . 38
1.5.2 Climatology and spatial variability . . . 41
1.5.3 Variability of gridded data . . . 48
1.6 Discussion . . . 52
1.6.1 Summary of results facilitated by gridded sections . . . 52
1.6.2 Daily to interannual variability . . . 53
1.6.3 Water mass definitions and comparison to previous work . . . 54
1.6.4 Gridded products facilitate model use and comparison . . . 55
1.7 Conclusions . . . 55
1.8 Code and data availability . . . 56
1.9 Acknowledgments . . . 57

Chapter 2 Water mass fraction methods in Greenland's glacial fjords with a case study in Sermilik Fjord, Southeast Greenland . . . 59
2.1 Introduction . . . 59
2.2 Methods . . . 63
2.2.1 Overview of Water Mass Fraction Methods in Ice-Ocean Environments 63
2.2.2 Linear Mixing Equations and Algebraic Solutions for Exact Systems . . . 66
2.2.3 Optimum Multiparameter Analysis (OMPA) . . . 69
2.2.4 Regularized least squares (RLS) formulation for underdetermined systems 73
2.2.5 Non-negativity constraint and SMW effective temperature . . . 74
2.2.6 Quadratic programming implementation . . . 76
2.2.7 Choosing **W** and **P** values . . . 77
2.2.8 Summary of diagnostic workflow . . . 84
2.3 Case Study: Sermilik Fjord . . . 85
2.3.1 Comparison framework . . . 89
2.3.2 2015 Survey Data Description . . . 90
2.3.3 Source Water Type Definitions . . . 92
2.4 Results . . . 100
2.4.1 Comparison of all solutions to reference case . . . 100
2.4.2 Uncertainties and residuals . . . 102
2.4.3 RLS-TSO vs RLS-TS: Is DO adding information? . . . 103
2.4.4 Spatially varying P vs. constant P . . . 104
2.5 Discussion . . . 105
2.5.1 Summary of results . . . 105
2.5.2 The non-negativity constraint: interpretability vs. accuracy . . . 106
2.5.3 Using diagnostics in iterative model construction . . . 107
2.5.4 2015 was an anomalously cold year . . . 107

2.5.5 From water mass fractions to improved parameterizations . . . . . 108
2.6 Recommendations for other fjord systems . . . . . 109
2.7 Conclusion . . . . . 110
2.8 Acknowledgments . . . . . 111

Chapter 3 Beyond temperature and salinity: Long-term water mass fractions reveal persistent composition and plume structure in Sermilik Fjord . . . . . 117
3.1 Introduction . . . . . 117
3.2 Methods . . . . . 119
3.2.1 Optimum Multiparameter Multi-Year Analysis . . . . . 119
3.2.2 Fjord region definitions . . . . . 120
3.2.3 Defining GMW extent and properties . . . . . 121
3.2.4 Limitations of the positive temperature anomaly approach . . . . . 123
3.2.5 AW and PW properties and variability . . . . . 124
3.2.6 OMPM fraction uncertainty estimation with Monte Carlo simulations . . 125
3.2.7 Weighted Regularized Least Squares (RLS) approach . . . . . 125
3.2.8 Simple plume model . . . . . 128
3.2.9 Subglacial discharge volume flux . . . . . 129
3.2.10 Estimating submarine melt rate from SMW fractions . . . . . 130
3.3 Results . . . . . 131
3.3.1 AW properties and variability . . . . . 131
3.3.2 PW properties and variability . . . . . 132
3.3.3 GMW properties and variability . . . . . 133
3.3.4 GMW spatial extent from positive temperature anomaly . . . . . 133
3.3.5 OMPM results: Time-averaged water mass fractions in different fjord regions . . . . . 134
3.3.6 Yearly Water mass fractions results from RLS . . . . . 136
3.3.7 Method comparison . . . . . 137
3.3.8 Plume properties, fractions, and melt rate . . . . . 138
3.4 Discussion . . . . . 140
3.4.1 Summary of results . . . . . 140
3.4.2 Methodological improvements and limitations . . . . . 142
3.4.3 Defining GMW from water mass fractions . . . . . 144
3.4.4 Interannual variability, GMW properties, and forcing . . . . . 145
3.4.5 Improving fjord process parameterizations? . . . . . 146
3.5 Conclusions: Summary and Future Work . . . . . 148

Chapter 4 Reflection and Reflexivity: Using the Greenland National Research Strategy as a guiding document . . . . . 159
4.1 Introduction . . . . . 159
4.2 Positionality statement . . . . . 162
4.3 Background . . . . . 164
4.3.1 Guidelines from the science community . . . . . 164
4.3.2 Background: Inuit Arctic Policy . . . . . 166

4.3.3 Background: The Greenland National Research Strategy . . . . . 167
4.3.4 Background: Why self-reflection and self-assessment matters . . . . . 168
4.3.5 Background: Other Inspiration . . . . . 169
4.3.6 Background: Physical sciences have been slower to adopt equitable research frameworks . . . . . 170
4.3.7 Background: Navigating the New Arctic Program . . . . . 172
4.3.8 Background: FISHEE and GRISO Project . . . . . 173
4.4 The GNRS as an evaluation tool . . . . . 174
4.4.1 GNRS as an anchor . . . . . 175
4.4.2 Rating level of each goal . . . . . 176
4.5 Reflection table . . . . . 176
4.6 Discussion . . . . . 176
4.6.1 Utilizing Greenlandic Research Vessels . . . . . 176
4.6.2 Working with Greenlandic students . . . . . 180
4.6.3 A StoryMap for sharing science with public audiences . . . . . 182
4.6.4 Interdisciplinary projects enable work that aligns with the research strategy 185
4.6.5 The role of graduate students . . . . . 188
4.7 Conclusion . . . . . 188

Chapter 5 Conclusion: Summary and Future Work . . . . . 192

Appendix A Supplementary Figures . . . . . 197

Bibliography . . . . . 213

LIST OF FIGURES


Figure 1. The town of Tiilerilaaq and traditional Greenlandic foods. . . . . 2

Figure 2. Greenland Ice Sheet mass loss from 2002 to 2025 based on satellite observations. . . . . 4

Figure 3. A schematic of the global Atlantic Meridional Overturning Circulation and the currents surrounding Greenland. . . . . 6

Figure 4. An introductory map of Sermilik Fjord and glacial retreat from 2000 to 2020, and photos of Sermilik Fjord. . . . . 8

Figure 5. A schematic of key freshwater processes in fjords, including subglacial discharge and submarine melt, and photos of plume region at Helheim Glacier. . . . . 10

Figure 6. The town of Tiilerilaaq, in Sermilik Fjord, in August 2025 with the R/V Tarajoq in the background of the fjord. Photo Alex Rivest. . . . . 14

Figure 7. A photo from historic protest in Nuuk, Greenland on January 17 2026 (AP/Evgeniy Maloletka). . . . . 15

Figure 1.1. Map of Sermilik Fjord region in Southeast Greenland with major regions labeled and bathymetry contours. . . . . 20

Figure 1.2. Locations of CTD (yellow dots) and XCTD (red dots) profiles for every summer survey in Sermilik Fjord included in this dataset. . . . . 26

Figure 1.3. A visual representation of the CTD and XCTD survey dates and time periods in the summer season (July–September). . . . . 31

Figure 1.4. The number of grids representing each survey that have data in each grid cell in the along–fjord standardized grid domain . . . . . 39

Figure 1.5. The conservative temperature objectively mapped gridded fields for 2009 (a) and 2019 (d) with associated residual (b,e) and mapping error estimates (c,f). . . . . 40

Figure 1.6. Histograms displaying the distribution of residual values between the gridded temperature (a) and salinity (b) fields. . . . . 40

Figure 1.7. Comparisons of original profiles and gridded data for years 2009 (a, b) and 2019 (c, d) in $\Theta$–$S_A$ diagrams (b, d). . . . . 42

Figure 1.8. Gridded 13 year mean summer state climatology of conservative temperature (a) and absolute salinity (b) for Sermilik Fjord derived from hydrographic observations between 2009 to 2023. . . . . 43

Figure 1.9. Conservative Temperature–Absolute Salinity ($\Theta$–$S_A$) diagram of the gridded summer state climatology for Sermilik Fjord. . . . . 45

Figure 1.10. Conservative temperature profiles from all the yearly grids at locations shown in (a): the near glacier (b), mid–fjord (c), and mouth regions (d). . . 49

Figure 1.11. $N^2$ (Brunt–Vaisala frequency), a measure of stratification, from the near glacier (a), mid–fjord (b), and mouth (c) regions for all yearly gridded data. 50

Figure 1.12. Conservative temperature anomalies from the climatological mean for yearly grids 2009 (a), 2015 (b), 2019 (c), and 2021 (d). . . . . 51

Figure 2.1. Map of Sermilik Fjord region in Southeast Greenland (a) with profile locations from 2015 survey and temperature (b), salinity (c), and oxygen (d) profiles in along-fjord sections. . . . . 87

Figure 2.2. A schematic of Sermilik Fjord identifying the origins and regions of input for the four source water types (SWT) used in this study: AW (red), PW (blue), SGD (purple), and SMW (yellow). . . . . 88

Figure 2.3. Schematic indicating the relationships between the different methods discussed in this section, defined by number of observed properties relative to SWTs and complexity/use of prior information. . . . . 90

Figure 2.4. $\Theta$–$S_A$ plot and b)DO–$S_A$ plot of CTD data from the 2015 survey. . . . . 93

Figure 2.5. Spatially varying penalty matrix $\mathbf{P}$ values for each source water type across the Sermilik Fjord domain. . . . . 99

Figure 2.6. Comparison of reference case OMP-NG water mass fraction solutions (a–d) to the solutions of the other configurations (e–p). . . . . 112

Figure 2.7. Profile-depth comparison of water mass fraction solutions of each analysis configuration to the reference case. . . . . 113

Figure 2.8. Along-fjord sections of RLS-TS SWT fraction solutions (a–d), associated Monte Carlo uncertainties (e–h), and property residuals (i–l). . . . . 114

Figure 2.9. RLS-TS analysis solutions using a constant $\mathbf{P}$ matrix. . . . . 116

Figure 3.1. An example of the positive temperature anomaly calculation along isopycnals to define mean GMW properties of profiles in the 2019 Sermilik Fjord survey. . . . . 122

Figure 3.2. Timeseries of AW, PW, and GMW water mass properties in different fjord regions—plume (purple), mélange (light blue), mid-fjord (yellow) and mouth (red). . . . . 150

Figure 3.3. Temperature anomaly (fjord profiles minus mean shelf profile), calculated along isopycnals for each year in the Sermilik Fjord gridded dataset. . . . . 151

Figure 3.4. Example of uncertainty calculation for OMPM fraction results utilizing Monte Carlo simulations for the mid-fjord region. . . . . 152

Figure 3.5. Temperature and salinity properties of PW endmembers (squares), AW endmembers (circles), and mean GMW as calculated at different fjord regions (diamonds). . . . . 153

Figure 3.6. RLS method fraction solutions (%) for all SWTs (AW, PW, SGD, and SMW) derived from individual years of gridded data (2009, 2016, 2019, and 2021). . . . . 154

Figure 3.7. RLS method fraction solutions (%) from specific fjord regions for all years in the Sermilik Fjord gridded dataset (colored lines). . . . . 155

Figure 3.8. Spatial comparison of three different water mass fraction methods: OMPM (black line), RLS method for three years (2015, 2019, and 2021), and noble gas-derived water mass fractions from 2015 (Beaird et al., 2018). . . . . 156

Figure 3.9. Temperature and salinity properties in $\Theta - S_A$ space for four different survey years (2010, 2016, 2019, and 2021) at four different fjord regions. . 157

Figure 3.10. Key areas of water mass transformation in Sermilik Fjord and associated SWT fraction contributions as Glacially Modified Water moves down-fjord. 158

Figure 4.1. The R/V Tarajoq in Sermilik Fjord outside of Tiilerilaaq in August 2025. . 180

Figure 4.2. An example of the coloring page activity I developed for students in Tiilerilaaq. . . . . 182

Figure 4.3. Examples of various outreach activities with students in Kullorsuaq and Tiilerilaaq. . . . . 183

Figure 4.4. A screenshot of Greenland's Living Fjords StoryMap project, showing the range of videos and topics presented. . . . . 184

Figure 4.5. Members of the NNA FISHEE team discussing interdisciplinary intersections of the Sermilik Fjord system on the R/V Tarajoq in August 2023. . . . 187

Figure 4.6. NNA FISHEE field team, R/V Tarajoq crewmembers, and students and teachers from Tiilerilaaq posing on the bow of the R/V Tarajoq. . . . . 190

Figure 4.7. Painting of Tiilerilaaq in August 2025 by Aurora Roth. . . . . 191

Figure A.1. he conservative temperature objectively mapped gridded fields for all years with potential density anomaly isopycnals (black contours). . . . . 198

Figure A.2. Conservative temperature anomalies from the climatological mean for all yearly grids. . . . . 199

Figure A.3. Conservative temperature residuals between the profile data and gridded data interpolated to the same position of every data point. . . . . 200

Figure A.4. Conservative temperature mapping relative error. . . . . 201

Figure A.5. The absolute salinity objectively mapped gridded fields for all years with potential density anomaly isopycnals (black contours). . . . . 202

Figure A.6. Absolute salinity anomalies from the climatological mean for all yearly grids. . . . . 203

Figure A.7. Absolute salinity residuals between the profile data and gridded data interpolated to the same position of every data point. . . . . 204

Figure A.8. Absolute salinity mapping relative error. . . . . 205

Figure A.9. $\Theta - S_A$ plots for each year in the hydrographic gridded dataset for Sermilik Fjord. . . . . 206

Figure A.10. Freshwater runoff discharge partitioned for subglacial discharge outlets for Helheim Glacier alone (a-b), for the other dominant tidewater glaciers in Sermilik Fjord with subglacial discharge (c). . . . . 207

Figure A.11. Half-violin plots of AW fjord salinity properties across the full fjord domain for each year. . . . . 208

Figure A.12. Atlantic Water (AW) fractions (%) as calculated from the RLS method for every grid points of every year in the Sermilik Fjord gridded hydrography dataset. . . . . 209

Figure A.13. Polar Water (PW) fractions (%) as calculated from the RLS method for every grid points of every year in the Sermilik Fjord gridded hydrography dataset. Note the scale is 0-50% for PW. . . . . 210

Figure A.14. Subglacial discharge (SGD) fractions (%) as calculated from the RLS method for every grid points of every year in the Sermilik Fjord gridded hydrography dataset. . . . . 211

Figure A.15. Submarine meltwater (SMW) fractions (%) as calculated from the RLS method for every grid points of every year in the Sermilik Fjord gridded hydrography dataset. . . . . 212

LIST OF TABLES

Table 1.1. Information about each shipboard CTD summer survey in Sermilik Fjord. 27

Table 1.2. Information about each XCTD survey in Sermilik Fjord. *One winter survey was conducted on March 15-16 2010 (Straneo et al., 2011). These profile data are available, but have not been gridded or included in the summer season climatology. . . . . 28

Table 1.3. Description of assigned parameters in objective mapping method . . . . . 38

Table 2.1. Summary of previous water mass fraction estimates from Greenland glacial fjords or fjord entrances. Abbreviations: OMPM = Optimum Multiparameter Multi-Year Analysis, CE = algebraic conservation equations used, MC = Monte Carlo simulation used for uncertainty . . . . . 64

Table 2.2. Source water type (SWT) end-member properties of conservative temperature ($\Theta$), absolute salinity ($S_A$), and dissolved oxygen (DO) and the combined measurement and definition uncertainty ($\pm\sigma$) for each. . . . . 92

Table 2.3. Regularization diagnostics for assessing the balance between the weight matrix $\mathbf{W}$ and penalty matrix $\mathbf{P}$ and conditioning of the system in the regularized least squares (RLS) water mass fraction method. . . . . 115

Table 3.1. Water mass fractions (%) estimated from OMPM analysis for each region. . 135

Table 3.2. Water mass fraction estimates (depth mean across GMW extent $\pm$ standard deviation, in %) by dataset and fjord region. . . . . 138

Table 4.1. An example of the Project Reflection Framework based on the Greenland National Research Strategy filled out for the work discussed in this dissertation. . . . . 177

ACKNOWLEDGEMENTS

It should surprise no one that knows me that this is, perhaps, an unusually long dissertation acknowledgements section, emphasizing that science is a team sport and a relational human endeavor.

One of my favorite **Fiamma** moments was when we were in Nuuk for Greenland Science Week and she invited two other female scientists over for dinner. In a somewhat sterile AirBnB kitchen, she whipped up a tasty dinner for all of us and they shared stories about being on ships together over 10 years ago. There was laughter, warmth, sharing, and a sense of belonging. In many ways this was an ordinary moment, and I have countless favorite memories of Fiamma like this, from eating dinner with her family or grabbing a quick coffee with colleagues, but they all show how she values the people around her and keeps "the science" positioned within the larger perspective of who we all are as people.

When I reached out about the possibility of working with her as a PhD student in 2019, I had no idea what I was actually signing up for—a community of some of the most thoughtful and caring people I know. I feel so lucky that I get to learn from and work with and laugh with an extraordinary ecosystem of humans brought together by Fiamma. I don't actually feel capable of articulating the many positive ways she has impacted my life as a person and scientists. I see more possibilities for myself now, and I have become more of who I authentically am in the world because of her guidance and collaboration. Learning from how Fiamma's brain organizes ideas, how she asks the exact question that needs to be asked, and hones in on a tractable problem has taught me so much.

I am grateful for her trust in me as I navigated a non-standard approach to being a PhD student and figured out what I needed to be a healthy and happy human (an on-going project). I am proud of both of us for making the most of hours and hours and hours of zoom meetings together. It has been life changing to get to know Sermilik Fjord through Fiamma's eyes and to be part of the joy that she shares when she is doing science in one of her favorite places with

good people. I hope I can give this same gift to students in the future, and I am excited for more collaboration and science scheming (qajaq oceanography or Tasilaaq science week?!) in the future. Thank you for everything, Fiamma. And thank you to Rosalba, Kea, Yani, and Maple for welcoming me to San Diego and then Cambridge, for all the incredible dinners and conversations, and for supporting Fiamma in her work as a sea-going mentor to all of her students.

My committee has been fabulous to work with. **Sarah Giddings** taught one of my first classes at Scripps, Fluid Dynamics. Her teaching style clicked with my brain and her class was a bright spot in an otherwise very hard 2020-2021 pandemic year of zoom classes. After we had a lecture on hydraulic control I went out to the Scripps beach, based on her advice, and watched as the outflow on the beach formed hydraulic jumps and transport sand around. I knew I was a wierdo then and it was the first time I felt like maybe I had put myself in the right place to become the scientist I wanted to be. We were able to have a more normal classroom experience with her in Estuaries a couple years later—again, one of my favorite classes. I have learned a lot from Sarah's work about using rigorous physics to help answer questions that communities and coastal managers need answers to. If I didn't love the Arctic so much I would be studying the Tijuana River Estuary. Thank you Sarah for being an empathetic and supportive mentor in my time at Scripps, and for taking over beaurocratic advising duties after Fiamma moved.

The work in this dissertation has been largely shaped and strengthened by **Matt Mazloff**, and I am so grateful for his guidance. Several committee meetings went by with him saying "You know, you can solve water mass fractions differently and only use temperature and salinity" before I finally was curious enough to learn what he was hinting at. I went down the rabbit hole of matrix algebra and least squares and did what I think a PhD is supposed to make you do—become an expert in one super niche thing and try to make everyone around you care about it too! My confidence in approaching problems with more complex math expanded a lot because of this work and Matt's help. I appreciate how Matt helped me connect the tensions I was grappling with in my application to larger questions around modeling and observations and doing science. Thank you Matt for the many hours on zoom interpreting Carl Wunsch's book and navigating

matrix algebra together.

Finally, **Karen Kovaka** came on to my committee later into my PhD, but our conversations and her support have been impactful even in a short time. I was able to take Chapter 4 more seriously and trust that it could be part of this dissertation with her advice and mentorship. I'm so looking forward to continue learning from her and excited to see what we can collaborate on in the future!

**Jamie Holte** and **Margaret Lindeman** are unofficial committee members, advisors, and friends. I could not have done any of this work without them. Jamie makes everything happen in our group with humility, kindness, and lots of tasty baked goods. Thank you Jamie for always calmly listening to my rants about the state of the world and for being the best person to troubleshoot a CTD with. I have learned so much by watching how you navigate the dynamics of academia and how you've prioritized a full life while also being a scientist. Margaret is my science thought partner in crime (though the only crime we are committing is making too many TS plots). It has been a joy to watch her step into mentorship and teaching roles in our group and to see how students love learning from her, just as I do. I'm so glad the universe conspired such that we could think about Sermilik Fjord together for more years.

I have made countless memories with the members of our research group over the years and I'm grateful to have them in my life. There are no better people to have a CTD dance party with than **Monica Nelson** and **Bobby Sanchez**. **Kylie Kinne's** pink color schemes in slides are iconic, her biscuits are delicious, and Bonnie the dog is the best office mate. Thank you for making my more recent brief San Diego times much better. I'm so proud of **Lucy Wanzer** for making hard choices to navigate grad school in a way that is best for her—what a delight that the universe has given us this time to be lab mates! **Natalie McGee** was incredible to work with and it was inspiring to watch her run with the projects we gave her. Watching **Amelie** get excited about OSNAP data was delightful! I can't wait to see what they get up to in the coming years. Honorary research group members include filmmakers **Alex Rivest** and **Morgan Burger**. They were both critical in reminding me that what we do as scientists matters and I loved getting to

brainstorm and create with them both! Chris Basque is also an honorary group member—his mooring deployments are calm, choreographed works of art.

I've had so many other mentors and guides through this process, a testament to how collaborative our group is. **Mark Carey** has been a mentor and a thought partner for my more philosophical and historical questions (and we will write a paper together one day). **Mattias Cape**, **Lorenz Meire** (the professor), **Paty Matrai**, **Maria Vernet**, **Lorenzo Ciannelli**, **Donald Slater**, **Helene Seroussi**, **Chris Little**, **Adrienne Silver**, **Aqqaluk Sørensen**, **Karl Zinglersen** have all impacted the way I've approached science and impacted the work in this dissertation. **Twila Moon** and **Dave Sutherland**, in addition to supporting the GRISO Summer School, have always been available for advice when needed. **Leigh Stearns** and **Michael Shahin** have been so wonderful to work with as we try to bridge glaciology and oceanography in Sermilik Fjord. **Kirsty Tinto**, **Margie Turrin**, and **Casey Brayton** of the Greenland Rising project were so generous with their Kullorsuaq contacts, time, and learning. **Nick Beaird** and **Morven Muilwijk** provided code and thoughts about water mass fractions that were incredibly helpful, especially as I was just starting out with no concept about where I was going with any of this.

I would not have survived grad school in the pandemic without the "Lost Cohort" of Scripps PO students. I am so grateful for **Helen Zhang**, **Sophie Shapiro**, **Andrea Rodriguez-Marin Freudmann**, and **Kerstin Bergentz**. We managed to get one photo of all of us together! They are each brilliant and kind scientists. Special thanks to Kerstin for sharing her apartment and for so many coffee/lunch dates trying to make sense of life together. Other Scripps students that I'm grateful for include **Eva Hidalgo Pla**, **Chance Roberts**, **Emmet Norris**, **Hayden Johnson**, **Austin Barnes**, **Duncan Wheeler**, **Susheel Adusumilli**, **Philipp Arndt**, **Matt Luongo Allison Cusick**, **Isa Arzeno-Soltero**, **Jessica Ng**, **Noel Brizuela**, and **Emelia Chamberlain**. The Scripps Polar Center and **Helen Fricker** were central to my time at Scripps. **BT Werner** and their commitment to justice showed me a different way of using power in academia and what creating a space for students to align their work with their values can look like.

The Fostering Indigenous-Led Research Group an NNA Convergence Working Group

was a grounded learning space for me. Infinite gratitude to **Mary Beth Jager**, **Margaret Rudolph**, **Heather Sauyaq Jean Gordon**, **Dylan Blaskey**, **Stas Ksenofontov**, **Kitrea Takata-Glushkoff**, **Stacey Lucason**, **Courtney Carothers**, **Valerie Tony**, and **Lauren Divine**. Our meetings were a balm for me, taught me better facilitation skills, and I'm proud of the conversations our group hosted in the broader NNA research community. I'm excited to continue learning from you all.

The outreach and education work shared in this dissertation would not have happened without **Maxi Audibert**, **Nino Brønlund**, and **Lars Demant-Poort**. It was absolute magic to sit with Maxi in his home, share some Arctic Char he had caught, and talk about the place he loves (despite him suffering from a bad stomach due to french cheese!). The way kids in Kullorsuaq gravitated toward Nino as he taught them about the ocean and science was a joy to watch, and we gained so much from his translation work with hunters in Kullorsuaq.

The measurements in this dissertation would not have been possible without all the crew members on board the ships facilitating all aspects of our work. A special shoutout to the CTD deck crews of the R/V Tarajoq and R/V Sanna: **John Egede**, **Tønnes Hard**, **Silas Knudsen**, **Klaus Nielsen**, **Johan Petersen**, **Hans**, **Isaias**, **Johan (Erni) Egede**, **Rene Lange**, **Rikka Nielsen**, and **Magnus (Maanu) Petersen**. Their work facilitated safe and numerous CTD profiles, sometimes with lots of bergy bits needing to be pushed away from the winch line.

The work of university administrators is key to our field work logistics, funding, and payments, and often goes unrecognized in the machinations of science. Special thanks to **Tomomi Ushii**, **Sabrina Leitner**, **Sabrina Azinheira**, **Molly Carlson**, **Gilbert Bretado**, and **Dana Jimenez**.

Our people outside of our identities as scientists are just as important in this process! First, I need to thank my parents, **Mitchell Roth** and **Dorothy Corbett**, for all their support my entire life. I am a curious person who thinks about dynamic systems because of them! and the values that define who I want to be as a scientist have come from what I've learned from them. They have generously supported me (and have not been too anxious) as I traveled from

Antarctica to Greenland for science. Fergus, the best goldendoodle in the world, has my infinite gratitude. **Laura Crews** has shared this journey with me from the beginning and I can't imagine my life without her. Thank you for everything Laura, truly. And thank you for starting the garden right now while I write these words in a windowless conference room. Thank you to my housemates at La Querencia for helping me find home in San Diego. Thank you to Borderlands Relief Collective for helping me better understand borderless Kumeyaay lands and life beyond La Jolla in San Diego.

In no particular order these are friends and mentors I have not yet mentioned who have played a role in bettering my life during my PhD and have helped me carry on: **Joanna Young**, **Klara Maisch**, **Sarah Clement**, **Chris Carr**, **Hannah Mode**, **Emilie Sinkler**, **Kirsten Arnell**, **Alex Ravelo**, **Haley Carlton**, **James McMahan**, **Ella Carpenter**, **Maia Willis**, **Precious Symonette**, **Nicole Abib**, **Victoria Benson**, **Claire Sharp**, **Erin Petit**, **Regine Hock**, **Andy Aschwanden**, **Martin Truffer**, **Claudine Hauri**, **Gwen Flowers**, **Amy Jenson**, **Nick Parlato**, **Rachel Kaplan**, **Chase Hensel**, **Phyllis Morrow**, **Carrie Heimer**, **Katie Spellman**, **Noel Fitzpatrick**, **Anna Crawford**, **Kevin Blackwell**, **Gabby Markel**, **Nick Crews**, **Amy Davis**, **Elaine Kelly**, **Maddie Halloran**, **Max Graham**, **David Kreiss-Tompkins**, **Alex Petkanas**, **Sydney Scout**, **Rachel Christiansen**, **Polly Murray**, **Julian Childs-Walker**, **Lily Cohen**, **Chandler Kemp**, **Casey Chandler**, **Tav Ammu**, **Nat Herz**, **Journey Berry**, **Megan Pittas**, **Tamie Parker Song**, **Jason Katz-Brown**, **Diana Saverin**, **David Carel**, **Ben Sullender**, **Rosie Frankowski**, **Eliza Ramsey**, **Fannie Watkinson**, **Sarah Histand**, **Danielle Dittmer**, **Kavitha George**, **Lokesh Jain**, **Ravenna Koenig**, **Tanguy Sandre**, **Laurel Carothers**, **Kate Bollen**, **Louie Glick**, **Lizzy Miner**, and the Anchorage Ultimate Frisbee community.

Chapter 1, in full, is a paper from Aurora Roth, Fiamma Straneo, Jamie Holte, Margaret Lindeman, Matthew Mazloff, "A dataset for multidisciplinary applications: Thirteen years of ocean observations in Sermilik Fjord, Southeast Greenland" published in Earth Systems Science Data, Volume 17, Issue 11, 2025, 6025–6048, https://doi.org/10.5194/essd-17-6025-2025. The

dissertation author is the primary author of this paper.

Chapter 2, in full, is based on a paper from Aurora Roth, Matthew Mazloff, Fiamma Straneo, and Margaret Lindeman ”Water mass fraction methods in Greenland’s glacial fjords with a case study in Sermilik Fjord, Southeast Greenland”, 2026, and is currently being prepared for submission. The dissertation author is primary author of this paper.

AI tools, specifically Claude.ai from Anthropic, were used to assist with code development, complex literature landscape searches, language polish and editing, and LaTeX formatting represented in this dissertation. Every word of this dissertation was reviewed and accepted by a very real human (Aurora Roth, the author of this dissertation).

VITA

| | |
|---|---|
| 2013 | B.A., Physics and Astronomy, Carleton College |
| 2016 | M.S., Geophysics, University of Alaska Fairbanks |
| 2017–2020 | Polar Field Engineer, EarthScope Primary Instrument Center (formerly IRIS PASSCAL Instrument Center) |
| 2026 | Ph.D., Scripps Institution of Oceanography, University of California San Diego |

ABSTRACT OF THE DISSERTATION

Meltwater, Matrices, and Mattak: Ocean Observations in Kalaallit Nunaat's Changing Glacial Fjords

by

Aurora Roth

Doctor of Philosophy in Oceanography

University of California San Diego, 2026

Fiamma Straneo, Chair
Sarah Giddings, Co-Chair

The glacial fjords of Kalaallit Nunaat (Greenland) are critical connectors between the Greenland Ice Sheet (GrIS) and the global ocean—delivering freshwater from the melting ice sheet to the ocean and channeling deep, warm ocean waters back toward the ice. The GrIS has been losing mass at an accelerating rate since at least 1990 due to unabated rising global air temperatures from industrial human activities. This increasing addition of fresh glacial meltwater to the salty ocean has cascading local to global impacts. A challenge for improving projections of ice loss and ocean changes is the representation of local fjord processes in large-scale models. Addressing this and improving fjord parameterizations requires coordinated,

accessible, long-term datasets spanning multiple fjords and timescales—essential, also, to furthering multidisciplinary fjord ecosystem understanding. While fjord dynamics play an outsized role in determining future global sea level rise and ocean circulation dynamics, it has become increasingly recognized that ice-ocean processes are also the foundation of local ecosystems that Kalaallit rely on for subsistence, economy, and culture.

This dissertation addresses these data and science goals using hydrographic observations from Sermilik Fjord, Southeast Greenland. Chapter 1 produces a long-term, standardized, gridded dataset spanning 2009–2023, advancing methods toward a future Greenland-wide fjord atlas and use of data across disciplines. Chapter 2 develops a water mass fraction methodology tailored to fjord environments, with guidance for cross-study comparability. Chapter 3 applies this methodology to assess interannual variability in Sermilik Fjord, finding a stable near-glacier environment and a highly variable fjord mouth driven by shelf Polar Water fluctuations, with implications for improving ice-ocean parameterizations.

A common mathematical thread runs through Chapters 1–3: matrix algebra, least squares estimation, and linear inverse methods—raising enduring questions in observational oceanography: What makes a model useful? How do we balance complexity with interpretability? This dissertation engages these questions technically and philosophically, centering the challenge of making meaning from imperfect observations of our dynamic ocean.

Finally, Chapter 4 reflects on this work in relation to the Greenland National Research Strategy, examining what ethical, beneficial, and collaborative research can look like in the current political and social context of U.S.–Kalaallit Nunaat relations.

# Introduction

## 0.1 Kalaallit Nunaat: Land of the People

Kalaallit Nunaat[1], the Greenlandic name for Greenland, is home to Kalaallit (Greenlanders) and home to one of Earth's largest ice sheets. When outsiders think of Kalaallit Nunaat, they often think only of the uninhabited ice sheet—a stark, icy landscape with a white color palette. But Kalaallit Nunaat and Kalaallit people are largely defined by the ocean or "imaq" (Figure 1). There are coastal communities with bustling harbors and industrial fish packing operations, families cook seal soup over a campfire with their kids, small boats weave around towering icebergs to go fishing for the day, giant cruise ships full of tourists anchor outside of major towns in the summertime. Sassuma Arnaa, the mother of the sea, is a foundational figure in Kalaallit and Inuit cosmology—a figure of abundance and consequence—reflecting how central imaq is to Kalaallit life (Vebæk, 1995).

### 0.1.1 Glacial fjords are meeting places

Kalaallit Nunaat's glacial fjords, in particular, are critical zones where the sermersuaq ("the big ice", the ice sheet) meets the ocean. This meeting of ice and ocean ultimately supports the marine ecosystem which has sustained communities for generations. It is not a coincidence that most communities are located at fjord mouths because this is where fishing and hunting are often best.

[1]Throughout this dissertation both "Kalaallit Nunaat" and "Greenland" will be used interchangeably, however, I want to recognize that language is not neutral and holds power. Referring to Kalaallit Nunaat by its original name is a tiny act of solidarity with Kalaallit to assert their sovereignty, particularly in the global political context of 2026. Official Kalaallisut place names are used here when possible.

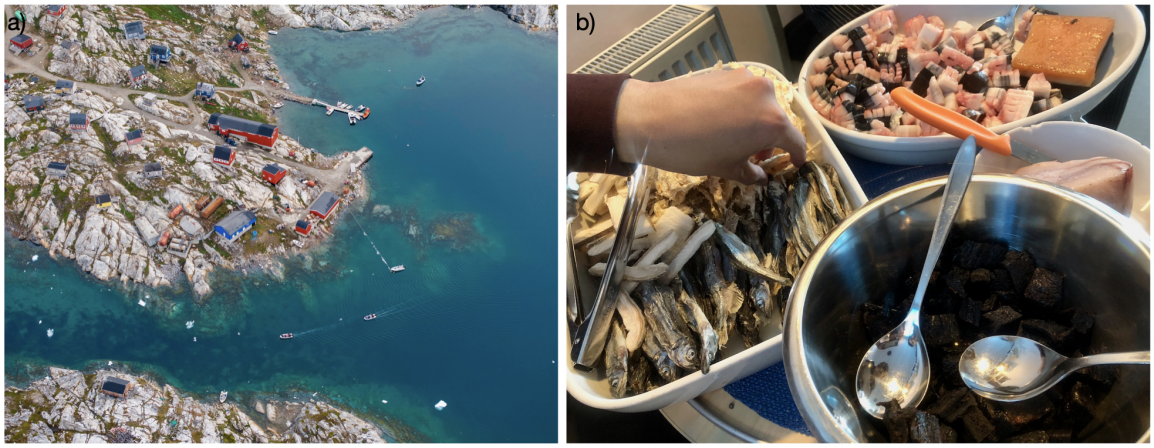


**Figure 1.** a) Boats head out for the day in the town of Tiilerilaaq in Sermilik Fjord in Southeast Greenland, the site of this dissertation, in August 2025. Photo by Alex Rivest. b) Traditional Greenlandic foods from the sea prepared on the R/V Sanna in Northwest Greenland in August 2024. Foods include puisi orsua (seal fat), ammassak (capelin), mattak (whale blubber) from qilalugaq qaqortaq (beluga) and qilalugaq qernertaq (narwhal), saarullik panertoq (dried cod) and qullulikat (dried halibut). Photo by Aurora Roth with translation assistance for caption by Nino Brønlund.

Importantly, it is through fjords that the rapid changes of the Greenland Ice Sheet are translated to the global ocean, and vice versa. The current unprecedented changes to our global climate system impact the ice of Kalaallit Nunaat through fjord pathways. Glacial fjord dynamics play an outsized role in determining future sea level rise and global ocean circulation. In a sense, glacial fjords host conversations between ice and ocean, between scales of local and global dynamics, and increasingly between international scientists and Kalaallit communities.

This dissertation explores elements of each of these conversations, and the remaining introduction provides important context and motivation for subsequent chapters. First, I describe the climate change context driving Greenland Ice Sheet mass loss and the global to local consequences of this immense change. Next, I provide an overview of glacial fjord dynamics, further introducing the processes and water masses important to the larger questions of global and local significance. Together, these set up the key scientific questions this dissertation addresses, including grappling with the ethics and responsibilities of being an outside scientist working in

Kalaallit Nunaat today.

Throughout the dissertation, and in practice as a scientist, I balance the dual significance of glacial fjords: as drivers and symbols of global environmental change, and the foundations of local ecosystems that support life in Kalaallit Nunaat.

## 0.2 The Climate Change Context

### 0.2.1 Warmer global temperatures are melting the Greenland Ice Sheet

The Greenland Ice sheet has lost 264 gigatons of ice per year over the period 2002–2025, with rates of loss accelerating over that period (Figure 2; The IMBIE Team, 2020; Landerer et al., 2020; NASA Jet Propulsion Laboratory, 2025). This translates to 18.4 mm or 0.72 inches of global sea level rise over that time period. Ultimately, this ice loss is caused by rising global air and ocean temperatures, primarily due to our industrial burning of fossil fuels[2]. In 2024, Earth experienced the hottest global average surface temperatures since observations began, and the last 10 years have been the hottest 10 years on record (World Meteorological Organization, 2025; Copernicus Climate Change Service, 2025). From October 2024–September 2025, the Arctic region experienced the warmest year on record, and Arctic air temperatures have continued to increase at faster rates than the global average (Druckenmiller et al., 2025). Notably, earlier this year, Nuuk logged its warmest ever January on record. The average monthly temperature in January 2026 was just above freezing (in winter!) at 0.1°C–7.8°C above the average over the last three decades (Danish Meteorological Institute, 2026).

Under intermediate to high emissions scenarios, the Intergovernmental Panel on Climate Change (IPCC) projects the Greenland Ice Sheet alone to contribute between 0.04–0.18 m of sea level rise by 2100 (Fox-Kemper et al., 2021), with higher-end estimates from expert elicitation studies reaching considerably beyond that (Bamber et al., 2019).

[2]Fossil fuel combustion for electricity, heat, transportation, and other industrial uses accounts for 65–75% of global carbon emissions. The Agriculture, Forestry and Other Land Use (AFOLU) sector, which includes deforestation and land use change, accounts for a further 13–21% of global anthropogenic GHG emissions (2010–2019) (Shukla et al., 2022; Nabuurs et al., 2022).

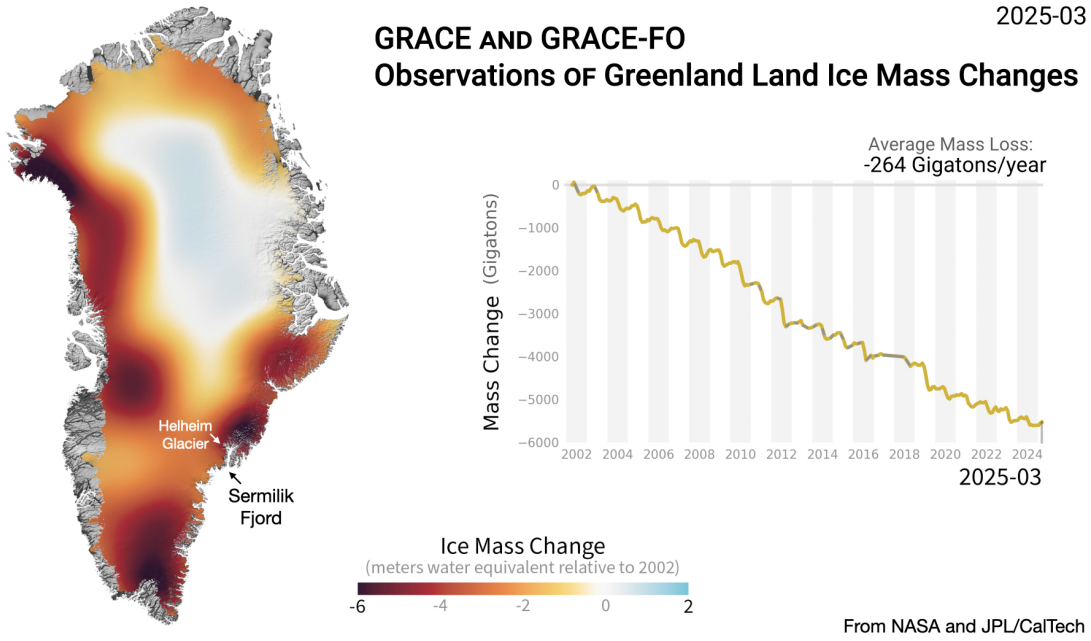


**Figure 2.** Greenland Ice Sheet mass loss from 2002 to 2025 based on observations from the Gravity Recovery and Climate Experiment (GRACE) satellites (2002-2017) and GRACE Follow-On (since 2018-present) (Landerer et al., 2020; NASA Jet Propulsion Laboratory, 2025). Sermilik Fjord and Helheim Glacier locations are indicated.

The addition of freshwater to the ocean from a melting Greenland Ice Sheet has global to local impacts beyond rising sea levels. First, more freshwater entering the ocean changes ocean density structure with potential impacts to global ocean circulation. And second, freshwater routed through the base of the ice sheet and released in glacial fjords at depth drives more ice loss and local upwelling at the ice-ocean interface. The following sections address these two topics and motivate the work of this dissertation.

### 0.2.2 Meltwater impacts global ocean circulation

The addition of fresh meltwater from the melting Greenland Ice Sheet does not just increase sea levels—it changes the ocean density structure with potential to destabilize, slow, or even shut down the Atlantic Meridional Overturning Circulation (AMOC), a globally important ocean current (Figure 3) that redistributes heat around the planet and regulates the climate in Europe and North America (Rahmstorf, 2024). The intensity and timescale for impacts to the

AMOC is a currently debated subject. Some modeling studies suggest the AMOC is already weakening (Caesar et al., 2018; Boers, 2021), while others provide time horizons of decades to centuries for a significant slow-down (Fox-Kemper et al., 2021). Direct observations of the AMOC strength from the past two decades show a picture dominated by strong interannual variability and decadal climate oscillations, making long-term trend detection challenging (Smeed et al., 2018; Lozier et al., 2019).

We rely heavily on coupled climate-ice-ocean models to explore these questions because these dynamics unfold on decadal to century timescales at large spatial scales. However, this means that local ice-ocean processes occurring in fjords are heavily parameterized, if included at all, despite their importance (Straneo and Cenedese, 2015; Hager et al., 2024; Slater et al., 2025b). The amount, location, and timing of freshwater, originating from the Greenland Ice Sheet and then subsequently mixed and transformed in fjords, is a critical variable in determining the fate of global ocean circulation (Sutherland et al., 2019). Currently, this freshwater is often crudely represented as a surface layer in large-scale models (Schmidt et al., 2025), despite observations and many recent studies showing that freshwater is also exported at depth and heavily mixed with salty ocean waters (Straneo et al., 2011; Mortensen et al., 2020; Beaird et al., 2018).

### 0.2.3 Melting glaciers impact marine ecosystems

For many years, the international science community was most concerned with the global impacts of a rapidly melting Greenland Ice Sheet and the physical ice-ocean system in glacial fjords. In essence, we were asking "What does all this melting ice in Greenland mean for the rest of the world?" While that is still of urgent concern (and needed action), it is now also recognized that glacial fjords and ice-ocean processes play an important role in supporting local and regional marine ecosystems, primarily through the upwelling of nutrient rich deep ocean waters at the fronts of marine terminating glaciers (described in detail in Section 0.3). Marine terminating glaciers are "ecosystem engines" and a widespread transition of marine terminating glaciers to land-terminating glaciers as outlet glaciers recede could lead to drastic shifts in nutrient and

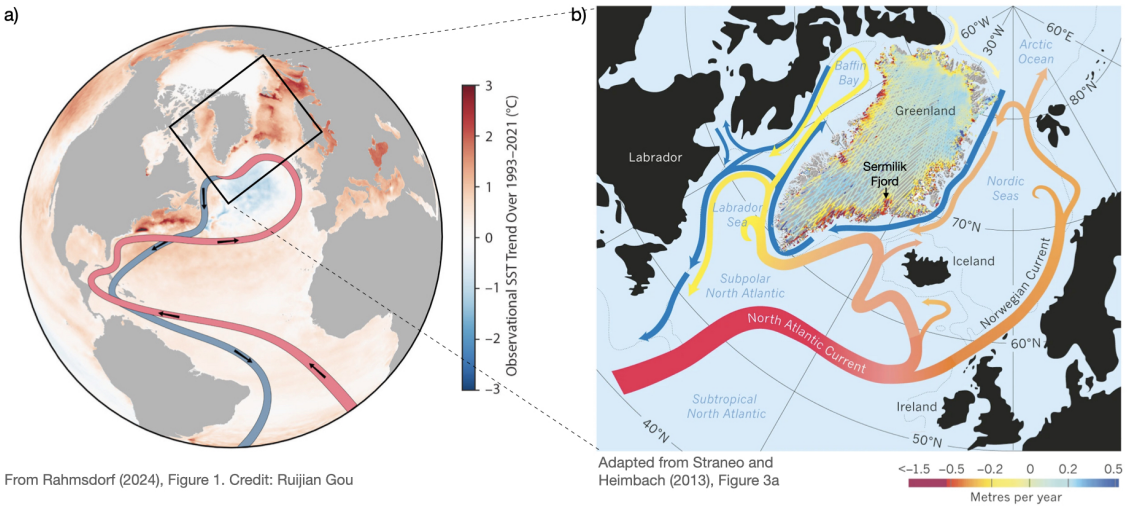


**Figure 3.** a) A simplified schematic of the global Atlantic Meridional Overturning Circulation (AMOC). The backdrop colors are the sea surface temperature trend since 1993 from the Copernicus Climate Change Service (https://climate.copernicus.eu/). Credit: Ruijian Gou. (Rahmstorf, 2024). b) Zooming in on the North Atlantic region of the AMOC and a schematic representation of the important ocean currents around Greenland. Atlantic Water (AW) is shown in red to yellow, and Polar Water (PW) is shown in blue. The dynamic thinning of the Greenland Ice Sheet is shown by the color scale. Adapted from Straneo and Heimbach (2013), Figure 3a.

sediment dynamics, with consequences to biodiversity and abundance of phytoplankton and zooplankton—the basis of the marine foodweb (Hopwood et al., 2020; Meire et al., 2017, 2023). Many questions remain unanswered about the specific links connecting the physical ice-ocean system, biogeochemical cycling, plankton ecology, and the higher trophic levels that people depend on like capelin, halibut, and seals. Making progress on these interdisciplinary questions requires not only working with scientists across distinct disciplines, but working with community members, fishers, and hunters who have local knowledge and are experiencing changes directly (Schiøtt et al., 2022; Rathcke et al., 2025).

## 0.3 Anatomy of a glacial fjord

Here we summarize the mechanics of glacial fjord processes, at the scale of a single fjord, to better understand how fjords mediate the global and local impacts described above.

Glacial fjords are long, narrow, deep channels carved into the bedrock by glaciers when the Greenland Ice Sheet was much larger during past glacial periods. The fjords of southeast Greenland are characteristically deep (often exceeding 500–900 m) and narrow. Today, where the ice sheet has retreated, marine-terminating glaciers sit at the heads of these fjords—meaning the glacier terminus is in direct contact with the ocean. The most significant dynamic changes to the Greenland Ice Sheet have occurred at these marine-terminating outlet glaciers (Rignot et al., 2010; Straneo and Cenedese, 2015; Mouginot et al., 2019; Wood et al., 2021).

Sermilik Fjord in southeast Greenland, the focus of this dissertation, is a representative example and one of the most well-studied glacial fjords in Kalaallit Nunaat (Figure 4; Straneo et al., 2016; Roth et al., 2025a). It has three branching fjords at its northern end each with a marine-terminating glacier at the head: Helheim Glacier, Apuseerajik (Fenris Glacier), and Nigertiip Apusiia (Midgård Glacier). Helheim is the largest of the three and one of the fastest-flowing outlet glaciers of the Greenland Ice Sheet. Tasilaaq, the largest town in East Greenland, with a population of $\sim$1800, is located near the mouth of Sermilik Fjord, and Tiilerilaaq, a small settlement of $\sim$100 people is located within the fjord (Figure 6). People fish, hunt, and recreate within Sermilik Fjord and there is increasingly more tourism activity in the area.

**Glacial meltwater**

Meltwater from the ice sheet has three primary pathways to the ocean: surface runoff, subglacial discharge, and submarine melt (Figure 5). Meltwater generated on the glacier surface can stay on the surface and drain directly into the ocean as runoff. It can also work its way down through crevasses into the subglacial system, traveling along the glacier bed before entering the ocean at depth—a giant submarine river emerging from the glacier bottom. This is called "subglacial discharge" or "subglacial runoff". Because this water is fresh and less dense than the ambient ocean waters, it rises as a turbulent buoyant plume, often reaching the surface and entraining large volumes of ambient ocean water on the way up. Subglacial discharge plumes are important for driving circulation in the fjords, increasing ocean melting of the ice, and upwelling

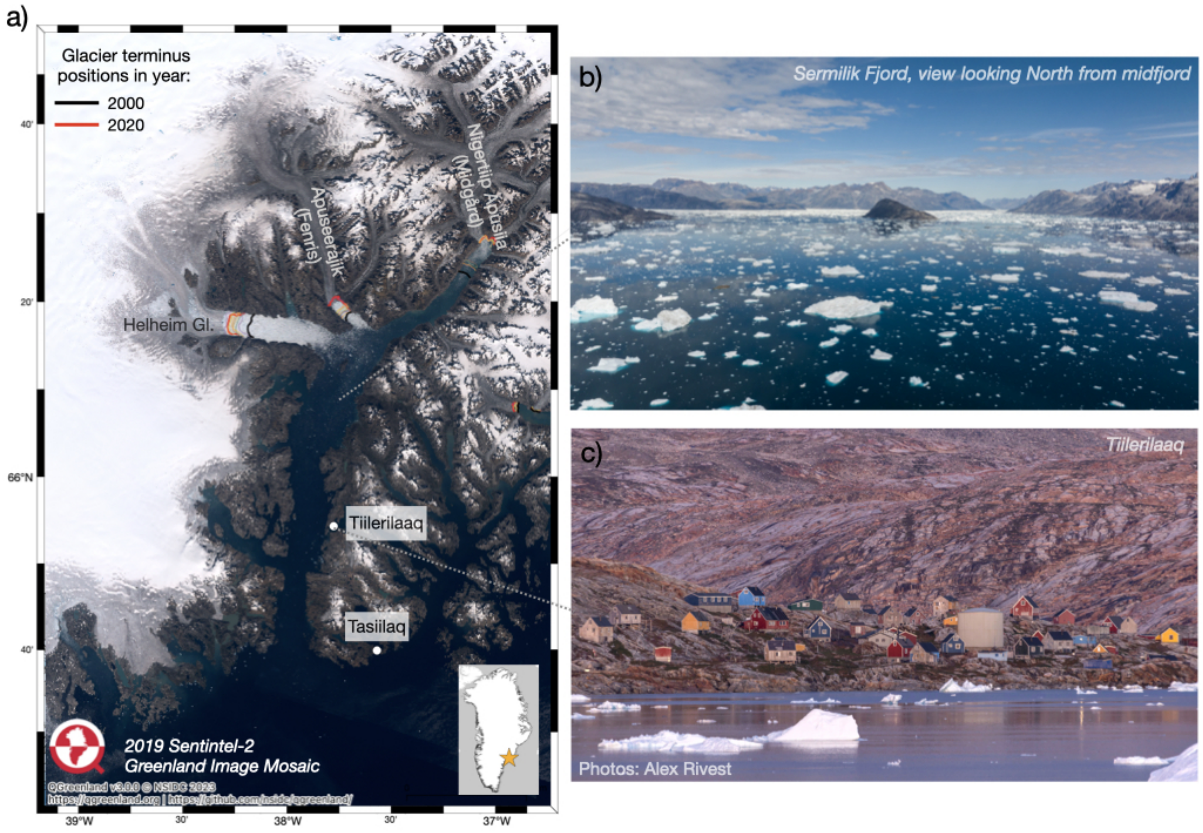


**Figure 4.** a) Introductory map of Sermilik Fjord with its three branching tidewater glaciers noted. Terminus positions from 2000 (black) and 2020 (red) are noted, as are the towns of Tasiilaq and Tiilerilaaq. Map and terminus positions visualized using QGreenland (Moon et al., 2023); Background is 2019 Sentinel-2 Greenland Image Mosaic product (European Space Agency and Copernicus Programme, 2019), and terminus positions are from Howat (2022). b) View of looking North from mid-fjord in Sermilik Fjord in August 2023. Photo by Alex Rivest. c) View of Tiilerilaaq inside Sermilik Fjord in August 2023. Photo by Alex Rivest.

nutrients locked away in deep fjord waters and making them available at the surface (Straneo and Cenedese, 2015; Hopwood et al., 2020; Slater and Straneo, 2022; Jackson et al., 2022; Oliver et al., 2023). For Sermilik Fjord, peak subglacial discharge from Helheim is estimated at roughly 500–650 $m^3\ s^{-1}$ in July (Mankoff et al., 2020). For reference, this is roughly a quarter of the average discharge rate of the Copper River in Alaska. At the scale of the whole ice sheet, the partitioning between surface runoff and subglacial discharge is an active area of research, and the balance is shifting as surface melting intensifies (Nienow et al., 2017; Bamber et al., 2019;

Mankoff et al., 2020).

Submarine melt is the process of ocean heat directly melting ice. This occurs everywhere the glacier terminus and icebergs are submerged in the ocean. We have learned in recent years that far more melt is happening this way than was previously assumed—a realization that has significant consequences for how we model ice-ocean processes and the future of the Greenland Ice Sheet (Sutherland et al., 2019; Jackson et al., 2020; Wood et al., 2021; Wengrove et al., 2023). For glacial fjords crowded with icebergs or choked with ice mélange, like the Helheim-Sermilik Fjord system, submarine melt of icebergs is an important driver of fjord water properties and freshwater export (Enderlin et al., 2016; Moon et al., 2018; Moyer et al., 2019; Davison et al., 2022; Kinne et al., 2025).

Helheim Glacier has an average of 30 Gt $yr^{-1}$ of solid ice discharge in the form of icebergs (Mankoff et al., 2020). If all this ice were instantly melted to freshwater, this would be equivalent to a discharge rate of $\sim$950 $m^3$ $s^{-1}$, compared to the peak subglacial discharge rate of 500–650 $m^3$ $s^{-1}$. This means that the freshwater input from Helheim Glacier to the broader ocean is largely controlled by the processes governing the melting of icebergs within the fjord, including the heat from Atlantic Water that is upwelled by the subglacial discharge plume.

**Ocean water masses**

The ocean side of the fjord conversation involves a more simple two-layer structure (Figure 5a). Cold, fresh Arctic-origin Polar Water (PW; temperature ¡ 0°C, salinity $<$ 33.3 g $kg^{-1}$) is carried southward along the Greenland coast by the East Greenland Coastal Current (Figure 3), filling the upper $\sim$150–200 m of the water column (Sutherland and Pickart, 2008; Harden et al., 2014). Below this, warm and salty Atlantic Water (AW; temperature 3–5°C, salinity $>$ 34 g $kg^{-1}$) from the Irminger Sea fills the deep regions of the continental shelf. A pronounced pycnocline separates these two layers at $\sim$150–200 m depth (Jackson et al., 2014, 2018; Sanchez et al., 2024).

The deep bathymetry of Sermilik Fjord, with no shallow sill to block exchange, allows AW

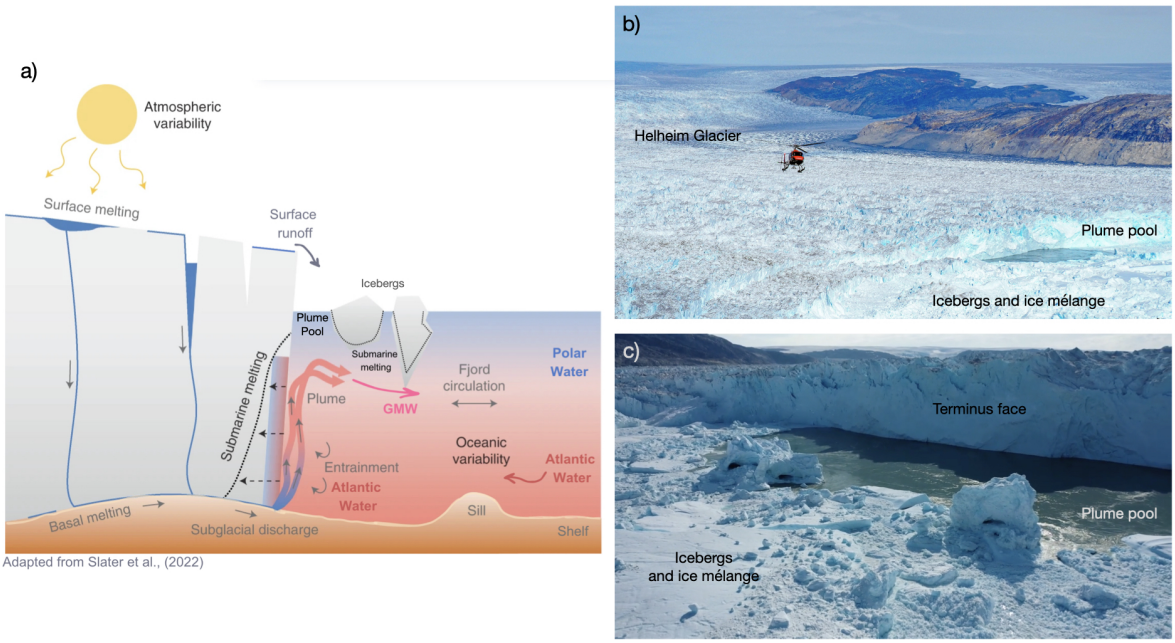


**Figure 5.** a) Diagram showing the pathways of subglacial discharge, surface runoff, and submarine melt into a glacial fjord and the key fjord processes controlling ocean properties in glacial fjords. The subglacial discharge plume and entrainment of deep ocean Atlantic Water is shown in detail which leads to the creation of Glacially Modified Water (GMW; see text). Depending on fjord stratification, the plume waters may have a surface expression as a plume pool that can be seen from the surface at the glacier terminus. Shelf waters of Atlantic Water and Polar Water are indicated. Figure adapted from Slater and Straneo (2022). b) An image of the terminus of Helheim Glacier with a plume pool showing at the surface. c) An alternate view of the same plume pool much closer to Helheim Glacier terminus. Both images are from July 2019. Photos by Paul Voosen/Science (Voosen, 2019).

to move freely from the shelf into the fjord and reach the termini of marine-terminating glaciers, where it drives submarine melt and is upwelled within subglacial discharge plumes (Straneo et al., 2011, 2012). Wind-driven variability on the continental shelf can rapidly change the depth of the shelf pycnocline relative to the fjord, driving intermediary circulation that exchanges fjord and shelf waters on timescales of days to weeks (Jackson et al., 2014, 2018). In summer, the addition of subglacial discharge and surface runoff complicates this picture, generating a third water mass—Glacially Modified Water (GMW), the product of AW entrained and upwelled by subglacial discharge plumes and mixed with glacial meltwater sources (Figure 5a). GMW appears in Sermilik Fjord as a relatively warm, salty intrusion in the upper 50–250 m of the

water column and is a tracer of glacier-ocean interaction (Straneo et al., 2011; Beaird et al., 2018; Lindeman et al., 2024). Partitioning the component water masses of GMW between ocean waters, submarine melt, and subglacial discharge and how the balance of these components evolves as GMW is exported from the fjord is a defining theme of this dissertation.

## 0.4 The key questions

In the 2000s, the scientific community began collecting more specific ice-ocean observations after documenting rapid outlet glacier retreat of key outlet glaciers. At this time, the ocean's role in these changes was uncertain (Straneo et al., 2016). For the last two decades, a concerted effort to measure the ocean near outlet glaciers using a variety of tools has occurred and we now know a lot more about the structure and properties of the ocean in fjords, and the changes ocean waters in fjords are causing, than we did previously (Straneo et al., 2019; Wood et al., 2021).

From this work, the sketch above of glacial fjord water masses and their interactions is accepted at this point—two ocean water masses on the shelf, multiple meltwater pathways, and forcing of circulation and mixing from both the glacier and the shelf (Figure 5a). What remains unknown is 1) how this picture varies from fjord to fjord, or from year to year in a single fjord, 2) what the most important drivers of that variation are, and 3) how much any variation (in both space and time) matters for projecting local and global impacts. These questions must be answered to complete a more generalized understanding of fjord physical dynamics and resulting ecosystem impacts, and to create robust parameterizations that can improve modeling efforts.

Making progress on these questions requires both the data infrastructure to make comparisons in space and time and consistent methodological tools to interpret those data. The chapters that follow address both areas.

## 0.5 Thesis structure and contributions

This dissertation addresses these questions through three chapters focused on Sermilik Fjord in Southeast Greenland. Chapter 1 tackles the foundation: before we can ask how the fjord varies, we need a consistent, accessible, long-term data record. We compiled thirteen years of summer hydrographic observations into a standardized, gridded dataset and produced a climatological mean—establishing what "typical" conditions are in Sermilik Fjord and where the greatest variability exists in space. This work provides a framework for other fjord datasets to improve our ability to compare datasets in different fjords by different research groups.

Chapter 2 shares an updated and more comprehensive water mass fraction methodology tailored specifically to glacial fjord environments. Water mass analysis is a powerful tool for tracing the origins and mixing of ocean waters, but applying it in fjords requires careful treatment of glacial meltwater end-members and the unique mixing processes near tidewater glaciers. We compare existing approaches and provide practical guidance for producing results that are comparable across fjords—a prerequisite for progress toward more generalized fjord dynamics parameterizations.

Chapter 3 then applies these updated water mass fraction methods to the long-term dataset produced in Chapter 1 to begin addressing the question of interannual variability of water masses in the fjord. What are the most important drivers in that variability? We find that the near-glacier environment is relatively stable interannually, while the fjord mouth is highly variable, driven primarily by fluctuations in how far Polar Water mixes into the fjord from the shelf. These results have direct implications for how freshwater export and submarine melt are represented in coupled ice-ocean models, and point toward the kinds of observations and parameterizations that will be needed to improve them.

### 0.5.1 Mathematical foundations

The first three chapters rely on similar mathematical frameworks including least squares estimation and matrix algebra. Chapter 1 uses objective mapping methods to produce a gridded dataset from scattered observations. Objective mapping is a way to model gaps in sparse data to create regularly spaced, filled-in fields of that data variable. Least squares estimation is used to best fit the data that do exist with the model that is constructed. Chapter 2 uses linear mixing equations and least squares estimation to determine water mass fractions. While in a slightly different form from objective mapping, this is another example of constructing a model of the system and finding the best fit to the data that are available. Both applications bring up philosophical questions of modeling and how to best fit data. In both cases, I emphasize the subjective choices that are required to make progress (true of any modeling effort) and the old adage "all models are wrong, but some are useful" is a guiding principle here. How do we balance interpretability with model complexity? What does "best fit" to the data actually mean and what metrics are most useful? How sensitive are different model parameters and how do we best account for those sensitivities in our given applications?

Additionally, the matrix algebra used here are simple versions of techniques used in machine learning and now ubiquitous A.I. chatbot models. The philosophical modeling and observational questions that we grapple with in this work are mirrored in those fields of study. There is also the potential of future studies to employ machine learning techniques to large, Greenland-wide fjord datasets to better generalize our understanding of fjord dynamics.

## 0.6 Kalaallit Nunaat Kalaallit Pigaat: Greenland belongs to Greenlanders

Chapter 4 steps back from physical science questions to reflect on the political, social, and historical structures of power that science and scientists are embedded within. Broadly, the science questions can be framed as "What does a melting Greenland Ice Sheet mean for the rest

of the world?" and "What does a melting Greenland Ice Sheet mean for Kalaallit Nunaat?". In Chapter 4, I ask "Why am I asking these questions to begin with and who am I to be doing this work?" and "Who benefits from this work?".



**Figure 6.** The town of Tiilerilaaq, in Sermilik Fjord, in August 2025 with the R/V Tarajoq in the background of the fjord. Photo Alex Rivest.

To make some progress on these large existential questions, I use the recently introduced Greenland National Research Strategy as an anchor (Naalakkersuisut (Government of Greenland), 2022). The strategy document is Naalakkersuisut's (the Government of Greenland) own vision of what beneficial international research in Kalaallit Nunaat should look like. I share a structured reflection exercise comparing our work to the goals stated in the document. The argument underlying this chapter is that reflection should not be separate from doing the science—we cannot improve what we don't identify and document. Conducting science in Kalaallit Nunaat as a U.S. researcher requires an honest reckoning of the historical and current relationship between

the U.S. military and science, the long legacy of extractive "hit and run" science in Kalaallit Nunaat, and an awareness that Kalaallit Nunaat is in the global spotlight more than ever.

In January 2026, in what Naalakkersuisut described as the largest protest in Greenland's history, thousands gathered in Nuuk, across Denmark, and internationally carrying the Erfalasorput flag and chanting "Kalaallit Nunaat, Kalaallit Pigaat" or "Greenland belongs to Greenlanders" in response to U.S. President Trump's threats to annex Kalaallit Nunaat by force (Figure 7). This dissertation is written in the context of this geopolitical moment, and all research in Kalaallit Nunaat is in the context of Kalaallit Nunaat's colonial history and present efforts toward sovereignty.




**Figure 7.** On January 17 2026, Kalaallit Nunaat had the largest protest in its history in response to threats of annexation and invasion by the U.S. and Trump administration. Thousands gathered in front of the U.S. consulate in Nuuk. Image from the AP/Evgeniy Maloletka.

The chapter closes with a practice common in social science but largely absent from

the natural sciences: a personal reflection on my own motivations and positionality. Many Kalaallit and indigenous scholars have advocated for approaching "research as relationship" (Inuit Circumpolar Council, 2022b; Graugaard, 2020; Gordon and Around Him, 2025). Ultimately, the foundations of any research are human relationships. Taking time to reflect on our motivations, positions within power structures, and values is not "self-indulgent", but a critical first step for developing relationships across cultures and research disciplines that make ethical, equitable, and beneficial research a reality.

# Chapter 1

# A dataset for multidisciplinary applications: thirteen years of ocean observations in Sermilik Fjord, Southeast Greenland

## 1.1 Introduction

The glacial fjords of Kalaallit Nunaat/Greenland are key climate connectors– delivering freshwater (in liquid and solid form) to the ocean and warm ocean waters to the ice sheet. As global air and ocean temperatures rise and the Greenland Ice Sheet (GrIS) melts at an accelerating rate, understanding fjord variability is critical to addressing large–scale questions of GrIS mass loss, freshening of the North Atlantic, and potential global ocean circulation changes (Straneo and Cenedese, 2015). Locally, fjords are home to Greenlanders and their livelihoods are dependent on the future of fjords in our rapidly changing climate (Holm, 2010; Nuttall, 2020; Schiøtt et al., 2022). While abundant fjord ecosystems have been observed and utilized by Greenlandic peoples for thousands of years, there is increasing scientific interest for how physical fjord processes impact local ecosystems and biodiversity around Greenland and how these may evolve in a changing climate (Meire et al., 2017; Hopwood et al., 2020; Straneo et al., 2022).

Long–term and concurrent observations of atmosphere, glacier, ocean, and ecosystem variables at Greenland's coastal margins are essential for improving our understanding of glacial fjord systems. Motivated by science needs, the last decade has seen a significant increase in

observations of all kinds collected in and near Greenland fjords. Notably, long–term (¿ 10 years) repeat oceanographic surveys have been carried out in Nuup Kangerlua (Godthåbsfjord) near Nuuk and in Young Sound in Northeast Greenland as part of the Greenland Ecosystem Monitoring MarineBasis Program (https://g-e-m.dk/gem-science-programme/marinebasis-programme) and Greenland Institute of Natural Resources research campaigns (Juul-Pedersen et al., 2009; Mortensen et al., 2018). In Northwest Greenland, long–term oceanographic observations have been conducted in Kangerlussuaq (Inglefield Bredning) region near Qaanaaq (Sugiyama et al., 2020, 2025). Sermilik Fjord in Southeast Greenland, the focus of this study, has had nearly annual summer season oceanographic observations since 2008.

While many of the ice or atmospheric data at the margin of GrIS are available through remote sensing, reanalysis, or regional climate model products (eg. Greenland Ice Sheet Mapping Project, ERA, RACMO), oceanographic data in fjords have been mostly collected by small research teams in isolated projects creating disparate datasets with widely varying characteristics distributed over many fjords (Schlegel and Gattuso, 2023). This makes it challenging to assemble these data in standard formats, typical of the large-scale oceanographic monitoring programs (eg. ARGO, GOSHIP), limiting their availability and usability.

Secondly, the environmental conditions and logistical constraints of working in fjords result in data being spatially and temporally disjointed. For example, repeat measurements at exact locations may be difficult to perform because of variable iceberg and sea ice presence and weather conditions. This makes it challenging to quantitatively compare different years or to provide modeling groups with mean properties instead of those based on a single survey. Even where repeat surveys exist, they may have been carried out using different instrumentation, sometimes within the same survey and/or by different groups over the years. Given the growing interest in understanding Greenland's fjords, it is important to develop data protocols and repositories that standardize fjord data from multiple surveys of a single fjord, facilitate comparisons between data collected in different fjords, and provide boundary conditions, forcings, and comparisons for ocean and ice sheet models (Juul-Pedersen et al., 2009; Straneo et al., 2019; Schlegel and

Gattuso, 2023).

Finally, as Greenland fjord research becomes increasingly interdisciplinary and collaborations with local Greenlandic communities and government are being further strengthened, it is necessary that data be provided in formats that are accessible and usable by a wide range of users, including scientists from other disciplines (glaciologists, marine ecologists, social scientists), policy makers, educators, and local tourism operators.

Here, we present 1) a quality controlled hydrographic dataset from Sermilik Fjord in Southeast Greenland for 13 summer field campaigns occurring from 2009 – 2023, consisting of ship–based Conductivity, Temperature, and Depth (CTD) profiles and eXpendable Conductivity Temperature Depth (XCTD) profiles deployed from helicopters, 2) a standardized, gridded along–fjord section dataset (**?**) combing both types of observations to increase usability by a diverse set of users, and 3) a summer climatological mean and root mean square deviation (RMSD), calculated from the gridded section dataset, summarizing the mean summertime fjord water properties and identifying regions with the greatest variability.

Data presented here include CTD profiles from ships and XCTD measurements typically deployed by helicopters in regions not accessible by ship. Some of these data have been described in previous studies (with data made available through data repositories) but the collective dataset and, importantly, the standardized gridded sections, which allow for survey–to–survey intercomparison and for the derivation of a robust summer season climatological mean, are new. Equally important, this study provides a procedure for the standardized gridding of the data, including an error estimate, where other observed variables in Sermilik Fjord (eg. dissolved oxygen, nutrients) can easily be gridded and incorporated into the database by multiple users. The method can also be easily adapted and used to build gridded section datasets from profile observations in other fjord systems.

The gridded sections, created using an objective mapping method, facilitate the comparison of coherent spatial patterns between surveys, comparison to model output, comparison with other scattered observational variables, and can be used for calculating fjord transport quantities.

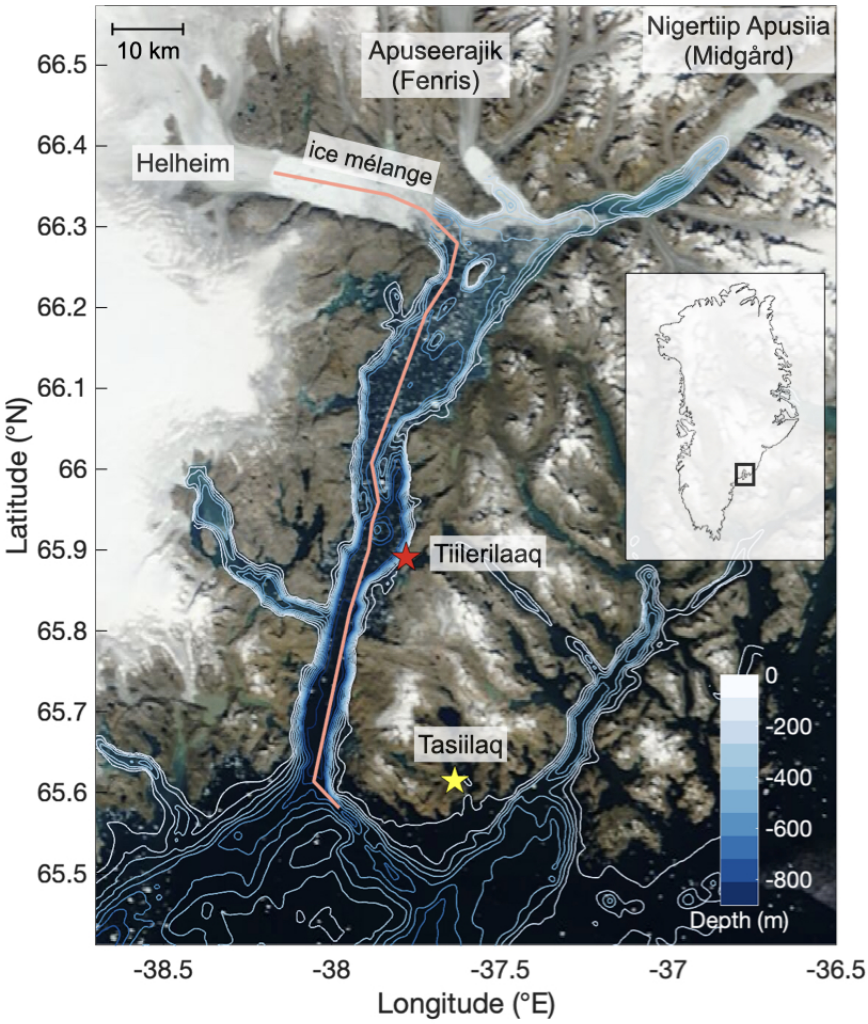


**Figure 1.1.** Map of Sermilik Fjord region in Southeast Greenland with major fjord branches and regions labeled. Bathymetry is shown as colored contours with 100 m increments and is derived from BedMachine Greenland v4 (Morlighem et al., 2017). The pink line represents the thalweg section of the fjord, used in plotting the bathymetry for the along–fjord sections (see text). The thalweg section end point is the Helheim Glacier terminus position in 2019. Background image is Terra MODIS corrected reflectance (true color) satellite image on August 12 2023. This image was obtained from NASA Worldview Snapshot application (https://worldview.earthdata.nasa.gov), part of Earth Science Data Information System (ESDIS).

They also address the needs of interdisciplinary researchers not familiar with CTD and XCTD data processing or treatment of observations from discrete profiles, but who are interested in

the mean and variable properties of the fjord for studies related, for example, to glaciers and ecosystems.

While more coordination and work is still needed within the science community, the approach shared here is a significant step toward creating a living data repository that standardizes long–term fjord observational records into a FAIR (Findable, Accessible, Interoperable, Reusable) data format to facilitate interdisciplinary research. The proposed framework for a larger, collaborative Greenland Ice Sheet-Ocean Observing System (GrIOOS) explicitly called for a repository such as this to facilitate the use of observations of Greenland's changing environment to address socially relevant questions at local to global scales (Straneo et al., 2019).

## 1.2 Sermilik Fjord setting

### 1.2.1 Glaciological context

Sermilik Fjord, located in southeast Greenland (Fig. 1.1), is long (∼90 km), narrow (5–10 km), and deep (550–900 m). The northern end of the fjord splits into three branching fjords with respective tidewater glaciers at the head of each branch– Helheim Glacier, Apuseerajik (Fenris Glacier), and Nigertiip Apusiia (Midgård, Midgaard, or Midgard Glacier) (Bjørk et al., 2015). Helheim, the largest of the three, is one of the largest and fastest flowing outlet glaciers of the GrIS. Due to Helheim's large volume of solid ice discharge, (∼30–38 Gt $yr^{-1}$ since 2000 from Mankoff et al. (2020)), freshwater input (∼500–650 $m^3$ $s^{-1}$ peak freshwater discharge in July from Mankoff et al. (2020)), and deep grounding depth (∼600 m) relative to the other glaciers, the physical dynamics of Sermilik Fjord are often studied by only considering the Helheim-Sermilik system. Since 2000, the terminus of Helheim has retreated ∼6 km and the glacier has lost an estimated 5–13 Gt $yr^{-1}$ of ice (Williams et al., 2021). Similarly, Apuseerajik (Fenris) and Nigertiip Apusiia (Midgård) have had consistently negative annual mass balance and terminus retreats (∼4 km and ∼11 km respectively) since 2000 (Williams et al., 2021; Huiban et al., 2024)).

### 1.2.2 Regional ocean context

The properties and circulation of the Sermilik Fjord region have been described in a number of earlier studies, and are briefly summarized below to provide context for this dataset.

The mouth of Sermilik Fjord opens onto the continental shelf where the East Greenland Coastal Current (EGCC) flows south carrying cold Polar Water (PW) (Conservative Temperature ($\Theta$) $< 0$ °C; Absolute Salinity ($S_A$) $< 33.3$ g kg$^{-1}$) of Arctic origin in the upper 200 m of the water column. Warmer, saltier Atlantic Water (AW) ($\Theta > 3$ °C; $S_A > 34.7$ g kg$^{-1}$) from the Irminger Sea underlies the PW on the continental shelf (Harden et al., 2014). A trough (400–900 m deep) extending from the fjord mouth across the continental shelf allows for the warm AW to be funneled from the shelf into the fjord (Straneo et al., 2010, 2011; Sutherland et al., 2014b; Snow et al., 2023). Shelf waters transported by the EGCC are known to enter Sermilik Fjord following the trough on the East side of the mouth, while there is strong preferential out fjord flow on the western side (Sutherland et al., 2014a).

### 1.2.3 Sermilik Fjord water masses

The deep bathymetry of Sermilik Fjord with no shallow sills allows for direct exchange of PW and AW shelf waters (Fig. 1.1). As a result, the same two-layer structure can exist in the fjord with a pycnocline at 150–200 m depth. AW fills the deep regions along the entire length of Sermilik Fjord and is present at the terminus of Helheim Glacier leading to submarine melting (Straneo et al., 2011). Regional wind dynamics on the shelf, primarily in the winter months during storms, result in oscillatory changes to the depth of the shelf pycnocline relative to the fjord, resulting in intermediary flow and fjord–shelf exchange (Jackson et al., 2014, 2018).

In the summer months, the addition of subglacial discharge, submarine meltwater, and surface runoff creates more complex fjord circulation, hydrography and ice–ocean dynamics. At glacier termini, buoyant subglacial discharge plumes entrain and upwell the deep, warm AW leading to enhanced submarine melting at the terminus and creating a water mass referred to as

Glacially Modified Water (GMW). In Sermilik Fjord, GMW appears as a relatively warm and salty intrusion in the upper 50–250 m of the water column (Straneo et al., 2011; Beaird et al., 2018; Lindeman et al., 2024). At the surface (¡ 50 m), the submarine meltwater of icebergs and the addition of surface runoff creates a fresh anomaly, referred to as surface GMW (sGMW) (Straneo et al., 2011; Lindeman et al., 2024).

### 1.2.4 Helheim Glacier ice mélange

Helheim Glacier has a perennial ice mélange consisting of icebergs and sea ice (Fig. 1.1). The ice mélange region regularly extends up to 30 km from the Helheim terminus, however the total extent and area varies seasonally and interannually with changing glacier and calving dynamics (Foga, 2016; Harcourt et al., 2025; Meng et al., 2025). The submarine meltwater of icebergs in the mélange contributes to GMW and creates a cold temperature anomaly in the upper 100 m of the water column in the upper fjord area (Straneo et al., 2011; Enderlin et al., 2016; Moon et al., 2018; Davison et al., 2022). Many questions remain about glacier–mélange–ocean feedbacks, in addition to questions about the role of subglacial discharge plumes in glacier–ocean dynamics at the terminus. Direct observations of these two fjord regions, ice mélange and subglacial discharge plume, are difficult and costly to obtain due to challenging ice conditions. The data presented here include observations from both regions for multiple summer seasons in Sermilik Fjord.

**Sermilik Fjord Western science context**

Sermilik Fjord became a site of intensive coordinated glaciological, atmospheric, and oceanic measurements starting in the late 2000s. Scientists aimed to understand the extent to which the ocean was playing a role in the retreat of Greenland's tidewater glaciers. At the time, there was little data from Greenland fjords and even high–resolution ocean models did not resolve fjord processes. Sermilik Fjord was chosen as a representative system of southeast Greenland glacial fjords because of the importance of Helheim Glacier to the dynamics of the

GrIS as a whole (Straneo et al., 2016). More recently, Sermilik Fjord has been identified as a site for a Greenland Ice Sheet–Ocean Observing System (GrIOOS) due to the availability of interdisciplinary measurements previously collected there (Straneo et al., 2019).

Studies in Sermilik Fjord have greatly advanced our understanding of fjord systems and the role of fjord dynamics in connecting GrIS and the ocean. Important findings that have previously utilized portions of the CTD and XCTD hydrographic dataset presented here include 1) showing unequivocally that warm AW contacts glacier termini and drives submarine melting (Straneo et al., 2010, 2011, 2012), 2) demonstrating that glacial melt water entrains ambient fjord water and is exported out of fjords as GMW at depth (Straneo et al., 2011; Beaird et al., 2018), 3) teasing apart drivers of complex fjord circulation beyond traditional estuarine two layer circulation (Sciascia et al., 2013; Sutherland et al., 2014b; Jackson et al., 2014), 4) the importance of shelf processes for ice–ocean interactions in fjords (Jackson and Straneo, 2016; Spall et al., 2017; Sanchez et al., 2024; Snow et al., 2023), and 5) the role of icebergs and the ice mélange in freshwater export and fjord properties (Enderlin et al., 2016; Moon et al., 2018; Davison et al., 2022; Hughes, 2022). The works listed have included analyses of these hydrographic data with other observational platforms in Sermilik Fjord (eg. moorings) or are modeling studies using these hydrographic data for validation and/or forcing. Additionally, many advancements in our understanding of ice–ocean–climate processes as a whole have been made utilizing a wide range of datasets from the Helheim–Sermilik Fjord system from many different research groups.

More recently, the Sermilik Fjord region has been the site of studies addressing the relationships between physical ice and climate processes, fjord biogeochemistry, ecosystems, and local communities (Cape et al., 2019; Laidre et al., 2022; Straneo et al., 2022; Lindeman et al., 2024; Rathcke et al., 2025). Though specific project goals have varied over the years, CTD and XCTD surveys have been reliably conducted almost every summer since 2009, excluding 2014 and 2020 (Fig. 1.2; Tables 1.1 and 1.2). This dataset is one of the longest oceanographic records of summer season water properties inside a southeast Greenland glacial fjord.

## 1.3 Data

### 1.3.1 CTD data

We present data from summer surveys conducted from 2009 to 2023, except for 2014 and 2020 (Fig. 1.2; Tables 1.1 and 1.2). 364 shipboard CTD profiles and 71 XCTD profiles are included in this dataset. A variety of vessels and instrumentation have been used as methods, logistics, and instrument technology were improved and refined (Table 1.1). From 2009–2013, conductivity, temperature, and pressure observations were collected with RBR XR–620 Titanium CTDs sampling at 6 Hz. Instrument accuracy is reported by the manufacturer as ±0.003 mS $cm^{-1}$, ±0.002 °C, and ±0.05 % of full depth scale for conductivity, temperature, and pressure sensors, respectively. Data from these CTDs required post–processing to correct unique pressure and conductivity offsets Straneo et al. (2010). Conductivity, temperature, and pressure were aligned prior to calculating salinity to account for the fact that the sensors are not physically co–located on the logger. Data were manually examined to address any salinity spikes or anomalous points.

Starting in 2015, a Sea–Bird SBE19plus CTD was used as the primary instrument, sampling at 16 Hz. Instrument accuracy is similar to the RBR XR–620 CTD and reported to be ±0.003 mS $cm^{-1}$, ±0.002 °C, and ±0.1 % of full depth scale for conductivity, temperature, and pressure sensors, respectively. A RBR Concerto CTD was also mounted on the rosette and used for redundancy, with the same instrument accuracy as the RBR XR–620 and sampling at 16 Hz. SBE19plus CTD data were processed using Sea–Bird SBE data processing scripts to correct for lags between sensors, despike data, remove loops, and smooth data. Data were manually examined and any remaining anomalous points were removed.

All CTD profile data were vertically averaged to 1 m depth bins. We used the TEOS–10 Oceanographic Toolbox (McDougall and Barker, 2011) to convert in situ temperature to Conservative Temperature ($\Theta$), conductivity to Absolute Salinity ($S_A$), and pressure to depth. All profiles were smoothed with a low–pass boxcar filter. The complete dataset of processed CTD profiles, grouped by cruise, are available with all metadata at the Arctic Data Center

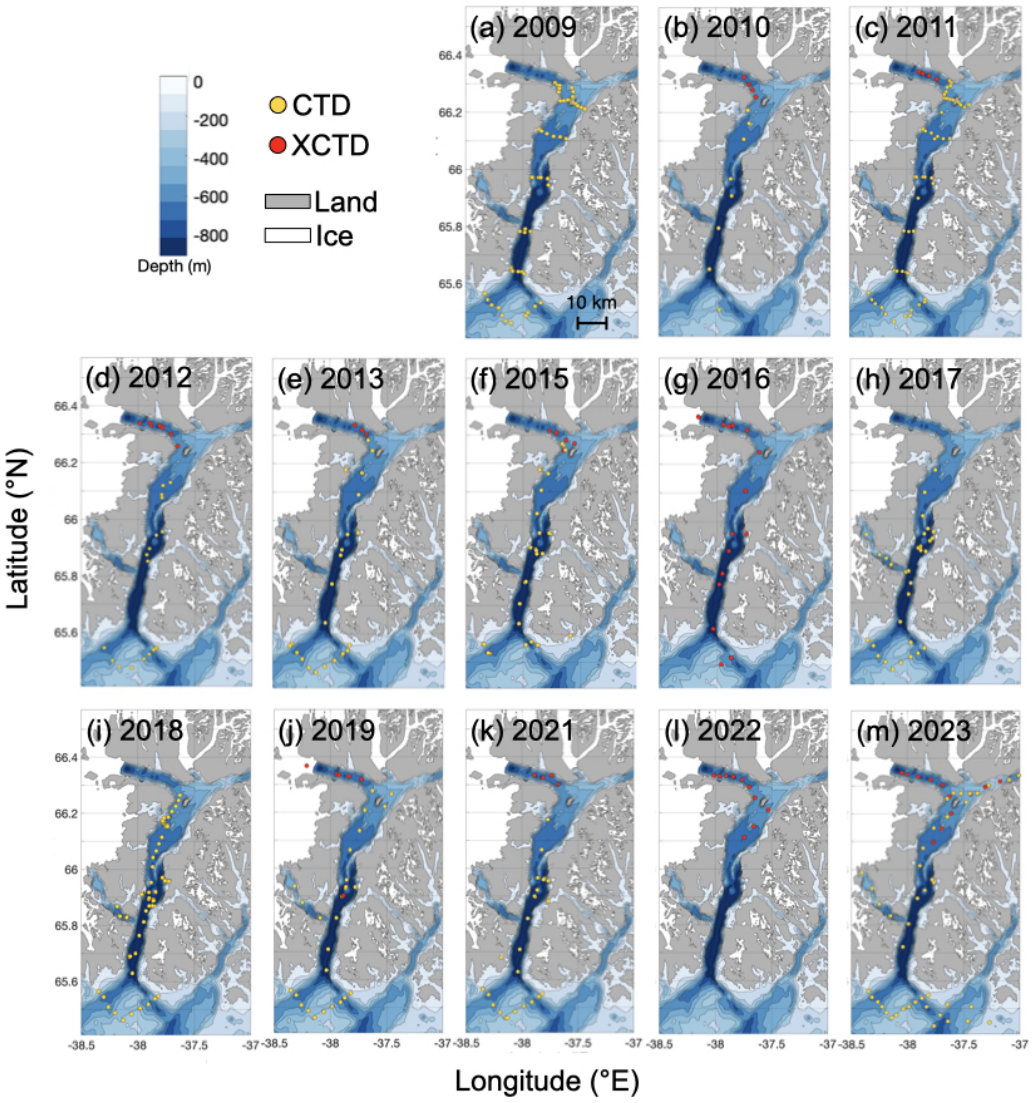


**Figure 1.2.** Locations of CTD (yellow dots) and XCTD (red dots) profiles for every summer survey in Sermilik Fjord included in this dataset. Bathymetry is shown as colored filled contours with 100 m increments. The bathymetry, land region, and ice regions are from BedMachine Greenland v4 (Morlighem et al., 2017). The land and ice regions correspond to outlines as they appear in the Greenland Ice Mapping Project (Howat et al., 2014) from the time periods 1999–2002 and 2013–2015. They are a static background for each year and do not represent specific ice extent and glacier terminus positions for a given year.

(https://arcticdata.io/catalog/portals/sermilik/Data).

**Table 1.1.** Information about each shipboard CTD summer survey in Sermilik Fjord.

| Year | Survey Dates | Vessel | CTDs Used | # fjord CTD profiles | # shelf CTD profiles |
|---|---|---|---|---|---|
| 2009 | Aug 19–25 | MY *Arctic Sunrise* | XR 620 Titanium RBR (s/n 18559) | 41 | 11 |
| 2010 | Aug 22–27 | *Pytur* | XR 620 Titanium RBR (s/n 18559) | 7 | 1 |
| 2011 | Aug 15–26 | *Viking Mads Alex* | XR 620 Titanium RBR (s/n 18559) | 39 | 12 |
| 2012 | Sept 14–20 | MV *Fox* | 2 x XR 620 Titanium RBR (s/n 17413, 18559) | 9 | 9 |
| 2013 | Aug 18–28 | *Viking Mads Alex* | 2 x XR 620 Titanium RBR (s/n 17413, 18559) | 13 | 14 |
| 2015 | Aug 2–11 | *Adolf Jensen* | SBEPLUS25 (s/n 251108); RBR Concerto (s/n 65584) | 22 | 8 |
| 2017 | July 15–22 | *Adolf Jensen* | SBEPLUS25 (s/n 251108); RBR Concerto (s/n 65584) | 21 | 10 |
| 2018 | Aug 3–14 | *Adolf Jensen* | SBEPLUS25 (s/n 251108); RBR Concerto (s/n 65584, 66129); RBR XR Titanium (s/n 18608) | 60 | 10 |
| 2019 | July 27–Aug 1 | *Adolf Jensen* | SBEPLUS25 (s/n 251108); RBR Concerto (s/n 66130) | 16 | 10 |
| 2021 | Aug 10–18 | *Adolf Jensen* | SBEPLUS25 (s/n 251108); RBR Concerto (s/n 66130) | 15 | 12 |
| 2023 | Aug 5–19 | RV *Tarajoq* | SBEPLUS25 (s/n 251108); RBR Concerto (s/n 66130) | 16 | 12 |

### 1.3.2 XCTD data

Starting in 2010, eXpendable Conductivity Temperature Depth (XCTD) probes were used in addition to shipboard CTDs (Straneo et al., 2011). The probes were deployed using helicopters to collect observations in the ice mélange and plume polynya regions where vessels cannot operate. Generally, the XCTD profiles are located in the near–terminus region of Helheim Fjord, but additional XCTD profiles have been collected in Midgård Fjord and the main branch of Sermilik Fjord in more recent years (Table 1.2).

XCTD instrument accuracy is reported as ±0.03 mS $cm^{-1}$, ±0.02 °C, and ±2.0 % of full

depth scale for conductivity, temperature, and depth respectively. The depth measurements are based on a constant fall speed and are thus less accurate than shipboard CTDs measuring pressure directly. All XCTD profiles were manually inspected and anomalous data points were removed. We removed the top 4 m of each profile because it takes several seconds for the probe to equilibrate to the ocean temperature once it enters the water and begins recording. The bottom of each profile was manually identified by spikes in the conductivity measurements and cross–checked with expected bottom depth. The profiles were vertically averaged to 2 m depth bins to reduce noise. In situ temperature and conductivity were converted to $\Theta$ and $S_A$, respectively, using TEOS–10 Gibbs–SeaWater Oceanographic Toolbox (McDougall and Barker, 2011), and a low–pass boxcar filter was applied to each profile. These processed XCTD profiles are available for use and released with the same data and metadata format as the CTD profiles at the Arctic Data Center (https://arcticdata.io/catalog/portals/sermilik/Data).

**Table 1.2.** Information about each XCTD survey in Sermilik Fjord. *One winter survey was conducted on March 15-16 2010 (Straneo et al., 2011). These profile data are available, but have not been gridded or included in the summer season climatology.

| Year | Survey Dates | Total # XCTD profiles | # XCTD profiles in ice mélange |
|---|---|---|---|
| 2010* | Mar 15–16 | 5 | 1 |
| 2010 | Aug 26 | 4 | 4 |
| 2011 | Aug 26 | 4 | 4 |
| 2012 | Sept 14 | 7 | 7 |
| 2013 | Aug 22 | 3 | 3 |
| 2015 | July 27 | 5 | 5 |
| 2016 | Aug 9–11 | 16 | 6 |
| 2019 | July 31, Aug 6 | 7 | 6 |
| 2021 | Aug 11 | 4 | 4 |
| 2022 | Sept 11 | 10 | 6 |
| 2023 | July 12 | 12 | 5 |

### 1.3.3 Combining CTD and XCTD data

XCTD measurements are less accurate compared to shipboard CTD measurements, and each XCTD profile uses a unique probe. Therefore we must consider whether any differences in measured water properties from each instrument type are due to biases in individual XCTD probes rather than real property variability. Because AW properties below 400 m have the smallest spatial and temporal variability throughout the fjord, we verified that the XCTD and CTD measurements for each year show matching AW properties within instrument error and known spatial variability, determined from the shipboard CTD measurements. No bias corrections were required for the XCTD data presented here, however, this is not always the case and this verification step is critical when working with combined XCTD and CTD data.

### 1.3.4 Profile locations and timing

There is a wide variety of profile locations and timing of the surveys during the summer season (Tables 1.1 and 1.2; Figs. 1.2 and 1.3). This is influenced by different logistical constraints and priorities of each field campaign and the fjord conditions at the time. The fjord has a high concentration of icebergs making exact repetition of profiling locations difficult. In general, an attempt is made each year to sample along the centerline of the fjord following the deepest bathymetric path (thalweg section) over a continuous time period (Fig. 1.1). Note that in 2009 and 2011 across–fjord sections were performed. From this data, it was determined that across–fjord variability is less significant compared to along–fjord variability, therefore surveys in the following years did not prioritize across–fjord sections (Straneo et al., 2011). Profiling locations are also influenced by recovering and deploying moorings, some of which are nearer to the coast than the fjord centerline. In 2018, the fjord survey was conducted in conjunction with specific iceberg surveys leading to many more profiles collected in the fjord that year. Other research priorities (eg. biogeochemical sampling) for a given year have influenced the final pattern of profile locations within the fjord.

XCTD profile locations in the ice mélange are limited to where gaps exist between icebergs and sea ice to deploy the probe. Notably, in 2016 and 2019, the Helheim subglacial discharge plume was visible at the ocean surface (known as a plume polynya) and created ice–free openings (Melton et al., 2022). This allowed for the rare opportunity to deploy XCTD probes directly into the subglacial discharge plume waters at the glacier terminus, collecting observations of this undersampled and critical region. In 2016 and 2022, only helicopter–based XCTDs were used for the complete fjord survey due logistical constraints.

In contrast, the sampling locations on the shelf are repeated at nearly the same locations each year because icebergs are less present on the shelf. The V–shape configuration is designed to cross the trough twice, observing shelf waters flowing into the fjord using the East section and fjord waters flowing out of the fjord and onto the shelf using the West section. All shelf profiles have been processed as described in Section 1.3.1 and are available with their associated fjord profiles for each year.

The surveys have occurred at different time periods in the summer season (Fig. 1.3). The seasonal dynamics of the fjord evolve over time and summer conditions can vary widely. Subglacial discharge and surface runoff begin to enter the fjord in June after the onset of the surface melt season. Both forms of freshwater entering the fjord peak in volume flux in late July and are usually negligible by late October (Mankoff et al., 2020). Buoyancy–driven circulation takes some time to set up with the addition of subglacial discharge. The continued addition of subglacial discharge throughout the summer can change the overall fjord stratification, altering the neutral buoyancy depth of the subglacial discharge plume over a summer season (Sanchez et al., 2023). Each year the surveys are capturing different time periods in this overall seasonal evolution of the fjord. Additionally, wind events on the shelf can drive shorter timescale (days to weeks) intermediary circulation on top of the buoyancy–driven circulation (Jackson et al., 2014, 2018). These events can quickly change fjord water mass properties over the timescale of a single fjord survey. Understanding the field campaign timing relative to freshwater inputs, wind conditions, regional climate conditions, is critical context for interpreting the data presented here.

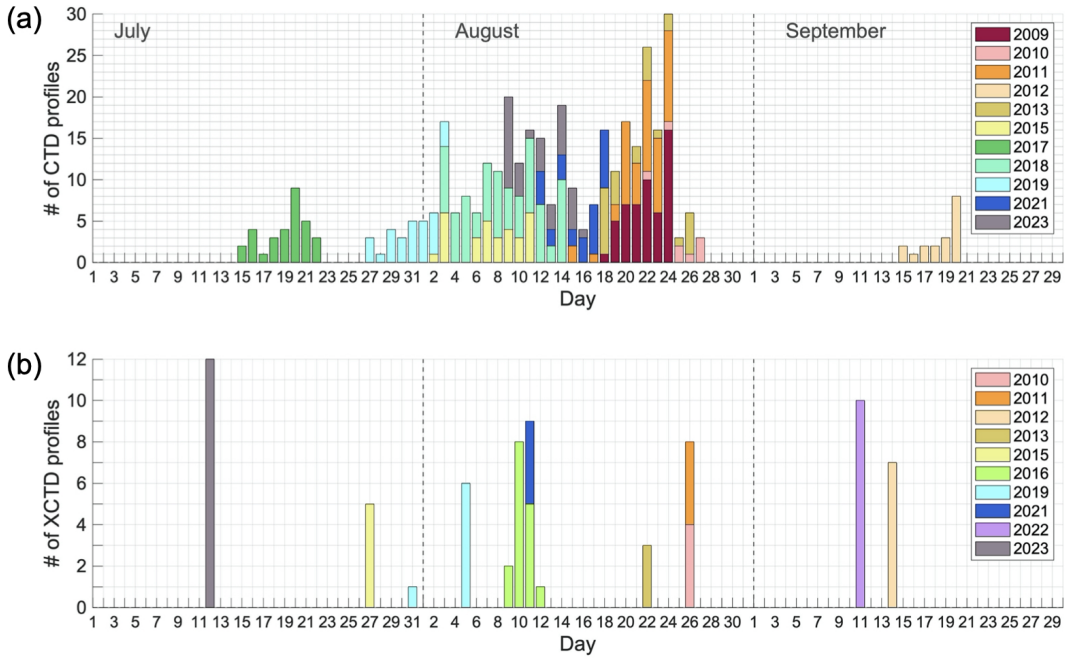


**Figure 1.3.** A visual representation of the survey dates and time periods in the summer season (July–September). Number of CTD (top) and XCTD (bottom) profiles collected on each day in the summer survey period across all years. Bar colors represent individual years. Dashed grey vertical lines denote the start/end of a month.

## 1.4 Methods

### 1.4.1 Profile selection for analysis

Prior to the gridding process, we constructed along–fjord sections for each survey following the thalweg transect line (Fig. 1.1). This required careful manual selection of profiles located nearest to the thalweg line and capturing similar fjord conditions within a certain time period. If profiles in similar locations existed, but were collected at different time periods during the survey (eg. collected while sailing upfjord and then downfjord several days later), we only retained the profile that created the best continuous synoptic section. If multiple profiles were collected in the across–fjord direction at the same along–fjord distance then those across-fjord profiles were averaged and the mean profile was used in the along–fjord section. Profiles near the shallower (¡ 300 m) fjord sides were not included. The final selection of individual profiles and

mean profiles (averaged in the across-fjord direction) making up the best synoptic along–fjord hydrographic section were then used as input data to create the gridded along–fjord dataset.

Data from inside the plume regions from years 2016 and 2019 are not included in the along–fjord sections. This is because the gradients of properties are at a finer scale in this dynamic region than we are accounting for in the objective mapping process. These plume data are discussed separately. Similarly, dynamics in the shelf region occur at different scales compared to the fjord and we do not use the shelf profiles for constructing the fjord sections.

Prior to objective mapping, we perform a "bottom fill" procedure for profiles extending beyond 550 m or deeper to enhance data density of the deep fjord regions for the objective mapping process. For all profile locations, properties below the sill depth of 550 m show little variability and are remarkably stable with respect to depth, but they do vary in the along–fjord distance. Without bottom filling of these profiles, the deepest profile informs the properties at that depth across the fjord when it is more likely that properties are similar to their nearest vertical neighbors. First, for all profiles extending 550 m or deeper, we calculated the average temperature and salinity value of the deepest 10 m of that profile. Then, we extrapolated these properties uniformly to the bottom. This extrapolation procedure was used for 128 profiles out of a total of 172 used in the along–fjord sections.

### 1.4.2 Creating gridded data using objective mapping

The challenge of creating gridded fields from scattered observations is well known in the earth sciences and there are many possible approaches. Objective mapping (also referred to as optimal or optimum interpolation) allows for the explicit use of input parameters and use of multiple spatial correlation scales to better represent physical processes. Objective mapping approaches are commonly applied to other hydrographic profile datasets including from the northern Antarctic Peninsula (Dotto et al., 2021) and the Weddell Sea (Reeve et al., 2016), and of biogeochemical profiles in the Southern Ocean (Mazloff et al., 2023). These previous applications are concerned with larger ocean basin–scale observations, often involving thousands

of profiles, and spanning decades. This is the first application of objective mapping for a Greenland fjord. Only recently have we been monitoring Sermilik Fjord long enough ($>$ 10 summer seasons) and with dense enough observations to appropriately inform the parameters and assumptions of the interpolation method. The increased utility provided by a gridded section dataset became apparent as research about Greenland fjords is maturing and data volume is increasing. We note that our use of "gridded data" here refers to gridded hydrographic sections (or transect) using a 2D coordinate system consisting of an along-fjord horizontal direction and depth. This is in contrast to other forms of gridded data with a 3D coordinate system (eg. outputs of regional ocean models using latitude, longitude, and depth levels) or a map view 2D coordinate system of latitude and longitude (eg. satellite data).

The along–fjord sections constructed with the final selected discrete profiles for each year were mapped onto a 2 km (horizontal) x 5 m (vertical) grid with the objective mapping procedure. The horizontal along-fjord coordinate system is referenced using 0 km at the 2019 location of Helheim Glacier's terminus and follows the thalweg section line. Associated latitude and longitude coordinates of gridcells this transect are included in the data products. The gridding process was performed independently for temperature and salinity variables. While each section is ultimately mapped to the same grid cell locations, the data extent of each gridded section varies because they are bounded by the minimum and maximum along–fjord distance locations of the profiles in each survey. The deepest vertical extent of each gridded section is bounded by the maximum depth profile for each survey (Fig. 1.4).

**Objective mapping algorithm**

First, a background field across the full domain (also referred to as a "first guess") was created by considering all summer season profiles selected by the process described above. The resulting background field, $\boldsymbol{g}_b$, represents the large–scale field which is well determined by the data and horizontal sampling locations.

For each year, the data anomaly $\boldsymbol{d'}$ was calculated as

$$\boldsymbol{d'} = \boldsymbol{d} - \boldsymbol{H}\boldsymbol{g}_b \tag{1.1}$$

where $\boldsymbol{d}$ is a vector of the original profile data for one year with n number of total data points at unique locations $(x_i, z_i)$. $\boldsymbol{H}$ is a matrix operator that linearly interpolates $\boldsymbol{g}_b$ to the same spatial coordinates as the original data points of $\boldsymbol{d}$.

The data anomalies for each year, $\boldsymbol{d'}$, are then objectively mapped using the gain matrix, $\boldsymbol{K}$, to produce the final gridded field by adding the background field, $\boldsymbol{g}_b$, back to produce the final gridded field, $\boldsymbol{g}_a$ (Eq. 1.2). It is common practice to objectively map the anomaly field (Bretherton et al., 1976; Roemmich, 1983). Prior to being mapped using Eq. (1.2), the anomaly data, $\boldsymbol{d'}$, were normalized by the standard deviation and the mean was subtracted.

The gridded field for each year, $\boldsymbol{g}_a$, is produced by

$$\boldsymbol{g}_a = \mathbf{K}\boldsymbol{d'} - \boldsymbol{g}_b. \tag{1.2}$$

The gain matrix, $\mathbf{K}$, objectively maps the data anomalies, $\boldsymbol{d'}$, and the background field is added back in. The core part of the objective mapping procedure is $\mathbf{K}$ (Ide et al., 1997). It's also referred to as the coefficient or weighting matrix (Wong et al., 2003; Reeve et al., 2016). $\mathbf{K}$ is constructed using the data–data spatial covariance matrix, $\mathbf{C_{dd}}$, and the data–grid spatial covariance matrix, $\mathbf{C_{dg}}$, where

$$\mathbf{K} = \mathbf{C_{dg}} \cdot [\mathbf{C_{dd}} + \mathbf{R}] - 1. \tag{1.3}$$

We assume the covariances are each a sum of a large–scale Gaussian and a small–scale Gaussian (Eq. 1.4 and Eq. 1.5). The decay scales of each Gaussian are determined by four scale parameters: large– and small–scale horizontal correlation scales, $L_{x_1}$ and $L_{x_2}$; and large– and

small–scale vertical correlation scales, $L_{z_1}$ and $L_{z_2}$. Each Gaussian has an amplitude parameter which determines the relative weighting of the large–scale ($A_1$) and small–scale ($A_2$) functions in the final map. The sum of $A_1$ and $A_2$ must be equal to 1 and must both be positive values. These six parameters were prescribed and determined by prior knowledge of scales of variability in the system, and tuned such that they yield a realistic field that best captures the conditions and dynamics of the fjord.

$$\mathbf{C_{dd_{ij}}} = A_1 \cdot \exp\left\{ -\left[ \frac{dist_{x_{ij}}^2}{L_{x1}} + \frac{dist_{z_{ij}}^2}{L_{z1}} \right] \right\} + A_2 \cdot \exp\left\{ -\left[ \frac{dist_{x_{ij}}^2}{L_{x2}} + \frac{dist_{z_{ij}}^2}{L_{z2}} \right] \right\} \tag{1.4}$$

$$\mathbf{C_{dg_{ig}}} = A_1 \cdot \exp\left\{ -\left[ \frac{dist_{x_{ig}}^2}{L_{x1}} + \frac{dist_{z_{ig}}^2}{L_{z1}} \right] \right\} + A_2 \cdot \exp\left\{ -\left[ \frac{dist_{x_{ig}}^2}{L_{x2}} + \frac{dist_{z_{ig}}^2}{L_{z2}} \right] \right\} \tag{1.5}$$

The data–data spatial covariance matrix, $\mathbf{C_{dd}}$,is a function of the distances between every i data point location to every other j data point location in the horizontal ($dist_{x_{ij}}$) and depth ($dist_{z_{ij}}$) directions. $\mathbf{C_{dd}}$ is thus a n x n square matrix where n is the number of original data points. The diagonal values of this matrix are 1 as this represents the distance of each profile data point to itself. The data–grid spatial covariance matrix, $\mathbf{C_{dg}}$, is a function of the distances between every i data point location to every g grid point location in the final gridded domain. $\mathbf{C_{dg}}$ is an m x n matrix where m is the total number of grid point locations.

To represent noise in the system, we define the noise matrix, $\mathbf{R}$, as

$$\mathbf{R} = \varepsilon^2 \cdot \mathbf{I}. \tag{1.6}$$

The value of $\varepsilon^2$ is a prescribed noise-to-signal parameter of the data anomalies. A larger value of $\varepsilon$ means that the map is less able to represent the data anomalies and the final map is

less influenced by those data values because more "noise" is assumed to exist in the system. The choice of $\varepsilon$ strongly impacts the final map (Mazloff et al., 2023). Our choice here is $\varepsilon = 0.5$ times the standard deviation of the data anomalies, $\boldsymbol{d'}$, and this is a parameter that can be adjusted depending on application or the question of interest. $\varepsilon = 0$ would represent that the values of the final map at the data locations must be equal to the original data values. However, it is not possible to use $\varepsilon = 0$ because the sum of $\mathbf{C_{dd}} + \mathbf{R}$ in Eq. 1.3 produces a non-zero diagonal for the matrix inversion, which is mathematically necessary for this objective mapping procedure. A non-zero value for $\varepsilon$ acknowledges that we are modeling the system with smoothness at the lengthscales specified in Eq. 1.4 and Eq. 1.5 and signals at smaller scales than these are considered "noise" not represented by the chosen lengthscale parameters.

Objective mapping allows for the calculation of the error variance of the gridded field as

$$\boldsymbol{\sigma}_g^2 = \mathrm{diag}(\mathbf{I} - \boldsymbol{C_{dg}} \cdot [\boldsymbol{C_{dd}} + \boldsymbol{R}]^{-\mathbf{1}} \cdot \boldsymbol{C}_{\mathbf{dg}}^{\mathrm{T}}) \cdot \boldsymbol{\sigma}_d^{\mathbf{2}}. \tag{1.7}$$

$\boldsymbol{\sigma}_d^2$ is the variance of the original data, $\boldsymbol{d}$. We report uncertainty in units of the observed data by taking the square root of Eq. 1.7. We share the gridded fields of the uncertainty (also referred to as mapping relative error) so that a user can gauge the amount of uncertainty in the map.

After deriving the gridded fields, we apply a correction to the temperature field. For the coldest temperatures at the freezing point of seawater with limited data points nearby, the objective mapping procedure interpolates the gridded temperature to be colder than the freezing point. We identify these values and correct them to be at the freezing point of seawater, calculated using the gridded salinity value of that gridded data point. This correction was applied to 27 out of 77,521 total gridded data points in all the final gridded temperature fields.

### 1.4.3 Choosing a background field

The background field, $\boldsymbol{g}_b$, is an important parameter in the objective mapping method and can be constructed in a number of ways. The constant hydrographic features we aimed to capture in a background field were the two–layer temperature structure of the fjord (cold water on top of warmer water), colder surface waters in the ice mélange relative to the mouth, and a large salinity range with nearly fresh water at the surface and increased salinity with depth. For both temperature and salinity fields, we plotted all selected along–fjord profiles from every summer season in the fjord onto one along–fjord axis, linearly interpolated these profiles to the 2 km x 5 m standardized grid. We then heavily smoothed this grid in the vertical and horizontal using a boxcar filter to achieve the desired large–scale background field features. We explored alternative methods for choice of background field, including creating individual background fields for every year from linearly interpolating between spatial endmember profiles closest to the glacier and mouth. We determined that any reasonable method for creating a background field that results in a representation of the average large–scale hydrographic features described above leads to similar objective mapping performance.

### 1.4.4 Choosing appropriate parameters

In the objective mapping method used here, there are seven parameters chosen based on knowledge of the system and the observations (Table 1.3). The same parameters were used for every year and for both temperature and salinity fields. Other applications of objective mapping in fjords could use more or fewer Gaussian lengthscale functions with different values and relative weights in order to capture the dynamics of a specific system. Initial lengthscale values were tested based on visual inspection of the scattered data and an error value was chosen informed by previous objective mapping applications and known instrument error (Dotto et al., 2021; Mazloff et al., 2023). Following other studies, we performed a series of tests exploring the parameter space to choose a parameter combination that yielded minimized residual values

and an appropriate representation of smoothed hydrographic features for the whole domain each summer. By making the code for this method available, we stress that others can adjust parameters to produce gridded fields that best match features of interest within Sermilik Fjord or best match features in other fjords with different spatial patterns.

**Table 1.3.** Description of assigned parameters in objective mapping method

| $L_{x_1}$ (km) | $L_{z_1}$ (m) | $A_1$ | $L_{x_2}$ (km) | $L_{z_2}$ (m) | $A_2$ | $\varepsilon$ |
|---|---|---|---|---|---|---|
| 50 | 100 | 0.6 | 15 | 10 | 0.4 | 0.5 |

### 1.4.5 Calculating a climatology

We calculated a climatology representing the average summer state properties of Sermilik Fjord from the summer along–fjord gridded sections. For both temperature and salinity, the mean and root mean square deviation (RMSD) at every grid cell was calculated. The 2009–2023 grids for each survey cover different fjord extents based on the locations of the original profiles for each year. As a result, each grid cell mean and RMSD was calculated from a different number of years ranging from 1–14 (Fig. 1.4). The 2023 CTD and XCTD data are not combined and treated as two separate instances of a summer fjord state, yielding a maximum of 14 available grids to be used in calculating each grid cell mean. Grid cells between 40–50 km from the terminus use all 14 grids while grid cells 12 km from the terminus only have 3 grids to calculate the mean. This reflects the challenge of obtaining repeat observations in the ice mélange region. Grid cells with fewer than 3 years were not included in the final climatology.

## 1.5 Results

### 1.5.1 Objective mapping performance

We judged the parameter choice performance based on the root mean squared error (RMSE) values, the pattern of residuals across the domain, and the visual representation of hydrographic features in the final gridded fields. Residuals were calculated by subtracting the

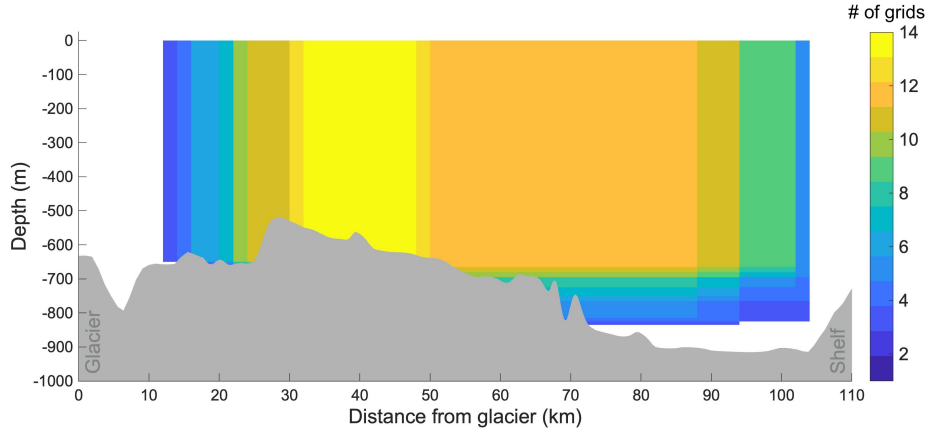


**Figure 1.4.** The number of grids representing each survey that have data in each grid cell in the along–fjord standardized grid domain. The number in each grid cell is used to calculate the property mean and RMSD. Grid cell size is 2 km (horizontal) by 5 m (vertical). Grid cells with only 1 or 2 surveys of coverage have been removed.

gridded value from the observed value, where the gridded data were linearly interpolated to match the exact along–fjord and depth coordinates of each observed data point. The gridded temperature fields at the profile locations, residuals at those locations, and the associated temperature relative mapping error for the years 2009 and 2019 are shown in Fig. 1.5a-f. We highlight these two years with differing hydrographic patterns and spacing between profile locations to demonstrate the objective mapping performance across a range of input profile data characteristics.

We evaluated the residuals and RMSE for each survey individually and across all surveys in bulk for both temperature and salinity fields. For the final parameter set presented here for all surveys, 88 % of temperature residuals are within a difference range of ± 0.1 °C and 67 % are within a difference range of ±0.04 °C. 91 % of salinity residuals are within a difference range of ±0.05 g $kg^{-1}$ and 77 % are within a range of ±0.02 g $kg^{-1}$ (Fig. 1.6). The bulk RMSE is 0.09 °C and 0.08 g $kg^{-1}$, for temperature and salinity respectively. The observed salinity profiles are more spatially smooth compared to the temperature profiles resulting in slightly smaller RMSE values.

The pattern of residuals across the domain is equally important to understand which hydrographic features are and are not represented well in the interpolation method. Sharp thermoclines within the upper 200 m at length scales smaller than the prescribed vertical

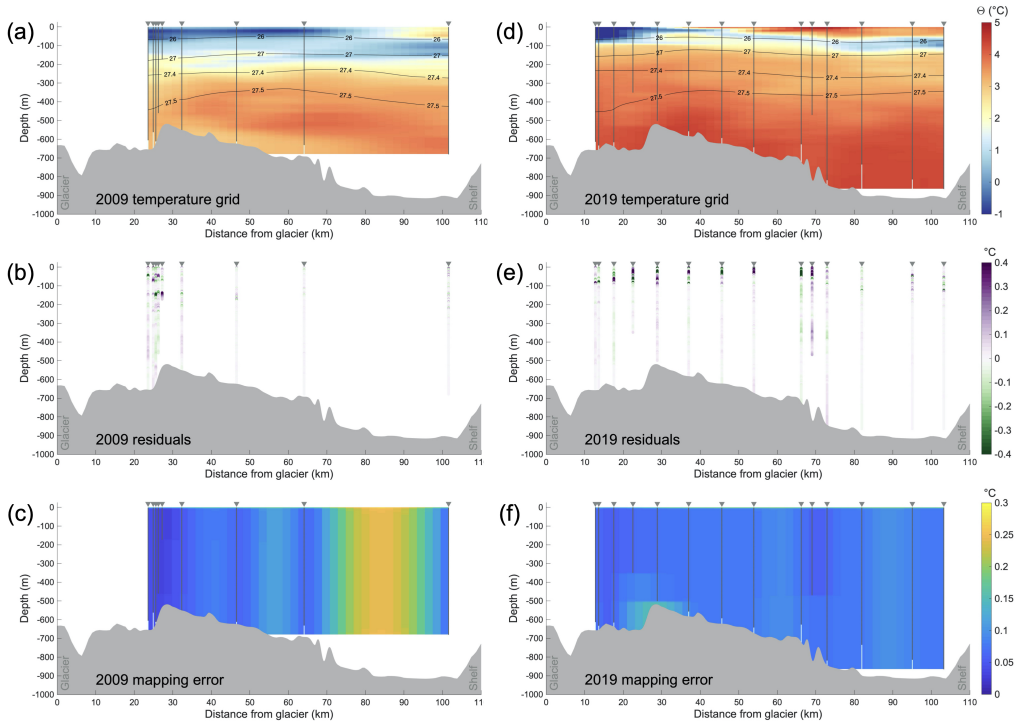


**Figure 1.5.** The conservative temperature objectively mapped gridded fields for 2009 (a) and 2019 (d) with potential density anomaly isopycnals (black contours). Original CTD and XCTD profile locations in the along–fjord direction are shown by triangle markers with vertical black lines representing the depth extent of each profile. White lines show where the bottom of a profile was filled in to facilitate greater data coverage for mapping. The 2009 (b) and 2019 (e) residual values are shown by filled dots at each original data point. The mapping relative error (c, f) is shown for each year. The bathymetry (grey area) is derived from a thalweg line (Fig. 1.1) of BedMachine Greenland v4 data (Morlighem et al., 2017). Distance 0 km is the location of the Helheim Gletsjer terminus in 2019.

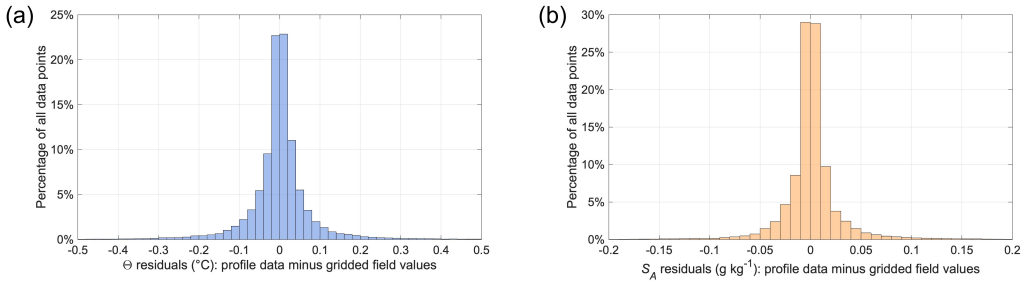


**Figure 1.6.** Histograms displaying the distribution of residual values between the gridded temperature (a) and salinity (b) fields and the profile observations considering all years in bulk. Bin size is 0.02 °C (a) and and 0.01 g kg$^{-1}$ (b)

smoothing ($L_{x_2}$ = 10 m) result in the highest residual values in the domain. These are often present near the fjord mouth where interleaving of different water masses between the fjord and shelf is known to occur. High residuals also consistently occur in the ice mélange region at ∼150 m depth where there is a sharp thermocline transition between cold ice mélange meltwater and warmer waters at depth.

We also provide the mapping relative errors in the same format as the temperature and salinity gridded sections. The user is able to choose a relative error value to work with, if needed. The mapping relative error magnitudes of all sections are acceptable for most use cases as shared here. Considering all sections, the range of error is 0.03 to 0.30 °C and 0.04 to 0.40 g $kg^{-1}$ for the temperature and salinity grids respectively. As expected, the error increases as the distance between data points increases beyond the lengthscale parameters.

Finally, parameter choice was aided by visual inspection of the original profiles and gridded data for each year in $\Theta$–$S_A$ diagrams (Fig. 1.7). This was to ensure that the gridded sections did not introduce density classes beyond the range present in the observations. The final parameter set shows good agreement between the gridded data and observations in $\Theta$–$S_A$ space.

### 1.5.2 Climatology and spatial variability

The complete set of $\Theta$ and $S_A$ along–fjord gridded sections are available to view in the Supplementary Material (Figs. S1–S8). Combining the CTD and XCTD datasets extends the along–fjord spatial coverage for years where both types of profiles were collected concurrently. Despite differences in original profile locations and fjord coverage from year to year, the standardized gridded along–fjord sections allow us to calculate a summer state climatology and associated RMSD for the Helheim–Sermilik Fjord system (Fig. 1.8). This is one example of the increased utility of the gridded dataset compared to utilizing individual surveys or less explicit interpolation methods. The climatology product provides novel context for the yearly variability of summer season fjord water properties and improves the interpretation of previously published work from Sermilik Fjord.

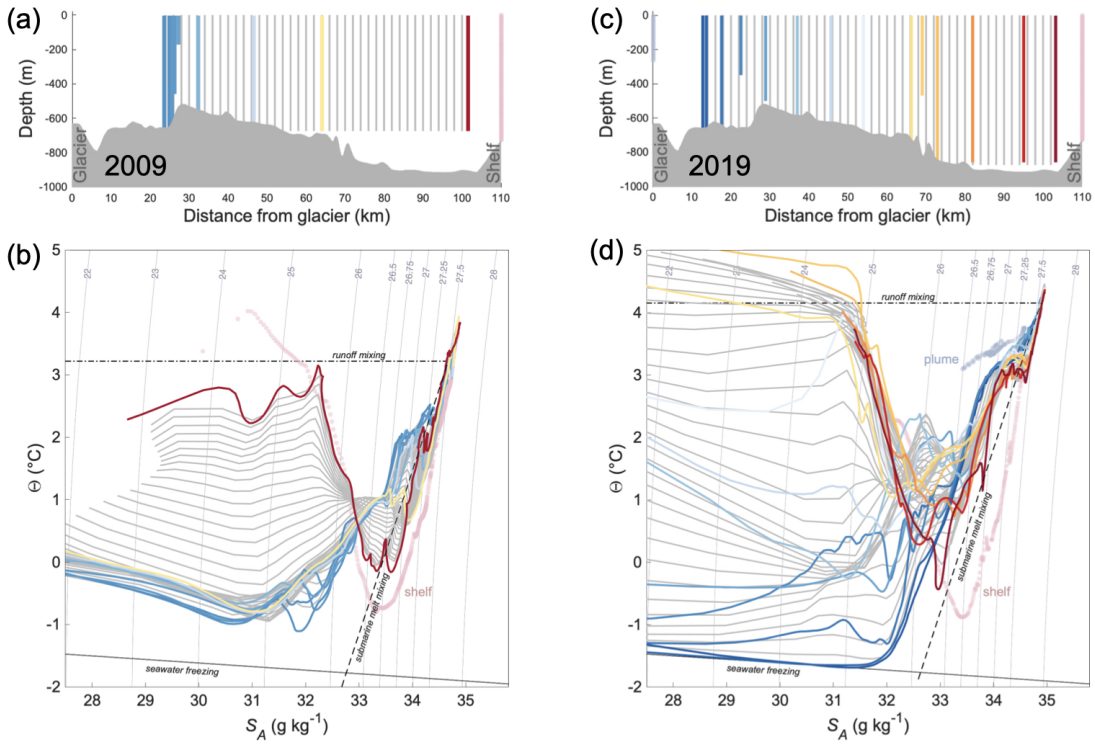


**Figure 1.7.** Comparisons of original profiles and gridded data for years 2009 (a, b) and 2019 (c, d) in Θ–$S_A$ diagrams (b, d). Panels (a) and (c) show the along–fjord location of the original profiles, colored by distance from the glacier, in comparison to location of the grid cells (grey lines). Θ–$S_A$ diagrams (b,d) show original profiles, colored by distance from the glacier in panels (a) and (c). Grey lines are the gridded data with every column in the grid plotted as an individual profile. Shelf profiles from both years are shown in light pink and two plume profiles from 2019 are shown in light blue. Mixing lines are plotted for submarine ice melt (dashed line) and melt runoff (dot–dash line) and the seawater freezing line is the black solid line. Grey contours are potential density anomaly isopycnals in kg m$^{-3}$.

Typical of Greenland glacial fjords, the climatology shows salinity is the dominant driver of stratification. The basic salinity structure is consistent throughout the fjord, with a maximum salinity of 34.95 g kg$^{-1}$ below 400 m, gradually freshening toward 34.40 g kg$^{-1}$ at 200 m depth (Fig. 1.8b). The halocline steepens in the upper 200 m, with the surface layer having the sharpest vertical salinity gradients over the entire along–fjord extent.

Below 400 m, temperature is also relatively uniform along the length of the fjord (Fig. 1.8a). The mean properties of this layer (3.81 ± 0.15 °C, 34.89 ± 0.04 g kg$^{-1}$, potential density anomaly $\sigma_0$ ¿ 27.5 kg m$^{-3}$) are consistent with established characteristics of inflowing AW

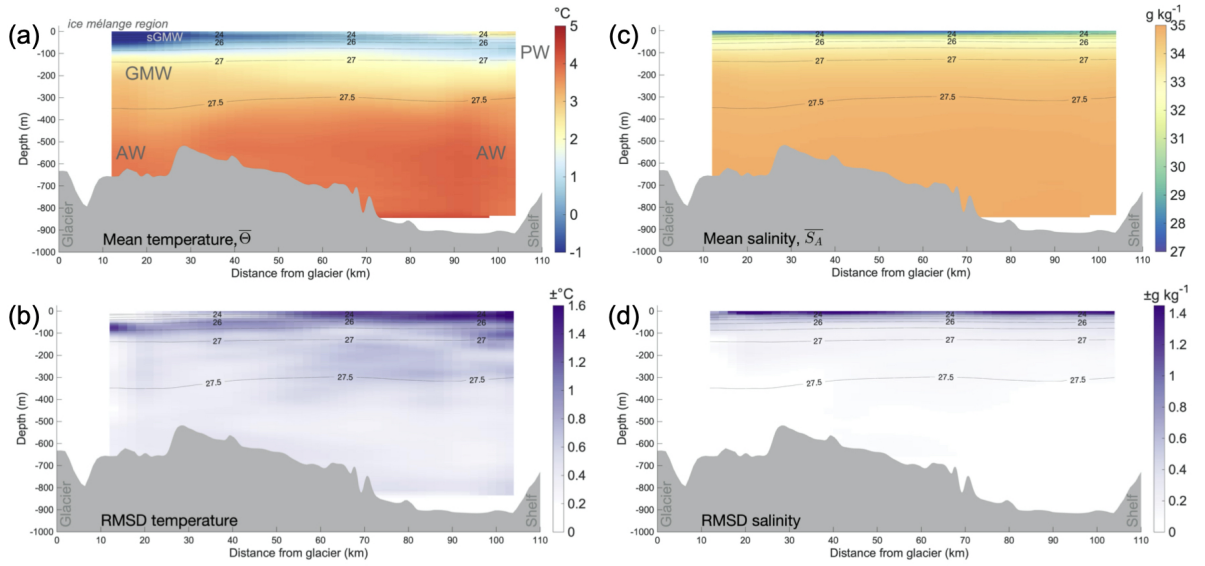


**Figure 1.8.** Gridded 13 year mean summer state climatology of conservative temperature (a) and absolute salinity (b) for Sermilik Fjord derived from hydrographic observations between 2009 to 2023. Associated RMSD about the mean for conservative temperature (c) and absolute salinity (d) show an estimate of spread of values in time at every grid cell. The $\sigma_0$ = 24, 26, 27 and 27.5 kg m$^{-3}$ potential density anomaly isopycnals are represented by grey contours in every panel and water masses discussed in the text (Atlantic Water (AW), glacially modified water (GMW), Polar Water (PW), and surface GMW (sGMW)) are labeled in panel (a).

from the continental shelf (Straneo et al., 2011; Jackson and Straneo, 2016; Beaird et al., 2018; Lindeman et al., 2024).

Above 400 m, we see more spatial variability in temperature indicative of different water masses and ice–ocean processes. To identify characteristics of along–fjord variability above 400 m, we have separated the fjord into three regions based on the water mass properties and established process understanding. We proceed by first describing water properties at the mouth region where we expect the fjord to be influenced by exchanges with the shelf. Second, we describe the near glacier region and address the glacial forcing on water properties, and finally we describe the mid–fjord region which shows gradients between the mouth and near glacier water properties.

**Fjord mouth properties**

At the fjord mouth (averaged over 94 km–104 km from the glacier), we see a mean temperature structure similar to the established, typical summer properties on the continental shelf nearby. A thermocline centered on the 27 kg $m^{-3}$ isopycnal separates a subsurface temperature minimum from the underlying warm AW. The AW properties at the mouth vertically averaged between 400–700 m are 3.85 ± 0.13 °C and 34.88 ± 0.04 g $kg^{-1}$.

In the upper water column, there is a subsurface temperature minimum (50 m–100 m, $\sigma_0$ = 26.5 kg $m^{-3}$) below a near–surface warm layer. This subsurface temperature minimum is at a similar depth and density to the cold, unmodified PW layer typically observed on the shelf (**?**). However, the fjord mouth subsurface temperature minimum is 1 °C warmer than the established properties of unmodified shelf PW (¡ 0 ºC).

To better interpret the properties at the fjord mouth, we identified unmodified PW properties from shelf profiles included in this dataset. Shelf profiles were collected during each survey, but are not included in the creation of the gridded data for the fjord. We created a single representative shelf profile for each survey by taking the temperature minimum of each isopycnal band across all East section shelf profiles, which sample the inflowing shelf waters, for a given survey (Fig. 1.7). We then calculated a mean profile from all representative East section shelf profiles from each survey. The subsurface temperature minimum of the mean profile indicates the coldest unmodified PW present on the shelf, on average, across all surveys from 2009–2023 and is comparable to the fjord summer climatology properties (Fig. 1.9). The mean East shelf coldest PW properties are -1.22 ± 0.35 °C and 33.17 ± 0.25 g $kg^{-1}$, occurring at a mean depth of 77 m and ranging from 50–115 m depth. These properties agree with previous observations of unmodified PW on the shelf outside of Sermilik Fjord (Sutherland and Pickart, 2008; Harden et al., 2014). However, the properties we calculated here are representative of more surveys allowing for improved understanding of the stability and variability of PW properties, and their influence on fjord properties. From this brief analysis, we can conclude that, on average, the

temperature minimum at the fjord mouth in the 50–100 m layer represents a mixture of PW and fjord-origin GMW that is nearly 1.5 °C warmer than unmodified shelf PW.

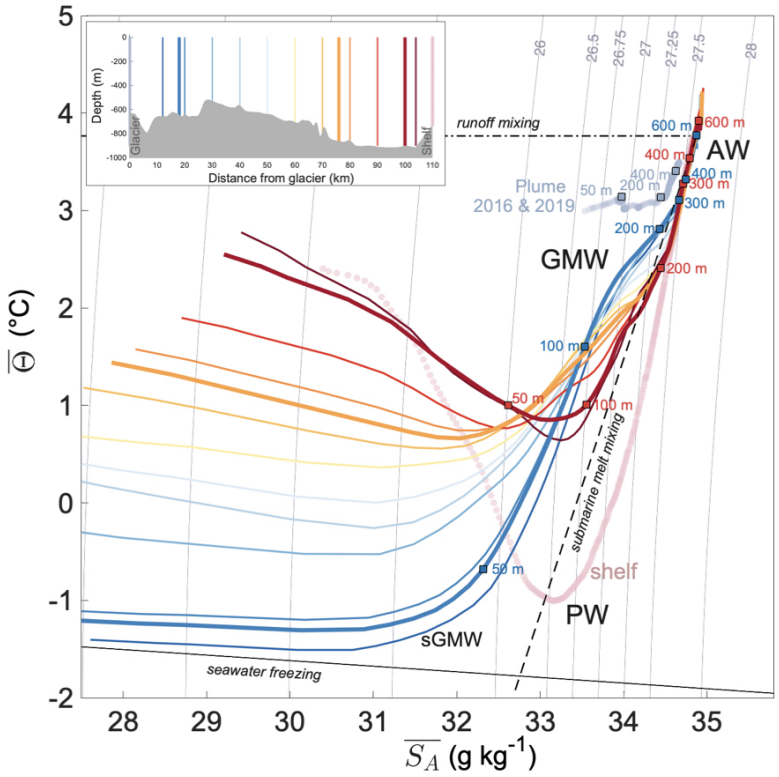


**Figure 1.9.** Conservative Temperature–Absolute Salinity ($\Theta$–$S_A$) diagram of the gridded summer state climatology for Sermilik Fjord. Grid cells every 10 km in the along–fjord direction are plotted, with cool to warm colors representing increasing distance from the glacier terminus. Bold lines are representative of the three regions (mouth, mid–fjord, and near glacier) discussed in text and referred to in Figs. 1.10 and 1.11. The mean representative shelf profile is plotted in faded pink dots. The average of profiles from the subglacial discharge plume polyna in 2016 and 2019 are faded blue dots. Mixing lines are plotted for submarine ice melt (dashed line) and melt runoff (dot–dash line) and the seawater freezing line is the black solid line. Grey contours are potential density anomaly isopycnals. Water masses discussed in text (Atlantic Water (AW), glacially modified water (GMW), Polar Water (PW), and surface GMW (sGMW)) are labeled.

### Near glacier properties

In the near glacier ice mélange region (horizontally averaged between 12 km–22 km from the glacier), the climatological mean AW properties vertically averaged between 400–700

m are 3.59 ± 0.17 °C and 34.84 ± 0.05 g kg$^{-1}$, within one standard deviation of the properties at the mouth.

Above the AW layer, the near glacier region has a positive temperature anomaly when compared to the mouth (between 75–300 m) and shelf (between 55–300 m), calculated by subtracting along isopycnals. The temperature anomaly and features of the near glacier profiles in $\Theta$–$S_A$ space (Fig. 1.9) are characteristic of GMW (Straneo et al., 2011; Muilwijk et al., 2022). Building on previous work, we can identify the fingerprints of different freshwater sources and determine their relative importance for setting the GMW water properties throughout the fjord.

We use the mixing lines displayed on the $\Theta$–$S_A$ plot to differentiate between SGD, surface runoff, or SMW influence (Fig. 1.9). The runoff mixing line shown represents the expected water properties for the mixing of averaged unmodified AW at 550 m and SGD (with assumed properties of 0 °C and 0 g kg$^{-1}$). The SMW mixing line, or Gade line, represents the combined influence of latent heat uptake and mixing with meltwater (Gade, 1979). The two XCTD profiles collected directly in the plume at the glacier terminus from 2016 and 2019 strongly parallel the runoff mixing line slope. Between 165–300 m (27.22 kg m$^{-3}$ $< \sigma_0 <$ 27.49 kg m$^{-3}$), the slope of the near glacier profiles (20 km from the glacier terminus; dark blue profiles in Fig. 1.9) deviate in the composite direction of the runoff mixing line and submarine melt line. This is consistent with a mixture of plume waters and SMW from the ice mélange. The inflection of the slope at depths shallower than 165 m ($\sigma_0 <$ 27 kg m$^{-3}$) suggests that this is the upper limit of SGD, which can be used as an estimate of the climatological average neutral buoyancy depth range of plume waters in this region of the fjord.

Between 50 m and 165 m (26.0 kg m$^{-3}$ $< \sigma_0 <$ 27.22 kg m$^{-3}$), the slopes of the near glacier profiles directly parallel the submarine melt mixing line, indicating the addition of SMW from the ice mélange as a primary driver of water properties at these depths. Above 50 m, the $\Theta$–$S_A$ properties converge toward the local freezing temperature as the near surface waters are both cooled by SMW and freshened by surface runoff. The surface water properties nearest to the glacier (12 km) are the coldest in the entire domain, with a minimum temperature of -1.49 °C

at 15 m depth. This cold pool is characteristic of the ice mélange region, which extends 30 km into the fjord. This also leads to the near glacier region showing the strongest thermocline (Fig. 1.10b-d) and, consequently, the strongest surface stratification of all the regions (Fig. 1.11b-d). Following Lindeman et al. (2024), we identify this as sGMW occurring at less than 50 m depth where $\sigma_0 < 26$ kg m$^{-3}$.

**Mid–fjord properties**

Considering the characteristics of the mid–fjord region (40–90 km from the glacier) in $\Theta$–$S_A$ space reveals that the water properties are a progressive mixture between the two endmembers of the mouth and near glacier profiles (Fig. 1.9). We assume along–isopycnal mixing is occurring in the upper 400 m of the mid–fjord region ($\sigma_0 < 27.5$ g kg$^{-1}$) where GMW is being exported down the fjord and meeting waters of the same density coming into the fjord from the shelf. Above 50 m, the surface waters are warmer than the sGMW found in the mélange, with minimum temperatures above 0 ºC.

The AW properties in the mid–fjord are similar to those at the mouth. The mid–fjord AW properties vertically averaged between 400–700 m and horizontally averaged between 60–70 km are 3.83 ± 0.05 °C and 34.90 ± 0.02 g kg$^{-1}$.

The middle of the fjord is at 60 km in the along–fjord distance coordinate axis. However, the map view of the fjord geometry is defined by a constriction at 75 km (at 65.60 ºN in Fig. 1.1) which influences the exchange of waters between the fjord mouth and upper fjord. Previous studies have described mooring records at this location (Jackson et al., 2014; Jackson and Straneo, 2016; Snow et al., 2023). To easily compare the findings of this study with the moored data, we define "mid–fjord" as 76 km. As Figs. 1.8 and 1.9 show, the water properties are similar between 60 km and 76 km from the glacier.

### 1.5.3 Variability of gridded data

While the climatology shows the average summer hydrography, there is yearly variability and unique hydrographic patterns represented in the individual survey grids which are important to consider (see Supplement to view all yearly grids). The temporal RMSD of the properties climatology grids (Fig. 1.8c-d) provide an initial sense of the year–to–year variability in different regions of the fjord. Below 400 m, in the largely unmodified AW layer for the whole along–fjord domain, we see consistent RMSD values. The spatial average of the RMSD between 400–700 m and horizontally from 12–104 km are ±0.39 °C and ±0.06 g $kg^{-1}$.

The year–to–year variability above 400 m is relatively greater, with maximum RMSD values of both temperature and salinity occurring at the surface. While salinity RMSD vertical structure is similar between the fjord mouth to the near glacier region, the temperature RMSD vertical structure varies along the fjord above 400 m and most prominently in the surface layers.

**Fjord mouth variability**

The mouth region shows the most variability from year to year in temperature properties (Fig. 1.8b). We speculate this is due to shelf processes, occurring on multiple timescales from seasonal to daily, influencing the properties measured at the mouth during a given field campaign (Jackson and Straneo, 2016; Jackson et al., 2018). While we showed that, on average, the fjord mouth temperature minimum is warmer than unmodified shelf PW, the 2015 and 2017 surveys have properties at the mouth that are equivalent to the unmodified shelf PW for those surveys. In other years (2010, 2018, 2019, 2020), more representative of the average, shelf PW properties are not present in the fjord and the fjord mouth temperatures are much warmer than shelf PW. Many of the mouth profiles show characteristic interleaving patterns above 200 m, where shelf and fjord GMW waters of similar density are meeting and mixing. Note that the average mouth profile is less smooth compared to the average near glacier profile due to multiple intrusions with sharp thermoclines at various depths being averaged together. This also impacts the stratification, which shows the largest range of yearly values between 50–200 m at the mouth (Fig. 1.11).

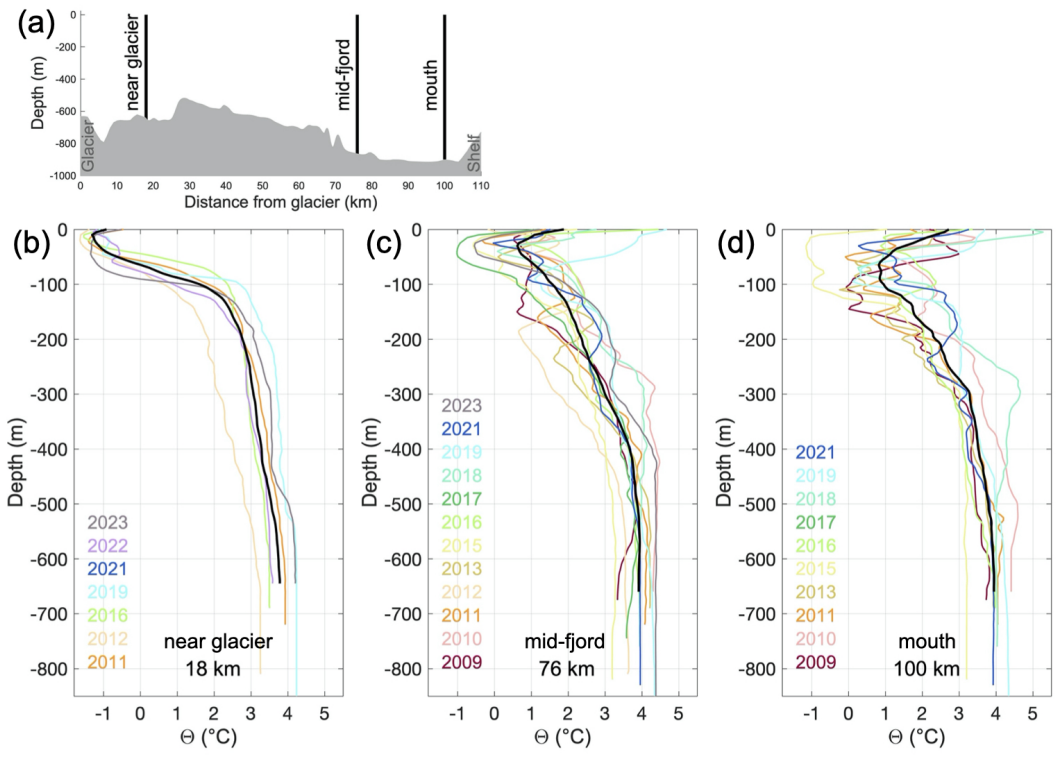


**Figure 1.10.** Conservative temperature profiles from all the yearly grids at locations shown in (a): the near glacier (b), mid–fjord (c), and mouth regions (d). Colored lines represent individual years and the bold black line is the time mean climatology profile.

### Near glacier variability

In the near glacier region, the upper 50 m has the smallest temperature RMSD of the fjord domain. This highlights the consistency of the ice mélange in setting the temperature properties in this area. From 50–100 m, there is an increase in the temperature RMSD (maximum ± 1.09 °C) as the thermocline is more variable– likely in response to variability in GMW extent in the water column and properties. Below the thermocline, the average RMSD of the GMW layer properties between 165–300 m are ±0.51 °C and ±0.14 g $kg^{-1}$. As previous studies have noted, the properties of this GMW layer vary with the unmodified AW properties at depth near the glacier as these are the waters being upwelled (Muilwijk et al., 2022). When AW near the glacier is cooler (warmer) than average for a given year, the GMW properties resulting from upwelling in the SGD plume are cooler (warmer) than average.

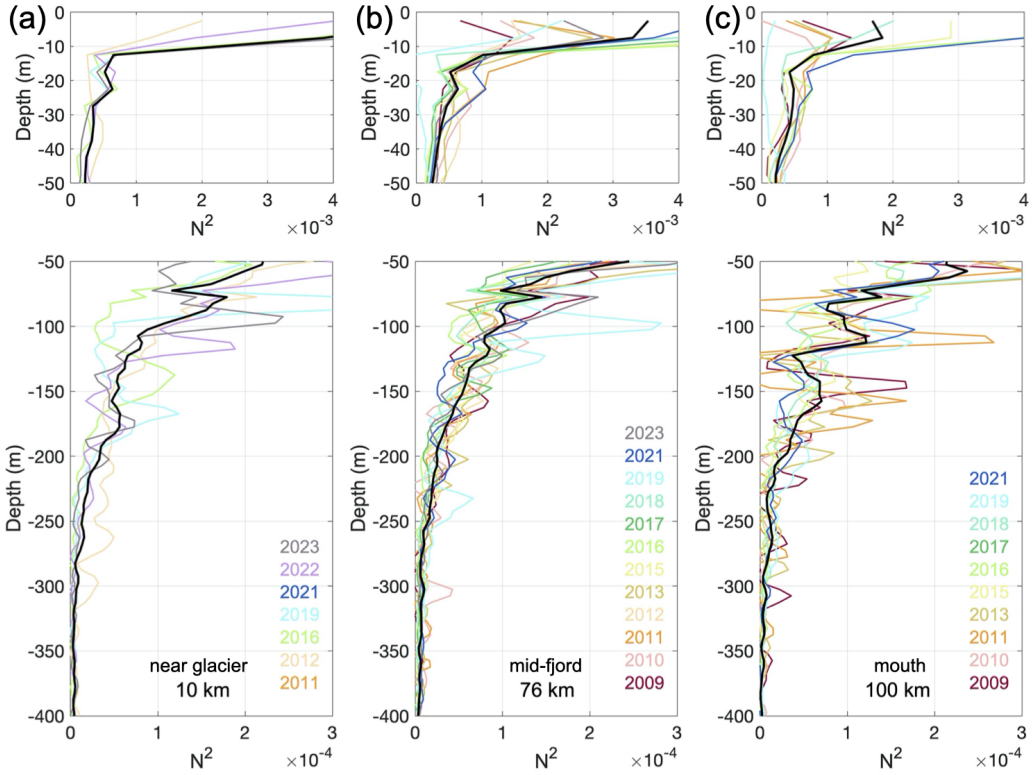


**Figure 1.11.** $N^2$ (Brunt–Vaisala frequency), a measure of stratification, from the near glacier (a), mid–fjord (b), and mouth (c) regions for all yearly gridded data. The profiles are from the same locations as in Figure 10. The upper panels have a different vertical scale to emphasize the surface. The horizontal scale in the upper panels is an order of magnitude larger than the lower panels. $N^2$ was calculated from conservative temperature and absolute salinity gridded data using the TEOS–10 Oceanographic Toolbox (McDougall and Barker, 2011). Black bold lines represent the mean $N^2$ profile for all years in each region.

### Mid–fjord variability

Profiles from the mid–fjord region for each survey show similarly variable interleaving and intrusion features as the mouth profiles, though the mid–fjord intrusions are less sharp overall. Some years, properties in the mid–fjord region are more similar to an average near glacier profile (2015, 2017, 2023) with $< 0$ °C temperatures in the upper 50 m and exhibiting a strong thermocline between 50–100 m and relatively weak intrusions. Other years are more similar to a mouth profile (2011, 2012, 2021) with warmer surface waters and multiple stronger intrusions. The along–fjord location of the transition between near glacier properties and mouth

properties varies from year to year. This variability is not captured in the time mean mid–fjord profile and climatology of the mid–fjord region.

**Yearly anomalies from the mean**

To further investigate the temporal variability, we subtracted the climatology from each summer grid to produce the temperature and salinity anomaly for each grid (selected years shown in Fig. 1.12). The temperature anomaly fields show summers where nearly the entire fjord domain is warmer (e.g. 2019) or colder (e.g. 2015) than average. 2021 is the year with the smallest average anomaly across the whole domain, however, there are still areas in the domain that are warmer and colder than the summer average.

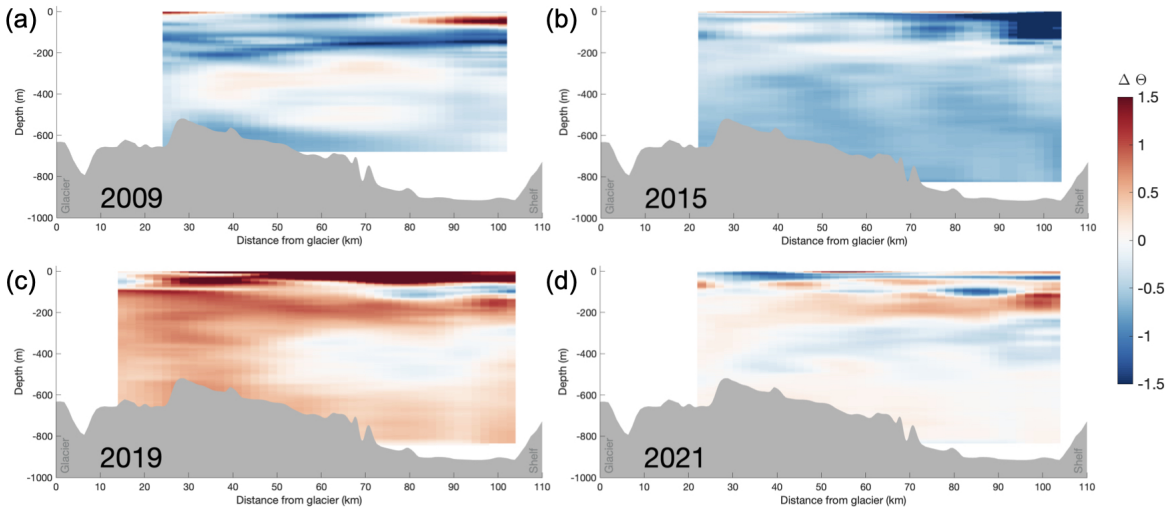


**Figure 1.12.** Conservative temperature anomalies from the climatological mean for yearly grids 2009 (a), 2015 (b), 2019 (c), and 2021 (d). Cooler (warmer) colors show values less (greater) than the mean for each grid cell.

The pattern in the gridded anomaly field can be both due to variability in the properties and variability in the depth of the thermocline. For example, the properties of the temperature minimum at the mouth could match the mean temperature minimum properties, but if the thermocline is at a different depth the anomaly will be nonzero.

## 1.6 Discussion

### 1.6.1 Summary of results facilitated by gridded sections

The method presented here, and the creation of gridded sections from discrete, irregular profiles, enables novel insights and quantification of water properties in Sermilik Fjord. Most notably, the summer climatology product, along with complementary information on the range and patterns of variability, is only possible with regularly gridded sections and could not have been constructed from the original profiles alone. The same is true for the calculation of the anomalies relative to the climatological state, which allow direct interannual comparisons against a mean field. For example, our analysis shows that 2015 was an anomalously cold year in the fjord, suggesting that conclusions from previous studies based solely on 2015 data should be interpreted with caution.

Beyond climatology and anomalies, the gridded sections also reveal coherent fjord-scale property structures that are less evident in scattered profile data. For instance, variability in Atlantic Water along the fjord is more readily discerned in the gridded fields than in the raw profiles. The gridded format also enables straightforward calculation of spatially averaged water properties in different parts of the fjord, both for individual surveys and for the summer climatology. These mean properties, presented in the Results, are robust quantities that can be directly used in modeling and comparative studies. Together, these examples demonstrate that the gridded sections are not just improving the accessibility of the data, but also the interpretive power, producing results that would not otherwise be attainable.

Hydrographic data from fjords are relevant to a wide range of users— from climate and earth scientists interested in ice–ocean interactions to local communities that depend on the ecosystem. Our aim is to make this dataset both usable and useful across disciplines. In the following sections, we identify several important considerations regarding the use of these gridded data and the original profile observations.

### 1.6.2 Daily to interannual variability

While all the data are from the summer season (July–September), each along–fjord section is a snapshot capturing the combined influence of processes occurring on a range of timescales (days, months, years). Single wind events within the fjord and the adjacent shelf can influence fjord exchange and hydrographic properties over a timescale of days (Jackson and Straneo, 2016). Integrating data collected before and after a single wind event during one survey can be challenging and creates discontinuities in the domain. Some profiles were not used in the construction of each along–fjord section because of these discontinuities.

All data and gridded products should also be interpreted within the context of the seasonal runoff cycle relative to the timing of data collection. Fjord properties change dramatically over the course of the surface melt season, with subglacial discharge input typically beginning in June and reaching its peak in August. Earlier studies have shown a progressive acceleration of fjord circulation, and associated modification of fjord properties, as a result of this seasonal forcing (Sanchez et al., 2023). For 2023, we did not combine the XCTD (collected on July 12) and CTD (collected August 9–16) surveys because the fjord properties had evolved significantly in the time between surveys. These data are treated as two different along–fjord sections. Because this data set incorporates sections collected at different points in the summer season (Fig. 1.3), the temporal variability reflects both interannual variability and the intraseasonal development of fjord conditions over the discharge period. Additionally, the high variability in properties directly at the surface (Fig. 1.8b, d) can be attributed to the variation of solar radiation forcing and terrestrial surface runoff (as opposed to subglacial discharge) at the seasonal timescale.

Variable regional atmospheric and ocean conditions occurring on larger spatial scales and longer time scales must also be considered. For example, in 2015, there was significant sea ice within the fjord and on the shelf during the summer survey, indicative of a prolonged winter. This is supported by findings that 2015 had an anonymously cold and long winter associated with a positive state of the North Atlantic Oscillation in Southeast Greenland and the Irminger Sea

(de Jong and de Steur, 2016). Making any conclusions about interannual variability from this dataset must be done within the context of understanding the combined effect of these multiscale forcings on hydrographic patterns of each year. This will be the subject of future studies, and we are careful not to attribute hydrographic patterns discussed here to particular forcings as this requires further analysis outside the scope of this work.

### 1.6.3 Water mass definitions and comparison to previous work

The average summer water mass properties calculated here are consistent with previously reported definitions of summer AW, PW, and GMW in Sermilik Fjord from CTD, XCTD, and moored observations (Straneo et al., 2011; Jackson and Straneo, 2016; Beaird et al., 2018; Sanchez et al., 2021; Lindeman et al., 2024). Notably, CTD data from 2009 (Straneo et al., 2011), 2015 (Beaird et al., 2018), and 2021 (Lindeman et al., 2024) were used in previous studies to identify the properties and depth range of GMW in these individual years. Reinterpreting the conclusions of these previous results within the context of the climatological mean and long term dataset is now possible. For example, Beaird et al. (2018) relied on the 2015 CTD survey. We now know that this is a year when nearly the entire fjord domain was 1 °C colder than the 13 year climatological temperature mean (Fig. 1.12b).

How water mass properties are defined and averaged has varied between studies based on particular applications. Different isopycnal ranges, depths, and/or horizontal extents are used to average and report water properties. The availability and format of the gridded sections allows a user to calculate any quantity they may need for a specific spatial extent or particular years based on the research question of interest. The gridded sections can also be combined with previously reported velocity data if a user wishes to calculate transport weighted means (Jackson and Straneo, 2016; Beaird et al., 2018).

### 1.6.4 Gridded products facilitate model use and comparison

Robust climatological means and consistently gridded surveys provide quantitative means for forcing or validating models. This is preferred over the use of single surveys or ad hoc choices made by earlier studies which used temperature and salinity profiles from Sermilik Fjord as initial conditions of idealized two–layer fjord models, boundary conditions and validation data for more complex numerical models, and ocean conditions for iceberg melt models and plume models (Sciascia et al., 2013; Moon et al., 2018; Davison et al., 2022; Schild et al., 2021; Sanchez et al., 2024). The gridded products presented here now make it easier to find average conditions for different fjord regions depending on the research question, model initialization, and time period of interest.

While we have not included the plume polynya profiles in the gridded products, the individual profiles are available in the original data and these can be useful in studies employing plume models. Similarly, the shelf profiles were not included in the gridded data presented here as the shelf environment dominated by different dynamics, but the individual profiles are available for use and provide important context for interpreting fjord water properties. We chose to create an average East section shelf profile to aid in the interpretation of properties at the fjord mouth. A more rigorous analysis of shelf water mass properties and the creation of a shelf summer climatology is possible with this dataset and will be considered in future work.

## 1.7 Conclusions

The dataset and gridded products presented in this study provide a crucial step toward standardizing and centralizing long–term fjord observations in Greenland. By compiling 13 years of hydrographic data from Sermilik Fjord, we offer a comprehensive and accessible resource for studying fjord dynamics and ice–ocean interactions. The combined CTD and XCTD observations lead to greater spatial coverage of the fjord, including the mélange region for multiple years and the subglacial discharge plume polyna region for two years. The objective mapping method

enabled necessary and novel analyses that are not possible from the raw profiles alone, including the construction of an along-fjord summer climatology, quantification of interannual anomalies, and identification of water property features. Importantly, these results provide context for interpreting previous work in Sermilik Fjord. We demonstrated how other quantities (eg. $N^2$) and water properties of specific regions can easily be calculated from the gridded sections depending on questions of interest. Finally, the method used to generate gridded sections is adaptable for different variables and fjord settings and can facilitate interdisciplinary research– enabling comparisons with models, biological data, and other observations.

This work highlights the need for a coordinated approach to fjord data collection and sharing. Establishing a structured, FAIR–compliant data repository for Greenland fjords will improve the accessibility and utility of these critical datasets, ultimately enhancing our understanding of glacial fjord systems and strengthening collaboration within the international science community and with Greenlandic partners.

## 1.8 Code and data availability

The gridded data products for each individual year and the climatology are available at the Arctic Data Center (https://doi.org/10.18739/A2513TZ0P, Roth et al. 2025b) as netCDF files. The files contain gridded section of $\Theta$ and $S_A$, as well as their respective mapping relative error matrices, for every summer survey. Derived variables, like potential density or $N^2$, can be calculated by the user. The thalweg along–fjord gridded coordinates in distance (km) from the 2019 Helheim Glacier terminus position and in latitude and longitude coordinates are included in the files.

The original CTD and XCTD profiles from every year of sampling are all available at the Arctic Data Center as netCDF files (https://arcticdata.io/catalog/portals/sermilik/Data, last access: 7 November 2025). Individual entries and DOIs have been created for each field campaign. All files include in situ temperature and practical salinity. Some years have additional

variables from the CTD rosette, such as dissolved oxygen and turbidity. All files include latitude and longitude coordinates of every profile and standardized depth levels (meters). As more hydrographic surveys are conducted in Sermilik Fjord, we plan for the data to be archived in this format and available at the Arctic Data Center in the Sermilik Hydrography Data Portal (Straneo et al., 2025).

The code developed to create gridded along–fjord sections is available at https://zenodo.org/records/17563180 (last access: 7 November 2025). While this code is set up for Sermilik Fjord profiles, it can easily be adapted to other regions with discrete profiles that have been compiled into along–fjord sections. The parameters of the objective mapping method can be manually adjusted for different length scales and error input. Ancillary code for plotting and deriving other variables is also available (Roth et al., 2025c).

## 1.9 Acknowledgments

Chapter 1, in full, is a paper from Aurora Roth, Fiamma Straneo, James Holte, Margaret Lindeman, and Matthew Mazloff "A dataset for multidisciplinary applications: thirteen years of ocean observations in Sermilik Fjord, Southeast Greenland" published in Earth System Science Data, Volume 17, Issue 11, 6025–6048, 2025. The dissertation author is the primary investigator and author of this paper.

The authors thank the many crew members, scientists, technicians, and logistics staff who have supported data collection efforts since 2008. These data would not exist if it were not for the knowledge and skill of the ships' crewmembers, most of them Greenlandic, including those of the M/Vs Viking, Adolf Jensen and R/V Tarajoq. The XCTD data were collected thanks to the patience and expertise of the many helicopter pilots, mostly from Air Greenland. FS acknowledges the essential role played by the late Gordon Hamilton in motivating and initiating the collection of these data. We acknowledge the many scientists who contributed to this data collection. In particular, we acknowledge the contributions of D. Sutherland, R. Jackson, N.

Beaird, M. Andres, D. Slater, L. Stearns, A. Lewinter, D. Finnegan and the late G. Hamilton. Invaluable technical support was provided by A. Ramsey, J. Ryder, W. Ostrom, M. Donahue and J. Kemp's entire group. Finally, we thank two anonymous reviewers for their time and contributions to improving the manuscript.

Successfully accomplishing and funding this work has required coordination and collaboration with multiple research groups across disciplines as we seek to answer increasingly complex and socially relevant questions. Maintaining positive collaboration with other research groups, Greenland–based scientists, logistics personnel, research vessels, and local people has been essential to ensuring observations are funded and conducted year after year.

# Chapter 2

# Water mass fraction methods in Greenland's glacial fjords with a case study in Sermilik Fjord, Southeast Greenland

## 2.1 Introduction

The fjords of Kalaallit Nunaat (Greenland) are connectors between the Greenland Ice Sheet (GrIS) and the ocean. Ocean water masses on the surrounding continental shelf flow into fjords, transporting heat that drives submarine melting of icebergs and glacier termini (Straneo et al., 2010, 2012; Straneo and Heimbach, 2013). Meltwater, both submarine melt and surface runoff, is mixed with oceanic waters within fjords before being exported to the regional ocean (Beaird et al., 2015, 2018; Mortensen et al., 2020). A set of interacting fjord processes controls glacier melt rates, freshwater export of the GrIS to the ocean, nutrient and sediment dynamics, and upwelling at glacier fronts, with impacts ranging from global sea level rise and ocean circulation to the sustainability of local marine ecosystems that Greenlanders depend on (Straneo et al., 2019, 2022; Heide-Jørgensen et al., 2023; Rathcke et al., 2025).

Despite their importance, the inclusion of relevant ice-ocean interactions and fjord processes within both fjord-scale and global-scale models is lacking. While there are increasingly more observations available from Greenland fjords, these data are still often spatially and temporally limited due to the challenging environment, and many key processes, including

subglacial discharge plumes and submarine melting, are difficult to observe directly, thus further limiting the improvement of parameterizations (Straneo et al., 2019; Slater and Straneo, 2022; Morrison, 2022). In regional and global ocean models, fjords are typically unresolved, and freshwater input from the GrIS is commonly represented as a temporally invariant surface flux (Vries et al., 2025). This treatment contrasts with observations showing that freshwater in Greenland fjords is distributed throughout the water column, often extending to depths of order 200 m (Straneo et al., 2012; Mortensen et al., 2013; Beaird et al., 2018; Moon et al., 2018; Rysgaard et al., 2024).

Even fjord-scale models rely on a hierarchy of various parameterizations to represent key processes, and they are often constrained by a limited number of observations. Directly at the ice-ocean interface at the glacier margin, plume models—which parameterize mixing driven by subglacial discharge—are widely used to estimate entrainment, neutral buoyancy depths, melt rates, and nutrient upwelling (Slater et al., 2016; Mankoff et al., 2016; Slater and Straneo, 2022; Oliver et al., 2023). These models offer valuable insight into near-terminus dynamics, but are inherently local in scope and do not represent the subsequent redistribution and transformation of freshwater throughout the fjord (Muilwijk et al., 2022). Reduced-physics fjord models, including box and layer-averaged frameworks, extend beyond the ice front to capture first-order fjord circulation, stratification, and exchange with the continental shelf, but typically rely on simplified or tuned parameterizations of plume processes, melt rates, and mixing (Sanchez et al., 2023; Slater et al., 2025a). More complex three-dimensional numerical models resolve a greater range of dynamics, but still depend on parameterizations for key processes, and observations for model forcing and validation can be scarce (Hughes, 2022; Sanchez et al., 2024; Kinne et al., 2025). Consequently, agreement between modeled and observed water properties does not guarantee that the relative contributions of different freshwater sources or the pathways by which shelf waters are mixed within fjords are correctly represented.

Water mass fraction analyses of glacial fjord observations, where the fractions of oceanic versus glacially-derived water masses are estimated, have been an important tool for clarifying

the relative importance and distinct effects of fjord processes and their resulting influence on fjord hydrography. These quantitative fractions present a possible approach for improving model parameterizations and bridging the gap in scales between fjord-processes and larger-scale ocean models. In Greenland glacial fjords, such analyses have been used to 1) infer the depth-dependent distribution and export of freshwater from fjords (Mortensen et al., 2013; Beaird et al., 2018; Rysgaard et al., 2024), 2) diagnose the influence of subglacial discharge plumes on entrainment of deep, warm Atlantic Water, providing observational constraints that directly inform plume and melt parameterizations (Mankoff et al., 2016; Beaird et al., 2018; Muilwijk et al., 2022; Cowton et al., 2023) and 3) describe relative roles of subglacial discharge versus submarine melt on fjord water properties (Washam et al., 2019; Mortensen et al., 2020). Finally, when applied using nutrient, dissolved oxygen (DO), stable isotope, or other tracer observations, water mass fraction analyses can enable a deeper understanding of biogeochemical pathways and ecosystem impacts associated with glacial freshwater input (Kanna et al., 2018; Cape et al., 2019; Lindeman et al., 2024). Similar water mass fraction analyses have also been conducted in Svalbard glacial fjords, Antarctic ice shelf cavities, and in the regional oceans surrounding Antarctica and Greenland (Jenkins and Jacobs, 2008; Jenkins, 2011; Randall-Goodwin et al., 2015; Biddle et al., 2017; Rhein et al., 2018; Kim et al., 2025a; Lanham et al., 2025).

Although commonly applied, methods for calculating water mass fractions in glacial fjords can vary, falling largely into one of two distinct categories. One is a conservation-based approach, originally developed for Antarctic ice-shelf cavities to infer meltwater fractions from heat, salt, and mass balances (Jenkins, 1999). This was later extended into a ”composite tracer” approach (Jenkins and Jacobs, 2008). The other is optimum multiparameter analysis (OMPA), adapted from open ocean water mass studies and extended to ice–ocean systems through the use of multiple conservative and quasi-conservative tracers (Tomczak and Large, 1989). While these two approaches differ in complexity and observational requirements, they are based on the same underlying linear mixing and conservation equations. Additionally, important assumptions adopted in each individual application of water mass fraction analysis can vary

greatly, complicating the intercomparison of results, and the formal quantification of uncertainty and error is often neglected.

Here, we use a more unifying and exact method, originally introduced in Wunsch (1978) and formalized in Wunsch (2006), in which both the conservation methods and OMPA emerge as special cases under specific assumptions. This approach can solve the underdetermined inverse problem that often results from using temperature and salinity observations alone through the incorporation of prior knowledge and appropriate weighting schemes and constraints. This method has most recently been applied to similar problems by Lanham et al. (2025), Shrikumar et al. (2021), and Lawrence et al. (2026), but we note that the general class of problems—underdetermined inverse problems—have a long lineage of applications in oceanography and earth science. We apply this method to hydrographic observations from Sermilik Fjord, Southeast Greenland (Roth et al., 2025a) and compare the results with previous water mass fraction analyses at this location derived from numerous noble gas observations (Beaird et al., 2018), and from DO observations (Lindeman et al., 2024). This leads to a more comprehensive assessment of what can, and cannot, be inferred from temperature and salinity observations alone. We suggest how others might proceed in applying these methods to different Greenland fjord systems, especially where temperature and salinity observations from eXpendable Conductivity Depth Temperature (XCTDs) have become more common.

As more water mass fraction studies are conducted in Greenland glacial fjords and around rapidly melting areas of Antarctica, intercomparison studies across different study sites and from different times are becoming possible. However, there is a need to provide an overview of the assumptions, constraints, and uncertainty calculations used in these methods and how resulting water mass fraction solutions and associated uncertainty are impacted by different approaches. In this study, we calculate water mass fractions using a spectrum of data types, assumptions and constraints and provide suggestions to the ice-ocean community for best practices. We introduce spatially varying penalty matrices, and show that these can provide appropriate constraints for heterogeneous Greenland fjord environments. This work can inform future data collection needs

and help us make use of existing datasets to calculate water mass fractions across different Greenland fjords.

## 2.2 Methods

### 2.2.1 Overview of Water Mass Fraction Methods in Ice-Ocean Environments

The concept of water mass fractions has been used in oceanography to study a variety of applications, from global ocean circulation to biogeochemical cycling (Tomczak and Large, 1989; Poole and Tomczak, 1999). Around Greenland and Antarctica, water mass fraction calculations have been used to determine the amount and extent of meltwater in the ocean and to explore the processes of meltwater mixing and dilution. While there are different methods, calculating water mass fractions is essentially an inverse problem that results in a "recipe" of relative fractions of source water types (SWTs), also called endmembers, defined by specific ocean properties, also referred to as tracers. When added together, the recipe of source water type fractions can reproduce, or nearly reproduce, observed ocean properties. Here we focus specifically on water mass fraction analyses in Greenland fjord environments, with previous studies summarized in Table 2.1. However, this work raises relevant and important considerations that also apply to research questions in Antarctica and other glacial fjord regions (eg. Svalbard, Alaska).

**Table 2.1.** Summary of previous water mass fraction estimates from Greenland glacial fjords or fjord entrances. Abbreviations: OMPM = Optimum Multiparameter Multi-Year Analysis, CE = algebraic conservation equations used, MC = Monte Carlo simulation used for uncertainty

| Study/Location | Study Goal | Method | Dim. | Tracers | SWTs | Weighting Scheme | Uncertainty/Trust Metric |
|---|---|---|---|---|---|---|---|
| Mortensen et al. (2013, 2020); Nuup Kangerlua, SW Greenland | Quantify SMW and SGD* fractions; dilution of SGD* | CE | $m+1=n$ | T, S | SGD*, SMW, ambient water | None (equal) | None |
| Beaird et al. (2015); Kangilerngata Sermia and Eqip Sermia, Disko Bay; Beaird et al. (2018); Sermilik Fjord, SE Greenland; | Export and spreading of meltwater | OMPA | $m+1>n$ | T, S, $^3$He, He, Ne, Ar, Kr, Xe | AW, PW, SMW, SGD, WPW, AIM | SWT variance and measurement uncertainty | MC; residuals reported |
| Mankoff et al. (2016); Saqqarliup Sermia, W Greenland | Structure of a SGD plume; dilution, entrainment, submarine melt rate in plume | CE | $m+1=n$ | T, S | SGD, SMW, ambient water | None (equal) | None |
| Kanna et al. (2018, 2020); Bowdoin Fjord, NW Greenland | SGD plume-driven upwelling of macronutrients; iron and phytoplankton | CE | $m+1=n$ | S, $\delta O^{18}$ (2018); T, S (2020) | glacial runoff, snowmelt, PW (2018); SGD, SMW, ambient water (2020) | None (equal) | None |
| Cape et al. (2019); Sermilik Fjord, SE Greenland | Nutrient transport from SGD plume upwelling | OMPA | $m+1=n$ | T, S, $NO_3^-$, $Si(OH)_4$ | AW, PW, SGD, SMW, WPW | SWT variance and measurement uncertainty | Comparison to Beaird et al. (2018); % error of mass constraint |
| Washam et al. (2019); Petermann Fjord and ice shelf, NW Greenland | Ice shelf basal melt rates | CE | $m+1=n$ | T, S | AW, SGD, SMW | None (equal) | None |
| Ohashi et al. (2020); Bowdoin Fjord, NW Greenland | interannual SGD, plume dynamics, and stratification | CE | $m+1=n$ | T, S | SGD, SMW, ambient water | None (equal) | None |
| Muilwijk et al. (2022); Upernavik Isfjord, NW Greenland | Glacially modified water composition and export | OMPM | $m+1>n$ | T, S; multi-year | AW, PW, SMW, SGD | None (equal) | MC; residuals reported |
| Lindeman et al. (2024); Sermilik Fjord, SE Greenland | Mercury cycling/sources | OMPA | $m+1=n$ | T, S, DO | AW, PW, SMW, SGD | measurement uncertainty | None |
| Rysgaard et al. (2024); East Greenland shelf and fjord entrances | Spatial distribution of water masses and freshwater | OMPA | $m+1=n$ | T, S, $\delta O^{18}$ | AW, PW, meteoric water, glacial water | None | None |

In Greenland fjord environments, subglacial discharge and submarine melt are often defined as source water types, and the fractions of each are tracked in space and/or time. Previous studies show maximum submarine melt fractions ranging from 0.4–4% and maximum subglacial discharge fractions ranging from 1–12%, with patterns in depth and distance from the glacier, and differences between study sites and methods (Table 2.1). Water mass fraction methods can also be used to understand the structure of shelf water masses at fjord entrances, namely warm deep Atlantic Water and cold, subsurface Polar Water, and their role in fjord processes, stratification, and freshwater export (Beaird et al., 2015, 2018; Rysgaard et al., 2024).

Quantitative estimates of water mass fractions in ice–ocean environments have developed along two largely independent but mathematically related lines. One strand originates in work by Jenkins who formulated meltwater fraction calculations for Antarctic ice-shelf cavities using the conservation of heat, salt, and mass to infer submarine melting and ice–ocean exchange (Jenkins, 1999). This was later presented as the ”composite tracer” method, which uses a normalized scalar to quantify meltwater fractions, but still starts with the same conservation equations (Jenkins and Jacobs, 2008). These conservation-based methods were later adapted to Greenland settings, including applications by Washam et al. (2019) to Petermann Ice Shelf and fjord and by Mortensen et al. (2013, 2020) to Nuup Kangerlua, where similar mass and property balances are used to quantify freshwater inputs and their transformation. A second approach is optimum multiparameter analysis (OMPA), initially formulated for open-ocean water mass analysis and global ocean circulation studies (Tomczak and Large, 1989; Tomczak et al., 1994). OMPA was later extended to ice–ocean systems through the inclusion of many conservative and quasi-conservative tracers like isotopes and noble gases (Beaird et al., 2015; Biddle et al., 2017; Beaird et al., 2018; Kanna et al., 2018; Biddle et al., 2019). Although these two approaches differ in complexity and observational requirements, they are fundamentally based on the same conservation equations. A key difference between the application of the two approaches is that the conservation equations approach is an exact system of equations that can be solved algebraically, whereas OMPA is generally presented as an overdetermined

system (more observational tracers than the number of unknown water mass fractions) and uses non-negative weighted least-squares estimation to find the best solution set.

It has been overlooked in applications to Greenland fjord systems that underdetermined least squares problems can be solved by appropriately ”regularizing” the problem with prior knowledge and solving the problem explicitly (Wunsch, 2006). This presents an opportunity to calculate water mass fractions from many SWTs in Greenland Fjords using only temperature and salinity data inputs. This approach was used successfully by Lanham et al. (2025) in the Antarctic context with model output. A similar approach for underdetermined systems is outlined by Shrikumar et al. (2021) and Lawrence et al. (2026), with a key constraint that fraction solutions must be non-negative. We build on this more recent work and propose spatially varying penalty matrices for Greenland glacial fjords. These improvements allow for prior knowledge about fjord systems to be incorporated into solutions. The formulation of the method presented here is more mathematically unifying for glacial fjord applications.

In the following sections, we step through each approach and describe how they build upon each other mathematically, discussing shared assumptions, key differences, and the benefits and drawbacks of each. The goal is to inform other water mass fraction studies in glacial fjord environments about the best method for a given application and data availability.

### 2.2.2 Linear Mixing Equations and Algebraic Solutions for Exact Systems

All water mass fraction estimation methods begin from linear mixing equations that assume each observed property is a conservative combination of source water types (SWTs). The most general representation of this is given by

$$y_i = \sum_{j=1}^{n} x_j A_{ij}, \qquad i = 1, \ldots, m, \tag{2.1}$$

$$\sum_{j=1}^{n} x_j = 1. \tag{2.2}$$

$$x_j \geq 0, \qquad j = 1, \ldots, n. \tag{2.3}$$

where $m$ is the total number of observed properties or tracers (eg. temperature, salinity, DO, etc), $n$ is the total number of SWTs, $x_j$ are unknown SWT fractions to be solved for, and $y_i$ is a data point of observed properties. $\mathbf{A}$ is the matrix of SWT properties with elements $A_{ij}$. Equation 2.2 provides a mass conservation constraint where the fraction solutions must all add to 1, while Equation 2.3 states that all fraction solutions must be positive.

Consider the specific case used in previous Greenland glacial fjord applications of temperature and salinity as observed properties ($m = 2$) and three SWTs ($n = 3$): ambient water (aW), subglacial discharge (SGD) and submarine melt (SMW). Expanding Equations 2.1–2.3 results in the following system of equations:

$$T_{\text{obs}} = x_{aW} T_{aW} + x_{SGD} T_{SGD} + x_{SMW} T_{SMW}, \tag{2.4}$$

$$S_{\text{obs}} = x_{aW} S_{aW} + x_{SGD} S_{SGD} + x_{SMW} S_{SMW}, \tag{2.5}$$

$$x_{aW} + x_{SGD} + x_{SMW} = 1. \tag{2.6}$$

The data point properties ($T_{\text{obs}}$, $S_{\text{obs}}$) must equal the sum of SWT property values weighted by their unknown fractional contributions. This case is an exact system where the number of unknowns, 3, equals the number of equations, expressed by $m + 1 = n$, which includes the addition of the mass constraint. As an exact system, the unknowns can be solved by simple algebraic substitution, and there exists a unique solution set of fractions.

This approach is straightforward to solve, making it easy to understand and apply to different systems. An advantage is that the solution can often be visualized directly in a property-property diagram (eg. temperature-salinity diagram), providing intuitive graphical interpretations of mixing between source waters. It can be applied using only temperature and salinity observations along with a conservation of mass constraint (as the example above), or additional conservative observed variables can be used as long as the number of observed variables matches the number of unknown source water type fractions to maintain exactness ($m+1=n$).

At the same time, the simplicity of the method poses limitations, especially for applications in Greenland fjords, where assumptions are often needed to limit the number of SWTs to create an exact system of equations. These assumptions may not always be well justified in fjord environments characterized by multiple interacting water masses in different fjord regions. Additionally, solutions derived using these methods are often presented without explicit treatment of uncertainty associated with SWT definitions or observational error. Thus, the robustness and sensitivity of the water mass fraction results are not always straightforward to assess.

Note that the conservation equations above (Equations 2.4–2.6) can also be written compactly in matrix form, where

$$\mathbf{y} = \begin{bmatrix} T_{\text{obs}} \\ S_{\text{obs}} \\ 1 \end{bmatrix}, \quad \mathbf{A} = \begin{bmatrix} T_{aW} & T_{SGD} & T_{SMW} \\ S_{aW} & S_{PW} & S_{SMW} \\ 1 & 1 & 1 \end{bmatrix}, \quad \mathbf{x} = \begin{bmatrix} x_{aW} \\ x_{SGD} \\ x_{SMW} \end{bmatrix}. \tag{2.7}$$

The last row of 1s represents the mass conservation equation. The solutions of this exact system ($m+1=n$) can be found by setting up the problem

$$\mathbf{y} = \mathbf{A}\mathbf{x}. \tag{2.8}$$

and solving for $\mathbf{x}$ using the transpose of $\mathbf{A}$ where

$$\mathbf{x} = \mathbf{A}^T \mathbf{y}. \tag{2.9}$$

The second method, OMPA, uses this matrix algebra approach to solve more complex water mass fraction equations with more known observational tracers than unknown water mass fractions.

### 2.2.3 Optimum Multiparameter Analysis (OMPA)

OMPA is generally presented as an overdetermined system which can utilize many observational properties and is therefore capable of solving for many SWTs. The inclusion of multiple observational properties allows for more constrained definitions of unique SWTs. There are often a greater number of linear mixing equations used compared to algebraic methods, best represented and solved through matrix algebra. An exact solution is rarely possible with an overdetermined system based on observations of the real world with inherent uncertainty. The conservation equations, represented by matrices (Equations 2.7–2.8), are then written with a residual term $\mathbf{r}$ where

$$\mathbf{y} = \mathbf{A}\mathbf{x} + \mathbf{r}. \tag{2.10}$$

Classical OMPA then solves for $\mathbf{x}$ using weighted constrained least-squares estimation to minimize the square of the residuals $\mathbf{r}$. This is formally written as

$$\min_{\mathbf{x} \geq 0} \|\mathbf{W}(\mathbf{A}\mathbf{x} - \mathbf{y})\|_2^2, \tag{2.11}$$

where the non-negativity constraint on the solutions is applied. Mass conservation is still included as entries of 1 in the last row of both $\mathbf{y}$ and $\mathbf{A}$. A diagonal row weight matrix is included, $\mathbf{W}$, with size $m \times m$ that represents both measurement uncertainty and model uncertainty (the

model here being SWT definitions). In practice, **W** forces the solution to fit more closely to the most reliable observations. In some applications, **W** is not included, which is the same as a diagonal matrix of 1s where all observations are weighted equally.

Often not explicitly discussed is the normalization of **A** and **y** prior to solving the problem. Different properties have different units and numerical ranges, therefore normalization is needed such that larger numerical values due to units are not weighted more heavily in the solution. This step was formally included in OMP literature by Mackas et al. (1987) and Tomczak and Large (1989). There are different approaches to normalization, but here we normalize each value in **A** and **y** as

$$\tilde{A}_{ij} = \frac{A_{ij} - \mu_i}{s_i} \tag{2.12}$$

$$\tilde{y}_i = \frac{y_i - \mu_i}{s_i} \tag{2.13}$$

where $\mu_i$ is the mean of property $i$ across all endmembers in **A**, and $s_i$ is the standard deviation of property $i$ across all endmembers in **A**. The same mean and standard deviation used to normalize **A** are applied consistently to **y**, ensuring they are both expressed in the same coordinate system. We adopt this normalization in all methods described below prior to solving for water mass fractions.

Common packages that iteratively solve non-negative constrained weighted least squares problems are often used to apply OMPA, such as MATLAB's *lsqnonneg* function. Karstensen and Tomczak (1999) offer a MATLAB package using this formulation. This package also works for extended OMPA, which builds directly on classical OMPA by retaining the same linear mixing framework for physical water mass fractions but adds stoichiometric relationships to represent property changes caused by biological processes. When only conservative properties are used, the formulation reduces to classical OMPA. We concern ourselves here with only conservative, or assumed-conservative, properties and the physical mixing of water masses as

we are ultimately working toward a method that uses only temperature and salinity observations.

While OMPA solutions with more observational property types are often better constrained, it can be challenging and costly to obtain noble gas and isotope observations especially in Greenland fjord environments. Only one instance of noble gas measurements is available in the 13 year record of observations from Sermilik Fjord (Beaird et al., 2018). DO and nutrient measurements are more readily available and often integrated with other CTD measurements, however, using them as conservative properties requires additional assumptions. Additionally, SWT definitions in glacial fjord environments, particularly for subglacial discharge and submarine melt, can be highly uncertain, especially with variables like noble gases where direct observations of those pure glacial SWTs are difficult to obtain.

**OMPA solution uncertainty**

Water mass fraction solutions are highly sensitive to SWT property definitions, making uncertainty calculations important for interpreting results. Uncertainty in OMPA analysis is most commonly estimated using Monte Carlo simulations, in which SWT properties are randomly perturbed and the non-negative least squares problem is solved repeatedly to characterize the distribution of fraction solutions. This iterative approach is necessary because the non-negativity constraint requires an iterative solver and precludes explicit closed-form uncertainty propagation.

The residuals of the OMPA system—the difference between observed property values and those reconstructed from the optimized fraction solution—provide a complementary, and more direct, measure of solution quality. Large or spatially structured residuals suggest that the defined SWT properties cannot adequately explain the observations, whether due to poorly constrained SWTs, unresolved mixing of other water types or processes, or violations of the conservative mixing assumption. Mass balance residuals in particular are commonly reported, with values below roughly 5% typically taken as evidence that the solution is physically sound. However, residuals reflect the aggregate fit of the system and do not lead to specific uncertainty estimates for individual fraction solutions, which is where Monte Carlo is used.

An alternative and largely unexplored approach is to use the geometry of the cost function of the least-squares problem itself: a flat or ill-defined minimum indicates that multiple water mass fraction combinations fit the observations nearly equally well, providing a direct measure of solution uncertainty that is intrinsic to the optimization rather than dependent on assumed SWT property perturbations. Characterizing this uncertainty through the curvature of the cost function at the solution—which is widely used in machine learning methods (MacKay, 1992; Bishop, 2006; Daxberger et al., 2021)—has not, to our knowledge, been applied in water mass analysis. Given the growing accessibility of these methods, cost function-based uncertainty quantification represents a promising direction for future OMPA applications.

**Underdetermined Systems in Greenland Glacial Fjords**

Previous studies in Greenland fjords using conservation equations or OMPA to calculate water mass fractions have all required that their system of equations be exact or overdetermined as described above (Table 2.1). Greenland glacial fjords can present a problem with at least four source water types: subglacial discharge or runoff (SGD), submarine meltwater (SMW), Atlantic Water (AW), and Polar Water (PW). Thus, for these methods, at least three measured properties and mass conservation are required. Temperature and salinity are the most commonly available observations in Greenland glacial fjords, especially with recent large-scale XCTD and aerial XCTD campaigns. At least one other variable is then needed to avoid an underdetermined system, or a reduction of SWTs is needed, to perform water mass fraction analyses as previously described in OMPA literature.

Previous studies that have been limited by only having temperature and salinity observations have used assumptions to create exact or overdetermined problems. For example, if only temperature and salinity are available, a reasonable assumption could be made to solve for $n = 3$ SWT fractions instead of $n = 4$, as in Washam et al. (2019). PW was not detected in their hydrographic observations far from the fjord entrance, therefore it was disregarded as a SWT. Similarly, other applications use a single ”ambient water mass” representing a constant

mixture of AW and PW to reduce the problem to $n = 3$. Muilwijk et al. (2022) used yet a third approach and assumed that SWT fractions were constant in time in order to create an overdetermined system of equations with available temperature and salinity data from multiple years (OMP Multi-year Analysis (OMPM); see Chapter 3). The following sections present an alternate approach to these assumptions.

### 2.2.4 Regularized least squares (RLS) formulation for underdetermined systems

Underdetermined least squares problems can be solved by appropriately "regularizing" the problem and solving it in explicit form. Lanham et al. (2025) successfully used this approach to calculate water mass fractions of $n = 4$ SWTs from model output of temperature, salinity, and mass conservation around Antarctica. This approach uses well-known linear inverse methods, and their derivations are described in full by Wunsch (2006). Key to this approach is a "penalty matrix", $\mathbf{P}$, not included in classical OMPA. This matrix creates a "cost" to using a specific water mass relative to the others. In practice, this matrix is used as a way of incorporating previous knowledge about the prevalence of each water mass in the solution. For an underdetermined system, this information is mathematically necessary in order to stabilize what is otherwise an ill-conditioned system. Problems of this form are called "penalized weighted least squares problems" or "Tikhonov regularized weighted inverse problems" and are represented by the cost function

$$\min_{x} \ \|\mathbf{W}(\mathbf{A}\mathbf{x}-\mathbf{y})\|_2^2 + \mathbf{x}^{\mathbf{T}}\mathbf{P}\mathbf{x}. \tag{2.14}$$

For now, we ignore the non-negativity constraint imposed in the previous methods, but we will return to this in Section 2.2.5. We set the derivative of Equation 3.4 to 0 to find the minimum cost solution. From there, we can algebraically rearrange the equation and explicitly

estimate water mass fractions, $\mathbf{x}$, as:

$$\mathbf{x} = (\mathbf{A^T W A} + \mathbf{P})^{-1} \mathbf{A^T W y}. \tag{2.15}$$

A benefit of this explicit inverse formulation is that it is transparently solved analytically, in one line of code, rather than through a packaged iterative solver. The uncertainty of the estimated water mass fractions can also be calculated explicitly through linear propagation of observational error, as opposed to using Monte Carlo with OMPA. The uncertainty covariance in $\mathbf{x}$ is given by

$$\mathrm{Cov}(\mathbf{x}) = (\mathbf{A^T W A} + \mathbf{P})^{-1} \mathbf{A^T W A} (\mathbf{A^T W A} + \mathbf{P})^{-1}. \tag{2.16}$$

The diagonal elements of $\mathrm{Cov}(\mathbf{x})$ provide formal uncertainty estimates for each water mass fraction that arise from observational error and the structure of the mixing model,

$$\sigma_{x_i} = \sqrt{[\mathrm{Cov}(x)]_{ii}}. \tag{2.17}$$

With this formulation, the fact that a water mass fraction problem is underdetermined is not necessarily always an issue that needs resolving as it has been previously described in OMPA literature, especially in Greenland fjord applications. Assumptions to limit the number of water masses or increase the number of tracers do not need to be introduced solely to create equal matrix dimensions and "fix" an underdetermined problem. The prior-informed inverse formulation is also easily applied to determined and overdetermined systems by adding rows or columns in the SWT definition matrix ($\mathbf{A}$) and adding corresponding rows in the other matrices.

### 2.2.5 Non-negativity constraint and SMW effective temperature

Although the explicit inverse formulation provides a transparent solution and analytical uncertainty estimates, it does not guarantee non-negative water mass fractions. In principle, a well-posed mixing model with appropriate SWT definitions should not produce negative fractions

and therefore enforcing non-negativity would not be needed. Given the non-negligible prescribed uncertainty covariance **P** on **x**, one expects some negative estimates. Solutions with negatives larger than desired can be viewed as clues, like residuals, as to where the model may need to account for other processes or need adjusted SWT definitions. However, with Greenland fjord water masses, the PW and SMW property definitions are such that we benefit from a non-negativity constraint to select a physically representative solution for our problem set up. This is further explained below.

SMW is defined following the effective temperature framework of Jenkins (1999).The latent heat of fusion is used to define an effective temperature of approximately -80 °C to -100 °C, representing the thermodynamic cost of melting ice into the ambient water column (Gade, 1979). Because this value lies roughly 90°C below any temperature actually observed in the fjord, SMW in temperature-salinity space sits far outside the other SWT property values, giving it extreme geometric "leverage" over the temperature equation relative to all other SWTs even when the problem is normalized. As a consequence, the fraction solution is hypersensitive to small perturbations in SMW near zero: a shift of a fraction of a percent in SMW produces large temperature excursions comparable in magnitude to the full range of observed temperatures. Critically, a negative SMW fraction is not interpretable as noise—it would imply the ocean is losing heat to refreeze water rather than melt ice, which is physically not represented in the construction of the effective SMW temperature.

Two additional factors compound this sensitivity. First, PW temperatures are bounded below by the freezing point, making the temperature distribution asymmetric and poorly approximated by the Gaussian uncertainty assumed in **P**. This mismatch can bias fraction estimates near zero in ways the prescribed uncertainty covariance does not fully capture. Second, PW and SMW are nearly overlapping in salinity space— both are fresh relative to Atlantic Water and lead to mixing lines with AW of similar slopes in temperature-salinity diagrams. This means the system relies heavily on the temperature equation to distinguish between PW and SMW, concentrating the sensitivity associated with the extreme SMW effective temperature even further.

Considering all the above characteristics of the Greenland fjord problem, we enforce a non-negativity constraint as a principled way of selecting physically representative solutions. Admittedly, this does not address all the above concerns, but it provides a higher likelihood of producing solutions grounded in physical reality compared to allowing negative solutions.

### 2.2.6 Quadratic programming implementation

To enforce the non-negativity constraint, we reformulated the cost function as a quadratic minimization problem subject to inequality bounds. The cost function is now expressed in the form of

$$\min_{x \geq 0} \frac{1}{2}\mathbf{x}^{\mathbf{T}}\mathbf{H}\mathbf{x} + \mathbf{f}^{\mathbf{T}}\mathbf{x}, \tag{2.18}$$

where

$$\mathbf{H} = 2(\mathbf{A}^{\mathbf{T}}\mathbf{W}\mathbf{A} + \mathbf{P}), \qquad \mathbf{f} = -2\mathbf{A}^{\mathbf{T}}\mathbf{W}\mathbf{y}. \tag{2.19}$$

This formulation retains the physical interpretation of the weighting schemes and prior information while enforcing admissible solutions. Equations 2.18 and 2.19 directly come from expanding the squared norms in Equation 3.4 and grouping like terms. They are mathematically the same problem, but the quadratic form allows us to employ MATLAB's *quadprog* function which can incorporate a non-negativity constraint into our solution. Note that *quadprog* solves objective functions in the form of Equation 2.18 and uses a built-in factor of 1/2. A factor of 2 is therefore included in Equation 2.19 so that the *quadprog* formulation is consistent with the cost function in Equation 2.18.

PYOMPA (Shrikumar et al., 2021) is a python implementation using the same quadratic cost function formulation presented here. They use the Operator Splitting Quadratic Program (OSQP) solver (Stellato et al., 2020), called using the *cvxpy* python package (Diamond and Boyd, 2016; Agrawal et al., 2018), which is a numerical optimization package for solving convex quadratic programs in the form of Equation 2.18. OSQP solver has support for a variety of

languages including MATLAB, R, Julia, and C/C++. MATLAB's *quadprog* function and OSQP solve the same class of problems, but there are underlying algorithm, performance, and access tradeoffs between the two. We use *quadprog* here as our problem is relatively small and it was straightforward to implement in our legacy workflows. We recognize that OSQP may be a better choice for more data intensive applications or python users. Finally, note that PYOMPA is implemented with a hard mass constraint, meaning that no residuals in the mass conservation equation are allowed. This is a secondary constraint on top of the non-negativity constraint, and is thus a slightly different implementation than the method described here. Incorporating the mass constraint into the matrix equations, as we do here, is called a "soft" mass constraint, as residuals are allowed and the solution is not forced to uphold mass conservation perfectly.

A drawback of this approach is that Monte Carlo simulations are needed for uncertainty calculations, as we are no longer using an analytical form of the problem and have applied a constraint. The analytical uncertainty (Equation 2.16) can still be calculated, if desired, from the input matrices and serves as an approximation of the uncertainty on the water mass fraction solutions. For the case study in Section 2.3 we report the Monte Carlo uncertainties.

### 2.2.7 Choosing W and P values

A critical step in this method is that a user must define **W** and **P** matrices used in the objective function (Equation 2.19). Previous water mass fraction studies employing **W** and/or **P** matrices rarely document the rationale for how these values are selected. We address this by providing guidance below and metrics that can help assess the influence that each matrix is having on the solution. Critically, it is the relative magnitude between **W** and **P** governs the solution, not their absolute values (Shrikumar et al., 2021). Large values within **W** and **P** should be avoided as these can produce numerical instabilities, as quantified by the condition number (described below). In practice, **W** and **P** are iteratively tuned after initial guesses to produce physically consistent solutions. We recommend performing sensitivity analyses with different iterations of **W** and **P** to assess their influence on the solution.

**The data weight matrix, W**

From Equations 3.3 and 2.18, **W** scales the magnitude of the residuals for each observed tracer or variable. A larger weight should be assigned to tracers that are well-constrained by both measurements and SWT definitions, such that the objective function is more strongly influenced by those tracers compared to others with large residuals.

Ultimately, the magnitude of a given residual is determined by 1) whether a variable has been measured precisely and 2) whether the SWT definitions are appropriate for that variable. Often, **W** values are described as containing only the measurement uncertainty, but they should also include the SWT definition uncertainty. For example, temperature measurement uncertainty as listed by a manufacturer may be $\pm 0.002$°C. However, the temperatures used to define specific water masses may be subject to much larger uncertainty. The submarine meltwater SWT effective temperature can vary from -87 to -100°C depending on the choice of ice temperature used. In this case, an initial temperature uncertainty $\sigma_T$ is orders of magnitude greater than the instrument measurement uncertainty. In the case study in Section 2.3, we initially set $\sigma_T = 0.1$ informed by the range of SWT temperature values. Additionally, the uncertainty for mass conservation is usually set as the smallest relative to other uncertainty values, meaning that mass conservation is strictly applied. We initially set $\sigma_{\text{mass}} = 0.003$. Rather than following a prescriptive formula, the uncertainty values reflect informed judgment and should be validated through sensitivity analysis.

Next, the uncertainty values are normalized by the standard deviation of the endmember property values for each tracer, $s_i$. This places all properties on a common scale, ensuring that **W** reflects each tracer's uncertainty relative to its ability to distinguish between different endmembers, as opposed to differences in physical units or numerical magnitude. We define the normalized uncertainties as $\tilde{\sigma}_i$ where

$$\tilde{\sigma}_i = \frac{\sigma_i}{s_i}. \tag{2.20}$$

The diagonal values in **W** are then set to

$$w_i = \frac{1}{\tilde{\sigma}_i^2}. \tag{2.21}$$

Large values in **W** correspond to properties with more influence on the solution. Large values result from smaller $\tilde{\sigma}_i$ values, which ultimately arise from relatively smaller initial uncertainties ($\sigma_i$) and/or larger spreads ($s_i$) in endmember properties. One exception arises for the mass conservation constraint, whose endmember values are all identically 1, yielding $s_i = 0$. To avoid division by zero, $w_{\text{mass}}$ is set directly to $1/\sigma_{\text{mass}}^2$.

Once an initial diagonal **W** is determined, we can consider the penalty matrix, **P**.

**Spatially varying P in glacial fjords**

There are two considerations for choosing values of **P**. The first is the relationship between the values within **P** and the second is the relative magnitude of **P** compared to **W**. We provide guidance on each below.

The diagonal elements of **P** act as a soft constraint on each SWT water mass fraction. A larger value means stronger suppression of the corresponding SWT. For a Greenland glacial fjord context, AW receives the weakest penalty because it is expected to dominate, while SGD and SMW receive the strongest penalty as their fractions are small. PW is given a penalty value slightly greater than AW and less than SMW and SGD.

Our specific contribution here is developing a spatially varying penalty matrix based on prior knowledge of water mass fraction distributions and the fjord dynamics of Sermilik Fjord. For example, we do not expect any SMW below 400 m depth, so we can maximally penalize SMW in this region of the fjord. Conversely, we do not expect any AW near the surface and can heavily penalize AW in this region relative to the rest of the fjord. PW has the greatest variability of the water masses in the along-fjord direction. We heavily penalize PW in the mélange region while relaxing the penalty in the mouth region. For a given fjord application, the exact spatial

variability of each water mass penalty may need to be adjusted based on known information. We provide the specific values and spatial variation of **P** used for Sermilik Fjord in Section 2.3 and compare results with a constant **P** matrix to show the effect on results.

**Relative magnitude of P and W**

In a Bayesian interpretation, **P** is analogous to an inverse prior covariance matrix on the solution and represents the prior confidence about the likely magnitude of each water mass fraction. The solution then represents a balance between fitting the observations (governed by **W**) and respecting the prior expectations (governed by **P**). If **P** is too small relative to **W**, the penalty has negligible effect and the solution may admit physically unrealistic fractions; if **P** is too large, the prior dominates and the data are effectively ignored.

One way to assess this balance is through a Frobenius norm ratio (Wunsch, 1996; Hansen, 1998). The Frobenius norm measures the overall magnitude of a matrix in a single scalar—as the square root of the sum of squared entries—which means it captures the combined effect of all diagonal elements of **W** and **P** simultaneously.

$$\lambda = \frac{\|\mathbf{W}^{1/2}\tilde{\mathbf{A}}\|_F}{\|\mathbf{P}^{1/2}\|_F} \tag{2.22}$$

where $\tilde{\mathbf{A}}$ is the normalized endmember matrix. The Frobenius norm of $\mathbf{W}^{1/2}\tilde{\mathbf{A}}$ directly reflects the scale of the data term's contribution to the cost function (Equation 2.19). In a balanced system, $\lambda \approx 1$, but the desired magnitude depends on the goal and how strongly the solution should depend on the data versus the prior information. With a spatially varying **P**, $\lambda$ can be calculated at all points in the domain and will vary. A user can adjust **P** spatially so that regions where there is high confidence in data and endmember definitions produce $\lambda > 1$ or even $\lambda \gg 1$, and regions where the prior information should be expressed more strongly produce $\lambda < 1$. Along with condition numbers and data influence matrix, $\lambda$ is a practical diagnostic for assessing whether **W** and **P** are appropriately balanced and scaled.

**Solution diagnostics: condition numbers and data influence**

While condition numbers are standard diagnostics in numerical inverse methods (Hansen, 1998), they are often not reported explicitly in water mass fraction studies. We include them here as reproducible metrics for assessing solution quality and to provide guidance for future water mass fraction applications in glacial fjords.

The condition number of a given matrix $\kappa(\mathbf{M})$ quantifies how sensitive a solution is to perturbations in the data, defined as the product of the matrix 2-norm and the 2-norm of its inverse (Hansen, 1998):

$$\kappa(\mathbf{M}) = \|\mathbf{M}\|_2 \|\mathbf{M}^{-1}\|_2 = \frac{\sigma_{\max}(\mathbf{M})}{\sigma_{\min}(\mathbf{M})}, \tag{2.23}$$

where $\sigma_{\max}$ and $\sigma_{\min}$ are the largest and smallest singular values of $\mathbf{M}$. Following the structure of Equation 2.8, $\mathbf{Mx} = \mathbf{y}$, $\kappa(\mathbf{M})$ represents that a relative perturbation, $\varepsilon$, in the data, $\mathbf{y}$, can produce an error in the solution ,$\mathbf{x}$, as large as $\kappa(\mathbf{M}) \cdot \varepsilon$. Intuitively, a matrix with a large condition number is nearly singular—small changes in the input can produce large changes in the output, meaning the solution is numerically unreliable and amplifies observational noise. Ill-conditioning arises naturally in water mass fraction problems when endmembers have similar tracer properties, a particular concern here for PW and SMW, which both cool and freshen the water column, making them difficult to distinguish using temperature and salinity alone.

We track $\kappa$ through each stage of the problem formulation, as normalization, weighting, and regularization impact the condition number. The raw matrix $\mathbf{A}$ can carry a large $\kappa(\mathbf{A})$ due to unit disparity across tracers. Normalizing should reduce the condition number. If $\kappa(\tilde{\mathbf{A}})$ is not improved at this stage it could indicate poorly separated endmembers (Mackas et al., 1987; Tomczak and Large, 1989). Forming the weighted normal equations $\mathbf{A}^T\mathbf{WA}$ can increase $\kappa$ again, establishing the baseline conditioning of the unregularized problem. Adding $\mathbf{P}$ to form $\mathbf{H} = \mathbf{A}^T\mathbf{WA} + \mathbf{P}$ raises the smallest eigenvalues and reduces the condition number, which is the fundamental stabilizing mechanism of this regularization technique (Hansen, 1998). The

condition number ratio

$$r_\kappa = \frac{\kappa(\mathbf{A}^T\mathbf{W}\mathbf{A})}{\kappa(\mathbf{H})} \tag{2.24}$$

quantifies this improvement. A value of $r_\kappa \gg 1$ confirms that $\mathbf{P}$ is meaningfully stabilizing the system.

The diagonal elements of the data influence matrix $\mathbf{S} = \mathbf{H}^{-1}\mathbf{A}^T\mathbf{W}\mathbf{A}$ can provide a complementary diagnostic for each SWT solution:

$$S_{ii} = \left[\mathbf{H}^{-1}\mathbf{A}^T\mathbf{W}\mathbf{A}\right]_{ii} \in [0,1], \tag{2.25}$$

where values near 1 indicate a data-driven estimate and values near 0 indicate that prior information is dominating the solution. The effective degrees of freedom $\nu = \mathrm{tr}(\mathbf{H}^{-1}\mathbf{A}^T\mathbf{W}\mathbf{A}) \in [0,n]$ summarizes this across all $n = 4$ source water types. Together, $\kappa(\mathbf{H})$, $r_\kappa$, the data influence diagonals, and $\nu$ provide a comprehensive picture of solution stability and how the problem is balancing the data and prior information. Noting these diagnostic values can assist in further iterating on values in $\mathbf{W}$ and $\mathbf{P}$ such that a problem becomes well-conditioned even if the initial endmember matrix is not.

These diagnostics and their interpretations are summarized in Table 2.3. Specific values for the case study in Section 2.3 are provided.

**Correlation diagnostics for SWT separability and tracer redundancy**

Finally, we identify two correlation diagnostics as important metics, often overlooked in previous studies, for assessing how well-posed the overall mixing model is. Note that these correlation diagnostics are also applicable to classical OMPA implementations, and the mass conservation row should be masked out and not used in the following correlations.

The first diagnostic is the $n \times n$ SWT–SWT correlation matrix $R_{\mathrm{SWT}} = \mathrm{corr}(\mathbf{W^{1/2}}\tilde{\mathbf{A}})$, which measures how similar each pair of SWTs appears in weighted property space. If two water

masses have nearly the same values across all tracers after normalizing, then there is no way to distinguish between their individual contributions to the solution—any combination of their fractions that satisfies the mass conservation constraint will fit the data equally well. This is collinearity: not that the two water masses are necessarily identical, but that the chosen tracers in the mixing model cannot resolve them. Values of $R_{ij}$ near $+1$ flag this problem; values near zero indicate well-separated, independently resolvable pairs. Collinear SWT pairs should prompt a user to consider adding a tracer that can more significantly distinguish between the two water masses.

The second diagnostic is the $m \times m$ property–property correlation matrix $R_{\text{prop}} = \text{corr}((\mathbf{W}^{1/2}\tilde{\mathbf{A}})^{\top})$, which measures how similarly two properties behave across all SWT definitions. A value near $+1$ means two properties carry nearly the same information—if temperature increases from one SWT to the next, so does salinity—making one of them potentially redundant. And a value near $-1$ means that two properties are anti-correlated, also an indication of possible redundancy. Values near zero indicate that two properties vary independently across the SWT definitions and are contributing unique information.

High property–property correlation or anti-correlation does not necessarily indicate a problem. A property that looks redundant on average may still be the one feature that distinguishes two otherwise collinear SWTs. For example, if temperature and dissolved oxygen are anti-correlated across all four SWTs, oxygen appears redundant with temperature globally—but if two specific SWTs happen to have very similar temperatures yet different oxygen signatures, oxygen is precisely what tells them apart. Removing it on the basis of global correlation alone would eliminate the only information separating that SWT pair. Tracer inclusion decisions should therefore be made by testing whether adding or removing a property improves or degrades the condition number $\kappa(\mathbf{A}^{\top}\mathbf{W}\mathbf{A})$ and by inspecting the raw SWT property values for collinear pairs directly.

### 2.2.8 Summary of diagnostic workflow

For regularized least squares (RLS) water mass fraction analyses incorporating prior information, the recommended sequence for creating a mixing model of SWTs, followed by choosing values within $\mathbf{W}$ and $\mathbf{P}$ is below. These diagnostics are for the user to better understand the overall behavior of a given mixing model. Reporting the diagnostics creates more transparent assumptions and allows for more comparable and trustable results. As noted in the text, some of these diagnostics are also applicable to classical OMP analysis.

1. Identify observed variables available for use as conservative tracers and the SWTs needed to represent the water mass dynamics of interest for a given fjord system.

2. Determine SWT endmember property values and construct the system matrix $\mathbf{A}$ ($m \times n$, properties $\times$ SWTs). Normalize to obtain $\tilde{\mathbf{A}}$, removing the effect of different units and scales.

3. Choose tracer uncertainties $\sigma_i$ informed by instrument specifications and the range of SWT property definitions. Convert to the normalized coordinate system, then construct the diagonal weight matrix, $\mathbf{W}$. Set $\sigma_{\text{mass}}$ to a small value to enforce mass conservation strictly.

4. Compute the SWT–SWT and property–property correlation diagnostics on the weighted normalized matrix $\mathbf{W}^{1/2}\tilde{\mathbf{A}}$ to assess whether the SWT definitions are distinguishable and whether the chosen tracers provide independent information. Iterate on SWT definitions, the tracer set, and $\mathbf{W}$ until the correlation structure is acceptable for the system.

5. Compute $\kappa(\mathbf{A})$ and $\kappa(\tilde{\mathbf{A}})$ to confirm that normalization reduces the condition number. If it does not, the SWT endmembers are poorly separated in tracer space and steps (2)–(4) should be revisited.

6. Choose an initial $\mathbf{P}$ by setting the relative diagonal values to reflect prior physical knowledge (e.g. AW least suppressed, SGD and SMW most suppressed). Scale $\mathbf{P}$ using the Frobenius norm ratio $\lambda = \|\mathbf{W}^{1/2}\tilde{\mathbf{A}}\|_F / \|\mathbf{P}^{1/2}\|_F$ as an initial guide to bring $\mathbf{W}$ and $\mathbf{P}$ to comparable magnitude.

7. Compute $\kappa(\tilde{\mathbf{A}}^\top \mathbf{W}\tilde{\mathbf{A}})$ and $\kappa(\mathbf{H})$ and verify that $\kappa(\mathbf{H}) \ll \kappa(\tilde{\mathbf{A}}^\top \mathbf{W}\tilde{\mathbf{A}})$, confirming that $\mathbf{P}$ is meaningfully stabilizing the system, and that $\kappa(\mathbf{H})$ is appropriate relative to the noise level of the observations.

8. Examine the diagonal elements of the data influence matrix $\mathbf{H}^{-1}\tilde{\mathbf{A}}^\top \mathbf{W}\tilde{\mathbf{A}}$ to assess per-SWT balance between data fidelity and prior information. Values near 1 indicate data are driving those fractions; smaller values reflect prior influence. Compare the effective degrees of freedom $\nu = \mathrm{tr}(\mathbf{H}^{-1}\tilde{\mathbf{A}}^\top \mathbf{W}\tilde{\mathbf{A}})$ against the number of SWTs $n$ as a global check. Iterate over steps (6)–(8) with adjusted $\mathbf{P}$ values until the diagnostics confirm a solution that is physically motivated, numerically stable, and balanced appropriately between data and prior information.

A question that remains is whether a specific application of water mass fraction analysis should choose classical OMPA or RLS with prior information. The following case study presents a comparison of results utilizing both methods across a spectrum data types, leading to final suggestions and conclusions for factors that should influence water mass fraction methodology and problem setup in glacial fjords.

## 2.3 Case Study: Sermilik Fjord

Sermilik Fjord, located in Southeast Greenland (Figure 2.1), offers an ideal case study for comparing the data requirements, assumptions, and uncertainties associated with water mass fraction analyses in glacial fjord systems. Its well-documented physical setting, long-term data record, and previous estimates of water mass fractions make it uniquely suited for this methodological comparison study.

A defining characteristic of Sermilik Fjord is the absence of a shallow sill, allowing for relatively unmodified, deep (∼450 m) Atlantic Water to reach and interact with the Helheim Glacier terminus (Straneo et al., 2010). This configuration means that four distinct water masses converge within the fjord in the summer season: warm, saline Atlantic Water (AW) from the shelf; cold, fresh Polar Water (PW) of Arctic origin that overlies AW on the continental shelf; subglacial discharge (SGD) delivered at depth at the glacier terminus base and then subsequently mixed with AW in a buoyant plume; and submarine meltwater (SMW) produced by direct ocean melting of the terminus ice and icebergs (Figure 2.2). The interaction of unmodified AW with PW on the shelf, combined with large glacial freshwater inputs during the summer season, creates a characteristic Greenland glacial fjord water mass structure (Straneo et al., 2012; Beaird et al., 2018; Muilwijk et al., 2022). We focus specifically on the summer season water masses as this is when there is the most glacial freshwater input into the ocean and ice-ocean dynamics are amplified.

Sermilik Fjord contains three major branches with marine terminating glaciers at the head of each (Figure 2.1). While all three glaciers add SGD and SMW into the fjord system, Helheim Glacier is the dominant source of glacial input as one of the largest and fastest-flowing outlet glaciers of the Greenland Ice Sheet, with solid ice discharge of approximately 30–38 Gt $yr^{-1}$ since 2000 and an average freshwater discharge of roughly 500–650 $m^3\ s^{-1}$ in July and August, with peak discharge rates exceeding 1000 $m^3\ s^{-1}$ for short periods (Mankoff et al., 2020). There is a perennial ice mélange extending up to 30 km from the terminus of Helheim Glacier, producing SMW in the upper water column, creating distinctly colder and fresher surface waters compared to the other fjord regions (Roth et al., 2025a).

The most rigorously constrained water mass fraction estimates for Sermilik Fjord come from Beaird et al. (2018), who used classical OMP methods with dissolved noble gas observations as conservative tracers collected during an August 2015 survey. The number of observational properties—including temperature, salinity, and $^3$He, $^4$He, Ne, Ar, Kr, Xe, plus mass conservation—exceeded the number of SWTs in the study, creating an overdetermined

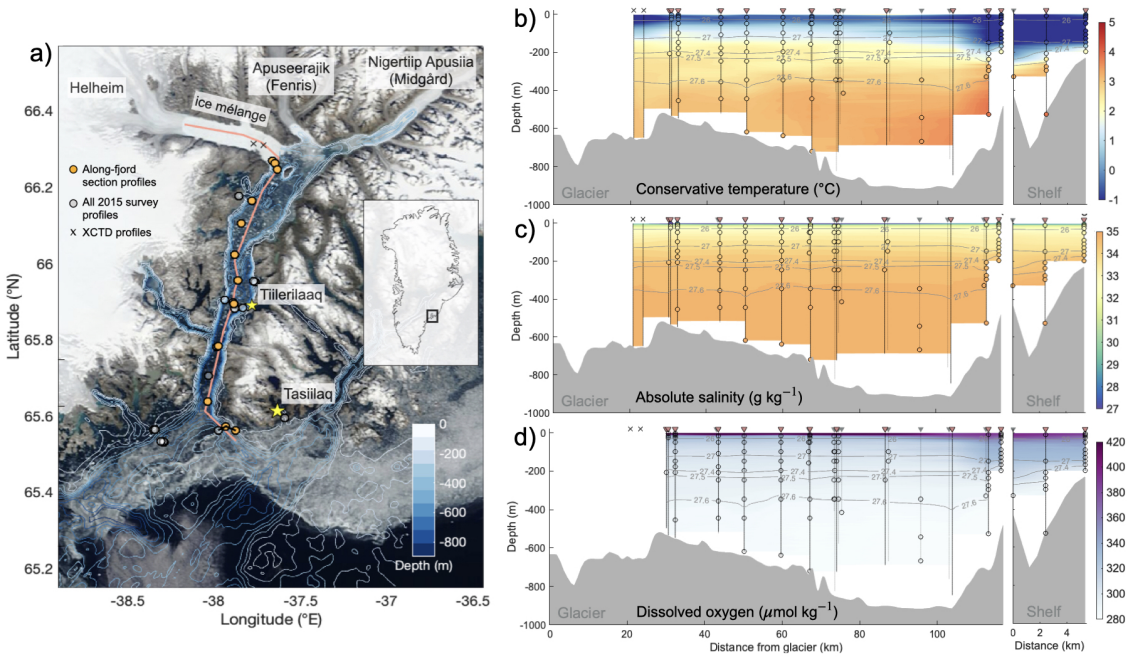


**Figure 2.1.** a) Map of Sermilik Fjord region in Southeast Greenland with major fjord branches and regions labeled. All profiles from the 2015 survey are shown (grey), with selected profiles shown in the along-fjord sections (b–d) in orange. XCTDs from 2015 and used in this study are labeled. Bathymetry is shown as colored contours with 100 m increments and is derived from BedMachine Greenland v4 (Morlighem et al., 2017). The pink line represents the thalweg section of the fjord, used in plotting the bathymetry for b–d. The thalweg section end point is the Helheim Glacier terminus position in 2019. Background image is Terra MODIS corrected reflectance (true color) satellite image on August 9 2015. This image was obtained from NASA Worldview Snapshot application (https://worldview.earthdata.nasa.gov), part of Earth Science Data Information System (ESDIS). Along-fjord sections of b) conservative temperature (°C) c) absolute salinity g kg$^{-1}$ and d) dissolved oxygen ($\mu$mol kg$^{-1}$. Vertical lines are CTD profile extents used in the contour plot. Circles represent bottle sample locations. $\sigma$= 26, 27, 27.4, 27.5, and 27.6 isopycnals are shown in each plot as grey lines.

linear system. This enabled a robust and unambiguous separation of SWT constituents.

Subsequent studies have applied different methods to estimate water mass fractions in Sermilik Fjord, not as their primary scientific objective, but as a necessary component of investigations into fjord biogeochemistry. Cape et al. (2019) quantified water mass fractions in service of estimating nutrient fluxes associated with buoyancy-driven upwelling at Helheim Glacier. They used the classical OMPA approach on data from the same 2015 survey as Beaird et al. (2018). Instead of noble gases, they treated nitrate and silicate as conservative tracers

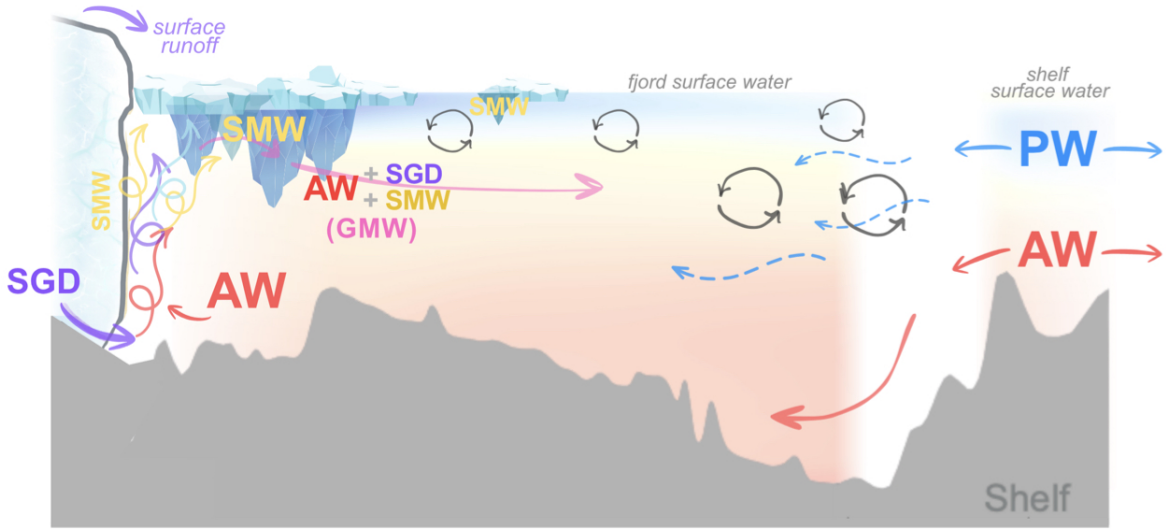


**Figure 2.2.** A schematic of Sermilik Fjord identifying the origins and regions of input for the four source water types (SWT) used in this study: AW (red), PW (blue), SGD (purple), and SMW (yellow). Glacially Modified Water (GMW), the product of SWT mixing, is shown in pink. The size of the lettering corresponds to the expected amount of input of each SWT. Grey arrows indicate areas of mixing. Dashed blue arrows indicate the variability of PW extending into the fjord. The background color gradient approximates ocean temperature such that red (blue) indicates generally warmer (colder) temperatures. The depths and lengths are not to scale. The glacier represented is Helheim Glacier, with a mélange region indicated, for an along-fjord section of the Helheim - Sermilik fjord system approximated by the pink thalweg line in Figure 2.1.

below the surface layer (¿ 30 m depth) to create an exactly determined system of equations. Lindeman et al. (2024), in a study focused on mercury cycling within the fjord, applied the same OMPA framework using data from a 2021 survey with DO as a conservative tracer to create their exactly determined system of equations. This approach utilized the fact that SMW is typically supersaturated in DO, and that AW and PW on the East Greenland shelf are characterized by distinct DO values.

Taken together, these studies illustrate the spectrum of data types and SWT assumptions that have been applied to the same physical system—from the maximally constrained noble gas approach to the more data-limited, yet more accessible, configurations using nutrients and DO—while each making different tradeoffs. Here, we present the first study comparing these

approaches and reporting uncertainty values informing data requirements and methods for water mass fraction analyses in glacial fjord systems.

We use the noble gas-derived water mass fraction estimates from Beaird et al. (2018) as a reference case and apply the methods developed in the preceding sections to the same data inputs. This allows a direct and quantitative comparison of how different data requirements, observation choices, and SWT assumptions propagate into different estimates of water mass fractions.

### 2.3.1 Comparison framework

We define three primary analyses that vary the method and observational inputs while holding the input observations fixed. The results from these analyses are compared against each other and the noble gas-derived reference case ($\mathbf{OMP_{NG}}$).

$\mathbf{OMP_{TSO}}$ applies classical OMPA using temperature, salinity, and dissolved oxygen, producing a unique algebraic solution at each data point with no prior information.

Regularized least squares with prior information analyses will be called RLS experiments. $\mathbf{RLS_{TSO}}$ applies the RLS method with temperature, salinity, and dissolved oxygen and a spatially varying $\mathbf{P}$, enabling formal uncertainty quantification and isolating the effect of prior information relative to $\mathrm{OMP_{TSO}}$.

$\mathbf{RLS_{TS}}$ applies the RLS method using only temperature and salinity, representing the most data-limited scenario. Observations from XCTDs are used as additional input in this experiment to extend the spatial extent of the water mass fraction results. Comparison of $\mathrm{RLS_{TS}}$ against $\mathrm{RLS_{TSO}}$ isolates the contribution of DO, while comparison against $\mathrm{OMP_{NG}}$ quantifies what is lost by relying on temperature and salinity alone.

Supplementary analyses presented in Appendix A include $\mathrm{RLS_{TSO}}$ and $\mathrm{RLS_{TS}}$ solutions with a spatially constant $\mathbf{P}$, exploring the contribution of spatially varying prior information, and a demonstration that the RLS framework recovers the $\mathrm{OMP_{TSO}}$ solution, confirming that classical OMPA is a limiting case of the more general RLS formulation.

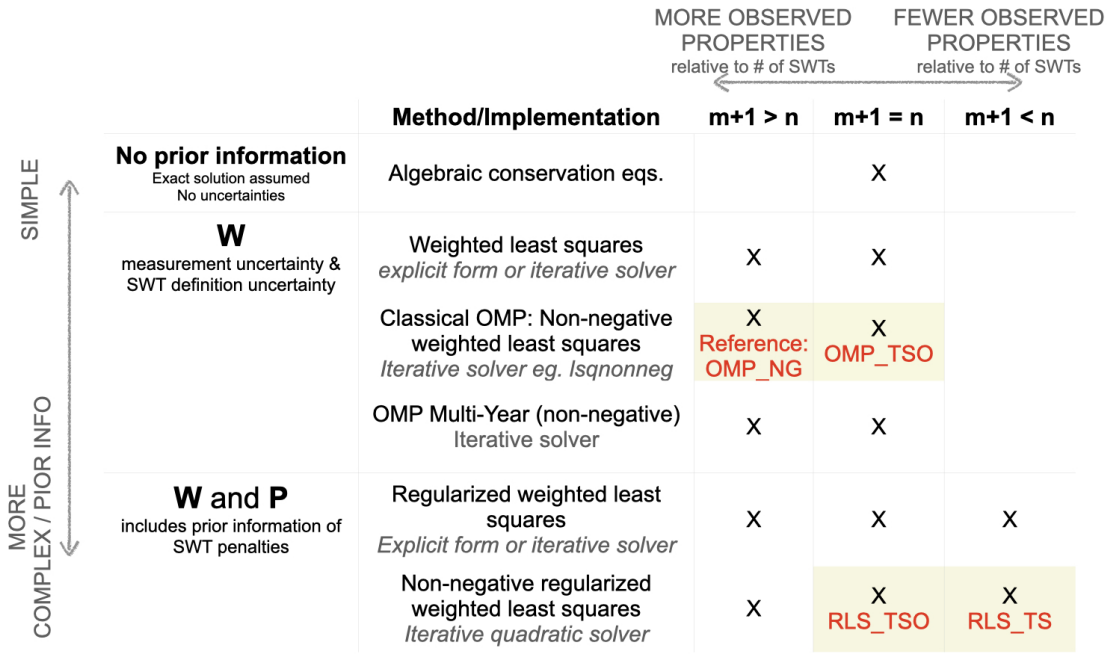


**Figure 2.3.** Schematic indicating the relationships between the different methods discussed in this section, defined by number of observed properties relative to SWTs and complexity/use of prior information. Shaded table cells indicate the methods tested and compared in the following Sermilik Fjord case study.

### 2.3.2 2015 Survey Data Description

We applied the different water mass fraction methods presented here to observations collected during an August 2015 survey of Sermilik Fjord (Figure 2.1). The data and survey are previously described in full in Beaird et al. (2018) and Cape et al. (2019), but we summarize key points for the intercomparison study here.

#### CTD and DO Data

33 profiles of conductivity, temperature and depth (CTD) were collected between the surface and 10 m above bottom using a SBE 25plus Sealogger CTD from Sea-Bird Scientific (Figure 2.1). In-situ temperature and conductivity were transformed to conservative temperature

(°C) and absolute salinity (g $kg^{-1}$) values using TEOS-10 and GSW (**?**). All values of temperature and salinity reported here are in these units. Dissolved oxygen (DO) profiles were collected using a SBE 43 DO sensor integrated into the CTD's pumped flow path. In-situ DO values were transformed from mL/L to $\mu$mol $kg^{-1}$ using Garcia and Gordon (1992). Measurement uncertainty from the manufacturer is listed as ±2% of equilibrium saturation (SeaBird). For DO values in this dataset, this results in measurement uncertainty of ±6.4–8 $\mu$mol $kg^{-1}$. Note that Winkler titrations of water samples were not conducted to calibrate DO values, therefore values reported here should not be compared directly to other studies. Despite this, we can still treat the relative DO values within this particular survey as a conservative tracer. We note that the DO values fall within the range of other observations from Sermilik Fjord and the East Greenland Shelf (García-Ibáñez et al., 2018; Lindeman et al., 2024).

**Discrete bottle samples**

In contrast to continuous profiles of temperature, salinity, and DO, discrete bottle samples were collected at a variety of depths and profiles and later analyzed for nitrate, silicate, and dissolved noble gas concentrations (Figure 2.1). Details of those measurements and methods are available in Beaird et al. (2018). Note that water mass fraction estimates derived from discrete bottle sample observations have decreased spatial vertical density relative to continuous profile observations. The water mass fraction results at each bottle sample are then interpolated within $\Theta$–$S_A$ space to the full profiles to produce contour plots of water mass fractions covering the full fjord domain.

**XCTD Data**

The method presented here allows us to use temperature and salinity from XCTD profiles because other variables are not needed. XCTD profiles were collected July 27 2015, approximately one week to two weeks prior to the ship-based CTD survey conducted between August 2–11 2015. Two XCTD profiles were located in the ice mélange region where the ship could

**Table 2.2.** Source water type (SWT) end-member properties of conservative temperature ($\Theta$), absolute salinity ($S_A$), and dissolved oxygen (DO) and the combined measurement and definition uncertainty ($\pm\sigma$) for each. These property values are used in the $OMP_{NG}$ (excluding DO), $OMP_{TSO}$, $RLS_{TSO}$, and $RLS_{TS}$ (excluding DO) solutions. The uncertainties are used in $OMP_{NG}$ (excluding DO) and $OMP_{TSO}$, both applied in traditional OMP weighting schemes. The relative uncertainty values are used to inform values for the $RLS_{TSO}$ and $RLS_{TS}$ **W** matrices.

| Source Water Type (SWT) | $\Theta$ (°C) | $\pm\sigma_\Theta$ (°C) | $S_A$ ($g\,kg^{-1}$) | $\pm\sigma_{S_A}$ ($g\,kg^{-1}$) | DO ($\mu mol\,kg^{-1}$) | $\pm\sigma_{DO}$ ($\mu mol\,kg^{-1}$) |
|---|---|---|---|---|---|---|
| Atlantic Water (AW) | 3.89 | 0.1 | 34.99 | 0.1 | 275 | 10 |
| Polar Water (PW) | -1.55 | 0.1 | 33.80 | 0.1 | 348 | 10 |
| Subglacial Discharge (SGD) | 0 | 2 | 0 | 0.01 | 457 | 30 |
| Submarine Meltwater (SMW) | -87 | 4 | 0 | 0.01 | 1050 | 50 |

not sample and the other three profiles were located at the confluence of Helheim Fjord and the main Sermilik Fjord branch. Using the XCTD profiles spatially extends the temperature and salinity section of the fjord. They were not used in the previous water mass fraction studies as more variables beyond temperature and salinity were needed. We add the XCTD profiles to the CTD temperature and salinity record to showcase the use of the underdetermined system method presented here with XCTD data. We assume that the general hydrographic structure of the fjord was unchanged between the time of XCTD and CTD data collection. Comparison of the XCTD and CTD profiles show deep AW with similar properties and no measurement bias in the XCTD data. Roth et al. (2025a) includes detailed methodology and data treatment of the XCTD profiles from this survey and others in Sermilik Fjord.

### 2.3.3 Source Water Type Definitions

A critical step in any water mass fraction analysis is the definition of SWTs, both which SWTs are used and the specific property and uncertainty values assigned to define them. These are subjective choices that, part of every water mass analysis regardless of method, and should be well-justified and reported. The properties used for each SWT can be defined in numerous ways depending on the focus of a given study. Below, we justify our choice of definitions, but there may be more appropriate definitions for different fjords or studies.

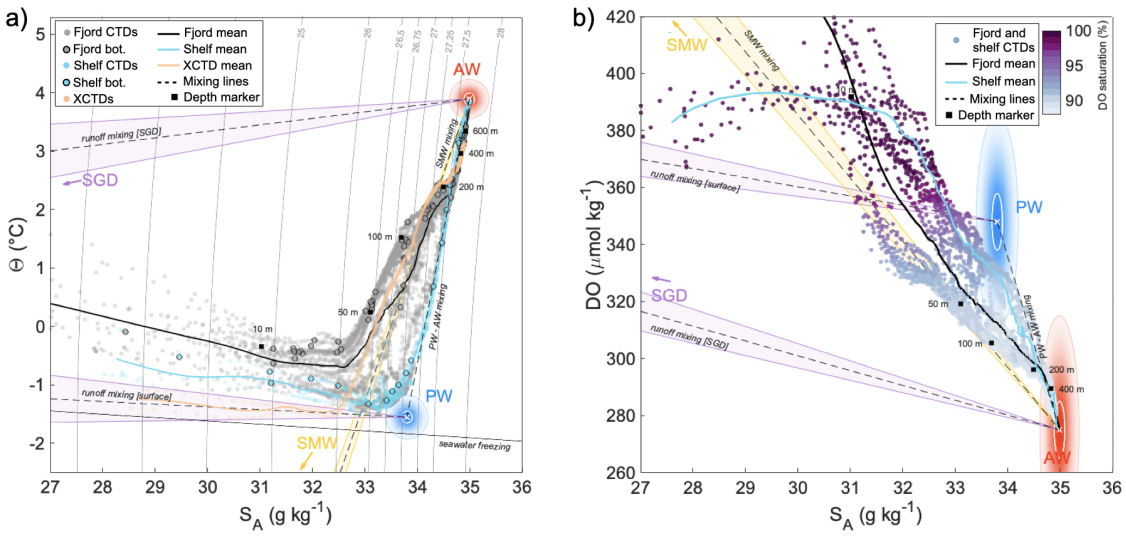


**Figure 2.4.** a)Θ–$S_A$ plot and b)DO–$S_A$ plot of CTD data from the 2015 survey. For a) Profiles from within the fjord are grey and shelf profiles are light blue. Bottle sample locations are shown as black outlined circles. XCTD data from 2015 are shown in orange. Isopycnals are plotted in the background as grey lines. For b) data points are colored in with oxygen saturation percentage. For both panels, SWT endmembers (AW, PW, SGD and SMW) used for the OMP-TSO, RLS-TSO, and RLS-TS configurations are plotted with values from Table 2.2, and mixing lines between them are indicated by dashed lines. The white circle around the AW and PW endmember property points indicate the $\sigma$ uncertainty used to define the W matrix. The outermost circle represents the range of values used in Monte Carlo experiments to calculate endmember uncertainty. The shaded purple and yellow lines represent the $\sigma$ uncertainty values for SGD and SMW, respectively. Black squares indicate depth for one fjord profile in each plot.

### Atlantic Water

Atlantic Water (AW) is the primary source of heat and salt in the subsurface fjord waters. AW in the Sermilik Fjord region is characterized by temperatures and salinities ranging from 3–5 °C and 34.5–35 g kg$^{-1}$ respectively. The DO concentrations are the lowest of the water masses in our system, ranging from 275–285 $\mu$mol kg$^{-1}$. AW properties are not completely uniform in deep fjord waters and do have some along-fjord variability due to temporal variability of AW arriving on the shelf, which then works its way into the fjord at depth.

Here we defined AW SWT properties using the Θ–$S_A$ maximum observed in all hydro-

graphic profiles, where AW properties are least modified by mixing. The other variables (DO, noble gas concentrations) were then selected from the corresponding maximum $\Theta$–$S_A$ point. For studies specifically at the terminus or in the plume region, an option is to define the AW properties at the depth of the grounding line to capture the properties of the water entrained by the plume. Here, because we are considering the full fjord section and shelf, we define the AW by the maximum properties of all profiles.

**Polar Water**

Polar Water (PW) originates from the Arctic Ocean and is transported southward along the East Greenland shelf by the East Greenland Coastal Current, mixing further with exported fjord waters and sea ice melt along the way. PW occupies the upper water column on the shelf, distinguished from AW by near-freezing temperatures ($<$0 °C) and comparatively fresh salinities (30–33 g kg$^{-1}$).

PW SWT properties were defined by extending the PW–AW mixing line to meet the coldest observed PW temperature in the dataset from the shelf profiles. This results in a $\Theta - S_A$ property pair that was not actually observed. Instead, it is represents the properties that can best capture the water mass fractions both along the AW–PW mixing line and mixing with the subsurface waters exported from the fjord. The choice of DO endmember is more subjective. We chose to use a value that follows the PW–AW $S_A$–DO mixing line and matches the endmember salinity value defined in $\Theta - S_A$ space. This results in a DO value that is below equilibrium saturation, meaning that it has not equilibrated with atmospheric surface conditions. Ignoring any biological processes, we assume this is a DO signature of subsurface PW without any influence of atmospheric exchange.

**Runoff: Subglacial Discharge**

Subglacial discharge consists of meteoric meltwater routed beneath the Greenland Ice Sheet and discharged at the grounding line of outlet glaciers, often hundreds of meters below

the ocean surface. The grounding depth for Helheim Glacier is estimated to be between 500–650 m (Morlighem et al., 2017), though recent work has revealed there may channels along a heterogenous grounding zone that reach nearly 900 m(Kim et al., 2025b). While observations of pure SGD do not exist, we assume SGD is effectively fresh ($S_A = 0$), and because it is in contact with glacial ice at the bed, we assume it is 0 °C. Dissolved oxygen in subglacial discharge is more uncertain and likely more variable, as it depends strongly on subglacial routing, microbial activity, and seasonal discharge regime. We assume that meltwater and precipitation are at the surface long enough before entering the subglacial system to reach equilibrium saturation and calculate the equilibrium concentration for freshwater at 0°C under standard atmospheric pressure ($\sim$456 $\mu$mol kg$^{-1}$). The runoff mixing lines in Figure 2.3b approximate the slope of the data in $S_A$–DO space where we expect AW and SGD to be mixed providing reassurance that the chosen values are appropriate.

Our temperature and salinity uncertainties for SGD are ±2°C and ±0.01 g kg$^{-1}$ respectively, based on previous OMP studies (Beaird et al., 2015, 2018). We calculated the associated range of equilibrium saturation values using the temperature uncertainty range to find a DO uncertainty value (±30 $\mu$mol kg$^{-1}$).

**Submarine Melt Water**

Submarine melt water is produced by the oceanic melting of glacier ice (both at the terminus and icebergs) below the water surface. Unlike SGD, which is assumed to be liquid as it enters the ocean, SMW is defined as glacial ice taking up necessary heat from the ocean to reach the melting point. An effective temperature calculated using the latent heat of fusion is used (Gade, 1979; Jenkins, 1999; Straneo and Cenedese, 2015). Depending on the assumed ice temperature, the effective temperature of SMW can range from -85 to -95°C. For tidewater glaciers in Greenland, it is often assumed that the SMW effective temperature property is -87 ± 4°C.

Like SGD, SMW DO concentration is more uncertain. SMW is formed by glacial ice

melting beneath the ocean surface, therefore we calculate the resulting oxygen concentration assuming that all gases contained in the ice are forced into solution (Beaird et al., 2015; Lindeman et al., 2024).

**Surface Water treatment and additional SWT considerations**

Many OMP analyses include a surface water endmember to account for warmer buoyant water found near the ocean surface from solar heating and air-sea interaction. However, this endmember is not strictly representative of a distinct water mass formed through conservative mixing processes, but rather reflects non-conservative modifications to water properties driven by surface dynamics.

One option to account for this is to relax the mass conservation constraint at the surface to accommodate these non-water-mass-mixing influences. This approach avoids introducing an artificial endmember while still allowing the system flexibility where conservative mixing assumptions are least appropriate. This would create a spatially varying **W** matrix similar to a spatially varying **P** matrix introduced below. We choose not to address this in order to focus on the effects of **P** in our methodological choices and keep **W** spatially constant. Therefore, we accept that the mixing model we have constructed is not appropriate for the surface and we will not interpret results above 50 m.

The SGD endmember (0°C, 0 g $kg^{-1}$) is permitted to contribute at the surface layer, serving as a proxy for surface runoff, which shares the same temperature and salinity properties. This allows the analysis to capture near-surface freshening driven by terrestrial runoff. Different observed properties would be needed to distinguish between surface runoff and subglacial discharge explicitly. For this application, we assume that any SGD values at the surface are from surface runoff and any SGD fraction appearing below 50 m must be true subglacial discharge.

Additional SWTs have been employed in the literature depending on the regional context and scientific objective. Sea ice melt and ancient glacial ice melt, for instance, have been used in studies where isotopic or chemical signatures allow these sources to be distinguished from SMW

(Beaird et al., 2018; Rysgaard et al., 2024). Whether such endmembers are warranted depends heavily on both the research question and the properties available in the observational dataset; without sufficient tracer contrast, the inclusion of additional endmembers risks under-constraining the system and producing non-unique solutions.

It is also worth noting that SMW need not be treated as actively melting ice using a latent heat formulation. In regions distant from glacial margins or significant iceberg concentrations, SMW may be better represented as a liquid freshwater source, as the ocean is not necessarily losing substantial heat to drive in situ melting. In such cases, the thermal signature typically associated with meltwater may be diminished or absent. Careful analysis of $\Theta$–$S_A$ diagrams and relevant property plots is therefore essential to assess which endmember configuration is most physically appropriate for a given study region and dataset.

**Constructing user-defined data weights, W**

The diagonal values of **W** are constructed from the combined instrument and SWT definition uncertainties listed in Table 2.2. As described in Section 2.2.7, the relevant uncertainty for each tracer reflects both the measurement precision and confidence in the SWT property definition, whichever is larger. For temperature and salinity, instrument uncertainties are small ($\pm 0.002$ °C and $\pm 0.005$ g kg$^{-1}$ respectively); SWT definition uncertainty dominates for all four water masses. For SGD, the temperature uncertainty of $\pm 2$ °C reflects the range of plausible runoff temperatures, while the salinity uncertainty of $\pm 0.01$ g kg$^{-1}$ reflects our high confidence that SGD is effectively fresh. For SMW, the temperature uncertainty of $\pm 4$ °C captures the range of effective temperatures arising from different assumed ice temperatures, while the salinity uncertainty is similarly small at $\pm 0.01$ g kg$^{-1}$. For DO, uncertainties of $\pm 10$ $\mu$mol kg$^{-1}$ are assigned to AW and PW reflecting sensor precision and definition uncertainty, while larger values of $\pm 30$ and $\pm 50$ $\mu$mol kg$^{-1}$ are assigned to SGD and SMW respectively, reflecting the greater uncertainty in their DO endmember definitions. Mass conservation is assigned a tight uncertainty of $\sigma_{\text{mass}} = 0.003$, enforcing it as a near-strict constraint. Each uncertainty value was

then normalized following methods in Section 2.2.7.

**Constructing user-defined SWT penalties, P**

The penalty matrix **P** encodes our prior physical knowledge about the expected spatial distribution of each SWT into the equation machinery. We construct a spatially varying **P** as described in Section 2.2.7, with diagonal elements varying as a function of depth and along-fjord position (Figure 2.4). The base penalty values reflect the expected dominance of each SWT across the full fjord domain: AW receives the weakest penalty as the dominant water mass in the deep fjord; PW receives a moderate penalty reflecting its presence in the upper water column and at the fjord mouth but absence in the mélange and deep fjord; SGD and SMW receive the strongest penalties, particularly at depth, consistent with their small fractions.

For this Sermilik Fjord case study, we constructed **P** in three steps: deriving a physically informed spatial structure from existing water mass fraction estimates, interpolating that structure across the full fjord domain, and scaling the result to achieve appropriate balance with **W**.

We created an initial field of each SWT penalty by interpolating the noble gas fraction results from the discrete water samples (Beaird et al., 2018) to the Sermilik Fjord climatology developed in Roth et al. (2025a) within $\Theta$–$S_A$ space. From these interpolated fields, representative profiles for the mélange, midfjord, mouth, and shelf regions were chosen. These profiles of water mass fractions were then linearly interpolated and heavily smoothed in the along-fjord direction to fill in the full fjord and shelf domains. The goal was to produce the persistent hydrographic patterns in Sermilik Fjord, without the specific details and small-scale perturbations of a specific survey, with smooth variation between fjord regions rather than discontinuities. The shelf and fjord regions are discontinuous reflecting their dramatic property difference from the fjord, particularly in 2015.

At this point, the magnitude of the each penalty field was between 0 and 1 since they were derived from fraction results. We scaled the spatial fields for each SWT so that their means and distributions were preserved relative to one another, while their overall magnitude was brought

to the scale required for $\mathbf{W} \approx \mathbf{P}$ balance as assessed by the Frobenius norm ratio $\lambda$.

Finally, we applied additional spatial variation with depth uniformly across the along-fjord domain. SMW and SGD were strongly suppressed below 400 m and near the surface ($< 50$ m), where AW is absent, we maximized the AW penalty.

To assess the effect of spatial variation in $\mathbf{P}$, we compared the $\mathrm{RLS}_{\mathrm{TS}}$ solutions obtained with the spatially varying $\mathbf{P}$ against solutions obtained with a constant $\mathbf{P}$ matrix using the domain-mean penalty values. The constant $\mathbf{P}$ values used were $P_{1,1} = 0.5$, $P_{2,2} = 8$, $P_{3,3} = 500$, $P_{4,4} = 500$, representing the penalties for AW, PW, SGD, and SMW.

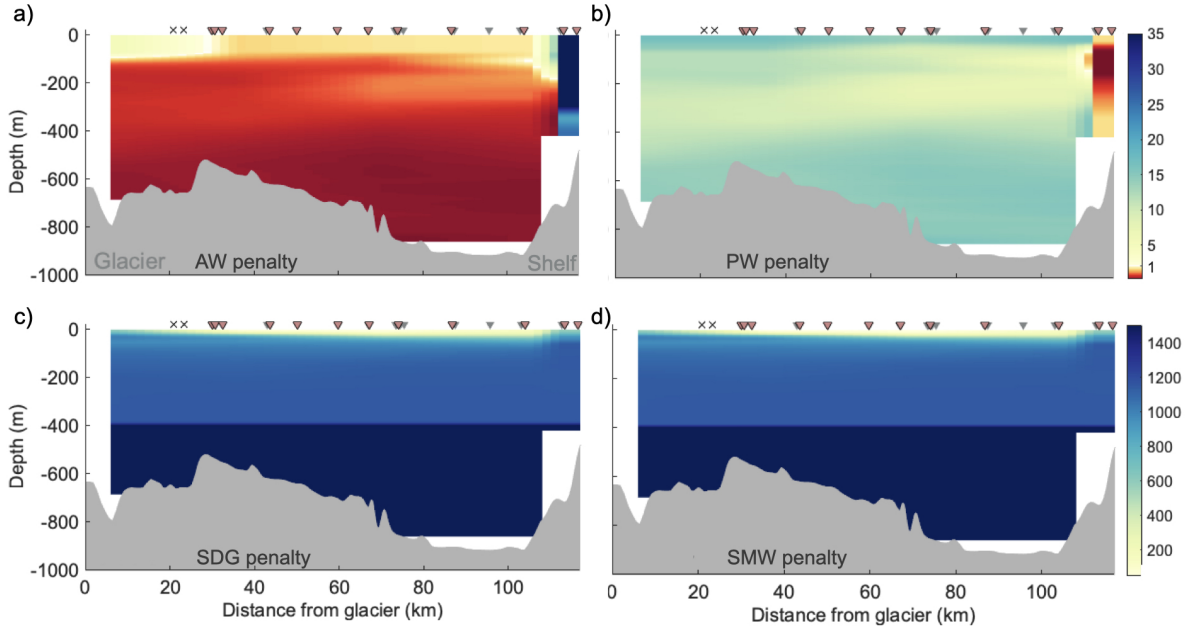


**Figure 2.5.** Spatially varying penalty matrix $\mathbf{P}$ values for each source water type across the Sermilik Fjord domain. Panels show the diagonal penalty values for a) Atlantic Water (AW), b) Polar Water (PW), c) Subglacial Discharge (SGD), and d) Submarine Meltwater (SMW). AW and PW panels share a non-uniform color scale from 0–35 to highlight the order-of-magnitude difference in penalty values between these water masses across the fjord. 0–1 is noted by red color scale. SGD and SMW panels share a uniform color scale from 200–1400. Larger values indicate stronger suppression of the corresponding SWT in the solution. Bathymetry is shown in grey and derived from BedMachine Greenland v4 (Morlighem et al., 2017). CTD (triangles) and XCTD (x) profile locations from the 2015 survey are indicated at the top of each panel. The horizontal axis represents along-fjord distance from the 2019 Helheim Glacier terminus.

## 2.4 Results

### 2.4.1 Comparison of all solutions to reference case

We compared the water mass fraction solutions from the three different configurations (OMP-TSO, RLS-TSO, and RLS-TS) to the reference case solutions from noble gas observations, with specific attention to average magnitude of the fractions across the domain and spatial patterns. We subtracted along-fjord sections of fraction solutions from the reference case to produce anomalies and evaluated the anomaly magnitudes and spatial patterns (Figure 2.6). The solutions are also presented in profile-depth space (Figure 2.7, where the four SWT fractions of every CTD profile are plotted on the same axes with their associated uncertainty values from Monte Carlo simulations.

Across all methods, the most general characteristics of the reference case were reproduced: 1) AW fractions dominate across the fjord, particularly at depth, with values ranging from 70–100% within the fjord, 2) PW fractions are inversely proportional to AW fractions, with the greatest PW fractions at the mouth and shelf above 200 m, and 3) SGD and SMW are small (¡ 5%) in the subsurface and are 0% below 300 m. In general, we will not compare surface values above 50 m as this region of the fjord is not well represented by the SWTs and mixing models we constructed.

AW and PW have anomalies ranging from -30% to +30%, with the largest anomalies concentrated at the surface, mouth, and shelf regions. The mean AW and PW anomalies are more promising, representing the majority of the fjord domain. All methods produce AW fractions (PW fractions) slightly less than (more than) the reference case. AW fjord mean anomalies are 6 ± 10%, 1 ± 9%, and 1 ± 9% and PW fjord mean anomalies are -9 ± 12%, -4 ± 9%, and -4 ± 7% for OMP-TSO, RLS-TSO, and RLS-TS respectively. OMP-TSO is the method that most underestimates AW and overestimates PW compared to the reference. This leads to OMP-TSO also presenting the greatest anomalies in the SGD and SMW fractions.

SGD fjord mean anomalies are -0.3 ± 1.1%, -0.2 ± 1.0%, and -0.2 ± 0.9% and SMW

fjord mean anomalies are 0.1 ± 0.6%, -0.2 ± 0.5%, and -0.2 ± 0.5% for OMP-TSO, RLS-TSO, and RLS-TS respectively. The spatial mean hides that OMP-TSO is underestimating subsurface SMW in the mélange to mid-fjord regions and overestimating SMW in the mouth to shelf region, therefore balancing out in the mean value. The pattern of the SMW anomaly is related to the underestimation (overestimation) of PW at the mouth (mélange to midfjord regions) in the OMP-TSO analysis.

Across all methods and SWTs, the mouth region above 300 m shows the greatest anomalies. This is not surprising given that the mouth region is defined by complex interleaving and mixing of PW and subsurface SMW and SGD (the latter two mixed heavily with AW). Without prior information, the uncertainty on the fractions is largest in this region, evident in the large uncertainty spread in the OMP-TSO profiles above 300 m (Figure 2.7b). Because all SWTs are present in this region, a perturbation in one SWT results in many possibilities for redistributing its fractional contribution to the other SWTs, increasing uncertainty. For methods using the spatially varying **P** matrix (RLS-TSO and RLS-TS), the solutions are pulled to match the **P** values which were specifically constructed from the reference case. Therefore, RLS-TSO and RLS-TS better match the reference case in the mouth region and the uncertainty is reduced. This does not necessarily mean that the RLS solutions are ”true” to the real world, but it reflects the methodological choice to define the reference values as true and construct a **P** to best match these results.

Overall, the two analyses incorporating prior information (RLS-TSO and RLS-TS) reproduce solutions more consistent with the reference case than OMP-TSO. This improvement has two sources. First, **P** enforces spatially distinct fraction structures between the shelf and fjord interior, preventing large anomalies at the mouth as seen in the OMP-TSO results. Second, **P** nudges the AW–PW balance toward the reference case values within the fjord interior, producing larger AW fractions and smaller PW fractions than OMP-TSO. Because SGD and SMW are small fractions superimposed on the dominant AW–PW background, correctly resolving the AW–PW background ratio is necessary for producing appropriate SGD and SMW values.

### 2.4.2 Uncertainties and residuals

For water mass fraction analyses to be comparable across different studies and methods, uncertainties are an important quantity to report. We report the uncertainties on the water mass fractions obtained from Monte Carlo simulations. The uncertainties are visualized in profile-depth space (Figure 2.7) and in along-fjord sections for the RLS-TS case (Figure 2.8) to better assess spatial patterns in uncertainties.

AW and PW uncertainties have a similar spatial pattern, with the greatest uncertainties occurring between 200–300 m in the water column in the mélange to mid-fjords region. This is an area where all four SWTs strongly occur together. As stated previously, in this configuration, a small perturbation in the property definition of one SWT results in multiple ways to redistribute that SWT's fractional contribution across the others, leading to larger uncertainty. SGD uncertainty is essentially zero where SGD fractions are negligible in the deep fjord waters. There is some amount of uncertainty for SMW fractions in the deep waters, despite the fractional values being zero or near zero. We attribute this to the similarity in slopes of the mixing lines between the AW-SMW and AW-PW. The background AW-PW properties in the deep fjord waters can be nearly replicated with a mixture of AW-SMW. Possible combinations of perturbed endmember definitions in the Monte Carlo simulations result in some solutions choosing SMW instead of PW in this region, and therefore this leads to some uncertainty.

The property residuals show how well the mixing model matches the original data points (Figure 2.8). The residual values are a reflection of the **W** values, where higher weighting forces smaller residuals in a given property. Overall, the RLS-TS solution shows the smallest residuals across all properties, including mass, and has the lowest weighted normalized residual norm (resnorm) values compared to the RLS-TSO and OMP-TSO analyses. The spatial pattern of the residuals indicate that the mixing model deviates most strongly from the observations in the shelf region and in the deep fjord. The model is producing deep fjord waters are 0.01–0.02 g $kg^{-1}$ fresher than the observations, an indication that the fraction of AW (a source of salt) is

not high enough. The SWT fraction anomalies also indicate that AW fraction in the deep fjord waters for the RLS-TS case are 5–7% lower than the reference case (Figure 2.6m).

Overall, a rule of thumb adopted in water mass fraction literature is that a mixing model is performing well when residuals are less than 5% of observational values. The residuals for RLS-TS, RLS-TSO, and OMP-TSO all satisfy this.

### 2.4.3 RLS-TSO vs RLS-TS: Is DO adding information?

While both RLS-TSO and RLS-TS analyses can closely reproduce the reference case, we compared the diagnostic metrics between the two methods (Table 2.3 to better understand 1) role of dissolved oxygen in distinguishing between SWTs and 2) the behavior of the minimal data system using only temperature and salinity.

The property–property correlation matrix computed from $\mathbf{W}^{1/2}\tilde{\mathbf{A}}$ shows that temperature and dissolved oxygen are nearly perfectly anti-correlated across all four SWT definitions ($R = -0.98$), which might suggest that oxygen is globally redundant with temperature and could be safely excluded. However, the SWT–SWT correlation matrix reveals that AW and PW are highly collinear ($R = 0.99$) in the weighted property space—meaning that temperature and salinity alone struggle to distinguish between these two dominant water masses. This may be surprising considering the distinct temperature difference between the two water masses, but AW and PW are nearest SWT pairs within the full range of $\Theta$–$S_A$ space defined by all SWTs. Although oxygen tracks temperature globally across all SWTs, AW and PW have meaningfully different dissolved oxygen signatures. Therefore, dissolved oxygen provides resolving power specifically for the AW–PW pair.

This distinction is quantified directly by the weighted condition number $\kappa(\tilde{\mathbf{A}}^\top \mathbf{W}\tilde{\mathbf{A}})$. For RLS-TSO, $\kappa(\tilde{\mathbf{A}}^\top \mathbf{W}\tilde{\mathbf{A}}) \sim 10^4$, indicating a moderately well-conditioned system in which the data provide meaningful constraints on all four SWT fractions. For RLS-TS, $\kappa(\tilde{\mathbf{A}}^\top \mathbf{W}\tilde{\mathbf{A}}) \sim 10^{16}$, indicating a nearly singular system in which temperature and salinity alone cannot reliably distinguish between SWTs. Critically, once the prior information is incorporated, the condition

numbers of $\mathbf{H} = \tilde{\mathbf{A}}^\top \mathbf{W}\tilde{\mathbf{A}} + \mathbf{P}$ are comparable between the two methods. This confirms that $\mathbf{P}$ is compensating for the near-singularity of the temperature and salinity only system—regularization is doing the work in absence of an additional tracer. The RLS-TS solutions are therefore prior-dominated in a way that RLS-TSO solutions are not, with the RLS-TS solutions reflecting the imposed penalty structure more heavily than the observations. This is also confirmed when comparing the Frobenius norm ratios and data influence matrix values of each method (Table 2.3).

The remaining SWT pairs are considerably better separated with temperature and salinity alone. From the correlation matrix, SGD and SMW are well-distinguished from both AW and PW with the SWT definitions used here. The SGD–SMW pair has moderate separation ($R = -0.44$), and oxygen contributes some additional resolving power between these two SWTs. However, the dissolved oxygen endmembers for SGD and SMW have the largest uncertainty, which reduces the effective weight of dissolved oxygen. The primary contribution of dissolved oxygen to the system is therefore distinguishing between AW and PW.

### 2.4.4 Spatially varying P vs. constant P

We performed the RLS-TS analysis with a constant $\mathbf{P}$ matrix to better isolate the effects of a spatially varying $\mathbf{P}$ on the solution. Within the fjord interior, the constant $\mathbf{P}$ solutions are nearly indistinguishable from the spatially varying $\mathbf{P}$ solutions, with anomalies close to zero across all four SWTs (Figure 2.9b–e). This indicates that a constant $\mathbf{P}$ matrix is a viable and practical approach for the fjord interior, and may be a reasonable first-order choice when applying these methods to other fjord systems where spatially resolved prior information about SWT distributions could be unavailable.

The most significant differences are concentrated at the shelf and in the upper water column above 200 m. At the shelf, the constant $\mathbf{P}$ approach underestimates PW and overestimates AW fractions, with the deficit compensated by an overestimation of SMW fractions. This is not a surprise: a constant $\mathbf{P}$ applies the same prior suppression of PW and AW everywhere in

the domain, including the shelf where the AW–PW structure differs markedly from the fjord interior. The spatially varying **P**, by contrast, relaxes the suppression of PW to reflect the reference case fractions in that region and the known two-layer PW/AW structure on the shelf. The misattribution of PW signal to SMW under a constant **P** is consistent with the moderate collinearity between these two SWTs ($R = -0.44$)— without spatially-varying prior information to guide the partitioning, the fractions are distributed according to penalty values that work best in the fjord interior rather than the shelf.

Despite these differences at the shelf, the RESNORM is nearly identical between the constant and spatially varying **P** solutions across the full domain, meaning that both solutions fit the observations equally well. However, the constant **P** temperature residuals are 0.1–0.2 °C warmer than observations throughout the fjord, and larger than the varying **P** temperature residuals. This warm bias is consistent with the underestimation of PW fractions. That RESNORM does change while the temperature residuals do highlights the importance of using the individual property residuals, which can cancel each other out when viewed in aggregate with RESNORM, to assess model behavior rather than just one goodness-of-fit metric.

## 2.5 Discussion

### 2.5.1 Summary of results

We evaluated three water mass fraction analysis configurations using different data types and prior information against a noble gas-derived reference case in Sermilik Fjord, Southeast Greenland. Across all methods, the dominant characteristics of the reference case were reproduced. OMP-TSO, using the most commonly applied OMPA method, produced the largest deviations from the reference case. In the upper water column (above 300 m) AW fractions were underrestimated and PW fractions were overestimated relative to the reference case. Incorporating prior information through regularized least squares reduced anomalies, with the greatest improvement in the mouth and shelf regions where the prior directly constrained the

AW and PW fractions to reflect shelf properties. Dissolved oxygen provides information to distinguish between AW and PW, despite being globally anti-correlated with temperature. For the solutions produced with temperature and salinity alone, regularization strongly compensates for an otherwise ill-conditioned system. We showed that an underdetermined problem setup can result in solutions consistent with the reference case. Finally, a spatially constant **P** matrix performs comparably to a spatially varying **P** in the fjord interior. Our results suggest that a path forward for other fjord water mass studies could be to utilize one **P** matrix for the fjord region and a second **P** matrix for shelf region, and that full spatial variation across a fjord domain is not necessary.

### 2.5.2 The non-negativity constraint: interpretability vs. accuracy

A fundamental choice in this work is the use of a quadratic solver in order to impose a non-negativity constraint on the solutions. This constraint was physically motivated—water mass fractions are by definition bounded between 0 and 1—and it was a necessary step to produce appropriate fractions of PW and SMW in our system. However, negative fractions produced by unconstrained least-squares do contain information and can be assessed, much like residuals, to inform the user of model limitations and successes.

Applying the non-negativity constraint transformed what would otherwise be a closed-form problem into a nonlinear, iterative optimization problem. This nonlinearity complicates uncertainty quantification, and we then used Monte Carlo simulations to assess the uncertainty rather than the covariance matrix.

The use of a quadratic solver places our method on a spectrum of modeling approaches, where interpretability—in the sense of explicit, analytical solutions—is traded for improved solution accuracy. Our results suggest this tradeoff is appropriate for the problem we presented here. Each application of these methods to a new system should assess whether the non-negativity constraint is truly necessary. In a well-conditioned system, unconstrained regularized least squares may produce non-negative solutions naturally, recovering the benefits of increased

model interpretability.

### 2.5.3 Using diagnostics in iterative model construction

Every water mass fraction analysis involves subjective choices: which SWTs to include, which observational properties to use, what endmember property values to assign, and how to weight the observations and SWT definitions. These choices are rarely made in a single step—they require iteration based on an understanding of how the mixing model is behaving. The diagnostics presented here provide guidance and a reproducible approach for model iteration.

The condition numbers $\kappa(\tilde{\mathbf{A}}^\top \mathbf{W}\tilde{\mathbf{A}})$ and $\kappa(\mathbf{H})$ are particularly useful. The first reveals whether the chosen tracers can actually distinguish the SWT definitions from one another, before introducing prior information. SWT–SWT and property–property correlation matrices provide complementary information, identifying which specific SWT pairs are causing conditioning issues and which tracers may be redundant.

$\kappa(\mathbf{H})$ confirms whether $\mathbf{P}$ is sufficiently stabilizing the system. The Frobenius norm ratio and data influence matrix $S_{ii}$ then translate system-level properties into per-SWT assessments of whether the fraction solutions are driven by observations or by prior information. Applied in sequence, these metrics allow a user to trace errors back to their root cause within the subjective choices of model construction and adjust the model accordingly. This iterative workflow is applicable to any water mass fraction problem and is not specific to the Sermilik Fjord system presented here.

### 2.5.4 2015 was an anomalously cold year

All results presented here are derived from the 2015 hydrographic survey and XCTD survey of Sermilik Fjord. This year was an atypical cold year in Sermilik Fjord and the surrounding shelf region relative to the climatological mean (Roth et al., 2025a). The background satellite image in Figure 2.1, taken at the time of the survey, shows dense sea ice being transported along the shelf, indicating cold ocean surface and atmospheric conditions. The consequences

of this are that this survey may represent a time where SGD and SMW input into the fjord are more limited relative to other years, PW may be dominating the hydrographic conditions more than other years, and the AW-PW interface may be deeper relative to other years. For water mass fraction analysis of observations from other time periods in Sermilik Fjord, the **P** may have to be adjusted to reflect different SWT prevalence and spatial patterns.

### 2.5.5 From water mass fractions to improved parameterizations

Water mass fractions have direct applications for quantifying ocean–ice interactions and fjord dynamics. In the near-glacier environment, entrainment within the subglacial discharge plume can be estimated by the ratio of deep water fractions (in this case AW) to SGD and SMW fractions. These values can be used to better inform entrainment coefficients in plume models (Carroll et al., 2015; Ovall et al., 2025). The SGD and SMW fraction fields, when combined with an independent estimate of subglacial discharge flux, can be used to infer the ratio of submarine melting to subglacial discharge and thereby constrain total melt volumes. When combined with velocity observations, spatially varying SMW and SGD fractions can enable the calculation of meltwater volume transports and their vertical structure, as demonstrated by **?**. Meltwater volume transports from Greenland fjords are important boundary conditions in regional and large-scale ocean models for accurately representing freshwater magnitude and distribution.

Determining robust empirical relationships and potentially improved parameterizations, however, requires a more extensive observational foundation than any single survey can provide. The results presented here represent a single summer season during an anomalously cool hydrographic year, and the fraction solutions are specific to this hydrographic state. Translating water mass fraction observations into improved parameterizations of fjord mixing, meltwater export, and submarine melting, requires repeat surveys spanning multiple years, seasons, and fjord systems to capture the full range of variability and to test whether the relationships can be generalized. The framework developed here is transferable to a broader range of surveys, including XCTD surveys where only temperature and salinity are available, providing a consistent

basis for intercomparison across studies.

## 2.6 Recommendations for other fjord systems

The methods and choices available for water mass fraction analysis in glacial fjords can be considered on a spectrum defined by data availability and number of water masses defining the hydrography of a system (Figure 2.2). While the number and identity of relevant SWTs can vary between fjord systems, the four water masses considered here—AW, PW, SGD, and SMW—represent the dominant components of many Greenland glacial fjords, particularly in Southeast Greenland. If we assume use of four SWTs, then data availability determines how one can proceed. If only temperature and salinity observations are available, as in an XCTD survey, then the method used must be regularized least squares with prior information. For each individual problem, the results can be assessed as to whether the non-negative or unconstrained approaches should be used.

Where more data types are available, such as from ship-based CTD surveys, classical OMP or RLS methods can be used. Our results show that the prior information used in the RLS method improves solution accuracy. However, we had high confidence in our prior information derived from constrained noble gas-derived water mass fraction estimates from a previous study. While few fjords will have similar results available to create a data-informed prior, our results show that general knowledge of fjord hydrographic structure is sufficient to construct a physically motivated **P** matrix. We recommend a two-zone approach: within the fjord interior, a spatially constant **P** is adequate, as demonstrated by the near-identical solutions between the constant and spatially varying **P** solutions in this region. At the shelf and mouth, a separate **P** should relax the suppression of PW to reflect the known two-layer shelf structure, with possibly some linear interpolation of the diagonal penalty values across the mouth transition zone.

If some information is known about the relative prevalence of SWTs, the RLS approach should be used. In contrast, if little is known about the relative prevalence of SWTs, OMP can

be used, provided that system is well-conditioned. Solutions should be reported with calculated uncertainties to reflect the larger uncertainty inherent to an approach lacking prior information.

Finally, the diagnostic workflow presented here, including SWT–SWT and property–property correlation matrices, condition number screening, and the data influence matrix, provides a principled basis for evaluating which data types should be used to best distinguish the SWTs of a given system. More tracers are not always better if the information is globally redundant, especially if the uncertainty of an endmember definition for that tracer is large. Adding a tracer without an assessment of its resolving power could lead to making the mixing model more complex for no reason. Redundancy should be assessed in the weighted property space using the correlation diagnostics rather than assumed from physical intuition alone.

## 2.7 Conclusion

We presented a unified framework for water mass fraction analysis in glacial fjords that reframes the problem as iterative model construction rather than a simple computation, with methodological approaches existing on a spectrum defined by data availability and defined water masses of the system. We demonstrated that physically meaningful water mass fraction solutions can be obtained from temperature and salinity observations alone—data types available from the full archive of historical and modern hydrographic surveys—when regularized with prior knowledge about fjord hydrographic structure. This result substantially expands the observational foundation available for water mass fraction analysis in Greenland's glacial fjords, extending it to XCTD surveys and previous ship-based CTD observations that predate routine dissolved oxygen or noble gas sampling.

The diagnostic framework presented here—comprising of SWT–SWT and property–property correlation matrices, condition number screening before and after regularization, uncertainty quantification, and the data influence matrix—provides the tools needed to evaluate, communicate, and compare the subjective choices inherent to every water mass fraction analysis.

Consistent reporting of these diagnostics alongside fraction solutions and their uncertainties is a prerequisite for quantitative intercomparison between studies conducted in different years, seasons, and fjord systems. Such intercomparisons, in turn, are the necessary first step toward the multi-fjord and multi-year empirical synthesis needed to develop generalized parameterizations and boundary conditions that better represent Greenland's rapidly changing glacial fjords in regional and global ocean models.

## 2.8 Acknowledgments

Chapter 2, in full, is based on a paper from Aurora Roth, Matthew Mazloff, Fiamma Straneo, and Margaret Lindeman "Water mass fraction methods in Greenland's glacial fjords with a case study in Sermilik Fjord, Southeast Greenland", 2026, and is currently being prepared for submission. The dissertation author is primary author of this paper.

The authors thank the crew of the *Adolf Jensen* and field team members that conducted the 2015 Sermilik Fjord ship-based hydrographic survey and XCTD survey, making these data possible. Data collection and original analysis in Beaird et al. (2018) were funded by the US National Science Foundation(NSFOCE-1536856). AR's analysis and the work of this manuscript were supported by the Heising-Simons Foundation and the US National Science Foundation. Additionally, we thank Nick Beaird and Morven Muilwijk for their collaboration and code that was incorporated into this analysis.

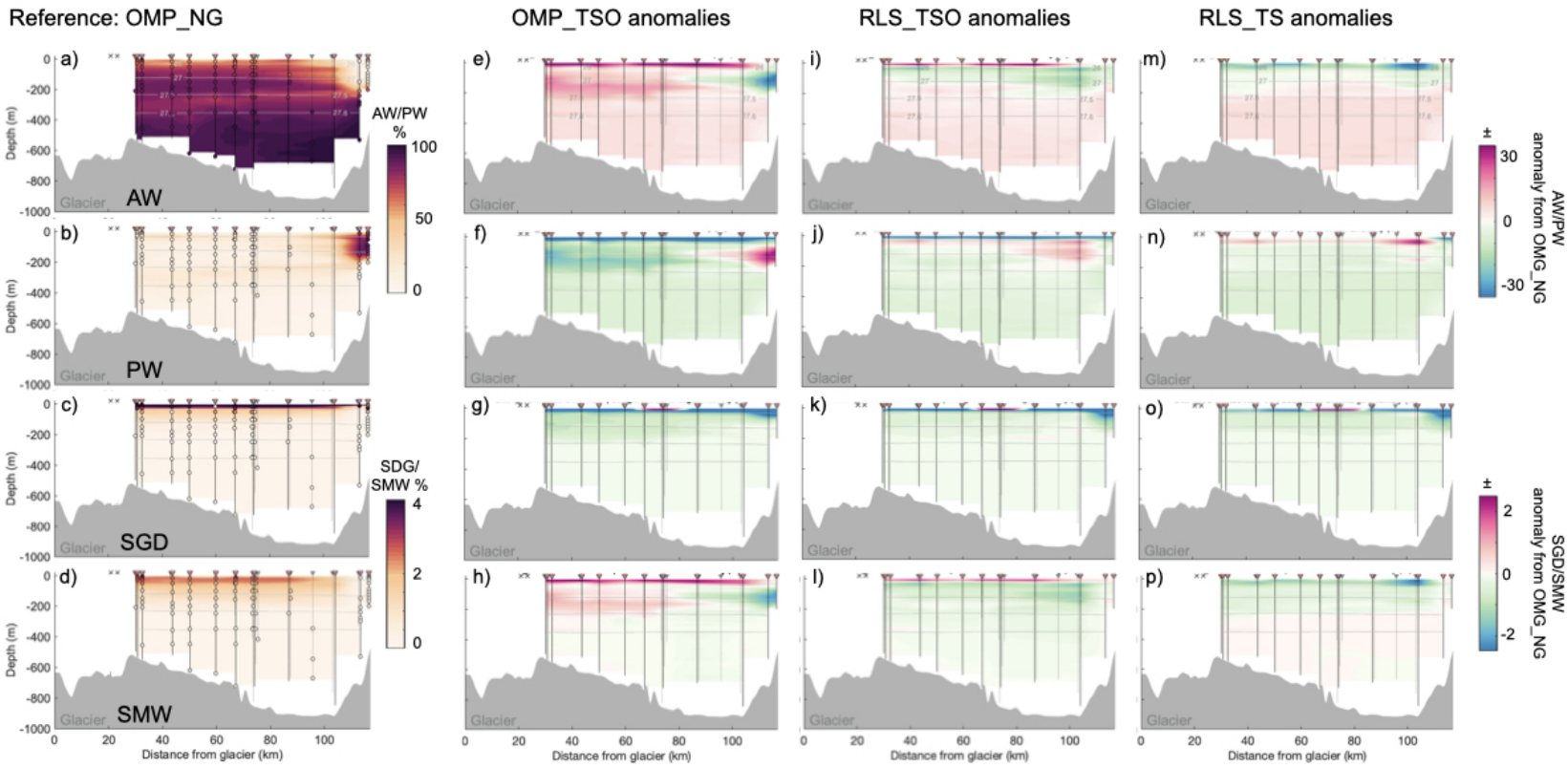


**Figure 2.6.** Comparison of reference case OMP-NG water mass fraction solutions (a–d) to the solutions of the other configurations (e–p). OMP-TSO, RLS-TSO, and RLS-TS solutions were subtracted from the reference case to display the anomalies—warmer colors mean that the reference case had larger fractions, while cooler colors indicate the reference case had smaller fractions. Each row corresponds to a SWT indicated in the reference case, while each column corresponds to the different analysis approaches. Note that AW and PW share a color scale, while SMW and SGD share a different color scale.

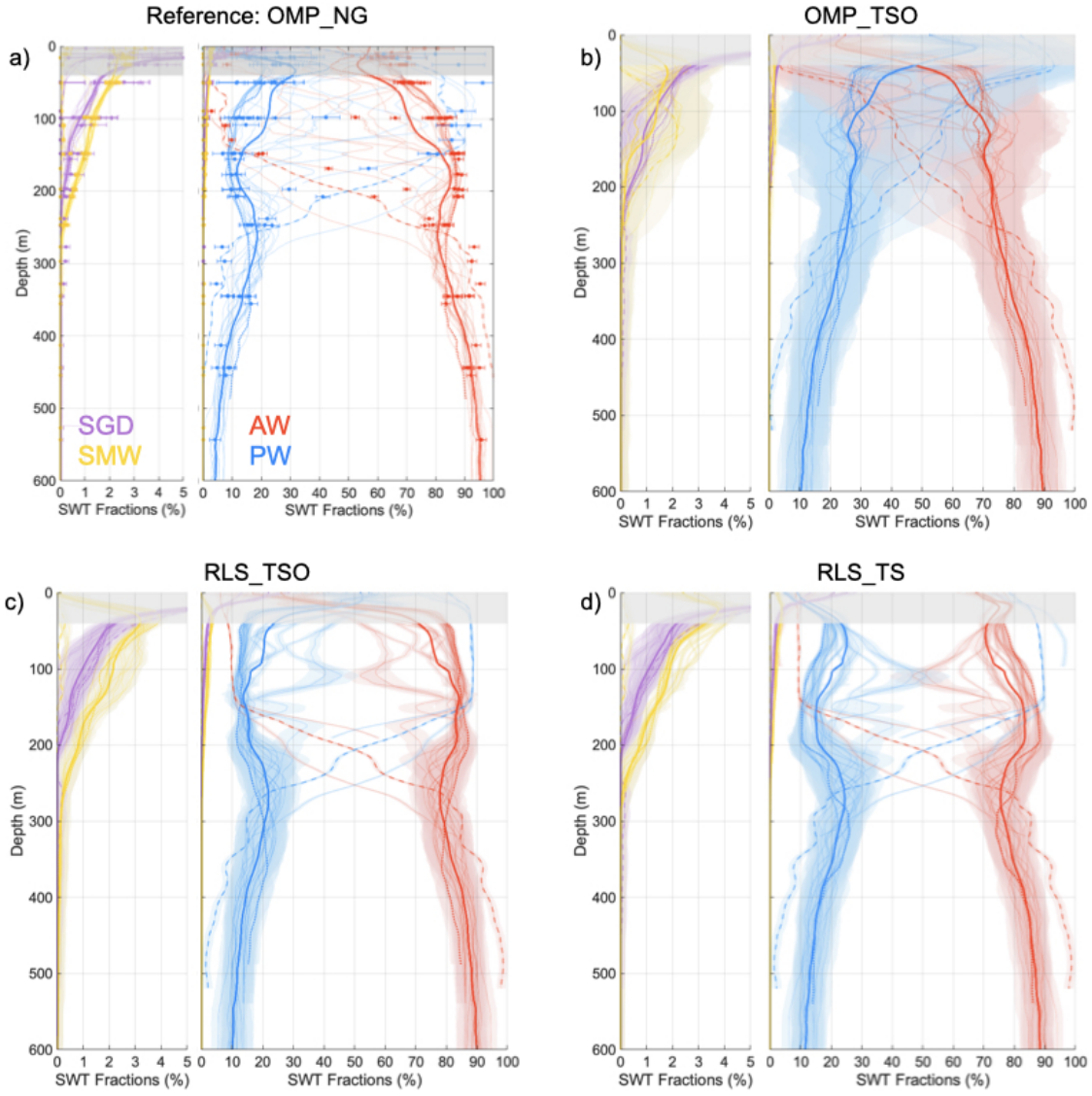


**Figure 2.7.** Profile-depth comparison of water mass fraction solutions of each analysis configuration to the reference case (a). Every profile's four SWT solutions are plotted (thin lines). Bold solid lines represents a fjord mean profile, while the dashed lines are from profile 32 on the shelf. Scattered points in (a) represent fractions calculated at bottle sample locations with associated Monte Carlo-derived uncertainty. For OMP-TSO, RLS-TSO, and RLS-TS, uncertainties are shown for every profile with shading. Grey shading from 0–50m depth indicated that the water mass fraction solutions at the surface are not to be trusted.

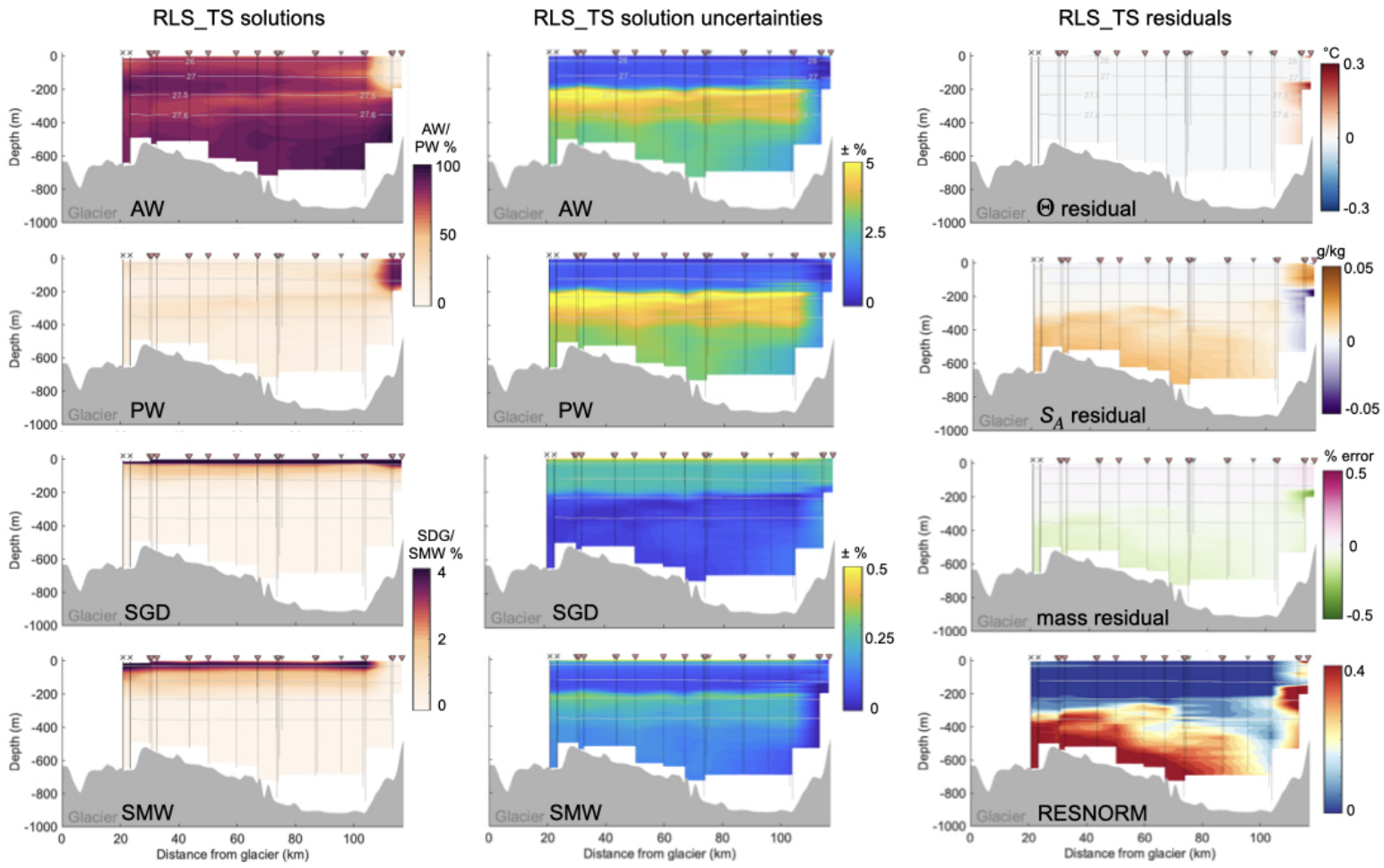


**Figure 2.8.** Along-fjord sections of RLS-TS SWT fraction solutions (a–d), associated Monte Carlo uncertainties (e–h), and property residuals (i–l). The weighted normalized residual norm (RESNORM) is defined as RESNORM $= \tilde{\mathbf{r}}^\top \mathbf{W}\tilde{\mathbf{r}}$ where $\tilde{\mathbf{r}}$ is all the residual values in their normalized space. Note the different color scales for AW/PW and SGD/SMW fractions and uncertainties.

**Table 2.3.** Regularization diagnostics for assessing the balance between the weight matrix $\mathbf{W}$ and penalty matrix $\mathbf{P}$ and conditioning of the system in the regularized least squares (RLS) water mass fraction method, evaluated for both the temperature–salinity (RLS-TS) and temperature–salinity–oxygen (RLS-TSO) formulations applied to the 2015 Sermilik Fjord dataset. The condition numbers, Frobenius norm ratio, and data influence matrix ($S$) are evaluated. Here $n$ denotes the number of source water types (SWTs) and $m$ denotes the number of observed properties. SWTs are Atlantic Water (AW), Polar Water (PW), Subglacial Discharge (SGD), and Surface Meltwater (SMW). Values for the data influence matrix represent the spatial mean across the fjord domain as every data point will have a unique value. Ranges are given for other spatially varying quantities influenced by a spatially varying $\mathbf{P}$.

| Diagnostic | Possible behavior | Interpretation | RLS-TS | RLS-TSO |
|---|---|---|---|---|
| $\kappa(\tilde{\mathbf{A}})$ | Large | Normalized endmember properties. If large, SWTs still not well separated even when normalized; Consider adding another observed property to better separate SWT. | 1.96 | 59.02 |
| $\kappa(\tilde{\mathbf{A}}^\top \mathbf{W}\tilde{\mathbf{A}})$ | Large | SWTs not well separated in observed property space; near-collinearity is a physical property of the endmember configuration. Expected and acceptable; motivates use of $\mathbf{P}$. Consider adding observed properties to improve SWT separation | $1.2\times10^{16}$ | $3.9\times10^{4}$ |
| $\kappa(\mathbf{H})$ | Large despite $\mathbf{P}$ | $\mathbf{P}$ is not sufficiently stabilizing the inversion. Increase diagonal entries of $\mathbf{P}$, particularly for poorly resolved SWTs | $6.7\times10^{2}$–$1.2\times10^{5}$ | $6.7\times10^{2}$–$2.3\times10^{4}$ |
| $\|\sqrt{\mathbf{W}}\tilde{\mathbf{A}}\|_F / \|\sqrt{\mathbf{P}}\|_F$ | $\gg 1$: data dominates; $\ll 1$: $\mathbf{P}$ dominates; $\approx 1$: balanced | Global scalar summary of relative influence of data term vs. penalty in $\mathbf{H}$ | 17–95 | 17–119 |
| $S_{ii}$ (AW, PW, SGD, SMW) | Near 1: data-driven; near 0: prior-dominated | Per-SWT fraction of solution determined by observations rather than penalty. If near 0, reduce P for that SWT or add observed properties | AW: 0.89; PW: 0.42; SGD: 0.94; SMW: 0.74 | AW: 0.93; PW: 0.48; SGD: 0.98; SMW: 0.94 |

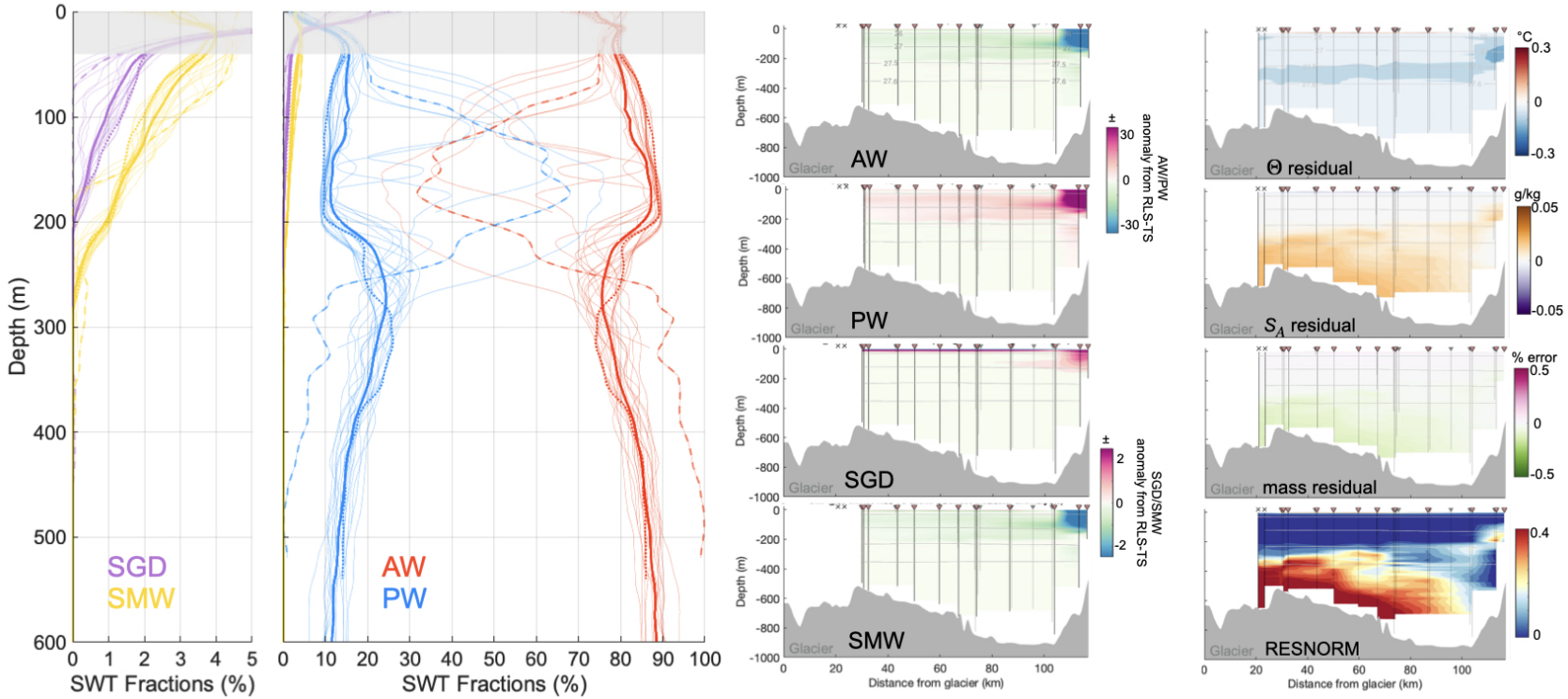


**Figure 2.9.** RLS-TS analysis solutions using a constant **P** matrix (a). The four SWT solutions for each profile are shown (thin colored lines). The bold solid line represents the fjord mean profile, while the dashed line is from profile 32 on the shelf. Grey shading from 0–50m depth indicates that the water mass fraction solutions at the surface are not to be trusted. Along-fjord section anomalies from the RLS-TS solutions using spatially varying **P** matrix for each SWT fraction solution (b–e). Constant **P** solutions were subtracted from the spatially varying **P** solutions. Residual results for each property in along-fjord section for the constant **P** matrix solution.

# Chapter 3

# Beyond temperature and salinity: Long-term water mass fractions reveal persistent composition and plume structure in Sermilik Fjord

## 3.1 Introduction

In Chapter 1, we established the characteristic summer water mass structure in Sermilik Fjord and identified regions with strong temporal variability by exploring deviations from the climatological mean. We showed Atlantic Water, originating from the shelf, fills the deep fjord regions below 400 m, and exhibits some variability in its properties along the fjord. Above this layer, there are strongly varying along-fjord gradients, controlled by Polar Water extending into the fjord from the shelf. Near the glacier, in the ice mélange region, a cold pool from the submarine melt of icebergs sets the properties and is consistent from year to year. Here, in Chapter 3, we now dive deeper into spatial and temporal variability of each particular water mass, with a focus on Glacially Modified Water—the water mass with the fingerprints of ice-ocean interactions in the summer season. This lays the foundation for connecting observed variability to forcing processes, a necessary step toward improved parameterization of fjord dynamics in ocean models.

The central questions motivating this chapter are 1) do constituent water mass fractions

of Atlantic Water (AW), Polar Water (PW), subglacial discharge (SGD), and submarine melt (SMW) within Sermilik Fjord vary in space and time, and 2) if so, can those variations provide insight into the variability and/or stability, and importance of different forcing processes?

Water mass fraction analysis decomposes observed hydrographic properties into a "recipe" of defined source water types (SWTs). Measured properties like temperature and salinity reflect the net result of mixing, while fractions reveal the explicit mixing recipe that led to those properties. Similar measured properties may result from a different set of water mass fractions, or the same fractions may result in different properties due to shifts in SWT endmember property definitions. Water mass fractions provide a distinct and complementary analysis to standard descriptive hydrographic analysis and provide a pathway for connecting observed variability to different forcing processes. A range of different water mass fraction methods have been used in glacial fjord settings in Greenland and elsewhere to track the spread of fresh glacial meltwater in the ocean and quantify water mass transformation driven by glacial fjord processes (see Chapter 2).

Calculating water mass fractions across time and space requires that we first define the source water type properties. Next, we compare two different water mass fraction methods and show how Optimum Multiparameter Multi-Year (OMPM) Analysis (Muilwijk et al., 2022) is not sufficient to determine SMW and SGD fraction changes in space and time. In contrast, the weighted regularized least squares (RLS) method with prior information allows for the estimation of water mass fractions for every survey year in Sermilik Fjord, and improves our ability to quantify SMW and SGD contributions across time and space—providing specific insight into ice-ocean interactions.

Finally, we closely examine where SGD and SMW are added into the water column in the near-glacier environment and compare our hydrographic and water mass fraction analyses to previous model results of Sermilik Fjord. We identify two distinct forms of transformation occurring to plume waters in the near-glacier region. We show that while near-glacier plume properties and mixing are well-captured by modeling studies, the dynamics occurring in the

subsequent ice mélange region are not.

## 3.2 Methods

### 3.2.1 Optimum Multiparameter Multi-Year Analysis

Optimum Multiparameter Multi-Year Analysis (OMPM) was developed to leverage temperature and salinity observations from different surveys, and was previously applied to Upernavik Fjord in Northwest, Greenland (Muilwijk et al., 2022). Unlike most OMP water mass fraction analyses, which use observations from a single time period or single survey, OMPM utilizes observations across multiple time periods with a key assumption that the water mass fractions are constant in time. In doing so, an overdetermined system of equations can be developed for four water mass fractions only using temperature and salinity observations, along with mass conservation (Equation 3.1. The solution yields a single set of water mass fractions representing the time- and space-mean GMW composition. The problem set up is as follows:

$$\mathbf{A} = \begin{bmatrix} T_{\mathrm{AW}_{2009}} & T_{\mathrm{PW}_{2009}} & T_{\mathrm{SGD}_{2009}} & T_{\mathrm{SMW}_{2009}} \\ S_{\mathrm{AW}_{2009}} & S_{\mathrm{PW}_{2009}} & S_{\mathrm{SGD}_{2009}} & S_{\mathrm{SMW}_{2009}} \\ T_{\mathrm{AW}_{2010}} & T_{\mathrm{PW}_{2010}} & T_{\mathrm{SGD}_{2010}} & T_{\mathrm{SMW}_{2010}} \\ S_{\mathrm{AW}_{2010}} & S_{\mathrm{PW}_{2010}} & S_{\mathrm{SGD}_{2010}} & S_{\mathrm{SMW}_{2010}} \\ \vdots & \vdots & \vdots & \vdots \\ T_{\mathrm{AW}_{2023}} & T_{\mathrm{PW}_{2023}} & T_{\mathrm{SGD}_{2023}} & T_{\mathrm{SMW}_{2023}} \\ S_{\mathrm{AW}_{2023}} & S_{\mathrm{PW}_{2023}} & S_{\mathrm{SGD}_{2023}} & S_{\mathrm{SMW}_{2023}} \\ 1 & 1 & 1 & 1 \end{bmatrix}, \quad \mathbf{x} = \begin{bmatrix} x_{PW} \\ x_{AW} \\ x_{SGD} \\ x_{SMW} \end{bmatrix}, \quad \mathbf{y} = \begin{bmatrix} T_{\mathrm{GMW}_{2009}} \\ S_{\mathrm{GMW}_{2009}} \\ T_{\mathrm{GMW}_{2010}} \\ S_{\mathrm{GMW}_{2010}} \\ \vdots \\ T_{\mathrm{GMW}_{2023}} \\ S_{\mathrm{GMW}_{2023}} \\ 1 \end{bmatrix}. \quad (3.1)$$

**A** is filled by endmember values of constituent SWTs, **y** contains the known mean GMW properties for each year, and **x** is the vector of unknown fractions of each SWT to be solved for. Mass conservation is explicitly included as the last row in the matrices dictating that the solution fractions must add to 1.

Similar to classical OMPA, we solve for $\mathbf{x}$ using non-negative constrained least-squares estimation to minimize the square of the residuals $\mathbf{r}$, formally written as

$$\mathbf{y} = \mathbf{A}\mathbf{x} + \mathbf{r}. \tag{3.2}$$

$$\min_{\mathbf{x}\geq 0} \|\mathbf{A}\mathbf{x} - \mathbf{y}\|_2^2 = \min_{\mathbf{x}\geq 0} \|\mathbf{r}\|_2^2. \tag{3.3}$$

Note that in this particular application we do not use any weighting, and therefore temperature, salinity, and mass conservation contribute equally to the solution. This is to replicate the methods of Muilwijk et al. (2022) in order to compare our results to theirs.

Values for AW and PW endmembers for each year in $\mathbf{A}$ (e.g. $T_{\mathrm{AW}_{2009}}$, $T_{\mathrm{PW}_{2009}}$) are determined from Figure 3.2. For each survey year, we use the fjord maximum AW temperature and associated salinity for AW endmembers, and use the mean coldest point on the shelf with associated salinity for the PW endmember value. SGD and SMW values are constant where $T_{\mathrm{SGD}} = 0\mathrm{C}$, $S_{\mathrm{SGD}} = 0\mathrm{g\,kg^{-1}}$, and where $T_{\mathrm{SMW}} = -87\mathrm{C}$, $S_{\mathrm{SMW}} = 0\mathrm{g\,kg^{-1}}$ as described in Chapter 2.

Whereas classical OMP often solves directly for individual data points of temperature and salinity, OMPM solves for the fractions that contribute to GMW mean properties. A consequence of this is that mean GMW temperature and salinity properties for each year must be defined prior to calculating the water mass fractions. These values are entered into $\mathbf{y}$. For example, $T_{\mathrm{GMW}_{2009}}$ and $T_{\mathrm{GMW}_{2009}}$ correspond to the mean temperature and salinity of the identified GMW extent in 2009. This raises the question of how to define GMW extent in a consistent way in order to calculate mean properties. We address this in Section 3.2.3.

### 3.2.2 Fjord region definitions

For their application of OMPM in Upernavik Fjord, Muilwijk et al. (2022) had only several CTD profiles from various surveys each year at non-standardized locations within the fjord. In contrast, we are utilizing full along-fjord hydrographic sections over a 13-year time

series (see Chapter 1). We therefore use the OMPM method over distinct fjord regions, assessing time-averaged spatial variability of water mass fractions within Sermilik Fjord.

We simplify the assessment of spatial variability to the along-fjord direction, reducing the fjord to four regions: plume, ice mélange, mid-fjord, and mouth, and include the shelf as a distinct fifth region from the fjord. Each fjord region has an associated distance from the Helheim Glacier terminus in the along-fjord direction: 0 km, 22 km, 76 km and 100 km, respectively. These regional definitions are informed by the distinct properties at each location and are supported by the analysis in Chapter 1. We also include a region between the ice mélange and mid-fjord region called ”north fjord” for the analysis in Figure 3.5 to better assess the spatial gradients in SWT fractions. Every survey year has data in the north fjord and mid-fjord regions, and most surveys have data in the mouth region. Only two surveys (2016 and 2019) have observations directly in the plume region.

### 3.2.3 Defining GMW extent and properties

The fjord temperature anomaly from shelf properties, calculated as a mean shelf profile subtracted from fjord profiles along isopycnals, is a standard method to identify GMW in fjords (Straneo et al., 2010; Beaird et al., 2018; Muilwijk et al., 2022; Lindeman et al., 2024). This approach assumes that GMW waters exist where the fjord is warmer than the shelf. The warming of fjord waters relative to the shelf below the surface layer is assumed to be caused by the entrainment and upwelling of warm AW in the subglacial discharge plume. Surface warming from solar radiation or the addition of warmer terrestrial runoff to the fjord is negated by only considering the water column below 50 m. An advantage of this method is that the vertical coordinates of the identified GMW are allowed to vary in time, as opposed to imposing a fixed depth range from which GMW properties are calculated.

Figure 3.1 shows an example of a temperature anomaly calculation and mean GMW properties for profiles from the 2019 survey. Mean GMW temperature and salinity values (yellow diamonds in Figure 3.1) were calculated from all data points that fell within the positive

temperature anomaly range. The salinity anomaly was also calculated for comparison and aligns with the same isopycnal range as the temperature anomaly.

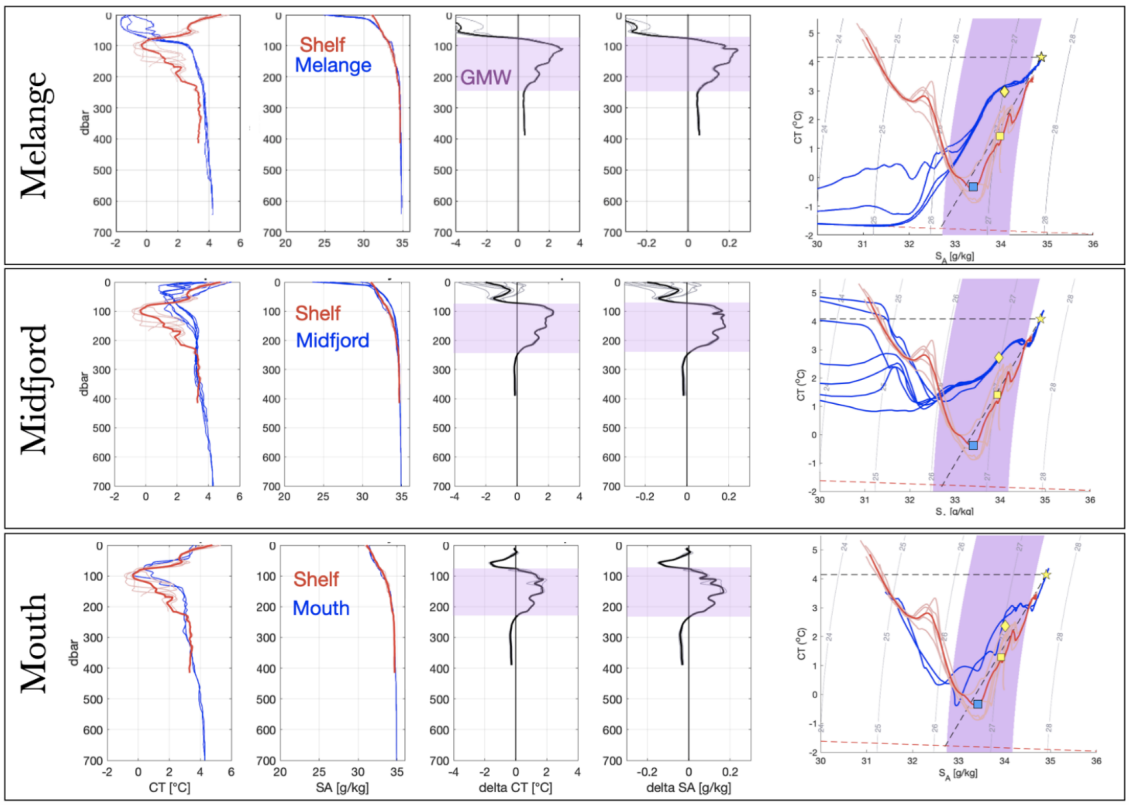


**Figure 3.1.** An example of the positive temperature anomaly calculation along isopycnals to define mean GMW properties of profiles in the 2019 Sermilik Fjord survey. The profiles are categorized into three separate fjord regions: ice mélange, mid-fjord, and mouth. The left most plots show temperature profiles from the shelf (red) and each fjord region (blue). The next plot over shows salinity of shelf and fjord profiles. The third plot from the left show the $\Delta$CT temperature anomaly from the shelf as calculated along isopycnals for every fjord profile. The bold black line represents the mean anomaly profile. The fourth plot over is the $\Delta S_A$ anomaly calculated in the same way. The purple swatches indicate where the anomalies are positive and define the depth of the GMW layer for each fjord region. The right most plots show the shelf and fjord profiles in $\Theta$-$S_A$ space. The purple swatch shows the same GMW range as in the preceding plots defined by an isopycnal range. The yellow diamond is the average GMW properties for each region calculated by averaging all data points within the GMW layer. The yellow square is the average properties of the shelf profiles across the same isopycnal range as the GMW. The blue square is the coldest point of the mean shelf profile and our defined PW endmember value.

The gridded dataset developed in Chapter 1 allows us to calculate the temperature anomaly from the mean shelf profile across the entire fjord domain of the gridded dataset (Figure

3.3). This provides a more complete picture of the temperature anomaly-defined GMW spatial distribution in an along-fjord section for each year.

### 3.2.4 Limitations of the positive temperature anomaly approach

The temperature anomaly approach broadly shows where warm upwelled waters exist in the fjord, but the specifics of the exact density and depth extent of GMW present some challenges. The true bottom extent of the GMW should represent the point at which a fjord profile deviates from the background AW-PW mixing line in the direction of the subglacial discharge mixing line, with warmer temperatures relative to that mixing line—a signal of plume waters. However, the background AW-PW mixing lines of the shelf and fjord do not always align due to temporal and spatial differences in the properties of the deep fjord waters.

Figure 3.1 shows an example in the mélange region where the shelf and fjord deep waters (below 250 m) do not overlap in properties and therefore the temperature anomaly method would overestimate the bottom depth of the GMW to the entire profile extent. In this case, we manually selected the bottom isopycnal, and associated depth, to be where the fjord profile deviated from its particular AW-PW mixing line. For the midfjord and mouth anomaly calculations in Figure 3.1, the GMW bottom extent is underestimated because the shelf AW-PW background mixing slope is slightly fresher than the fjord AW-PW mixing slope. The consequence of this is that the deepest, warmest, and saltiest parts of the true GMW for those fjord profiles are not included in the GMW mean property calculations. This results in reported mean GMW properties that are slightly colder and fresher than they would be if the true GMW extent was utilized.

The upper bound of the GMW is similarly challenging. In practice, we end up creating a cutoff of GMW at 50 m depth to not include positive temperature anomalies due to surface warming. However, significant input of SMW occurs above 50 m depth from iceberg melt, particularly in the mélange area. Additionally, the upper water column of the melange area is a negative temperature anomaly compared to the shelf. If we are using positive temperature anomaly-defined GMW as a proxy for all exported freshwater from glacier and icebergs, this

becomes a significant issue as both the 50 m cutoff and a positive anomaly definition prevent the inclusion of a major source of SMW from icebergs (Moon et al., 2018; Kinne et al., 2025).

There are several options to address this. First, we could manually choose an upper bound that captures more of near-surface iceberg melt. The iceberg melt is defined by a parallel slope to the SMW mixing line. Therefore, we could set an upper bound at the point where the profile slope deviates from the SMW mixing line. A consequence of this is that mean GMW properties are calculated as slightly colder and fresher compared to a rigid positive temperature anomaly method. However, this would still miss iceberg melt that was then warmed at the surface (and thus has a different slope in TS space). A second option is to adjust our definition of GMW to include the caveat that we are simply not capturing a portion of the SMW melt at the surface (no matter which approach we take) and that we are primarily concerned with using the temperature anomaly method to determine properties of the upwelled plume waters. Neither option is fully satisfying, but both allow for meaningful interpretation of the bulk GMW properties. Here, we choose to use an upper bound cutoff of 50 m and acknowledge that we are miss an important source of SMW at the surface. We do, however, manually select lower bounds of the GMW for years when the AW-PW background slopes of the temperature and shelf are not aligned.

### 3.2.5 AW and PW properties and variability

AW and PW are two water masses that define the shelf region and pycnocline, an important driver of fjord-shelf exchange, and AW primarily defines the deep fjord water properties. Both AW and PW are constituent water masses of the fjord system and their endmember property definitions are required for water mass fraction analyses. Assessing the temporal and spatial variability of each allows for a more informed choice of these endmembers and associated uncertainty values.

We considered AW to be all data points deeper than 500 m. Mean AW properties in different fjord regions were determined by averaging all data points below 500 m at each location. Shelf AW temperatures are determined from the properties of the deepest point ($\sim$400 m) in the

suite of East shelf section profiles every year. The East shelf section perpendicularly cross the trough connecting Sermilik Fjord to the continental shelf, and the deepest part of the trough has been identified as a pathway for AW to flow from the continental shelf into the fjord system.

We assessed Polar Water properties by considering all profiles from the East Shelf section every year. There are fewer profiles in this shelf section each year (1 - 8 profiles) compared to the fjord. The number of profiles on the shelf is determined by logistical and weather factors for each survey. For each year, we identified the core PW temperature as the coldest value of the shelf-wide mean. The associated salinity of every coldest data point are averaged to obtain the mean salinity property of the PW for each year.

### 3.2.6 OMPM fraction uncertainty estimation with Monte Carlo simulations

A key source of uncertainty in any water mass fraction analysis is the choice of endmember properties and observational uncertainty (see Chapter 2). Following Beaird et al. (2018) and Muilwijk et al. (2022) we assessed the sensitivity of our OMPM results to these sources of uncertainty using Monte Carlo simulations. Endmember property values were randomly perturbed within observationally informed ranges of uncertainty (Table **??**) and the OMPM system of equations was solved for each perturbed endmember set. We ran 5000 iterations for each fjord region.

### 3.2.7 Weighted Regularized Least Squares (RLS) approach

The OMPM method was developed to create an overdetermined system of equations that could be solved within the classical OMP framework. For a fjord system of four SWTs, classical OMP requires at least three observed properties plus the mass conservation constraint. With only two observed properties, temperature and salinity, progress was made by assuming time invariance of the SWT fractions and developing an overdetermined system of equations with profiles from multiple time periods. This is a large and previously untested assumption,

and limited our interpretation of the results produced by the OMPM method. We address this gap here, utilizing weighted regularized least squares (RLS) approach for water mass fraction analysis to estimate water mass fractions for each distinct survey year.

The RLS method allows for an underdetermined system of equations to be solved directly, with the addition of prior information in the form of a penalty matrix **P**. Rather than incorporating another property or tracer to resolve underdetermination, RLS uses regularization, a standard technique in inverse theory, where **P** penalizes the use of certain SWTs relative to others. Similar to OMP, RLS is a least squares problem with the form of

$$\min_{x} \ \|\mathbf{W}(\mathbf{A}\mathbf{x}-\mathbf{y})\|_2^2+\mathbf{x}^{\mathbf{T}}\mathbf{P}\mathbf{x}. \tag{3.4}$$

**A** is the endmember property matrix (rows: properties plus mass conservation; columns: SWTs), **y** is the vector of observed temperature and salinity for a given data point in the fjord, and **W** is a diagonal data weighting matrix reflecting measurement uncertainty and SWT property definition uncertainty. **P** the penalty matrix encoding the expected prevalence of each SWT. The penalty term regularizes the equations by selecting, among all solutions that adequately fit the data, the solution that remains closest to the prior.

As described in Section 2.2.5, we impose a non-negative solution constraint and reformulate the cost function as a quadratic minimization problem subject to inequality bounds. Using MATLAB's quadprog iterative solver, we solve

$$\min_{x\geq 0} \frac{1}{2}\mathbf{x}^{\mathbf{T}}\mathbf{H}\mathbf{x}+\mathbf{f}^{\mathbf{T}}\mathbf{x}, \tag{3.5}$$

where

$$\mathbf{H}=2(\mathbf{A}^{\mathbf{T}}\mathbf{W}\mathbf{A}+\mathbf{P}), \qquad \mathbf{f}=-2\mathbf{A}^{\mathbf{T}}\mathbf{W}\mathbf{y}. \tag{3.6}$$

Determining the values in **P** is not trivial. Here, we rely on the model comparison analysis in Chapter 2 and utilize the spatially varying **P** matrix developed there. This is appropriate

because every survey year is from the summer season where the same broad hydrographic patterns occur. The same **P** is applied to all observations across all survey years. We conducted a sensitivity experiment, calculating the RLS water mass fractions with a spatially constant **P** matrix. Differences were negligible between the spatially varying and constant **P** solutions throughout the fjord interior, except for the mouth region, where variations in **P** are need to resolve the appropriate AW and PW fractions along the AW-PW mixing line. Therefore, we use the spatially varying **P** matrix developed in Chapter 2 for this analysis here.

Given that the observations in Chapter 2 are from the same dataset of temperature and salinity used here, we also use the same values for **W** as they appear in Chapter 2. **W** incorporates measurement uncertainty of the data and the uncertainty of the SWT definitions for each measurement type. An important distinction between **W** and **P** is that we would adjust **P** if we were applying this method to winter observations where the SWT prevalence and structure is different from the summer season. In this case, we would not adjust **W** because the measurement uncertainty of temperature and salinity would not change. **P** relates to the expected solution and **W** relates to the uncertainty of the property measurement.

Finally, in the RLS method, we adjust the PW endmember salinity properties to better capture the background AW-PW mixing line in $\Theta - S_A$ space. We keep the coldest mean temperature as described above, but increase the salinity to a value that aligns with the measured AW-PW mixing line. This allows the model to better distinguish between PW and SMW and appropriately partition the deep fjord waters between AW and PW along the observed mixing line. The physical basis for this is that the PW properties on the shelf are more transient than the fjord interior. Therefore the measured PW properties on the shelf in a given survey do not necessarily match the PW properties that created the AW-PW background mixing line seen in the fjord profiles.

### 3.2.8 Simple plume model

In 2016 and 2019, the subglacial discharge plume at the Helheim Glacier terminus was visible as a plume polynya at the surface. XCTD profiles were collected directly in this region and those observations are used in this analysis to asses the dynamics in the region of formation of GMW. Following Muilwijk et al. (2022), we employ a simple analytical plume model adapted from bouyant plume theory (Slater et al., 2016) to compare with the direct observations of plume properties and water mass fractions.

We treat plume GMW as a mixture of ambient Water (aW), subglacial discharge (SGD), and submarine meltwater (SMW), where aW are the fjord waters entrained into plume at the grounding line. These waters are primarily AW but include some PW. To distinguish between a pure AW SWT endmember used in the OMPM and RLS analysis (the warmest AW measured in the full fjord domain) and the upwelled plume waters within this model (temperature of AW nearest the glacier) we use the term "ambient water" (aW). Plume GMW temperature and salinity are given by the volume-flux-weighted averages of the three contributing water masses:

$$T_{\mathrm{GMW}} = \frac{Q_{\mathrm{aW}} T_{\mathrm{aW}} + Q_{\mathrm{SGD}} T_{\mathrm{SGD}} + Q_{\mathrm{SMW}} T_{\mathrm{SMW}}}{Q_{\mathrm{aW}} + Q_{\mathrm{SGD}} + Q_{\mathrm{SMW}}}, \quad S_{\mathrm{GMW}} = \frac{Q_{\mathrm{aW}} S_{\mathrm{AW}} + Q_{\mathrm{SGD}} S_{\mathrm{SGD}} + Q_{\mathrm{SMW}} S_{\mathrm{SMW}}}{Q_{\mathrm{aW}} + Q_{\mathrm{SGD}} + Q_{\mathrm{SMW}}} \tag{3.7}$$

Following Muilwijk et al. (2022), we adopt the simplification of an unstratified water column at the glacier front, which permits an analytical solution and is more interpretable for our purposes here. For a linear plume in a homogeneous aW column with conservative temperature $T_{\mathrm{aW}}$, absolute salinity $S_{\mathrm{aW}}$, grounding line depth $h_{\mathrm{gl}}$, and channel width $w$, the volume flux of AW entrained by the rising plume is

$$Q_{\mathrm{AW}} = \alpha h_{\mathrm{gl}} w \left( \frac{Q_{\mathrm{SGD}} g'_0}{\alpha w} \right)^{1/3} \tag{3.8}$$

where $\alpha = 0.1$ is the entrainment coefficient and $g'_0 = 0.26$ m s$^{-2}$ is the reduced gravity of the plume at the grounding line. The SGD temperature $T_{\mathrm{SGD}}$ is taken as the pressure melting point of freshwater at the grounding line depth, $T_{\mathrm{SGD}} = \lambda_1 + \lambda_2 h_{\mathrm{gl}}$, where $\lambda_1 = 8.32 \times 10^{-2}$ °C

and $\lambda_2 = -7.53 \times 10^{-4}$ °C m$^{-1}$.

The SMW flux generated by oceanic melting of the glacier face is approximated as

$$Q_{\mathrm{SMW}} = A_1 \left(1 + A_2 (T_{\mathrm{aW}} - T_{\mathrm{SGD}})\right) \left(\frac{Q_{\mathrm{SGD}}}{w}\right)^{1/3} w\, h_{\mathrm{gl}} \tag{3.9}$$

where $A_1 = 1.56 \times 10^{-5}$ s$^{-2/3}$ and $A_2 = 0.84$ °C$^{-1}$ are meltwater flux coefficients. Together, Equations (3.7)–(3.9) show that the GMW properties are determined by four inputs: the ambient deep water properties (aW) determined from hydrographic observations, the grounding line depth ($h_{\mathrm{gl}}$) determined from Morlighem et al. (2017) and Kim et al. (2025b), the plume width ($w$) estimated and tuned to the observations, and the SGD volume flux $Q_{\mathrm{SGD}}$.

### 3.2.9 Subglacial discharge volume flux

The SGD volume flux ($Q_{\mathrm{SGD}}$) required as input to the plume model is estimated from the liquid freshwater runoff product of Mankoff et al. (2020), which provides daily runoff estimates for individual drainage basins around the Greenland Ice Sheet derived from regional climate model output and a drainage network model. Total catchment runoff integrates contributions from all outlet types within a basin, but only runoff routed through marine-terminating outlets reaches the fjord as subglacial discharge at the grounding line. Runoff draining through land-terminating glacier outlets is assumed to exit as proglacial surface flow and does not contribute to the buoyant plume dynamics at the glacier face. To isolate the subglacial component, we follow Moon et al. (2024) and partition catchment runoff by outlet elevation, attributing runoff from outlets at or below sea level located at the Helheim terminus as $Q_{\mathrm{SGD}}$, and excluding contributions from any land-terminating outlets. While there are several marine terminating glaciers with subglacial discharge plumes in Sermilk Fjord, we specifically use Helheim subglacial estimates to match the observations from directly in the plume. We average daily volume flux values over July and August to report a mean summer SGD volume flux for each year. Total runoff and other subglacial discharge input is compared to Helheim Glacier subglacial discharge in Appendix

A(Figure A.10).

### 3.2.10 Estimating submarine melt rate from SMW fractions

The observed SMW fraction $x_{\mathrm{SMW}}$ from the water mass fraction analysis of the plume profiles, combined with the estimated SGD volume flux $Q_{\mathrm{SGD}}$ and the plume-entrained aW volume flux $Q_{\mathrm{aW}}$, allows $Q_{\mathrm{SMW}}$ to be solved for directly without requiring an independent estimate of total plume volume flux. Rearranging the definition of $x_{\mathrm{SMW}}$ as the proportion of SMW in the total plume volume:

$$Q_{\mathrm{SMW}} = \frac{x_{\mathrm{SMW}}(Q_{\mathrm{AW}} + Q_{\mathrm{SGD}})}{1 - x_{\mathrm{SMW}}} \tag{3.10}$$

The resulting SMW volume flux is then converted to a spatially averaged melt rate across the subaqueous glacier face:

$$\dot{m} = \frac{\rho_w}{\rho_i} \cdot \frac{Q_{\mathrm{SMW}}}{w \cdot h_{\mathrm{gl}}} \cdot 86400 \quad [\mathrm{m\ d^{-1}}] \tag{3.11}$$

where $w$ is the plume width, $h_{\mathrm{gl}}$ is the grounding line depth, and the density ratio $\rho_w/\rho_i \approx 1.12$ converts from a seawater to an ice volume equivalent. Melt rates are computed for the two CTD profiles collected within the plume region.

The plume model also allows for an independent prediction of $Q_{\mathrm{SMW}}$ from Equation 3.9, derived from the ambient aW properties and $Q_{\mathrm{SGD}}$ alone without reference to the CTD observations. This model-predicted flux implies a corresponding SMW fraction:

$$x_{\mathrm{SMW}}^{\mathrm{model}} = \frac{Q_{\mathrm{SMW}}^{\mathrm{model}}}{Q_{\mathrm{AW}} + Q_{\mathrm{SGD}} + Q_{\mathrm{SMW}}^{\mathrm{model}}} \tag{3.12}$$

Comparing $x_{\mathrm{SMW}}^{\mathrm{model}}$ to the observed $x_{\mathrm{SMW}}^{\mathrm{obs}}$ from the water mass fraction analysis provides a direct test of the plume model's ability to reproduce the meltwater content of the observed plume.

## 3.3 Results

We first present the mean temperature and salinity properties of AW, PW, and GMW in the different fjord regions across every survey year (Figure 3.2). This enables us to discern any trends or anomalies in time and between the different fjord regions for each water mass. We also present the mean summer subglacial discharge for each survey year, representing one forcing mechanism of GMW properties and ice-ocean interaction, showing the variability in time. These values are used in the simple plume model and melt rate calculations.

Next, we present the quantitative water mass fraction solutions from the OMPM and RLS methods and compare their results. This comparison provides context for previous and future water mass fraction studies of other fjord locations.

Finally, we compare the plume properties and fraction results with the expectations of buoyant plume theory and melt model.

### 3.3.1 AW properties and variability

Half-violin plots (Figure 3.2a) show the distribution of AW temperatures across the full fjord for each year. The half-violin plots are histograms of all AW temperatures in the full fjord domain, and the vertical extent of the shaded region denotes the maximum and minimum temperature values. Where the maximum and minimum temperatures are close together, the overall temperature distribution is tight (2011, 2021, 2022, and 2023). In contrast, 2009 and 2017 show relatively large distributions of AW temperatures, spanning 1°C across the whole fjord.

In the along-fjord spatial dimension, AW in the mélange region is consistently cooler than in the mid-fjord and mouth regions, and also cooler than the fjord-wide mean. The exceptions to this are 2015 and 2019. Shelf AW temperatures vary widely relative to mean fjord temperatures—sometimes cooler and sometimes warmer—ranging from 3.10°C to 4.28°C. Five different years show shelf AW temperatures outside the fjord temperature range for that year. The difference in

properties between the fjord and shelf AW is independent of survey length. For instance, 2009 and 2010 surveys occurred over 6 and 5 days respectively, yet 2010 has much larger difference between fjord and shelf AW temperature properties.

Salinity of AW shows some variability across the fjord, though not as distinct of a pattern as temperature (Figure A.11). Six years show the mélange region with slightly lower salinity ($>$0.05 g kg$^{-1}$ difference) compared to the mean fjord salinity. Similar to temperature, the shelf salinity can vary widely from the fjord salinity for each year.

Fjord-wide mean AW temperatures span 3.1°C to 4.6°C over the 13-year record. 2010, 2019, and 2023 have the warmest mean fjord temperatures, while 2009, 2012, and 2015 are the coldest. 2017 was previously identified as a colder year in the fjord in Chapter 1 by the temperature anomaly from the climatological mean, but it has a larger range of AW temperatures leading to an overall warmer mean fjord temperature compared to 2015.

There is no significant linear trend over 13-year fjord mean AW temperature or salinity properties. The 13-year time mean of fjord averaged AW salinities is 34.90 ± 0.05 g kg$^{-1}$.

### 3.3.2 PW properties and variability

In addition to presenting PW mean coldest temperature, Figure 3.2b displays every individual shelf profile's coldest temperature value. No clear spatial pattern emerges across the East shelf section profiles and each year shows no more than a 1°C range between the coldest point of all profiles.

The overall 13-year temperature range of the PW (mean coldest point, as defined above) is $-1.60$°C to 0.20°C, and the mean is $-0.79$°C ± 0.50°C. PW mean salinity properties are 33.22 ± 0.28 g kg$^{-1}$. The coldest and freshest years are 2015 and 2023. Again, 2015 was already identified as an anomalously cold year throughout the region and surveying that year in Sermilik Fjord was impacted by dense sea ice presence outside and in the fjord—indicative of cold temperatures in the winter and spring seasons lasting into July.

### 3.3.3 GMW properties and variability

We report mean GMW properties calculated from the positive temperature anomaly method (Figure 3.2 and 3.3). Mean GMW properties in Figure 3.2 incorporated the manual lower bound adjustments described in Section 3.2.4. The gridded positive temperature anomalies (Figure 3.3) are not adjusted and show the rigid positive temperature anomaly approach.

The mean GMW temperature is warmest in the plume region and coolest at the mouth for each survey. For the two years with observations from the plume (2016 and 2019), the GMW cools over 0.5°C from the plume to the mélange. The largest temperature difference from mélange to mouth region is 1.50°C in 2011. Similarly, the GMW is saltiest in the plume and becomes fresher toward the mouth, and 2011 shows the largest salinity range with a change of 0.59 g $kg^{-1}$ from mélange to mouth.

Across all years and all regions, the mean GMW properties are 1.82 ± 0.59°C and 33.86 ± 0.20 g $kg^{-1}$. The GMW properties over time mirror the AW properties—warmer (colder) AW leads to warmer (colder) GMW. This is consistent with previous findings of GMW being predominantly composed of upwelled AW in both Sermilik and Upernavik Fjord (Beaird et al., 2015, 2018; Muilwijk et al., 2022).

### 3.3.4 GMW spatial extent from positive temperature anomaly

The gridded positive temperature anomaly results show the spatial extent of the GMW (defined as the positive temperature anomaly) in along-fjord sections (Figure 3.3). The maximum magnitude of the positive temperature anomaly does not necessarily correspond to the "core" of the plume waters, though it is tempting to view it as such. The overall magnitude is determined by the shape of the shelf profile and shape of the fjord profile in temperature space. The maximum magnitude of the temperature anomaly can be influenced by intrusions and deviations in the shelf profile, not corresponding to any GMW process, as much as it is influenced by the shape of the fjord profile (which does reflect GMW processes). The temperature anomaly below the $\sigma_\theta$=27.5

kg $m^{-3}$ isopycnal is greyed out to prevent interpretation of the anomaly in the deep fjord waters. Temperature anomalies below this isopycnal result from the properties of the deep fjord and deep shelf waters not aligning, as opposed to the fjord profiles presenting deviations from the shelf properties due to water mass transformation. For both reasons, we therefore caution against overinterpretation of the anomaly magnitudes, and instead focus on the trends in space and time of the bulk positive temperature anomaly as a whole.

In general, all years show the deepest positive temperature anomaly extent in the upper reaches of the fjord (20–30 km from the glacier). Some years show maximum depth values of >500 m (2009 and 2021), while others are much shallower maximum depths (200–300 m). The thickness and depth of the GMW is decreased and shallower at the mouth compared to the upper reaches of the fjord each year. The $\sigma_\theta$=27 kg $m^{-3}$ isopycnal, occurring between 100–200 m, reliably tracks positive temperature anomaly waters every year, even as the bottom and top boundaries of the positive temperature anomaly differ from year to year.

### 3.3.5 OMPM results: Time-averaged water mass fractions in different fjord regions

From the OMPM method, we produced a single set of water mass fractions, representing a time-mean constituent composition of depth-mean GMW properties integrated across all survey years, for each fjord region (Table 3.1). Uncertainty values for each fraction solution were derived from Monte Carlo simulations (Figure 3.4). We also visualized the problem setup, defined by input SWT endmembers and mean GMW properties for each region and every year, in $\Theta - S_A$ space and compared plume model results to observations (Figure 3.5).

Across all regions, Atlantic Water dominates the GMW composition, comprising 49–98% of the mixture. AW fractions decrease systematically from the plume toward the fjord mouth, while Polar Water increases in the opposite direction, reaching 50% at the mouth. SGD and SMW fractions are small across all regions ($\leq$2.1% and $\leq$ 1.3%, respectively). The interpretation of SMW fractions is limited by large uncertainties, which are comparable to or exceed the

**Table 3.1.** Water mass fractions (%) estimated from OMPM analysis for each region. Uncertainty values derived from Monte Carlo simulations. Dashes for Plume$_a$ and mélange$_a$ regions represent where PW was forced to contribute 0% as a way to investigate the mixing model limitations of distinguishing between SMW and PW. Plume$_b$ and mélange$_b$ include all four SWTs. AW = Atlantic Water; PW = Polar Water; SGD = Subglacial Discharge; SMW = Submarine Meltwater. †Result from Muilwijk et al. (2022) for comparison.

| Region | AW (%) | PW (%) | SGD (%) | SMW (%) |
|---|---|---|---|---|
| Plume$_a$ | $97.8 \pm 0.04$ | — | $2.10 \pm 0.06$ | $0.06 \pm 0.04$ |
| Plume$_b$ | $96.3 \pm 1.33$ | $1.6 \pm 1.40$ | $2.10 \pm 0.06$ | $0.02 \pm 0.03$ |
| Mélange$_a$ | $97.9 \pm 0.05$ | — | $0.79 \pm 0.07$ | $1.30 \pm 0.06$ |
| Mélange$_b$ | $63.7 \pm 1.6$ | $35.9 \pm 1.7$ | $0.76 \pm 0.05$ | $0.0 \pm 0.0$ |
| North | $82.6 \pm 4.9$ | $15.7 \pm 5.2$ | $0.94 \pm 0.05$ | $0.84 \pm 0.26$ |
| Midfjord | $74.7 \pm 5.3$ | $23.6 \pm 5.6$ | $0.85 \pm 0.05$ | $0.79 \pm 0.28$ |
| Mouth | $48.8 \pm 1.5$ | $50.7 \pm 1.6$ | $0.63 \pm 0.04$ | $0.0 \pm 0.01$ |
| *Upernavik*† | $57.8 \pm 8.1$ | $41.0 \pm 8.3$ | $1.0 \pm 0.1$ | $0.2 \pm 0.2$ |

estimated fractions. The mélange and fjord mouth both return SMW fractions of zero. This is a failure of the OMPM model and SWT definitions to resolve SMW against the dominant AW and PW endmembers. The high PW fraction for the mélange region (36%) is notably large and a concerning result as this is where SMW fractions should be highest with substantial iceberg melt. Thus our confidence is low in all results produced by this method with the model set up and SWT definitions described here.

We assessed what the SMW fraction contributions could be in absence of PW by excluding it in the plume and mélange region (Plume$_a$ and Mélange$_a$ in Table 3.1). Without PW, the SMW fraction in the melange is more appropriate— larger than SGD in the mélange region. The SGD fraction remains unchanged as the fractional composition is redistributed between AW and SMW without PW as a SWT. This provides more confidence in the SGD results, while the SMW and PW fractions remain suspect.

The failure of the OMPM model and SWT definitions to resolve SMW can be visualized within $\Theta - S_A$ space (Figure 3.5). The PW endmember properties for each year fall near or on the SMW-AW mixing line. Both PW and SMW act to freshen and cool water properties. Their

definitions, and the slopes of their respective mixing lines, in this OMPM model are not distinct enough from each other to reliably resolve their fractional contributions.

### 3.3.6 Yearly Water mass fractions results from RLS

The OMPM model setup here requires that we calculate fraction constituents for mean GMW properties. In contrast, the RLS method allows us to calculate the water mass fractions at every observation data point for every year in the gridded dataset without making assumptions about GMW extent and mean properties. We produced four fractional solution grids for every year (Figure 3.6 and Figure A.12-A.15).

Like the OMPM results, AW dominates the fractional composition overall and is never less than 40% anywhere in the fjord domain across all years. Each year shows that the depth integrated mean AW fractions are largest closest to the glacier and decrease toward the mouth, where PW fractions are generally largest. Each year shows a remarkably consistent pattern of upwelled AW, strongest closest to the glacier, indicated by a local maximum in AW fractions ($\sim$90%) between 100–200 m depth and reliably following the 27 isopycnal. This region indicates the core GMW plume waters spreading down-fjord from the region of mixing and formation at glacier terminus.

In contrast, the PW fraction patterns for each year are more variable. Each year shows a background PW fraction of 10–20% nearly everywhere in the fjord domain. Where both SGD and SMW fractions are largest ($\sim$100–200 m), PW fractions are slightly suppressed. There are variable "hot spots" of PW that extend from the mouth. 2021 shows two layers of "hot spots" indicating interleaving of PW with outgoing GMW fjord waters. Comparing the mouth to the midfjord region, we see the maximum PW fractions occur at deeper depths (200-250 m) in the midfjord (Figure 3.7. This indicates that PW from the shelf is reliably subducting below the core GMW waters and reaching further up fjord. Overall, maximum PW fractions are notably decreased in the fjord in the 2019–2023 time period compared to the 2009–2018 time period, though the background PW fraction levels remain fairly consistent (Figure A.13).

SMW and SGD fractions for each year are consistent in their spatial patterns and magnitudes, though there are small variations. SMW is present deeper in the water column (>400 m) compared to SGD (∼200 m), and SMW reaches maximum depths closest to the glacier for all years. This result is consistent with the noble gas-derived water mass fractions of the 2015 survey of Sermilik Fjord from Beaird et al. (2018). Below 50 m, SMW varies from 0-4% and SGD varies from 0-10% within the fjord domain across all years—results that are again consistent with Beaird et al. (2018).

### 3.3.7 Method comparison

To compare the RLS results with the OMPM results, the RLS results must be spatially averaged. For each survey year and each region, we calculate the depth mean of the fraction solutions over the GMW depth range as defined by the positive temperature anomaly for that region (Table 3.2). For comparison, we've also presented the depth mean fractions for each region of the 2015 noble gas-derived water mass fractions from Beaird et al. (2018). The standard deviations presented here represent standard deviation of the depth average. OMPM results represent a temporal average across the entire dataset range in addition to a spatial average. We choose to present individual years of the RLS results alongside the OMPM so that we can assess how much temporal variability is lost when calculating the OMPM time average fractions (Figure 3.8).

Spatial averaging of the SGD and SMW fractions creates large standard deviation values, making the information nearly meaningless. For the RLS solutions, SGD and SMW fractions are not distributed uniformly with depth and this information is lost in the depth-averaging process.

For AW and PW fractions, the OMPM and RLS solutions match in their along-fjord gradients despite the magnitude of the fractions in each region not matching exactly. The OMPM method overestimated PW fractions and underestimated AW fractions compared to the three years of the RLS method displayed (Figure 3.8).

**Table 3.2.** Water mass fraction estimates (depth mean across GMW extent ± standard deviation, in %) by dataset and fjord region. Mean values here represent the spatial average over the GMW extent defined by the positive temperature anomaly method. This is to be comparable with results in Table 3.1. Note that results from Beaird et al. (2018) use the shelf region rather than mouth.

| | Region | AW% | PW% | SGD% | SMW% |
|---|---|---|---|---|---|
| 2015 Beaird et al. (2018) | North | $84.82 \pm 4.50$ | $13.27 \pm 3.11$ | $0.89 \pm 0.81$ | $0.51 \pm 0.49$ |
| | Mid-fjord | $79.30 \pm 10.80$ | $16.00 \pm 9.40$ | $0.57 \pm 0.78$ | $0.52 \pm 0.45$ |
| | Shelf | $29.05 \pm 28.32$ | $68.60 \pm 26.55$ | $0.30 \pm 0.64$ | $0.05 \pm 0.06$ |
| RLS 2015 | North | $85.98 \pm 5.72$ | $11.56 \pm 4.58$ | $1.09 \pm 0.57$ | $1.37 \pm 0.64$ |
| | Mid-fjord | $80.35 \pm 4.58$ | $17.17 \pm 3.56$ | $0.92 \pm 0.47$ | $1.54 \pm 0.68$ |
| | Mouth | $66.78 \pm 11.99$ | $32.06 \pm 11.63$ | $0.06 \pm 0.11$ | $1.09 \pm 0.68$ |
| RLS 2019 | Plume | $91.96 \pm 0.13$ | $5.93 \pm 0.58$ | $1.35 \pm 0.52$ | $0.76 \pm 0.11$ |
| | Mélange | $91.38 \pm 1.72$ | $7.41 \pm 1.09$ | $0.60 \pm 0.66$ | $0.60 \pm 0.35$ |
| | North | $89.09 \pm 4.58$ | $9.00 \pm 3.26$ | $1.01 \pm 1.02$ | $0.90 \pm 0.60$ |
| | Mid-fjord | $84.46 \pm 2.57$ | $13.31 \pm 1.69$ | $1.16 \pm 0.55$ | $1.05 \pm 0.65$ |
| | Mouth | $82.20 \pm 4.18$ | $15.99 \pm 3.90$ | $1.01 \pm 0.29$ | $0.79 \pm 0.27$ |
| RLS 2021 | North | $88.37 \pm 5.07$ | $9.90 \pm 3.79$ | $0.74 \pm 0.63$ | $0.99 \pm 0.73$ |
| | Mid-fjord | $84.16 \pm 2.72$ | $14.23 \pm 2.13$ | $0.78 \pm 0.91$ | $0.83 \pm 0.55$ |
| | Mouth | $79.84 \pm 5.89$ | $18.46 \pm 5.55$ | $0.96 \pm 1.02$ | $0.73 \pm 0.55$ |

### 3.3.8 Plume properties, fractions, and melt rate

The consistency between the RLS fraction solutions of 2016 and 2019 in the plume region is notable. The mean July–August SGD volume flux is estimated to be 570 $m^3 s^{-1}$ and 590 $m^3 s^{-1}$ for 2016 and 2019, respectively. However, 2019 has much greater variation during the summer runoff season with a peak as high as 1200 $m^3 s^{-1}$.

The years have notably different temperature properties and spatial patterns, with 2019 being one of the warmest years overall relative to the climatological mean of the fjord (Roth et al., 2025a) and 2016 being cooler overall than 2019 (Figure 3.9). For the two plume profiles, the different temperature and salinity properties of the deep waters (below 300 m) between these years are due to both different SWT properties of AW and PW and slightly different fractions of PW and AW. However, in the core plume waters where SGD is highest (above 200 m), all SWT fractions are nearly identical within uncertainty.

We applied the simple plume model described by Equations 3.7–3.9. The plume width, $w$, is the most unknown parameter. We tuned $w$, holding other parameters constant, until the mean plume properties of the model best matched the mean observed properties from 2019 and 2016. The final parameter values of the model are reported in Figure 3.5, with $w = 200$ m. The mean fractions of SMW and SGD derived from the plume model results are $x_{SMW}^{model}$=0.05% and $x_{SGD}^{model}$=2.07%. The SMW fractions from the plume model are an order of magnitude less compared to the RLS results of the plume observations. This is also evident in the model plume properties which are warmer than the directly observed plume temperatures (Figure 3.5).

The plume model produces a mean submarine meltwater flux of $Q_{SMW}^{model} = 14.12$ m$^3$s$^{-1}$ corresponding to a melt rate within the plume area of the terminus of $\dot{m}^{model} = 9.6$ m d$^{-1}$. While high, this is of similar magnitude to other estimated submarine melt rates at tidewater glaciers in Greenland (1–4 m d$^{-1}$), which are often reported distributed across the full terminus face due to methodology rather than directly in the plume. Enderlin and Howat (2013) estimated a mean submarine melt rate of $\sim$0.56 m d$^{-1}$ at Helheim between 2000 and 2010. Rignot et al. (2010) estimated melt rates of between 1 and 4 m d$^{-1}$ at three grounded tidewater glaciers in West Greenland.

Everett et al. (2021) used a three-dimensional, high resolution plume model to estimate the melt rate within the Helheim plume at different SGD rates. For $Q_{SGD}$=500 m$^3$s$^{-1}$ the $Q_{SMW}$ was 212.5 x 10$^3$ m$^3$d$^{-1}$. We estimate the total plume area from their results with a 500 m terminus height (assumed in their model set up) and 100 m constant plume width, producing a melt rate within the plume area of the terminus of approximately 4.2 m d$^{-1}$. Using a 700 m terminus height, the melt rate is 3.0 m d$^{-1}$.

Using an RLS calculated SMW mean plume fraction of $x_{SMW}^{obs}$=0.5%, the submarine melt flux associated with this fraction is $Q_{SMW}^{obs} = 140$ m$^3$s$^{-1}$ corresponding to a melt rate within the plume area of the terminus of $\dot{m}^{obs} = 96$ m d$^{-1}$. This is an order of magnitude larger than our model estimate and other previous estimates listed above, and very suspect as a terminus melt rate. Likely, our fractional decomposition includes additional iceberg melt, rather than terminus

melt alone, integrated over the small plume area to produce such a large melt rate.

We can also compare the $Q_{aW}$ between the plume model and a derivation from fraction results of the observations. Using the simple plume model, $Q_{aW}^{model}$ is calculated from $Q_{SGD}$ based on an assumed entrainment coefficient. Assuming a mean discharge value from 2016 and 2019 as $Q_{SGD}$=580 $m^3s^{-1}$, we calculate $Q_{aW}^{model}$ to be 2.72 x $10^4$ $m^3s^{-1}$. We can estimate a $Q_{aW}^{obs}$ value by noting that total $Q_{SGD}$ must be about 1% of the total plume on average from our RLS fraction solutions in the plume. This provides a total plume volume flux of 5.80 x $10^4$ $m^3s^{-1}$. The mean ambient water fraction (combined AW and PW fractions) within the plume is roughly 98% of this total flux, leading to $Q_{aW}^{obs}$ = 5.68 x $10^4$ $m^3s^{-1}$. If we choose an upper end estimate of $x_{SGD}^{obs}$=2% within the range of our plume observations instead, we arrive at a $Q_{aW}^{obs}$ = 2.84 x $10^4$ $m^3s^{-1}$, which is closer to the model results, and consistent with the fraction of SGD derived from the simple plume model, which is $x_{SGD}^{model} = 2.07\%$.

Overall, the observed plume properties are cooler relative to the prediction of the simple buoyant plume model, and the fractional decomposition of the plume observations reveal an order of magnitude more SMW fractional contribution than predicted by the plume model. The upper end of observed SGD fractions correspond well to the plume model results. From this, we can infer that the assumed entrainment coefficient of ambient water is likely appropriate here. Taken together, these results indicate a source of SMW contribution not accounted for in the buoyant plume model.

## 3.4 Discussion

### 3.4.1 Summary of results

We applied the regularized least-squares water mass fraction framework developed in Chapter 2 to the full 13-year gridded dataset for Sermilik Fjord, producing the first multi-year record of Atlantic Water (AW), Polar Water (PW), subglacial discharge (SGD), and submarine meltwater (SMW) fractions across the fjord for the summer season. The general water mass

structure is consistent with the known hydrography of the system: AW dominates at depth throughout the fjord interior, PW occupies the upper water column and is most prominent near the mouth and shelf, and glacially derived freshwater fractions (SGD and SMW) are largest in the mélange and plume regions near the glacier terminus. Spatial patterns in water mass fractions are robust across the thirteen-year record, particularly in the plume and mélange regions. The implication of these results is that even as source water properties vary in time, the different fjord water masses are mixed together in similar amounts and with spatial consistency during the summer season.

The fraction solutions for each year help to define upwelled AW above 300 m, indicative of core plume waters and GMW. While the largest SMW and SGD fractions are both at the surface, SMW is consistently detected at deeper depths compared to SGD. PW fractions show the most spatially variability across all years, with PW sometimes extending past the mid-fjord region and subducting underneath GMW waters. Recent (2019–2023) maximum PW fractions in the fjord have been reduced compared to the previous time period of the data set. Interannual variability across all fractions is concentrated at the fjord mouth, where shelf forcing governs the exchange of water masses entering and exiting the fjord, though there are subtle differences in patterns across the fjord domain for each year and for each SWT fraction.

Overall, the RLS fraction solutions, which vary in space and time, are a meaningful improvement over the OMPM solutions which are time and depth-averaged across a defined GMW spatial extent. The OMPM solutions, when partitioned into distinct fjord regions, can match the general gradients of AW and PW fractions along the fjord predicted by the RLS solutions. The SMW fraction results from the OMPM approach should not be trusted as SMW and PW are not distinguishable enough within the OMPM mixing model as defined here.

Additionally, we demonstrated that despite varying subglacial discharge volume flux and different source water type properties, the fraction solutions within the plume region were consistent. From these results, we showed that submarine melt flux estimated from observed plume SMW fractions is an order of magnitude greater than SMW melt flux predicted by buoyant

plume theory and other estimates. Buoyant plume models do not include any representation of or interaction with icebergs or an ice mélange. Everett et al. (2021) show that the plume waters of Helheim Glacier meaningfully interact with its mélange, likely melting through the mélange to form open plume pool polynyas at times when the plume reaches the surface. Additionally, they showed that the plume waters extend beyond the area of the visible open plume pools, meaning that warm upwelled waters are in contact with mélange icebergs. It is likely that although the plume observations were from profiles directly in the open plume pool, that the water properties are significantly modified by iceberg melt, rather than only submarine terminus melt. This modification occurring within the plume is not accounted for in current plume models because complex plume-mélange interactions are not represented.

### 3.4.2 Methodological improvements and limitations

#### RLS versus OMPM

By comparing the RLS results with the OMPM approach, we now have improved context for the assumptions of the OMPM mixing model and interpretation of its results. In the OMPM approach, the system was rendered overdetermined by pooling observations across multiple years and over the defined GMW depth extent, implicitly treating both interannual variability and depth variability as noise in order to satisfy the algebraic requirements of the inversion. The water mass fraction solutions are assumed to be constant in time within the GMW defined layer. The results of the RLS method allow us to directly test this assumption for the first time. Within uncertainty, the AW and PW fractions of all individual years in the north and mid-fjord are the same. The OMPM results nearly match these RLS fractions for these two regions, though AW is underestimated and PW is overestimated by roughly 6–10%. At the mouth, the PW fractions are more variable in time and therefore an assumption of constant fractions in this region is not applicable. If a research question is concerned with the partitioning of AW and PW within the fjord interior, then there is perhaps a pathway where those fractions could be assumed constant in time and OMPM could provide valid results. OMPM, as applied here, should not be used to

understand glacial freshwater endmembers.

A critical step in adapting the RLS framework to each survey year is the adjustment of the PW salinity in the endmember definition. This adjustment is needed such that the AW-PW background mixing line that defines slope of the deep waters in $\Theta - S_A$ space is captured by the endmember definition used in the mixing model. PW properties are more variable on the shelf such that the directly observed PW in a given survey may not represent the PW properties that created the AW-PW background mixing properties. This adjustment also allows for more definition between SMW and PW fractions, ensuring more trustable results. We recommend this adjustment as a standard step in any application of the RLS framework to multi-year fjord datasets. Future work could include applying this adjustment to the OMPM framework and assessing whether this improves results between SMW and PW fractions.

**Resolving SMW and SGD**

The two freshwater endmembers — SGD and SMW — occur at much smaller quantities than AW and PW and their relative fidelity in the RLS solution warrants careful interpretation. SMW is characterized by a large temperature anomaly relative to the other source water types. This large temperature offset gives SMW disproportionate resolving power within the least-squares system— small SMW fractions produce a relatively large signal in temperature properties.

SGD, by contrast, is defined primarily by its salinity signature and is less thermally distinct from AW and PW. Its resolving power is lower compared to SMW as it is geometrically closer to AW and PW in $\Theta - S_A$ space—a larger fraction of SGD is needed relative to SMW to produce the same magnitude signal of property change. The practical consequence is that in regions where both freshwater endmembers are present— particularly at depth in the plume region, where subglacial discharge rises in a buoyant plume and rapidly entrains AW— a portion of what is physically SGD-influenced water may be attributed to SMW in the solution, because the SMW endmember can be calculated and resolved with smaller fraction resolution. SGD

fractions at depth should therefore be interpreted as conservative estimates, likely representing a lower bound on the true subglacial discharge contribution. In other words, the spatial footprint of the plume in fraction space should be understood as the region where the SGD signal remains resolvable, not necessarily as the full physical extent of all plume waters.

**Smoothing of PW intrusions in the gridded dataset**

The optimum interpolation scheme used to produce the gridded dataset in Chapter 1 applies spatial covariance weighting that smooths over sharp property gradients. PW intrusions into the fjord may be partially attenuated by this smoothing, resulting in an underestimate of peak PW fractions in the gridded product relative to what would be inferred from raw profile data. The PW fractions reported here should therefore be interpreted as spatially smoothed representations of the PW distribution and may underestimate the magnitude of individual intrusion events.

### 3.4.3 Defining GMW from water mass fractions

Glacially modified water has been identified using temperature anomaly relative shelf properties— an approach that integrates both SGD and SMW signals without distinguishing between them. Defining GMW directly from AW, SGD, and SMW fractions is possible with the RLS framework. The spatial distribution of AW in the upper water column is consistent with the expected GMW layer in the upper water column and mélange region, and the broad spatial patterns are robust across years. However, the precise boundaries of the GMW layer— the threshold fraction above which a water parcel is classified as glacially modified— remain challenging to define. SMW is consistently present at deeper depths than SGD, indicating the SMW fractions are not just within the core plume waters. This could potentially be from interaction with deep icebergs reaching below the neutral buoyancy of the plume. The results presented here capture the broad-scale structure of the core plume waters reliably; users should exercise caution in drawing quantitative conclusions that depend on the exact SMW and SGD boundaries.

Semantics and definition are somewhat at issue here: is GMW any water parcel that has interacted and mixed with SGD or SMW? Would deep iceberg interactions be considered GMW? Or is GMW specifically the plume waters where SMW, SGD, and upwelled AW occur together? The RLS method provides increased discernment between SMW and SGD making these questions more relevant than previous studies of GMW in Sermilik Fjord.

### 3.4.4 Interannual variability, GMW properties, and forcing

The interannual variability in GMW properties tracks AW properties at depth in the fjord, consistent with previous studies. We note that this is different than if GMW tracked properties of AW on the shelf. Some fjord parameterizations and ice-ocean models utilize properties from the shelf, but we note there is an along-fjord gradient in AW properties whereby AW is cooled closer to the glacier.

Beyond defining SWT properties and uncertainty for the mixing model, we assessed the defined properties for variability across time to make any connections with potential forcing mechanisms that could improve parameterizations. This is also a main motivation for calculating water mass fractions through time—is there a connection to forcing mechanisms, not just through changes in properties, but through changes in the mixing recipe? This is a future area of work, but we took a first step in considering subglacial discharge volume flux as a forcing mechanism and comparing the time series with that of water mass properties and fractions. We see no apparent connection between variations in Helheim Glacier summer mean subglacial discharge flux and the magnitude or pattern of water mass fractions. Rather, the water mass fractions are consistent across years, in the plume and mélange region most specifically.

The connections that do exist reflect larger regional forcing. AW and PW are both relatively cooler in 2015 time period, and SGD volume flux is relatively low those years also (Figure 3.2). We expect the AW temperatures to reflect larger climatic trends in the Subpolar North Atlantic, primarily influenced by decadal-scale processes in the ocean and atmosphere (e.g., subpolar gyre spin up or down and the North Atlantic Oscillation). The period between

2014 and 2016 is a well-known anomalously cold period in the Irminger Sea and SPNA due to increased heat loss to the atmosphere (Nelson et al., 2024), followed by a distinct warming trend from 2016 to 2020 (Desbruyères et al., 2021). The AW fjord temperatures broadly follow this trend. A component of this cooler period includes cooler than normal atmospheric conditions. This is a possible reason for slightly lower mean summer subglacial discharge values in 2014 and 2015 which could be connected to overall reduced ice sheet surface melt during these years.

We expect PW temperatures on the shelf to be controlled by dynamics of the EGCC, EGC, sea ice formation and transport, and surface heat flux. The East Greenland Polar Front, which varies on seasonal and annual timescales, plays a large role in dynamics on the shelf outside of Sermilik Fjord specifically. Sea ice front position and delivery of waters from the Arctic are largely controlled by the East Greenland Polar Front position—two processes that dictate the characteristics and properties of PW measured at a specific point and time (Gjelstrup et al., 2025). The seasonal timescales and dynamic nature of currents on the shelf, in combination with the relative timing of hydrographic sampling in relation to these processes, play an important role in the measured properties of PW reported here. Despite cooler than normal PW temperatures aligning with AW in 2015, recent PW properties from 2019–2023 have been cooler and fresher than average while AW fjord temperatures have been average to warmer than average.

Other forcings to be considered in future work include the thickness and extent of the mélange region, which could be a significant control on SMW fractions, and shelf processes including along-shelf barrier wind events (Snow et al., 2023), East Greenland Polar Front position, and spring sea ice extent. Some forcing processes likely have lag times from their observed occurrence to possible impact on fjord properties and water mass mixing processes.

### 3.4.5 Improving fjord process parameterizations?

Pathways to parameterization depend on the research questions of interest. Muilwijk et al. (2022) proposed a simple relationship between AW, PW, and GMW properties as a way of determining the bulk exported GMW properties out of Upernavik Fjord. While this could

also work in Sermilik Fjord as the GMW properties are between the extremes of PW and AW properties, this may result in the correct properties but for the wrong reasons. Our results show that GMW is initially cooled relative to AW because of the addition of SMW in the plume and mélange, and then variable PW fractions are added near the mouth. If the research question of interest is concerned with properties of waters exported from the fjord, then an AW–PW relationship may be acceptable, but if the interest lies in total amount of SMW and SGD exported, or partitioning between SMW and SGD to estimate melt rates, then another approach is needed.

The fact that water mass fraction patterns are fairly consistent within the plume and mélange regions independent of survey year, subglacial discharge volume flux, and source water properties, potentially provides simple pathways to improving model representation of these processes. Results by Sanchez et al. (2024) and Kinne et al. (2025) using three-dimensional, high-resolution modeling indicate the plume processes that add SGD and upwell AW are well-represented, but additional SMW from mélange melt and associated cooling of properties, even within the plume, are not captured. For results from Sanchez et al. (2024) this makes sense because icebergs were not included in the modeling framework. Kinne et al. (2025) did include iceberg representation, but even with this the water properties are not as cold as the observations. This has impacts for the overall model results as the stratification is impacted with additional SMW and cooled water properties. The consistency of the water mass fractions in the plume and mélange indicate that a simple temperature and salinity bias could be added to the plume or mélange properties of a model. While this does not dynamically represent the physics of increased SMW, it would allow for more appropriate fjord stratification.

Other recent work has specifically focused on subglacial discharge, plume, mélange, and melt feedbacks (Kajanto et al., 2023; Jain et al., 2025; Wood et al., 2025), with direct applicability to the Sermilik Fjord system. More work is needed to directly compare results here with these modeling studies, and the FAIR gridded dataset combined with water mass fraction understanding now makes this possible.

We summarize our understanding of key water mass transformation processes and regions

in Sermilik Fjord from combined hydrographic and water mass fraction analysis (Figure 3.10). Highlighting these key transformation steps, and their consistency in time, shows the major processes that must be included in models, if accurate process, rather than bulk exported properties, is a desired result. While the data represented in Figure 3.10 are from 2019 as an example, we stress that these highlighted transformation steps are consistently observed in all summer surveys.

## 3.5 Conclusions: Summary and Future Work

We applied the regularized least-squares (RLS) water mass fraction framework developed in Chapter 2 to a 13-year gridded hydrographic dataset of Sermilik Fjord, producing the first multi-year, spatially resolved record of Atlantic Water (AW), Polar Water (PW), subglacial discharge (SGD), and submarine meltwater (SMW) fractions for the summer season. The resulting decomposition reproduces the established hydrographic structure of the system while providing distinctly new information from that of bulk temperature and salinity properties. The along-fjord spatial patterns in constituent fractions are robust across the full record, most notably a local maximum in AW fraction ($\sim$90%) between 100 and 200 m that reliably tracks the 27 isopycnal and marks the core of upwelled, plume-derived GMW spreading down-fjord.

A central methodological result is that the RLS framework, applied year by year, resolves the temporal and spatial variability that the multi-year OMPM approach must discard to satisfy the overdetermined problem setup. OMPM recovers the broad along-fjord gradient in AW and PW but cannot reliably distinguish SMW from PW, and it should not be used to interpret glacial freshwater contributions. We further identify adjustment of the PW endmember salinity to the observed AW–PW background mixing line as a necessary step when applying the RLS framework to multi-year datasets, and recommend it as standard practice. The RLS method can be used on the growing archive of XCTD data around Greenland, including XCTD observations in more challenging-to-observe regions like plumes and ice mélange.

The interannual signal in GMW properties tracks AW at depth within the fjord rather than on the shelf, reflecting the down-fjord cooling of AW and arguing against the common modeling shortcut of forcing fjord parameterizations with shelf properties alone. The variability that does emerge reflects regional forcing: AW fjord temperatures broadly follow the well-documented mid-decade cooling of the Irminger Sea and subpolar North Atlantic (Nelson et al., 2024) and the subsequent post-2016 warming (Desbruyères et al., 2021), while PW properties on the shelf are governed by East Greenland Polar Front dynamics and sea-ice processes (Gjelstrup et al., 2025) and have remained anomalously cool and fresh in recent years even as AW warmed. We find no clear correspondence between summer subglacial discharge flux, GMW mean properties or the magnitude and pattern of water mass fractions.

The consistency of the water mass fraction results points toward a possible pathway for improving model representation of the near-glacier environment specifically. The gridded dataset and water mass fraction record presented here provide previously unavailable observational quantities to evaluate models with—not just hydrographic properties but distinguishing between the influence of subglacial discharge versus submarine melt on those properties. Quantifying the role of mélange thickness and extent in setting SMW fractions, and resolving the lagged influence of shelf forcing on fjord water mass composition, remain as future work for connecting the variability documented here to driving processes.

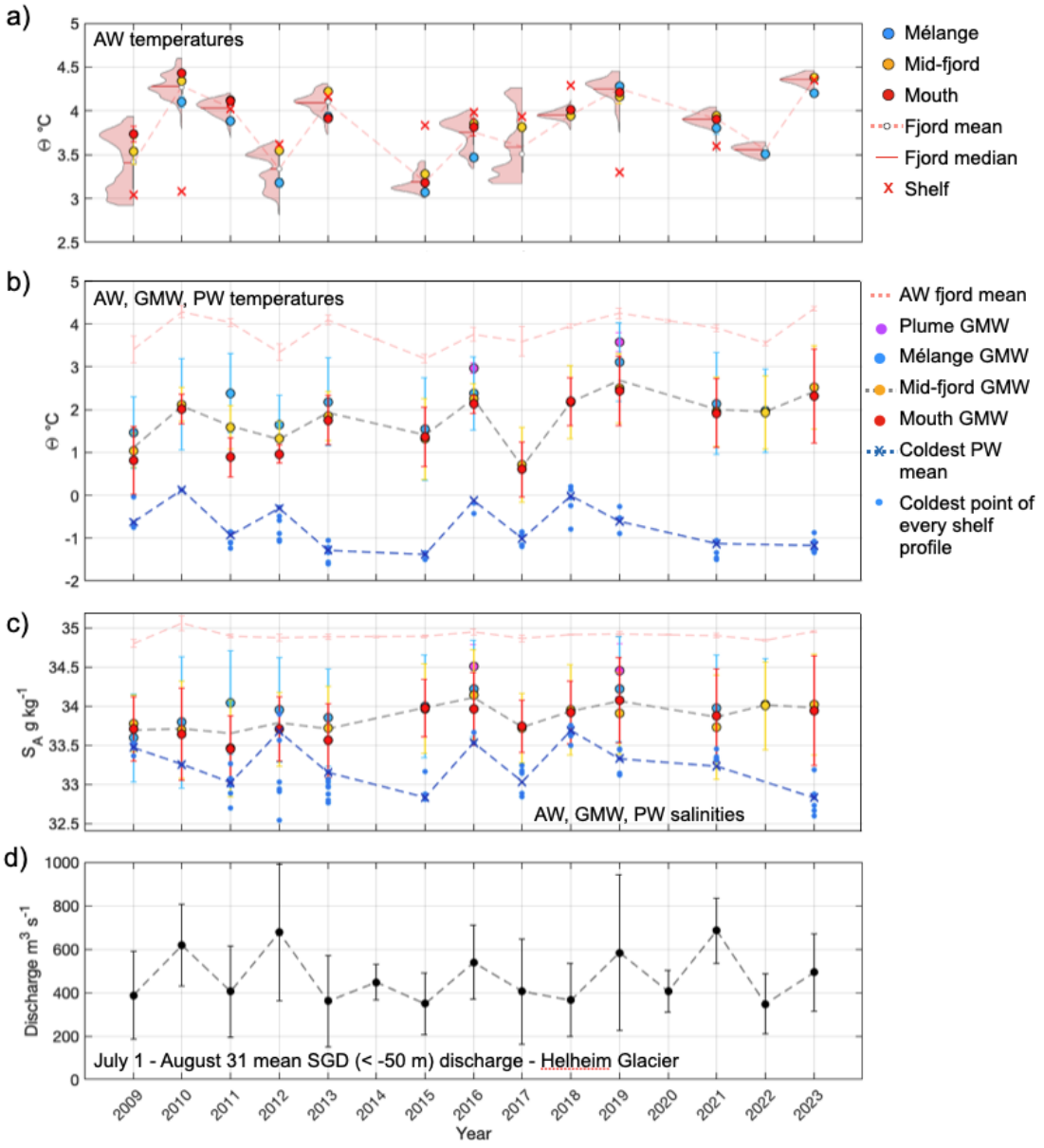


**Figure 3.2.** Timeseries of AW, PW, and GMW water mass properties in different fjord regions—plume (purple), mélange (light blue), mid-fjord (yellow) and mouth (red). a) AW temperatures as calculated from the mean of temperature observations below 500 m in each region. Half-violin plots (pink shading) represent the distribution of all temperature observations below 500 m in the full fjord domain and show the full fjord AW water mean and median values. b) All water mass temperature properties (AW, PW, and GMW). AW fjord mean temperatures that match results in (a) are represented by the light pink line. The mean GMW properties of each fjord region are shown with associated standard deviation. c) Mean salinity properties corresponding to the temperature properties for AW, PW, and GMW in each fjord region. d) Mean subglacial discharge from July 1–August 31 of each year. Error bars represent standard deviation around the mean.

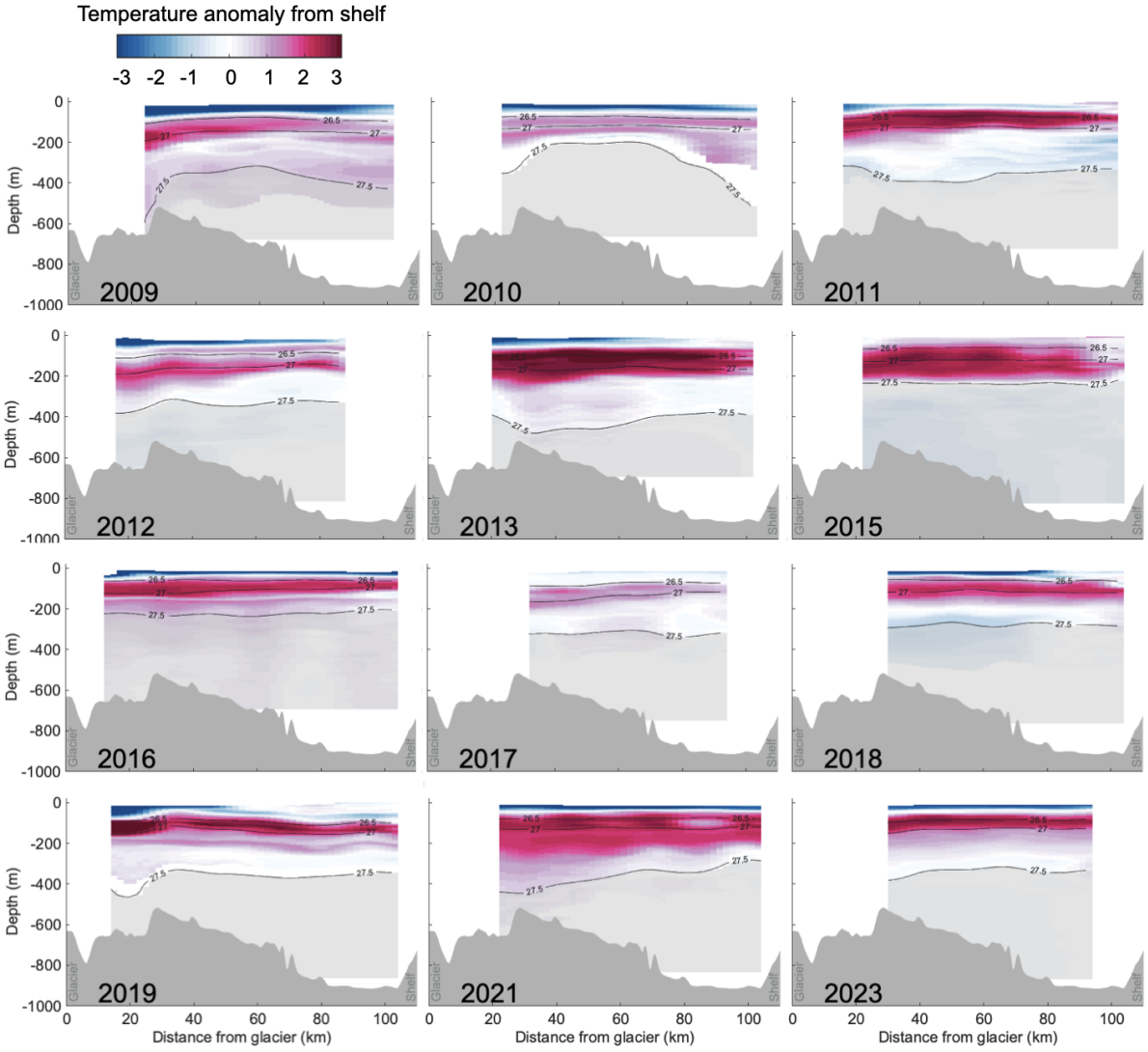


**Figure 3.3.** Temperature anomaly (fjord profiles minus mean shelf profile), calculated along isopycnals for each year in the Sermilik Fjord gridded dataset. Warm (cool) colors represent positive (negative) temperature anomaly from the mean shelf profile. $\sigma_\theta$=26.5, 27, and 27.5 kg m$^{-3}$ isopycnals are noted. Light grey shading blocks out the fjord area below the 27.5 kg m$^{-3}$ isopycnal. Dark grey shading is bathymetry of the along-fjord thalweg section, derived from Morlighem et al. (2017).

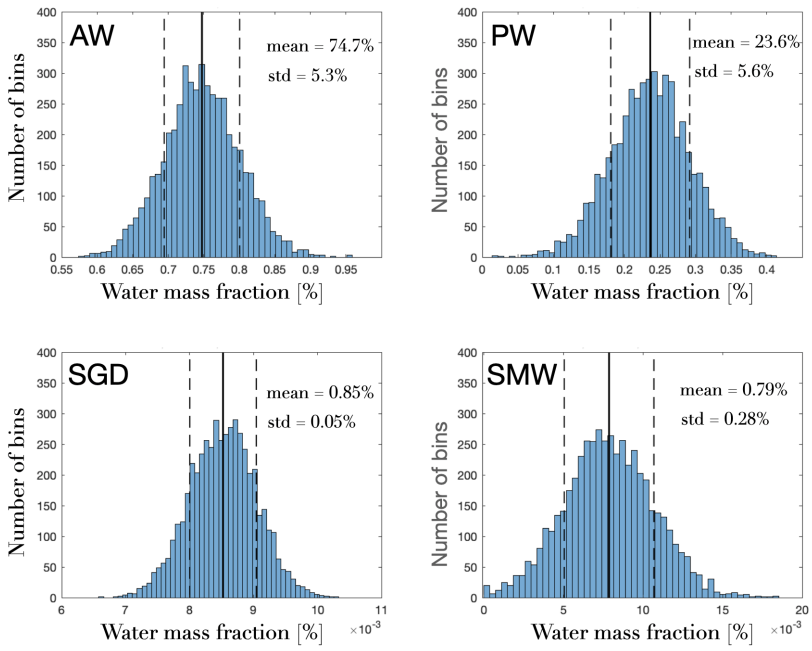


**Figure 3.4.** Example of uncertainty calculation for OMPM fraction results utilizing Monte Carlo simulations for the mid-fjord region. Each panel shows the fraction solutions from 5000 iterations of the OMPM system with perturbed SWT endmember values. The mean of this distribution is the reported water mass fraction solution and the standard deviation is the reported uncertainty.

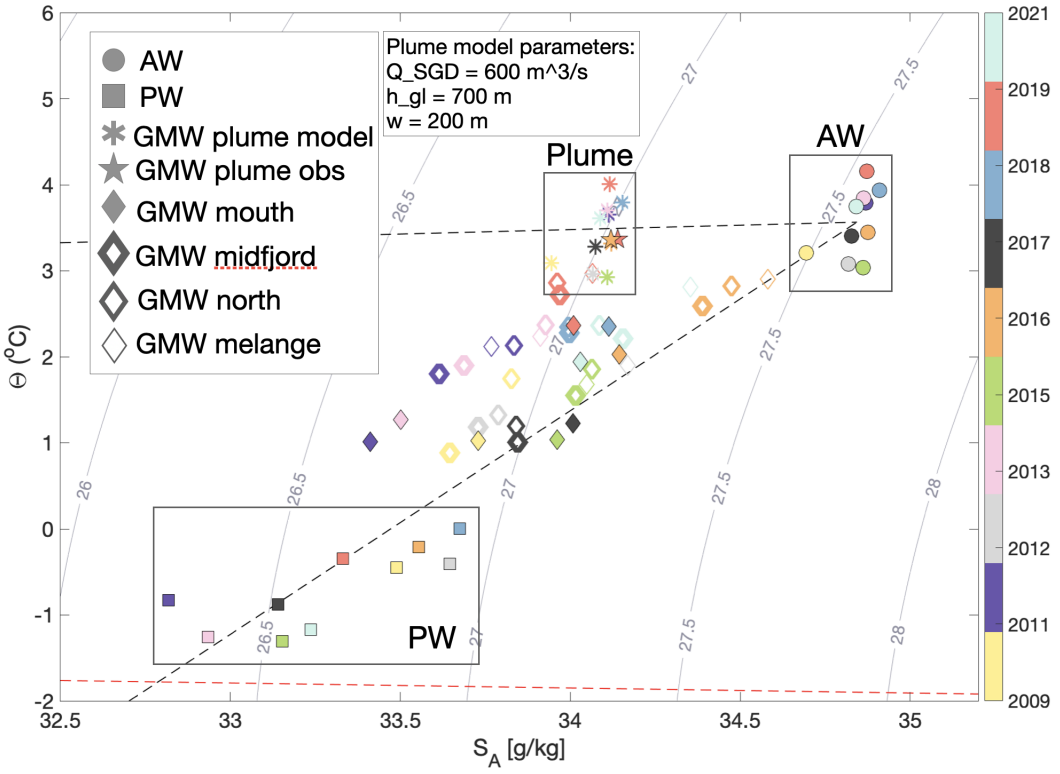


**Figure 3.5.** Temperature and salinity properties of PW endmembers (squares), AW endmembers (circles), and mean GMW as calculated at different fjord regions (diamonds). The top dashed line is the mixing line between AW and SGD. The second, angled dashed line is the mixing line between AW and the effective SMW endmember properties. The red dashed line is the freezing line. Colors denote years. The plume observations from 2016 and 2019 are also shown (stars) as mean plume properties. The asterik symbols represent the results of a plume model used for the other years without direct plume observations. Parameters for the plume model were consistent for each year.

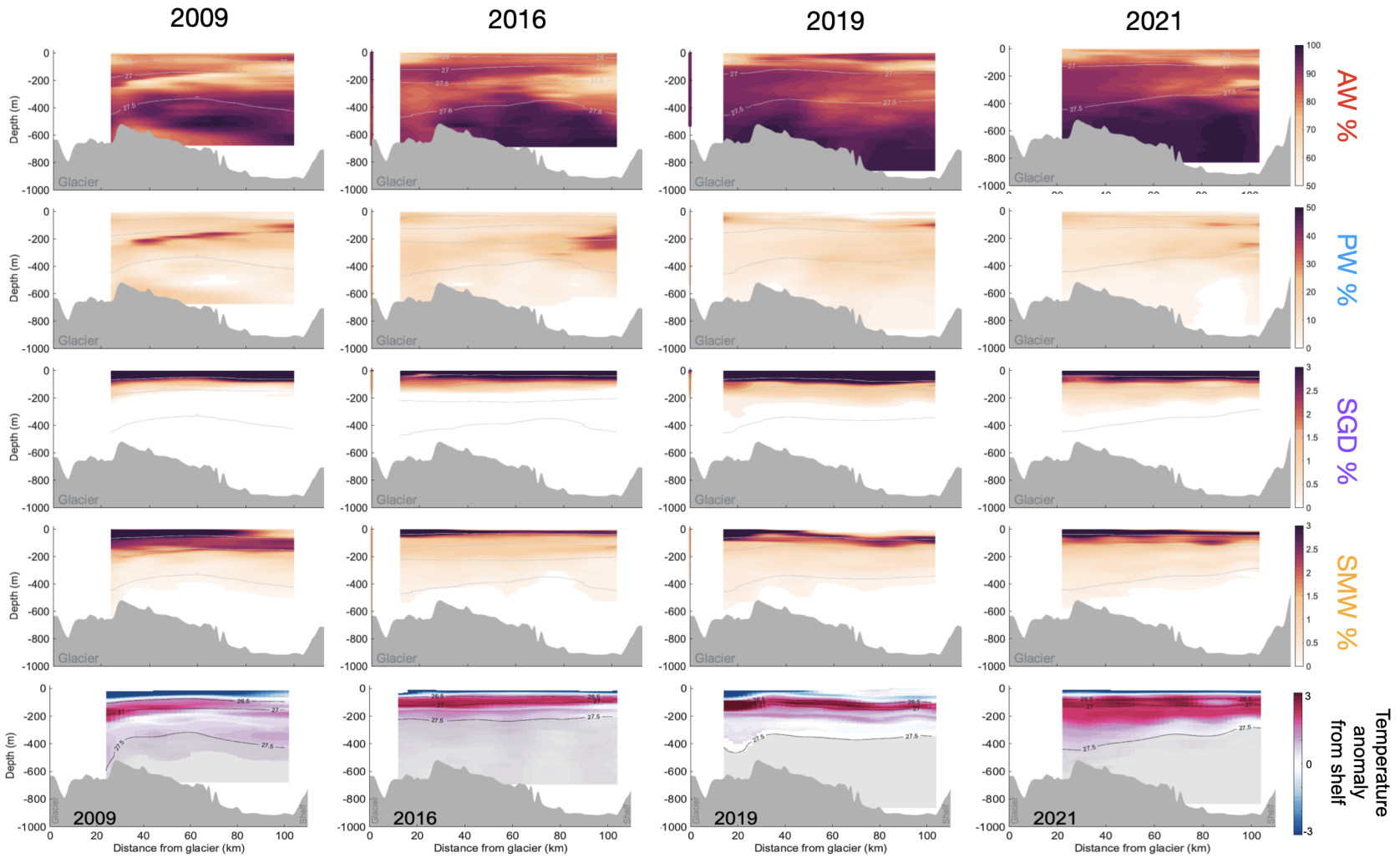


**Figure 3.6.** RLS method fraction solutions (%) for all SWTs (AW, PW, SGD, and SMW) derived from individual years of gridded data (2009, 2016, 2019, and 2021). Rows in the figure compare specific SWTs across the years and columns in the figure are the four SWT solutions for each year. Note that the color scale for each SWT fraction is distinct and covers different ranges. The temperature anomaly for each year is shown across the last row in the figure to compare GMW identification from the positive temperature anomaly method with SGD and SMW fraction solutions across each year.

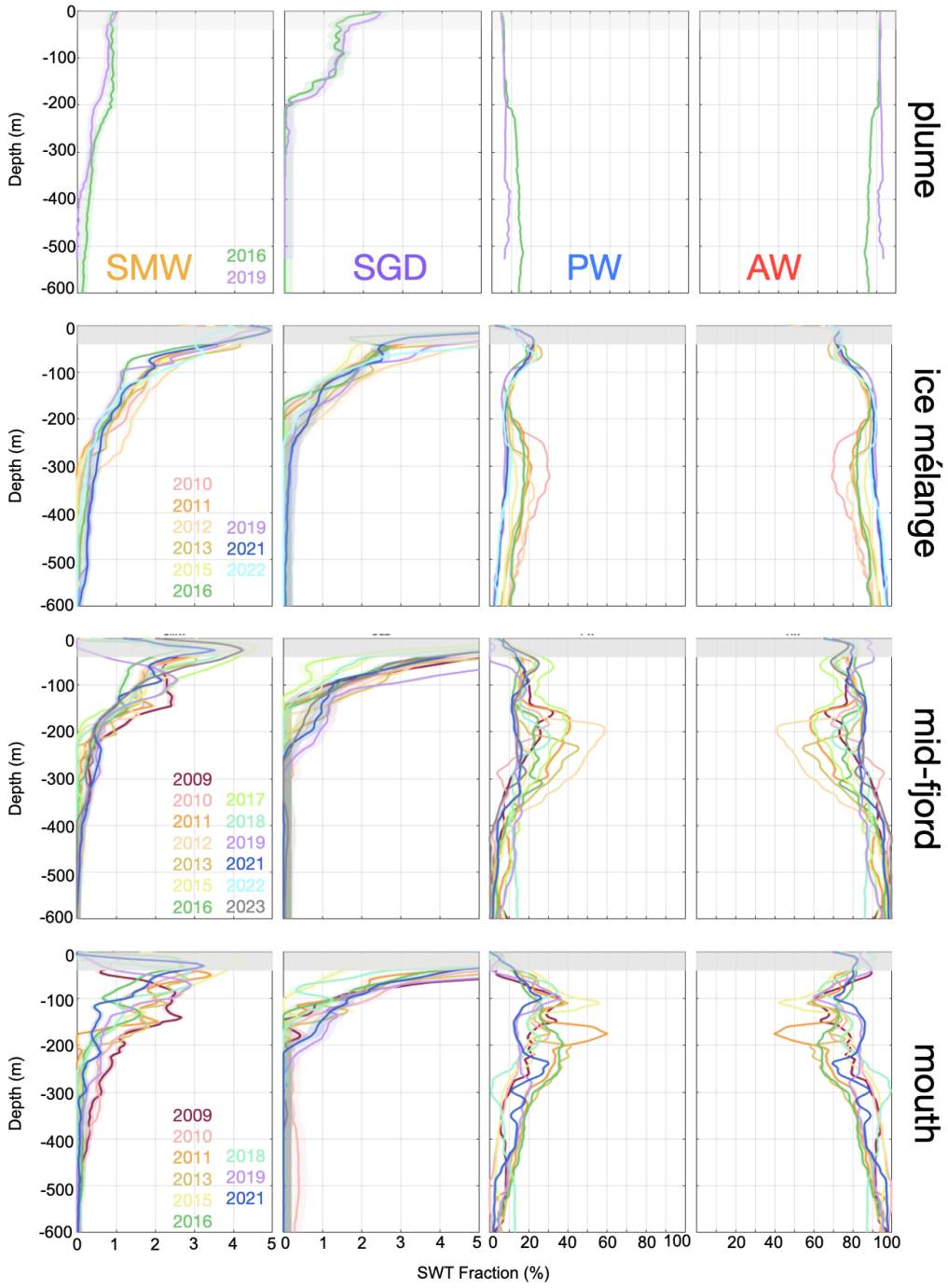


**Figure 3.7.** RLS method fraction solutions (%) from specific fjord regions for all years in the Sermilik Fjord gridded dataset (colored lines). Rows in the figure correspond to a single fjord region (plume, ice mélange, mid-fjord, and mouth) and columns of the figure correspond to specific SWT fractions (AW, PW, SGD, and SMW). The SMW and SGD x-axes are from 0–5% and the PW and AW x-axes cover 0–100%. The top 50 m of each panel are greyed out in order to prevent interpretation of the solutions at the surface where the mixing model does not represent the data well.

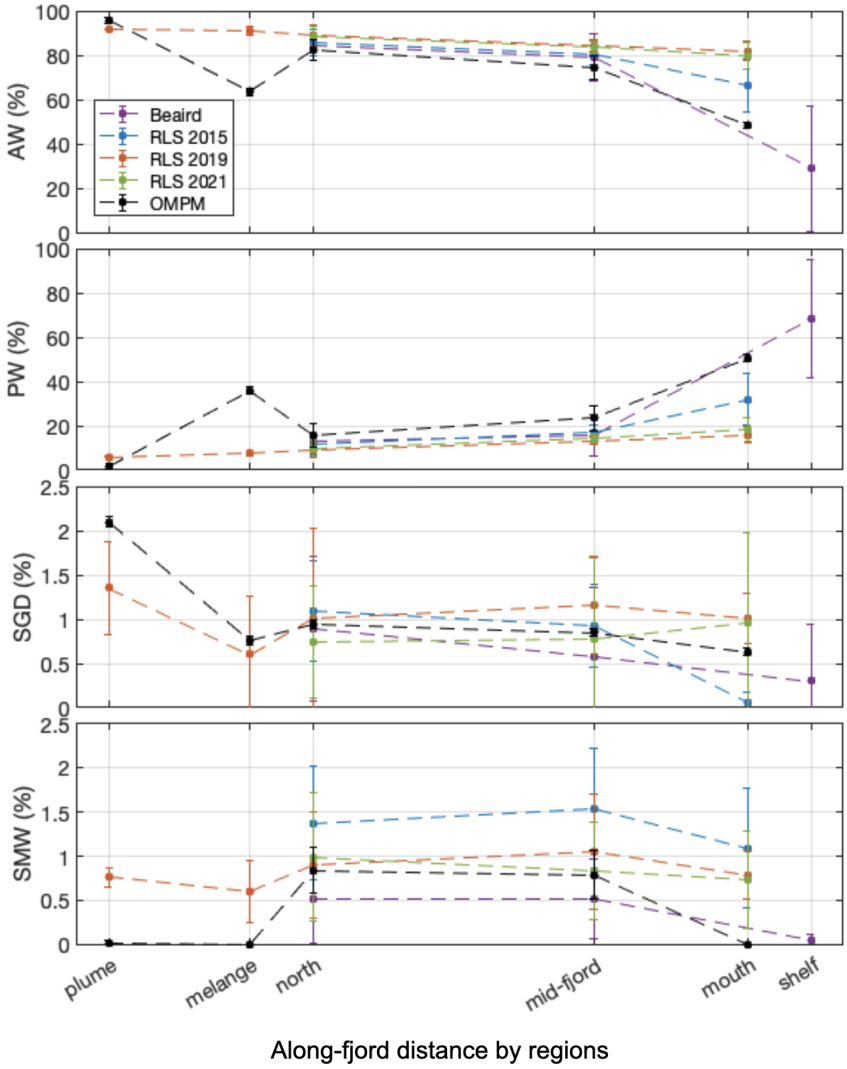


**Figure 3.8.** Comparison of three different water mass fraction methods: OMPM (black line), RLS method for three years (2015, 2019, and 2021), and noble gas-derived water mass fractions from 2015 (Beaird et al., 2018), for all SWT fractions across the different fjord regions. Data visualized here match the results in Tables 3.1 and 3.2

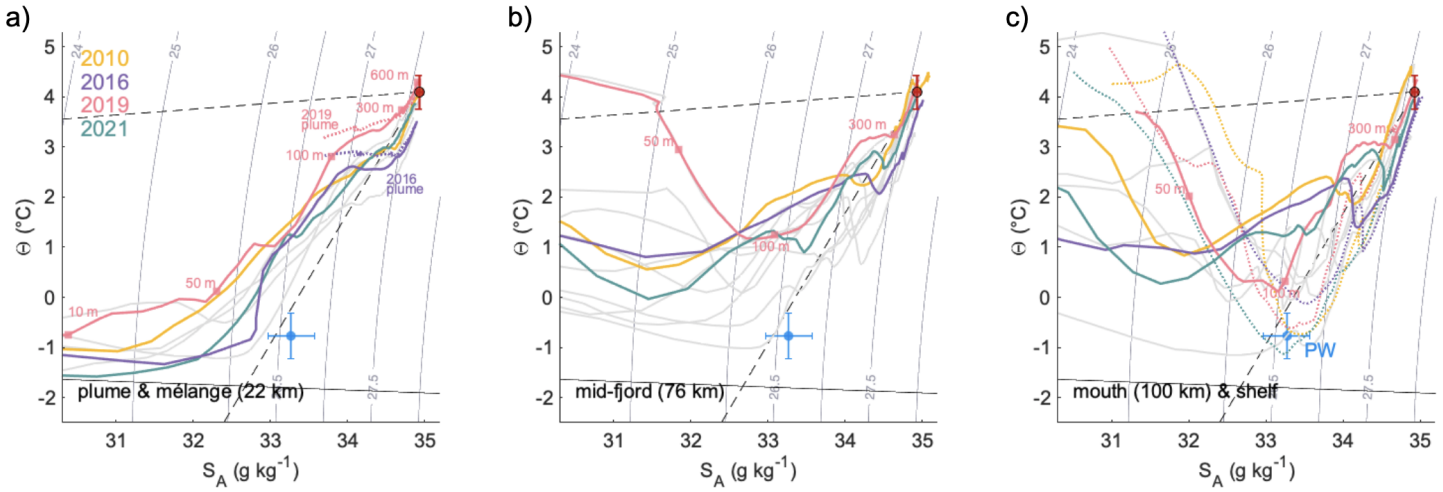


**Figure 3.9.** Temperature and salinity properties in $\Theta - S_A$ space for four different survey years (2010, 2016, 2019, and 2021) at four different fjord regions: a)plume and mélange, b)mid-fjord, and c) mouth. The properties of the plume profiles from 2016 and 2019 are represented by dashed lines in panel a). All other survey years (2009, 2011, 2012, 2013, 2014, 2015, 2017, 2018, 2022, and 2023) are represented as light grey lines in each panel. Mean shelf profiles are shown as dashed dark grey lines in panel c). In each panel, the mean AW (red) and PW (blue) properties are plotted with standard deviations in temperature and salinity. This are the mean values of the warmest AW in the fjord for all years and the coldest mean shelf properties across all year for defining the PW.

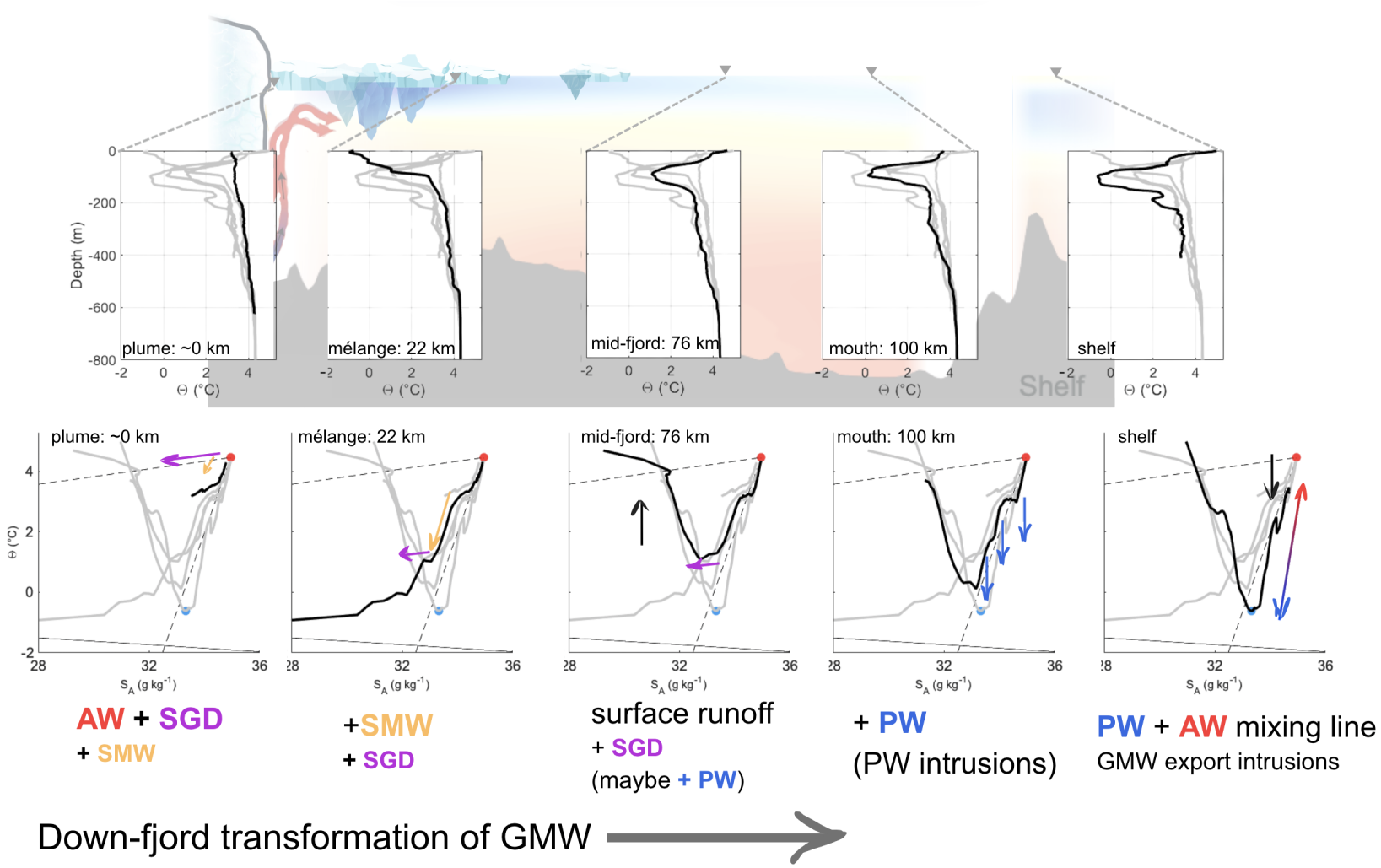


**Figure 3.10.** Key areas of water mass transformation in Sermilik Fjord and associated SWT fraction contributions as Glacially Modified Water moves down-fjord. Data represented is from the 2019 survey, but these transformation steps are persistent in time. Data are shown as temperature profiles (top row) and in $\Theta - S_A$ space. Arrows indicate directions of mixing along mixing lines between SWTs. Size of text for SWTs (AW, PW, SGD, and SMW) indicates relative fraction contribution.

# Chapter 4

# Reflection and Reflexivity: Using the Greenland National Research Strategy as a guiding document

## 4.1 Introduction

I first met the Greenland Ice Sheet in February 2017. I landed at Summit Station, a U.S. owned and operated research station at the ice sheet's highest point, in a twin otter ski plane from Iceland. It was -70°F. The Kalaallit Nunaat and U.S. flags flapped in the wind together above the main building of the station as I walked up the metal stairs of the "Big House" for the first time to attend orientation. My time at Summit Station was truly life changing. I saw snow and light do surreal things, I gained crucial skills as a scientist and teammate, I drove snowmachines for science and hosted U.S. government officials visiting the research station. It didn't occur to me until years later how odd it was that I spent months in Kalaallit Nunaat and barely had a single conversation with a Kalaallit person. The work of maintaining long-term climate records at Summit Station was important and rewarding, but it was a U.S. bubble inside another country and culture that I never questioned. Leaving Summit Station at the end of that season, I flew out to Kangerlussuaq in a hulking US military LC-130 cargo plane—standard transportation for scientists around the ice sheet. This is just the way international science in Kalaallit Nunaat was, and largely still is, performed—"parachute science" or "hit and run

science" as the Kalaallit/Danish scholar Naja Dyrendom Graugaard has called it.

Since then, the relationship between international scientists and Kalaallit Nunaat has changed and conversations have evolved, as have my own learning and values. Kalaallit people (academics, government officials, community members) speak strongly, publicly, and often about the need for Greenland to receive benefits from international research, and more structures are in place to work towards that. "Research fatigue" is discussed as a common problem in local communities and organizations like Arctic Hub have been established to better coordinate and prepare international scientists. The problems and barriers preventing equitable and mutually beneficial science are more widely discussed compared to a decade ago, as are the historical legacies of colonization and on-going marginalization of Kalaallit people.

The Greenland National Research Strategy (GNRS) 2022–2030 was the first document produced by Naalakkersuisut (the Government of Greenland) articulating what beneficial international research in Greenland should look like (Naalakkersuisut (Government of Greenland), 2022). It gives international researchers a clear, formally stated set of expectations grounded in Greenland's own priorities. Prior to the GNRS, Arctic Indigenous groups and nations have a long history of articulating standards and requirements for ethical, equitable, and mutually beneficial research in the Arctic. Despite this, the research community has been slow to adapt. Together, these guiding documents articulate a high-level collective vision for where the research community should be, rather than prescribing specific, project-scale choices. The work of translating that vision into action now lies with the international research community at the scale of individual projects and teams who must try new things, form new relationships, and work in genuinely new ways. This chapter documents one project's attempt at this.

First, I translate statements of the GNRS into characteristics of research projects that can be evaluated and propose a reflection exercise based on this. This could be a transferable tool that other research teams, especially in the natural sciences, could use to assess their projects. Second, I take a first step at reflecting on aspects of the larger projects that encompassed and fostered the science presented in this dissertation. These were complex, collaborative projects with multiple

PIs and spanning multiple years. Therefore, this is not a full accounting of the projects or a formal evaluation, but is a first step in both 1) identifying a structure that could support formal evaluation in the future and 2) reflecting on the work I've personally been involved with. The argument underlying these goals is that reflection should not be separate from actively "doing the science". We can't improve what we don't name and document. What are the honest gaps between the aspirations of the Greenland National Research Strategy and the actions/outcomes of the research I am part of today?

The current U.S.–Greenland political context, with the U.S. threatening invasion and control of Greenland, makes this reflection even more urgent. Science and data collection have never been neutral acts, but how science has been conducted in Greenland in the past and present by U.S. researchers, often with reliance on U.S. military infrastructure and U.S. government funding, is a present ethical discussion that cannot be ignored. Conducting science in Greenland as a U.S. researcher requires an understanding that we carry on a legacy of outsiders traveling to Greenland with their own agendas—extracting knowledge, adventure, geopolitical power, and resources—with Kalaallit Nunaat rarely receiving any benefits from these actions. We cannot change painful and violent history, but we can (and should) learn about it, and then work in ways that respond to what Greenlanders are asking for in the present.

There is already a growing body of academic work developed by social scientists, health researchers, fisheries researchers, public officials, and other academics on ethical and equitable research in Kalaallit Nunaat specifically, with a range of projects utilizing best practices and sharing their challenges and successes (Hansen and Ren, 2021). The problem is that this work is rarely connected to natural science projects. By including this chapter, we hope to alert ice-ocean colleagues about work occurring in other research fields that may lead to re-imagining what our collective ice-ocean and fjord dynamics research efforts can look like.

Ultimately, the best science comes from trusting collaborations, and at the heart of the science presented in this dissertation are human relationships—whether that's with crew members on the research vessel, Greenland-based science colleagues, our lab group, or local

community members. In many ways, moving toward more ethical and mutually beneficial science in Greenland is about prioritizing these relationships over science outcomes and prioritizing our own humanity over being "researchers". As indigenous researchers Heather Sauyaq Jean Gordon and Deana Around Him stated, "The first step in conducting ethical research with Indigenous Peoples is self-awareness as a researcher. Understanding one's own identity, perceptions, and roles is crucial for building sustainable, reciprocal relationships" (Gordon and Around Him, 2025). I weave reflexivity through this chapter—not only reflecting on our project's goals and execution, but my own experience and identity as a U.S. researcher working in Kalaallit Nunaat.

## 4.2 Positionality statement

*Positionality statements are common in the social sciences and humanities, with the premise that a researcher is never a neutral observer—who you are shapes what you pay attention to, what questions you ask, who you listen to, and what you consider worth knowing. A positionality statement makes these factors visible to the reader, who can then evaluate the research within that context. At Greenland Science Week in Nuuk in 2025, Mari Kleist, current Chair of the Greenland Research Council, shared remarks that included the following: "To recognize our own position is to show respect...True research humility begins with asking 'Who am I in this space' and 'How do I ensure my work gives back more than I am taking'".*

I am speaking as a white U.S. researcher, born and raised in Alaska on Tanana Dene lands, with economic privilege and access to academia and higher education. My parents were professors in computer science and math. I therefore have the privilege of feeling comfortable in a group of scientists and academics. I feel comfortable critiquing the processes of traditional western science and academia because I feel safe to do so and have been encouraged by academic mentors I trust. As a PhD student, I had limited decision-making power within our project and was not involved in the initial project creation, scoping, or budgeting. Typical for PhD

students, I joined the project after the science goals and team were mostly formed. Despite this, I had immense support from my advisor and co-PIs to develop aspects of our work that I was passionate about. Our team made me feel like the ideas and goals I had were worthwhile, and I was entrusted with building relationships in Kalaallit Nunaat. This felt unusual and I'm deeply grateful for that trust. I had previous experience as a researcher and had been doing field work in Kalaallit Nunaat as a field engineer prior to beginning my PhD. This put me in an unusual position as a PhD student where I had less spin up in navigating the norms of grad school, research environments, and collaborations—an overwhelming process for everyone who goes through a natural science PhD program.

Growing up and living in Alaska has shaped who I am as a scientist. I am connected to and inspired by the research community in Alaska, especially those that are doing community-based and knowledge co-production work. I have an identity of "being from Alaska and the Arctic", though I am a white settler. This allowed me to connect with Kalaallit people and friends with a shared understanding of fishing, hunting, connection to land, and being aware of how outsiders characterize Arctic people and Arctic narratives. This sometimes opened up different with Kalaallit colleagues compared to other colleagues. I am perhaps more sensitive to how Kalaallit view and relate to outside scientists because I also experience outside scientists, journalists, and filmmakers, working in Alaska and creating knowledge about my home through their specific lenses. With this, I have noticed that it can feel easy for me to over-generalize my experiences in Alaska to Kalaallit Nunaat, but each place has their own distinct history, cultures, politics, and challenges, and my role is different in each place. Comparing and contrasting Alaska and Kalaallit Nunaat, and the dynamics between scientists and communities in both, has been a useful way for me to learn. In Kalaallit Nunaat, I am a guest and I am building a career in understanding a place I do not spend a majority of my life in.

I struggle with being a non-Kalaallit person and outside researcher sharing and telling stories about a place that is not my home. Whether this is at scientific conferences speaking about my research in Sermilik Fjord or to U.S. journalists curious about what people eat in Greenland

and how they feel about Trump. I do my best to credit Greenlandic colleagues, academics, and activists that I've learned from in these communications, and provide ways for others to learn directly from Kalaallit people.

Colleagues on this project that I have had the joy of working with have different backgrounds and identities from me. They may draw different conclusions from our work than what I have shared below. Finally, I am largely speaking to other U.S. and international researchers here in this chapter versus researchers in Kalaallit Nunaat or to a general public audience.

## 4.3 Background

### 4.3.1 Guidelines from the science community

The Greenland National Research Strategy (GNRS) is part of a legacy of earlier documents and decades-long efforts identifying challenges and solutions to equitable research in Kalaallit Nunaat, and the Arctic more generally. The U.S. Interagency Arctic Research Policy Committee (IARPC) established the Principles for the Conduct of Research in the Arctic initially in 1990 and revised this document in 2018, providing guidelines for research in the Arctic by U.S. researchers (Interagency Arctic Research Policy Committee (IARPC), 2017). Also in 2018, U.S. National Science Foundation staff collaborated with Naalakkersuisut and Nunatsinni Ilisimatusarnermik Siunnersuisoqatigiit (Greenland Research Council), to host a workshop, followed by a public report, titled "Facilitating increased engagement between the research communities of Greenland and the U.S." (Culler et al., 2018). The results of this workshop both laid the foundation for many of the recommendations in the GNRS and led to funding supporting new outreach and collaboration initiatives. Additionally, a paper by Mercer et al. (2022) with co-authors from the Greenland Research Council, Greenlandic Government, U.S. National Science Foundation, and U.S. academic institutions, was developed from this workshop. This work specifically shared a summary of the history of U.S. research in Kalaallit Nunaat[1], the

[1]We do not provide a comprehensive review of U.S.–Kalaallit research relationship and history here and refer the reader Mercer et al. (2022)

current state of relations between the Kalaallit and U.S. research community, and shared tangible recommendations and actions to be implemented. Finally, another guiding document in the lineage of the GNRS is the Circumpolar Inuit Protocols for Ethical and Equitable Engagement developed by the Inuit Circumpolar Council (ICC) and released in 2022 (Inuit Circumpolar Council, 2022a).

Why continue to update and refine guidelines for ethical Arctic research when a document was established in 1990? There are several important points in the answer to this question. The first is that despite guidelines existing in 1990, there was a general consensus that researchers were not responding and shifting their practices—communities were still considered an afterthought by most Arctic researchers concerned with global environmental change (we would not need to keep having this conversation if that had meaningfully changed). A possible contribution to this lack of change is that the 1990 IARPC guidelines have much weaker language and motivation compared to recent documents. Despite saying that "**All** scientific investigations in the Arctic should be assessed in terms of potential human impact and interest" (emphasis mine), the need for prior informed consent and community involvement was aimed at social science researchers and those working directly with people. For instance, the statement "Researchers should consult with and, **where applicable**, include communities in project planning and implementation" (emphasis mine) allows space for a natural scientist to claim their research isn't applicable for including communities. This "out" is not an accident of language, rather it reflects an assumption, still common in the physical earth sciences, that studying the environment directly involves less connection to and input from people. In an academic system that prioritizes publishing output over long-term projects and relationships, it's easy to see how voluntarily taking on more work to build relationships and interface with communities was not done en masse by Arctic researchers if they didn't feel they needed to. Finally, a document from IARPC or the U.S. National Science Foundation is an attempt by the research community to organize ourselves to better align with the goals of science. This is distinct from guidelines and asks developed by Arctic indigenous governments, organizations, and communities themselves.

### 4.3.2 Background: Inuit Arctic Policy

In parallel to the science community developing guidelines for ethical engagement, the Inuit Arctic Policy was developed by the ICC beginning in the 1980s. Creating such a policy was central to the ICC since its founding in 1977. Initially, the idea for the Inuit Arctic Policy came from the threat of increased oil and gas development in the Beaufort Sea and the challenge of multiple national governments promoting resource development under different regulations in a region of Inuit Nunaat (Inuit Homelands) with no ecological borders (Stenbaek, 1985). If Canada allowed oil development in its Arctic waters and there was a spill, then damage to the environment would not be limited to Canadian waters alone. The fact that the Arctic as a whole is an interconnected ecological region motivated the need for an Inuit Arctic Policy. The policy also established Inuit as policymakers on an international stage, as opposed to having policies of disparate national governments enacted upon them (Stenbaek, 1985). The finalized Inuit Arctic Policy, released in 2010, has dozens of policy positions across a range of domains including housing, health, Inuit rights, nuclear proliferation, education, conservation, subsistence, energy, cultural and intellectual property and more. Section VII includes specific policies for Arctic Scientific Research, including:

> *8. Researchers should shift the focus from research about Inuit, to research with Inuit.*
>
> *13. Traditional knowledge should include both traditional ecological knowledge, environmental and cultural knowledge, either as handed down through generations or as engendered in contemporary times. Traditional knowledge should be integrated with western sciences into all research projects and education in the Arctic.*
>
> *14. Ethical and other basic principles for the conduct of northern scientific research should include the following:*
>
> *. . . In the case of researchers unfamiliar with the Arctic and its northern peoples and cultures, appropriate orientation and training programs should be mandatory prior to the commencement of research;*
>
> *. . . the duty of researchers to inform Arctic communities continues even after the initial approval to proceed with the research has been obtained. On-going*

*explanation of research objectives, methods, findings, and interpretations is required;*

*. . . where possible, research programs should anticipate and provide for meaningful training and involvement of Inuit researchers;*

*22. Private and public foundations and especially national and international research councils and funding agencies should insist on the inclusion and close co-operation with Inuit and other Arctic inhabitants in Arctic research projects. Such participation should be a pre-requisite for obtaining funding.*

*(Inuit Circumpolar Council, 2010)*

These policies, drafted in the 1980s and established as a living policy document in 2010, formed the backbone and foundation of the subsequent Circumpolar Inuit Protocols for Ethical and Equitable Engagement (2022) and GNRS. There is a distinctive strength in the language of these Inuit governance documents compared with the original IARPC documents from the research community. What we see in more recent documents with research community co-authorship, like Culler et al. (2018) and Mercer et al. (2022), is the practical work of elevating Inuit priorities to the same status as international research priorities within the governments that fund and administer Arctic research.

### 4.3.3 Background: The Greenland National Research Strategy

The Greenland National Research Strategy is that practical work distilled specifically for the Greenland context for the coming decade. While the ICC produced documents for the whole of Inuit Nunaat, the unique political and social forces within Greenland require more specificity. The strategy articulates four main goals:

*1. Research must be anchored in Greenland, with an emphasis on the integration of local and indigenous knowledge and expanding Greenland's own research capacity.*

*2. Research must support sustainable societal development.*

*3. Research results must be easily accessible to all.*

*4. Research efforts must be conducted at an international level.*

*(Naalakkersuisut (Government of Greenland), 2022)*

Importantly, and distinct from the ICC documents, is that the strategy highlights Greenland's own research capacity and institutions. The strategy welcomes international collaboration in growing Greenland's research community and in helping to support Greenlandic and Greenland-based scientists. As a result, a present challenge experienced by the Greenlandic research community is an overwhelming number of requests from international scientists to work with and partner with them. While the intentions of these requests are often genuine, the Greenlandic research community is small relative to the number of international scientists working in Greenland. This has created a tension where the Greenland research community does not have enough capacity to respond to offers of partnership that could lead to growing capacity. This has implications for individual Greenland-based researchers—they have to choose and discern which projects benefit them and Greenland the most.

### 4.3.4 Background: Why self-reflection and self-assessment matters

For international researchers, we must learn to accept any rejection or a lack of response to our requests as information to prompt reflection (true even if partnerships are welcomed and developed). Why are we are asking for partnership at all? Does our work truly help grow research capacity in Greenland, or are we trying to check a box to be perceived as ethical as expectations have evolved? Do our research questions have interest and value to Kalaallit and the Greenland research community? These latter questions and actions are not necessarily spelled out in official guidelines and policy documents, but emphasize the importance of self-reflection by individual international scientists as we work towards improved and responsive research practices.

The work, conversations, and relationships created by the documents described above and their evolution through time represent an important ongoing cultural shift and establishment of new norms within the U.S. and Kalaallit research communities. However, these documents have never been binding. U.S. projects do not currently face any material consequences (i.e. loss

of funding or lack of permission to conduct research) if they do not adhere to the protocols and best practices defined in these documents. In contrast to the Canadian Arctic and Alaska, there are fewer established formal protocols for seeking permission to conduct research or guidelines for ownership and access of data and knowledge. It is currently up to individual researchers and groups to opt-in and normalize equitable, beneficial, and just research practices. Though we may see a shift in the coming decade to more specific and binding requirements from the Government of Greenland, the current opt-in system once again highlights the need for self-reflection and self-assessment by international researchers.

### 4.3.5 Background: Other Inspiration

Much academic and practical work already exists for promoting and normalizing equitable research in Kalaallit Nunaat and other Arctic regions. Individual projects need not reinvent frameworks and best practices structurally designed to work towards the goals in the research strategy. There are research projects in a range of fields implementing best practices and publicly sharing challenges and successes. Specifically, Co-Production of Knowledge (CPK) and Community-Based Participatory Research (CBPR) frameworks have been applied in many Arctic research contexts with tangible benefits to communities. Key contributions that serve as touchstones for me personally include the CPK framework articulated in Ellam Yua et al. (2022), which argues that much of the structure of contemporary Arctic research is rooted in colonialism and calls for systematic change; Cana Uluak Itchuaqiyaq's practical guide to equitable Arctic research (Itchuaqiyaq et al., 2023); and the work of Rudolf (2025) on the factors that enable or undermine co-production partnerships, and questioning if CPK is all too often perpetuating colonial power structures.

CBPR frameworks, widely used in public health, assess how closely a project's actual practices match principles at each stage of research—from design through dissemination. They are built for iterative, honest reflection rather than only relying on post-project external audit (Wallerstein and Duran). An inspiration and resource specific to Kalaallit Nunaat is the edited

anthology Hansen and Ren (2021) which presents experiences from collaborative research in Greenland, including explicit CBPR projects, across multiple disciplines. Notably, the physical sciences are strikingly absent from this anthology, though this gap has been well-documented in other contexts and is summarized in the following section.

### 4.3.6 Background: Physical sciences have been slower to adopt equitable research frameworks

Brunet et al. (2014) and Brunet et al. (2024) empirically tested whether Arctic research has been transformed with an increase in local community involvement by reviewing and categorizing published research papers in the journal *Arctic* spanning 1965–2020. They found that despite growing rhetoric around community engagement and Indigenous knowledge integration, meaningful local participation remained limited and largely unchanged across this period. In Brunet et al. (2014), physical science papers (defined as climate, atmospheric, physical geography, geology, and cryosphere research) had the most traditional Western science approaches compared to social science and multidisciplinary papers.

Similarly, Monakhova et al. (2025) conducted a systematic literature review of Arctic sea ice research to assess the state of CPK practices specifically. Of more than 65,000 peer-reviewed articles on sea ice, only 461 mentioned any engagement with Arctic Indigenous communities, and just 25 explicitly described collaborative community engagement or CPK. While this work encountered challenges with consistent terminology and reporting of CPK/CBPR practices, the results are still striking. In particular, they note the lack of Indigenous co-authorship in sea ice literature. Sea ice, which has arguably the most connection to hunting and cultural practices of all physical systems in the Arctic, should be an area of physical sciences that can integrate equitable research frameworks and best practices most naturally.

These are not the only ways to assess whether the called-for cultural shifts in science practices are occurring, but they are two examples that highlight specific barriers faced by physical sciences in aligning with ethical Arctic research. The underlying reasons for why

physical sciences remains slow to adopt equitable research best practices in the Arctic are well-understood and structural: Physical scientists are trained in a system that treats community engagement as external to ”real” science; Physical scientists are specifically trained to view natural systems as ”mechanistic objects” separate from social systems; our institutions do not fund or reward equitable and engaged science; our career structures punish the slow timelines that genuine relationship-building requires; institutional barriers exist that make simple concrete actions, like paying honoraria to community members or elders, needlessly difficult; and the historical record of our disciplines and overarching histories of colonization give communities good reason to have distrust (Druckenmiller, 2022; Ellam Yua et al., 2022; Gvèret, 2022; Lauter, 2023; Stein et al., 2024).

This is not to say there are no positive examples of physical science research forming mutually-beneficial collaborations, utilizing CPK and CBPR frameworks, or applying ethical research best practices where possible. Projects for readers to learn from include Ikaagvik Sikukun (Ice Bridges) project, which integrates modern geophysical measurements of sea ice with indigenous knowledge to answer research questions that were co-developed with the community of Kotzebue, Alaska (Hauser et al., 2021); the Exchange for Local Observations and Knowledge of the Arctic (ELOKA), a long-running platform specifically designed to document and integrate Indigenous and local observations of sea ice alongside scientific data (Pulsifer et al., 2012). In Kalaallit Nunaat, physical science research led by Greenland Institute of Natural Resources scientists have long-standing community partnerships. Research groups based outside of Kalaallit Nunaat but collaborating with GINR scientists and Kalaallit communities include Kalaallit Nunaat Qaffappoq (Greenland Rising), a geophysics project in partnership with the Greenland Institute of Natural Resources and four Greenlandic communities to understand local sea level change and plan for community futures (Tinto et al., 2019). Finally, I highlight the work of Shin Sugiyama’s Japanese research group working in the Qaanaaq area researching questions about the connections between rapidly changing coastal and fjord environments and marine ecology and communities. For several years, they have held workshops with the residents

of Qaanaaq of Qeqertat to introduce their project, share results, build trust and work toward transdisciplinary mutually-beneficial research (Sugiyama et al., 2020; Otsuki and Sugiyama, 2025; Sugiyama et al., 2025).

This is not an exhaustive list, but rather meant to show that there are physical science-based projects working to follow best practices even if physical sciences more generally are still lagging behind other disciplines in responding to calls for equitable research practices in Kalaallit Nunaat and the Arctic as a whole.

### 4.3.7 Background: Navigating the New Arctic Program

The Navigating the New Arctic (NNA) Program, one of NSF's Ten Big Ideas, represented the largest and most ambitious attempt by the U.S. federal government to address the longstanding disconnect between Arctic research and the communities it affects (Druckenmiller, 2022). Running from 2017 to the end of fiscal year 2023, the program invested over $150 million across more than 100 individual and collaborative projects, spanning the social, natural, built, and computing sciences (National Science Foundation, 2023). Its defining structural feature was a requirement that projects scientifically engage with at least two of three domains: the natural environment, the built environment, and social systems. This convergence requirement pushed physical scientists toward interdisciplinary work and community engagement in ways that prior Arctic funding mechanisms had not.

The program had a rocky start. NSF vastly underestimated the research community's lack of literacy in CPK and CBPR practices, ethical engagement frameworks, and equitable research methods, and key structural barriers — including how to route funding directly to community members, pay honoraria to elders, or establish community-led data sharing agreements — were initially unaddressed (Bahnke et al., 2020; Stone, 2020; Druckenmiller, 2022). But it was progress. Over the lifetime of NNA, funding was routed to community members and outreach efforts, more extensive training opportunities for researchers were provided, and Arctic Indigenous ways of knowing were centered in academic meeting spaces in new ways.

### 4.3.8 Background: FISHEE and GRISO Project

The work in this dissertation was largely funded by the Navigating the New Arctic Program through the project Global changes, local impacts: Study of glacial fjords, ecosystems and communities in Greenland (Award No. 2127241) (Straneo et al., 2022). We later adopted the acronym FIord-SHelf Ecosystem Exchanges for the project, which included collecting ocean and fisheries observations in Sermilik Fjord in 2023 and 2025, and in Qimusseriarsuaq (Melville Bay region in NW Greenland) in 2024 and 2026. The efforts of our research to better align with the GNRS and my own learning (as is evident in this chapter) are a direct result of the NNA program and U.S. government investment in Arctic community priorities.

I want to be clear that our project did not follow initial steps of CPK or CBPR and should not be considered as such. Unexpected events including the passing of a Greenlandic colleague and the COVID-19 pandemic occurred in the early stages of the project development. The original intention was to design a mutually-beneficial project after hosting listening sessions with communities. The pandemic derailed this and project leaders reoriented in response, utilizing a more standard western science project structure and development path. Team member and co-PI changes occurred (which happens in any project) that impacted the project's connection to local communities. However, that does not mean that smaller actions taken within a more western science project structure were not and are not possible.

The GReenland Ice Sheet-Ocean (GRISO) Network also supported the science and outreach work represented in this dissertation. Founded in 2011, GRISO represents a network of scientists interested in problems related to Greenland Ice Sheet change, and its interaction with the ocean, the atmosphere, the marine ecosystems and local communities. Rather than being an individual research project, GRISO supports the interaction of different scientists across disciplines and with community members through workshops, summer schools, and other initiatives. GRISO has been funded by a variety of sources and most recently has been funded by the U.S. National Science Foundation. GRISO supported the creation of the StoryMap (see

below) and I was a participant in the GRISO summer school, where conversations and learning about conducting mutually-beneficial research in Kalaallit Nunaat are centered.

While the structures and goals of FISHEE and GRISO are unique, they are both bureaucratically complex, multi-disciplinary, and multi-PI projects spanning multiple years. A formal post-project evaluation of either project has not been completed they are still on-going and doing so will be a massive undertaking with involvement from the many project leaders and collaborators. That work is beyond the scope of this chapter or dissertation. However, grounded in the understanding of reflection as an on-going process, I present a possible framework by which to begin evaluation of these projects using the GNRS and I take some first steps in reflecting on the work I have personally been involved in during my time as PhD student.

## 4.4 The GNRS as an evaluation tool

The GNRS articulates the aspirations for research in Greenland, but translating those aspirations into tangible, project-level actions is the challenge facing international research teams. Bridging this gap requires creativity and a willingness to work in new ways. At this early stage, learning from other projects about what they have tried, what has worked, and what has not is itself a valuable part of the process. To support that kind of structured reflection, I present a self-reflection table organized around the four core goals of the GNRS. This tool is designed to be completed collaboratively by a project team, prompting discussion and serving as a reflective instrument rather than a pass/fail checklist. The goal is to create a systematic record—of what a project tried, what it did not try, what got in the way, and what it learned. By placing project-level actions alongside the goals of the GNRS, we can see how those actions connect to the broader vision, and how they might be built upon and scaled over time to work toward what the GNRS is asking for.

Given that this chapter is not a full project evaluation with all the co-PIs of FISHEE or GRISO, I will use the reflection table to document project actions that I was part of and how

those actions connect with the GNRS goals. After the table, I highlight and contextualize specific efforts and share broader takeaways which may be useful for other projects, PIs, or PhD students working in Kalaallit Nunaat.

I stress that this table is one tool for helping prompt reflection and organize ideas in a way that could be comparable across projects, but it cannot capture every detail or all the history of a project. Narrative reflection and evaluation is a necessary and complementary process alongside any visual aid.

### 4.4.1 GNRS as an anchor

The GNRS is used as the starting framework for this reflection because it is Naalakkersuisut's own articulation of its aspirations for research conducted in their country and communities. However, we note that a national government may not be representative of all communities and that research priorities are likely heterogeneous from community to community. Additionally, the language of the national research strategy is written as Naalakkersuisut's commitments that it will make as a governmental body at a national and international scale. Where applicable, we have interpreted the intent of the goals listed to actions at an individual project level and reported those in the table and reflection exercise, but not all goals listed in the document can be interpreted to the project level. For instance, we have omitted initiative 4.1—"Naalakkersuisut aims to ensure that aggregate research funding from the Treasury, research institutions and public and private companies amounts to at least 2.3% of GDP by 2030." from the table as this is beyond the scope of an individual project.

We note that the Greenland Research Council and Naalakkersuisut are developing specific ethical guidelines for research activities to be released in the near future. This is distinct from the GNRS and when those guidelines are published, this activity could be tailored to those specific guidelines.

### 4.4.2 Rating level of each goal

Each row in the table is rated on the following scale:

**Not addressed or applicable** This goal was not pursued in this project, or is not applicable at the individual project level.

**Partial** Some action was taken toward this goal, but meaningful gaps remain between what was done and what the goal envisions.

**Met** Deliberate and concrete action was taken in alignment with this goal.

**Ongoing/Embedded** This goal is built into the project structure across multiple field seasons and collaborations—not a one-time effort, but a sustained commitment.

Rating in this way has limitations, but helps provide an at a glance overview. Space in the table is given to further defining actions and gaps in the project, and the discussion section below includes expanded points.

## 4.5 Reflection table

## 4.6 Discussion

### 4.6.1 Utilizing Greenlandic Research Vessels

The NNA FISHEE project utilized the R/V Tarajoq and R/V Sanna—Government of Greenland-owned and -operated research vessels. The R/V Tarajoq (Figure 4.1), built in 2020, represents one of the largest investments by the government in their own science infrastructure, and our group was one of the first international science groups to utilize the vessel. By contracting with Greenland-owned vessels, our group supported the continuation of that infrastructure, showing that there is an international demand that Greenland can fill, along with salaries of Greenlandic crewmembers and logistics staff.

**Table 4.1.** An example of the Project Reflection Framework based on the Greenland National Research Strategy filled out for the work discussed in this dissertation.

## Project Reflection Framework

### Alignment with Greenland's National Research Strategy 2022–2030 (Naalakkersuisut)

*NRS language quoted directly from the English translation (nis.gl, December 2022).*

| Level Scale: | N/A — Not addressed or applicable | Partial | Met | On-going / Embedded |
|---|---|---|---|---|
| | *Not addressed in this project* | *Some action taken; meaningful gaps remain* | *Deliberate and concrete action taken* | *Built into project structure across field seasons; not a one-time effort* |

C

| NRS Goal / Initiative | Actions taken | Level | Possible future project actions |
|---|---|---|---|
| **Goal 1: Research must be anchored in Greenland** | | | |
| **Research institutions must continue to expand.** "Local researchers [must be able] to set the course for research in this country by pointing to the needs and potential that they are familiar with... local bodies and institutions [must have] the necessary resources to invite a growing number of external researchers to participate in projects." *(NRS pp. 23, 38)* | Projects included co-PI from GINR and GINR scientists were part of field work on Greenland owned and operated research vessels. Research agenda set by collective group of international scientists. | Partial | *Identify a Greenlandic co-PI or lead at the proposal stage. Contact Ilisimatusarfik and GINR directly. Accept that they are inundated with requests and may not have capacity to partner.* |
| **Improved overview of research activities.** "Naalakkersuisut aims to create a more comprehensive overview of research activities in the country... by requiring all research projects in Greenland to be entered into a central directory." Registration facilitates early contact between projects and local stakeholders. *(NRS pp. 28, 39)* | FISHEE project was registered on Isaaffik, Greenland's central research registry, prior to fieldwork. We also attended Arctic Hub webinars documenting and connecting researchers before each field season. | Met | *Register on Isaaffik (isaaffik.org) before field season. This is a concrete, low-effort action that immediately signals transparency and communication of activities. Follow Arctic Hub announcements and participate in events to coordinate researchers.* |
| **Ethical guidelines must define the parameters of research.** "The ethical guidelines are designed to ensure that the public is not unduly burdened by research activities... draw researchers' attention to local cultural differences and ensure that participants in projects receive feedback on the results and have a positive experience when contributing to research." *(NRS pp. 31, 44)* | Our project applied for appropriate permits with Naalakkeruisut. We communicated to contacts in communities about our presence, but did not necessarily "ask permission" or co-create research questions. Attempted to align our activities with research strategy and supporting Greenlandic education priorities where possible. Initial research design included listening sessions and co-creation but was canceled due to Covid-19 pandemic. | Partial | *Review Naalakkersuisut and ICC ethical research guidelines as a research team. Find small actions that move a project to be more in alignment with these guidelines, even if not a co-created or CBPR project.*<br>*Apply for appropriate permits with the government. Let communities know your research plan and be willing to adjust around activities like hunting, cruise ships, or other science groups.* |
| **Increased use of indigenous and local knowledge.** "Indigenous and local knowledge can be integrated — on an equal footing — into local and international research projects... [It] is knowledge that has been passed down from generation to generation and is bound to cultural, spiritual and linguistic values." *(NRS pp. 32, 48)* | Local knowledge was not formally integrated into the research design or data collection. No structured process existed for community members to contribute observations or co-interpret results. We did work with Maxi Audibert, local Tiilerilaaq school teacher, who shared his extensive knowledge in Sermilik Fjord and later developed bathymetric maps. In Kullorsuaq, we met with local hunters and | Partial | *This is one of the most significant gaps in standard U.S.-led Arctic research. It takes time to build relationships to truly integrate indigenous knowledge in an ethical and appropriate way. Greenland-based researchers have local partners and are integrating IK. We suggest learning from them and leaning on existing relationships and research partnerships.* |

**Table 4.1** Project Reflection Framework, Continued

| NRS Goal / Initiative | Actions taken | Level | Possible future project actions |
|---|---|---|---|
| | learned more about their home from them and their concerns. | | |
| **Strengthen local research institutions: use of Greenlandic infrastructure.** "[Resources must support] local bodies and institutions... to invite a growing number of external researchers to participate in projects." Using Greenlandic vessels and logistics providers directly supports the physical and financial sustainability of local research infrastructure. *(NRS pp. 23, 38)* | All sea-going fieldwork was conducted aboard Greenlandic-owned and operated research vessels. Logistical arrangements channeled funding to Greenlandic maritime and scientific infrastructure rather than U.S.-vessels. GINR scientists were paid by the project. | **On-going / Embedded** | *Contact GINR early to identify Greenlandic vessel options. Budget for them explicitly. This choice keeps research funding inside Greenland's economy and supports use and expansion of Greenland infrastructure.* |
| **Goal 2: Research must support sustainable social development** | | | |
| **Research must find solutions to future challenges.** "Intensifying our research efforts can help us to meet future social and environmental challenges... Naalakkersuisut aims to enhance the conditions for basic, strategic and applied research and their use in developing sustainable solutions." *(NRS pp. 19, 56)* | Project scope includes better understanding glacier and climate change impacts on fjord ecosystems, a significant environmental challenge in the present and future. However, the project results are not "solution oriented" – instead they are more about understanding system dynamics and predicting and projecting future changes. | **Not Addressed – Partial** | *Interdisciplinary projects that include social and humanities researchers likely have a better chance of being framed towards solutions to environmental and social challenges. Co-creating research questions with local partners has a greater chance of leading to research outcomes that can be applied and integrated to address challenges.* |
| **Private-public research collaborations and business development.** "Naalakkersuisut aims to enhance the conditions for private-public research collaborations and to increase the focus on business development through applied research." *(p. 58)* | Business development or connection was not part of the scope of this project. | **Not Applicable** | *More spaces of connection for the international research community to learn about the business sector (especially fisheries technology, aquaculture) could be facilitated by Arctic Hub or international researchers. DTU has many Greenlandic students that could be connected with researchers for internships or project ideas. Royal Greenland could be a potential partner for researchers.* |
| **Research as an attractive career option; support for Greenlandic PhD and postdoc researchers.** "Naalakkersuisut aims to support Greenlandic research institutions in their efforts to get the word out about research careers and to increase funding for PhD and postdoc programmes for Greenlandic researchers." *(NRS pp. 20, 64)* | While no Greenlandic science graduate students or early-career researchers were funded on this project, we created a paid internship opportunity for Greenlandic science teaching students at Iisimatusarfik during our 2024 and 2026 field seasons. In 2024, Nino was an invaluable team member.<br>Outreach to local schools in Tiilierilaaq and Kullorsuaq contributed informally to science career visibility for young people in each community. | **Partial** | *Reach out to Ilisimatusarfik's Sila program and GINR early, at least 5 months before fieldwork, to offer student opportunities for fieldwork. Even one funded field position is important. Maintain contact with Greenlandic-based colleagues to identify potential to financially support Greenlandic graduate students and post-docs.* |
| **Government use of research statistics**. "Naalakkersuisut aims to optimise cooperation with research institutions and Statistics Greenland on the development and use of research statistics." *(p. 68)* | Not applicable for our project | **Not Applicable** | *For a project more grounded in social science and/or population and health statistics this may be a relevant aim.* |
| **Goal 3: Research results must be easily accessible to all** | | | |

**Table 4.1** Project Reflection Framework, Continued

| NRS Goal / Initiative | Actions taken | Level | Possible future project actions |
|---|---|---|---|
| **Data must be handled according to open science principles (FAIR).** "To maximise the benefits of research, information must be accessible — to researchers, policymakers, industry, public authorities, students and the general public... Naalakkersuisut will work to increase the accessibility of knowledge on research projects in Greenland, and on the results of this research, and to actively disseminate this knowledge." *(NRS pp. 21, 71)* | Oceanographic data from Sermilik Fjord were archived and published in open-access repositories (Roth et al. 2025, ESSD), fully consistent with FAIR principles and available to Greenlandic institutions and researchers. However, disseminating results beyond the research community remains an on-going activity. | **On-going / Embedded** | *Publish data in open-access repositories (e.g., ICES, Arctic Data Center) and register datasets with Isaaffik. Adopt FAIR data practices and work toward implementing CARE data practices as applicable and led by Greenlandic institutions.* |
| **Results disseminated beyond peer-reviewed journals.** ".. [results] must be made widely available and used to promote development." The expectation is that knowledge reaches not only researchers but communities, policymakers, and the general public. *(pp. 8, 21, 71)* | Presentations to school children in Tiilierilaaq and Kullorsuaq shared project goals and early findings. Other than teachers, we did not include many adults. Creation of online StoryMap presented at Greenland Science Week and hopefully used in science classes around Greenland, translated to Kalaallisut (on-going work). | **Partial – On-going** | *Budget for a return visits or time to share results with communities visited during fieldwork. Partner with KNR (Kalaallit Nunaata Radioa) radio or TV. Even a one-page summary in Kalaallisut is an important step. Participate in Greenland Science Week Qaagitsi science fair event.* |
| **Goal 4: Research efforts must be at an international level** | | | |
| **International research cooperation must be enhanced.** "Naalakkersuisut aims to prioritise collaborative research with governmental and supranational bodies, and to take part in international research forums with a focus on research in the Arctic." Cooperation must generate mutual benefit — not extractive data collection. *(NRS pp. 22, 81)* | We did not have specific collaborations or connection to supranational bodies (Arctic Council or ICC). Project structure is internationally collaborative (U.S. - Greenland researchers) with research goals defined by the group. We attended Greenland Science Week and other international science meetings. Some benefits to GINR and Greenland scientists from the project. | **Partial** | *Participate in Arctic Council working group meetings relevant to your science — particularly the Arctic Monitoring and Assessment Programme (AMAP) and the Protection of the Arctic Marine Environment (PAME) working groups, These forums directly connect physical science findings to policy at the governmental level. Fund Greenlandic collaborators to present rather than U.S. researchers presenting about Greenland to an international audience alone.* |
| **Supporting UN Decade of Ocean Science**. "As a special initiative, Naalakkersuisut intends to give priority to supporting the UN Decade of Ocean Science for Sustainable Development (2021–2030) by establishing a 10-year ocean research programme." (p. 86) | | **Not Addressed** | *Potential for future alignment with this goal and requires communication with government and Greenland scientists.* |



**Figure 4.1.** The R/V Tarajoq in Sermilik Fjord outside of Tiilerilaaq in August 2025. Photo by Alex Rivest.

Working on the Greenlandic vessels is an opportunity for cross-cultural and two-way learning. One of the most joyful parts of field campaigns for me was learning Greenlandic words from crew members. Through informal conversations, I learned about Greenlandic politics and sports, hunting and fishing, and Greenlandic musicians. Several crewmembers expressed that they preferred working on the research vessels to cargo ships or other maritime jobs because it felt more meaningful.

### 4.6.2 Working with Greenlandic students

In 2021, Fiamma met Max Audibert, the schoolmaster in Tiilerilaaq. Max, originally from France, has been living there for decades and has dedicated himself to the kids of the community. This relationship provided further opportunities for us to share science with the handful of students in the school. In 2023, Max stayed with us on the R/V Tarajoq for several

days to learn more about our work and provided him with some simple tools for making ocean measurements of temperature and turbidity with students. I developed a coloring page activity (Figure 4.2) that communicated the temperature of the ocean in the fjord, something the students may have never seen before. In 2025, the students in the school were able to come onto the the ship and interact with our instruments and the crew (Figure 4.3). This would not have been possible without our Greenlandic science colleague Aqqaluk Sørensen and the support and help of the Greenlandic crew members. While sharing the science is fun for us, our primary goal was to expand their worlds just a little bit and provide some fun. One of the crewmembers told me, "Everyone loves kids in Greenland. We all want to see them happy".

Logistically, making time for this required us to deprioritize science for a day—this was a day of expensive ship time that did not go to collecting measurements. Being able to do this required that the U.S. National Science Foundation and program manager responsible for our project felt this was a good investment. And they did, because of the Navigating New Arctic's emphasis on community connection and engagement. This illustrates how priorities at the highest level do matter for what becomes possible for individual projects, scientists, and relationships.

We also worked with a science teaching student at Ilisimatusarfik. Nino Brønlund was a part of our field team in 2024 for our work in Northwest Greenland (Figure 4.3). This collaboration was designed for two-way learning and to be mutually beneficial. Nino was able to participate in real scientific research, learning about the sometimes tedious tasks and, at other times, the fun team work that goes into learning about the ocean. This directly informs how he gets kids excited about science as a teacher. Nino led our outreach day with the school in Kullorsuaq, communicating with students of all grades about what we were doing in their fjord with a big research ship. He also coordinated a meeting with local hunters and fishers in Kullorsuaq, serving as a translator and liaison. Our project was able to pay for Nino's travel and time to participate, making this a more possible experience for him compared to if it was an unpaid opportunity. I personally learned so much from Nino and we worked together to create

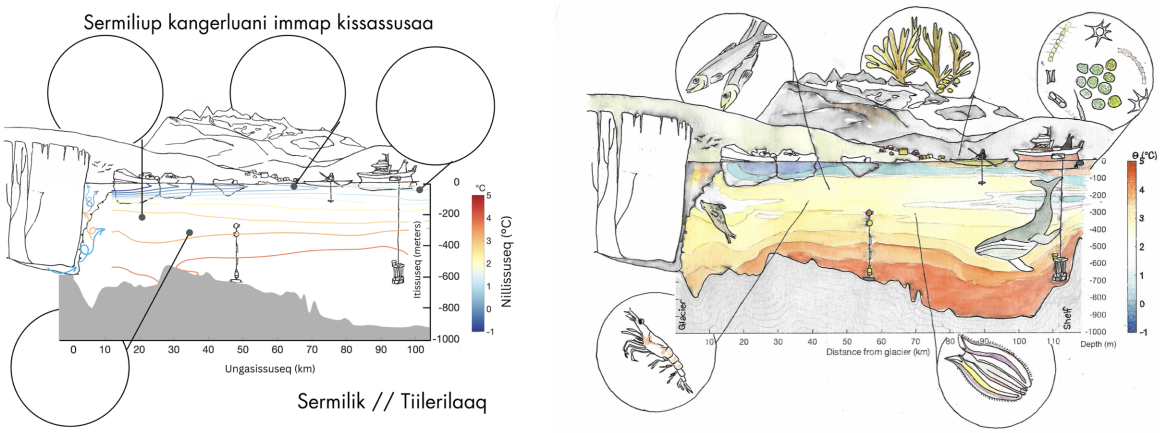


**Figure 4.2.** An example of the coloring page activity I developed for students in Tiilerilaaq. Student learn about the temperature of the ocean in their fjord and can identify where the find certain animals, including learning about phytoplankton and zooplankton. Greenlandic translation by Aqqaluk Sørensen.

activities for the students in Greenlandic. We were able to have conversations with people in Greenland that we would never have been able to have otherwise because of Nino.

Creating this opportunity for Nino and our group to work together required the bureaucracy in place to transfer funds to be able to pay Nino, and it required this payment to be allowed by the National Science Foundation. Nino's participation meant giving a spot to a "non-scientist" on the field team and prioritizing more that just science goals during our time on the ship.

### 4.6.3 A StoryMap for sharing science with public audiences

A rewarding and concrete action for making science accessible to Greenlandic audiences is the StoryMap *Kalaallit Nunaata Kangerluisa Uumassuseqarneri* (Greenland's Living Fjords), created by filmmaker Morgan Burger (FORSEAS), myself, and Fiamma with input from GRISO project partners including Twila Moon and others. The StoryMap is designed for Greenlandic and U.S. high school students and the general public, and it is designed to provide an interactive understanding of converging stories in Greenland's glacial fjords (Figure 4.4). The topics covered include geology, oceanography, chemistry, physics, and biology of Greenland's fjords alongside




**Figure 4.3.** a) Students from Tiilerilaaq on board the R/V Tarajoq, learning about water sampling with Aqqaluk Sørensen and Maia Willis (Photo: Alex Rivest). b) Nino Brønlund assisting with water sampling procedures during our research cruise in Northwest Greenland in 2024 (Photo: Fiamma Straneo). c) A student in Kullorsuaq places their an animal in a depiction of the fjord with ocean temperatures (Photo: Fiamma Straneo) d) Nino Brønlunc leads an outreach activity about density of ocean water with Bobby Sanchez at the Kullorsuaq school in August 2024 (Photo: Aurora Roth).

the perspectives of hunters, fishers, and community members—centering the life in fjords rather than only telling stories of ice loss. We created videos highlighting the work of Greenlandic and Greenland-based scientists, and made an effort throughout to make science more human and relatable. The first version was presented at Greenland Science Week in 2025, where we received enthusiastic feedback and generated ideas for continued development.

As a result of sharing the StoryMap at Greenland Science Week, the StoryMap was used in a Nuuk high school physics class, where the teacher incorporated real hydrographic data from Sermilik Fjord to teach students about ocean density. This is a small but concrete example of research results returning to Greenland in a form that has immediate educational impact. It's a paradigm shift for Greenlandic high schools students to learn from the international research

happening in their home.

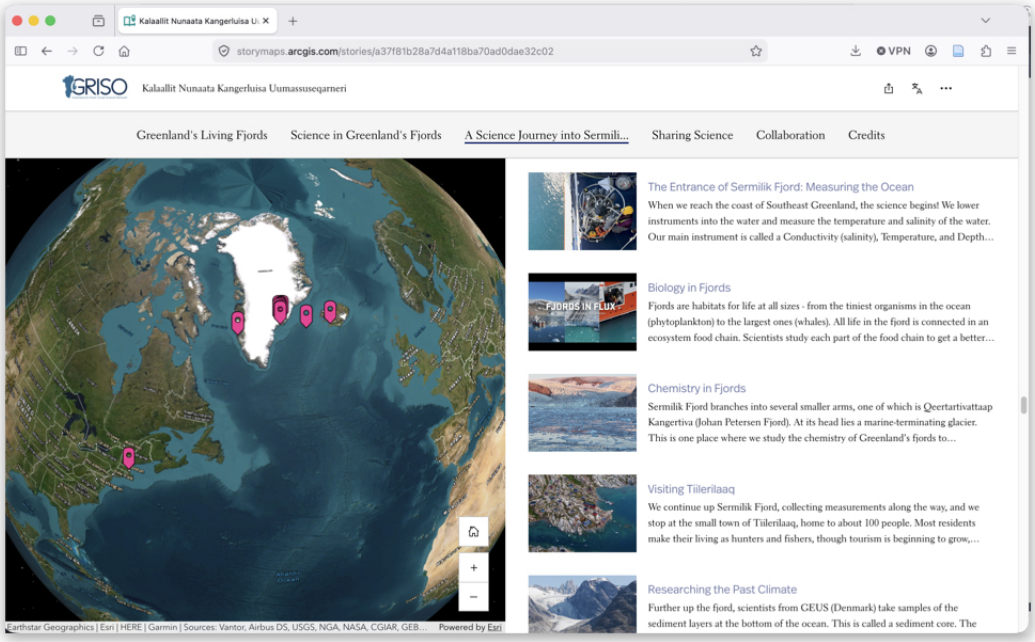


**Figure 4.4.** A screenshot of Greenland's Living Fjords StoryMap project, showing the range of videos and topics presented. (Screenshot from May 23 2026).

However, gaps remain. The initial concept and development were not co-created with Greenlandic partners, and the StoryMap is currently available only in English and Danish—a Kalaallisut translation is in progress. Funding this work required piecing together resources from multiple sources outside the core dissertation project. On a personal level, completing the StoryMap required prioritizing it alongside—and sometimes over—PhD work, absorbing extra labor that is not formally recognized or compensated within standard graduate research structures. Making science accessible and beneficial requires real time and resources, and if those costs fall entirely on individual researchers rather than being built into project budgets and institutional expectations, equitable dissemination will remain the exception rather than the norm.

To view the StoryMap, visit: `greenlandslivingfjords.com`

### 4.6.4 Interdisciplinary projects enable work that aligns with the research strategy

One observation from these projects is that an interdisciplinary project structure may be a prerequisite—or is at least a significant enabler—for more equitable and ethical research practices in the physical sciences. Lauter (2023) notes that transdisciplinary research, which goes beyond disciplinary collaboration to transcend disciplinary borders altogether, is a promising approach for bridging Indigenous and western knowledge systems, and that difficulties remain even within Western interdisciplinary efforts. O'Brien et al. (2024) draw an analogy between co-production of knowledge and cross-disciplinary research, noting that both require treating different forms of knowledge as having equal value. Having a genuinely interdisciplinary team built into the project structure changes how a research group functions, what questions it asks, and what kinds of relationships and outputs become possible. The following points highlight how inter- and multi-disciplinary aspects of our projects facilitated mutually-beneficial science.

**Including environmental humanities changed how our group functioned**

Our project included an environmental history and humanities co-PI, Mark Carey, whose presence shaped the project in ways that are subtle but important. The discussions we had as a science group were shaped by his curiosity and lines of questioning. Mark was able to name tensions or structural contradictions that we physical scientists were sitting with but had not articulated. Scholars trained in environmental humanities are accustomed to asking: whose knowledge counts? Who benefits from this work? What narrative are we telling, and who does it serve? These are not questions that emerge naturally in a physical oceanography group meeting. Having someone in the room for whom these questions are routine changed the texture of our conversations.

We struggled to make direct connections between the environmental humanities and our physical science research outcomes. But even without producing a jointly-authored paper, the value of having our group function differently from a traditional western science project in a

disciplinary silo was real. A physical science project that regularly asks "who benefits?" and "what story are we telling?" is better positioned to pursue equitable research than one that does not.

**Making space for filmmakers, artists, and journalists**

We collaborated with filmmakers Alex Rivest and Morgan Burger and a journalist, Caroline Beeler. Alex and Caroline joined us on the R/V Tarajoq during research cruises. These were valuable structural decisions of our project. Non-scientists notice different things during fieldwork. They are not optimizing for data collection and so can they pay attention to other aspects of the work—the story a crew member is telling, the expression on a student's face when they first come onto the ship, the quality of the light on an iceberg. They connect with crew and community members in ways that scientists often can't because they are not trying to complete a sampling protocol or extract specific information.

Alex reflected back to us how he saw our work and why it mattered —from outside the frame of scientific productivity. On a very concrete level, high-quality documentation of fieldwork facilitated outreach products and making our science more accessible. The StoryMap described above would not exist without the visual material Alex produced and without the skills and talents of filmmaker Morgan Burger.

**Interdisciplinary teams normalize different ways of working**

A more structural benefit of genuinely interdisciplinary teams is that they normalize slower, more relational timelines. As a physical scientists, we often have to optimize for efficient data collection—the ship has a schedule, the weather window is finite, the CTD cast takes 45 minutes. This efficiency orientation is often incompatible with community engagement, which requires time to sit with people, to explain without extracting, to listen without an agenda. When a team includes multiple kinds of scientists, humanists building contextual understanding, and filmmakers capturing process rather than product, the pace of work becomes more varied and

more relational (Figure 4.5). We made time for interdisciplinary discussions and new ways of thinking together. This normalization of slower timelines is not incidental—it is a structural aspect of the project that makes genuine engagement with communities more possible.

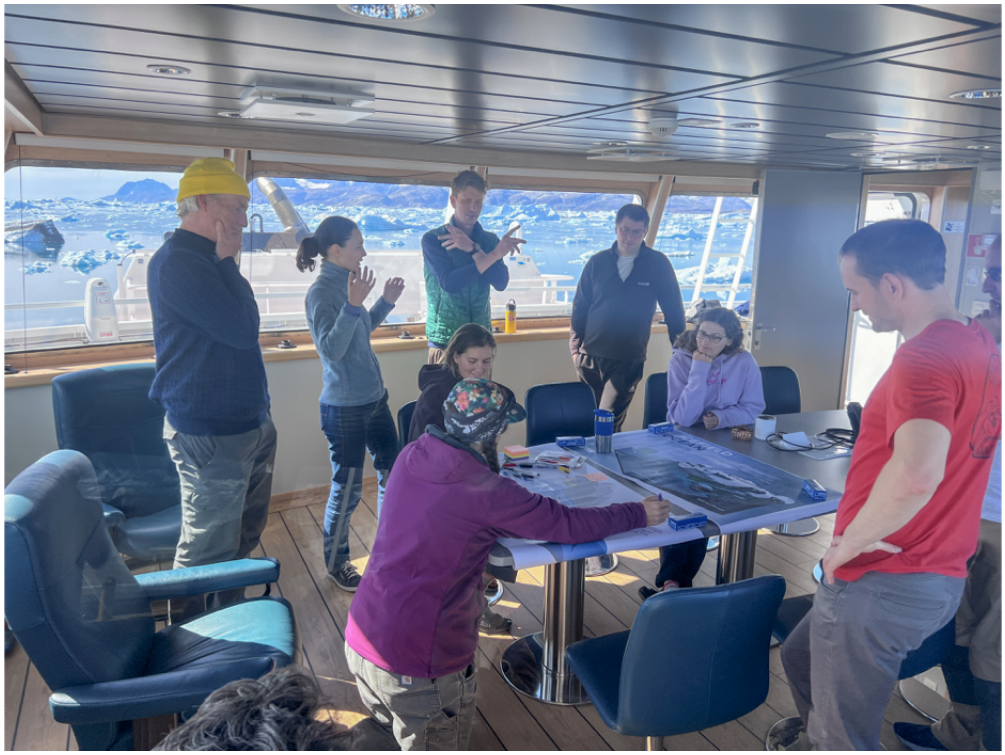

**Figure 4.5.** Members of the NNA FISHEE team discussing interdisciplinary intersections of the Sermilik Fjord system on the R/V Tarajoq in August 2023. Photo by Alex Rivest.

### A necessary caveat

I want to be clear that an interdisciplinary team of Western scientists, humanists, and filmmakers is not the same as genuine co-production of knowledge with Greenlandic partners, and should not be confused with it. A project can be highly interdisciplinary within a Western academic framework and still be fundamentally extractive in its relationship to the communities where it works. Interdisciplinarity is a step in the right direction—it disrupts disciplinary insularity and creates the conditions for more reflexive and relational science—but it is not a substitute for Indigenous leadership in research design and implementation. We offer it here as a structural recommendation for physical science projects that are working toward more equitable

practices, not as an endpoint.

### 4.6.5 The role of graduate students

Graduate students generally become part of projects after the scope, budget, and research objectives have been decided. However, small actions after the project initiation can be taken by graduate students to nudge projects into more in alignment with the goals of the GNRS. Even if project questions were not co-created with communities or designed to incorporate community needs and feedback, outreach and results dissemination can lead to building relationships that later become the foundation of more community-based research. At the same time, defined tasks like developing an outreach activity, sharing results in a public talk, or connecting with teachers, helps graduate students build skills that will make them more courageous and creative in leading future community-based work. I have learned that small actions at any point in the project process still matter and that we can keep iterating on these actions. Finally, I have learned to think on longer timescales beyond the funded years of one particular project, and to think instead about what building relationships can look like regardless of project. When I think about the future direction of my career, I am considering the relationships I've built in the last six years, who I feel accountable to, and what connections I want to grow.

## 4.7 Conclusion

Writing a chapter like this to share publicly feels uncomfortable, but it has been a useful personal process allowing me to articulate dynamics I experienced during my PhD work. It is even more uncomfortable to specifically write about my identity and role in this work, but necessary for putting my thoughts in context and continuing reflection. My hope is that including this chapter helps to normalize self-reflection and project evaluation more within the natural sciences. Overall, the work of formally evaluating multi-year, multi-PI projects is a huge effort and daunting task. How can we summarize and draw patterns from complex human and institutional dynamics that drive the work of research? Creating a structure for a process

utilizing the GNRS as guidelines for evaluation was a first and necessary step. This now serves as a proposal for how we can conduct an evaluation across each project with all team members involved. Continuing to invest in interdisciplinary understanding with colleagues who specialize in human systems and evaluation is also a key step.

Despite working through the reflection table as an individual rather than a team, it was a useful exercise. Connecting the dots of specific actions back to the goals of the GNRS allowed me to see the successes and gaps of our project and initiated a brainstorm of what further actions could be developed. Places where our work has fallen short include 1) a lack of project co-creation with local partners and integrating local knowledge into results, 2) developing research questions that are solution-oriented to community challenges, and 3) connecting with business and economic development aspects of communities. Making progress on these goals will involve, primarily, time, followed by further deepening relationships, imagination, and more creativity.

During my PhD, I tried to do this work differently than I would have before when I first started working at Summit Station. This chapter is a record of that work from the last six years. There have been times where I was out of my comfort zone, felt like I had failed, and felt like I was trying something new. I was empowered by my advisor, Fiamma, and our colleagues and team members to lead with my whole self. I do believe that naming the gaps, building the relationships, making the time is what changes things, slowly, over the course of whole careers and collaborations. While the overall political relationship between the U.S. and Kalaallit Nunaat is in a strange, tense, and uncertain period, I will keep taking small actions wherever and whenever I possibly can.



**Figure 4.6.** NNA FISHEE field team, R/V Tarajoq crewmembers, and students and teachers from Tiilerilaaq posing on the bow of the R/V Tarajoq. Photo by Alex Rivest.

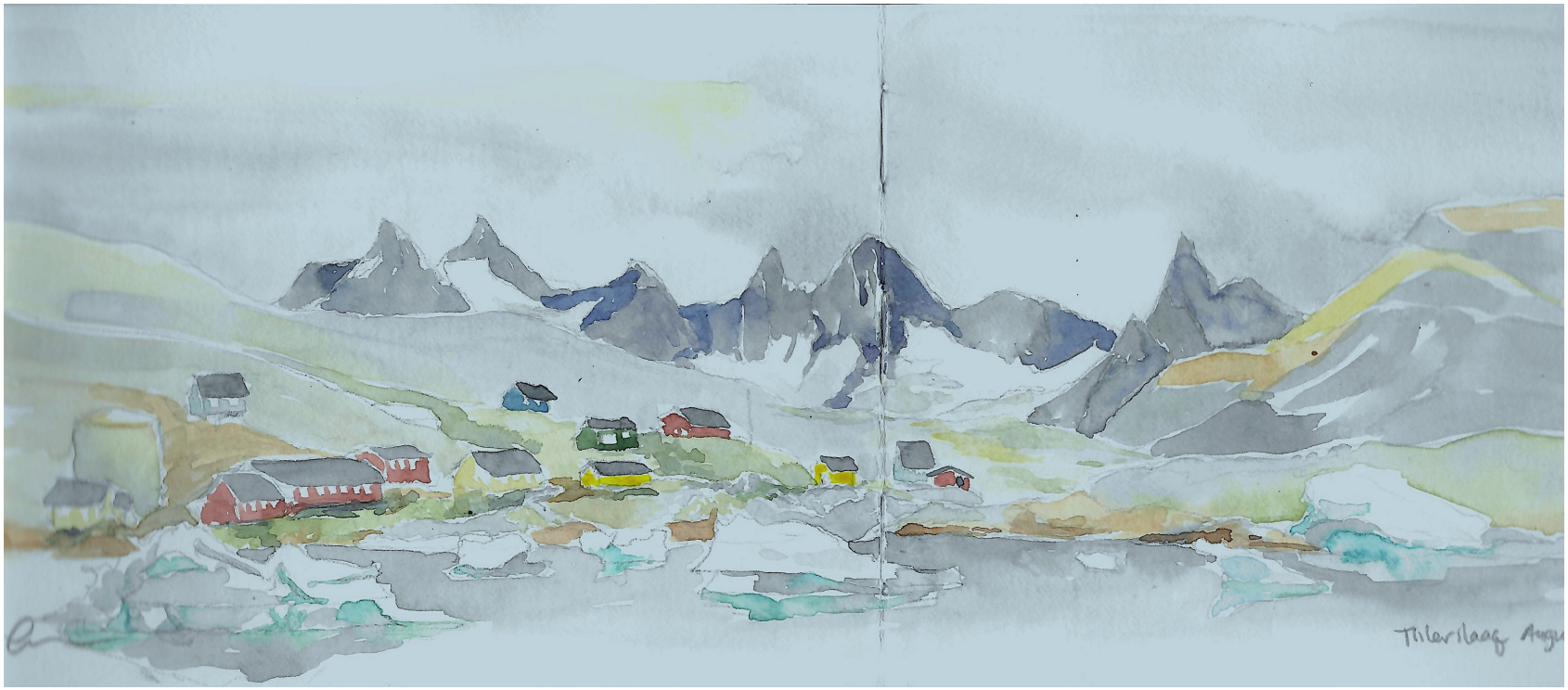

**Figure 4.7.** Painting of Tiilerilaaq in August 2025 by Aurora Roth.

# Chapter 5

# Conclusion: Summary and Future Work

The glacial fjords of Kalaallit Nunaat are critical places of exchange between the sermersuaq (Greenland Ice Sheet) and imaq (ocean), between local and global dynamics, and between international scientists and Kalaallit communities. The dynamics of glacial fjords are connected to both our shared global climate and the local ecosystems that support Kalaallit communities and culture. Both perspectives, the global and the local, are important and lead to questions with scientific and human value.

The foundation of this dissertation is observations from Sermilik Fjord, where one of the largest outlet glaciers of the ice sheet, Helheim Glacier, drains to the ocean. And where people live in the small town of Tiilerilaaq and the larger hub of Tasiilaq. While prior hydrographic work in Sermilik Fjord has been invaluable in shaping our understanding of glacial fjord dynamics, it was largely based on individual summer surveys or two- to three-year-long mooring records. Chapter 1 represents the first effort to treat the entire CTD record as a coherent dataset of summer fjord properties through time, extending from 2009 to 2023. By standardizing the data to a common grid using optimum interpolation, combining XCTD and CTD measurements, and making the dataset compliant with FAIR principles, Chapter 1 produced a resource that can support climatological analysis, model validation, and future multidisciplinary applications.

Temperature and salinity observations tell us that the ocean at a given location is warm and salty, or cool and fresh—but the properties do not directly tell us where that water came

from. Water mass fractions provide that information and present a quantitative pathway to improving parameterizations of glacial fjord processes in larger ocean and climate models. By decomposing properties into contributions from ocean source waters (Atlantic Water and Polar Water), subglacial discharge, and submarine meltwater, the analysis separates two distinct sources of variability: changes in the properties of the ocean source waters, and changes in glacial fjord mixing processes.

Previous analyses of water mass fractions in Greenland glacial fjord settings were hindered by the assumption that temperature and salinity observations alone could not resolve the four water types present in fjord systems. In Chapter 2, we developed a weighted regularized least squares (RLS) framework suited for glacial fjords that produced water mass fraction solutions from temperature and salinity observations alone. By incorporating prior information through a penalty matrix, the approach regularizes an otherwise underdetermined and ill-conditioned system, and produces results comparable to well-constrained noble gas-derived water mass fraction estimates. A key contribution was developing and utilizing a spatially varying penalty matrix that represented the general fjord characteristics. This method is applicable to the growing archive of XCTD observations, which provide only temperature and salinity information, expanding the spatial and temporal coverage of water mass fraction analysis to other fjords and the difficult-to-observe plume and ice mélange regions.

Chapter 3 applied the RLS framework from Chapter 2 to the full gridded dataset developed in Chapter 1, producing new estimates of water mass fractions that vary in both time and space. These results demonstrated that the RLS method is a meaningful improvement over the multi-year averaged approach previously used. Atlantic Water fractions dominate at depth throughout the record, varying between 70–100% below 300 m across all fjord regions and years. However, we showed that the background Atlantic Water and Polar Water mixing ratios that define the deep water are an important characteristic to resolve in the mixing models in order to produce reliable solutions. Near the glacier terminus, subglacial discharge and submarine melt fractions show a consistent signal of buoyancy-driven upwelling that drives summer circulation in the fjord.

Maximum Atlantic Water fractions above 300 m, representing upwelled Atlantic Water entrained within the subglacial discharge plume, trace the core plume waters as they extend down-fjord. The overall spatial pattern of water mass fractions is remarkably consistent. While properties of the source ocean waters change in time and space, the dominant mixing processes consistently mix fjord waters in similar ratios.

What is variable, by contrast, is concentrated at the shelf and mouth, where Polar Water dominates the upper water column. From both hydrographic property and water mass fraction analysis, the fjord mouth and adjacent shelf are the most variable regions. Winds, coastal currents, and the depth of the shelf pycnocline all modulate fjord-shelf exchange, and control the extent to which Polar Water can move into the fjord and Glacially Modified Water moves out of the fjord. Our results show that for years when Polar Water reaches further up the fjord, it does so by subducting underneath Glacially Modified Water. The fjord interior, and particularly the mélange region, is generally buffered from the higher-frequency variability of Polar Water at the mouth.

A thread that runs through all three scientific chapters is that both optimum interpolation and water mass fraction analysis are models—and all models require subjective choices in their problem setup, assumptions, and definitions. The gridded dataset of Chapter 1 reflects decisions about covariance length scales and the weighting of observations; the water mass decomposition of Chapters 2 and 3 reflects decisions about source water type definitions, the properties and observations used, and regularization. In each case these choices shape the final results and assumptions always have to be made with imperfect information about a system. Previously, water mass fraction analyses in glacial fjord regions were treated more like a simple calculation than a model with subjective choices. We provide an example of reporting uncertainties, residuals, and condition numbers—the reporting of which will facilitate intercomparison studies of different fjord locations.

Important questions remain. The persistent mismatch between observed fjord properties and the output of numerical models points to processes that remain poorly represented—most notably the role of icebergs, whose melt and freshwater input are difficult to constrain from

observations alone. The gridded dataset assembled here offers a natural benchmark against which such models can be tested, and improving the representation of iceberg melt is a clear priority for closing the observation–model gap. A second open question concerns what ultimately leaves the fjord. This dissertation has focused on conditions within Sermilik and at its mouth, but the fate of fjord-modified water on the shelf—captured in the west shelf section and left entirely unexamined here—remains essentially unexplored, despite its importance for how fjord processes feedback onto the shelf and the impacts on the larger regional ocean. Third, the datasets here are all snapshots in the summer season. Many questions remain about the evolution of fjord properties during the summer season and the transitions between summer and winter regimes in the fjord. A fourth concerns an assumption implicit throughout: that Helheim dominates the system. Sermilik is fed by other tidewater glaciers whose subglacial discharge plumes also reach the fjord, and how much these additional plumes contribute, and whether they interact with one another, is not resolved here. Finally, the gridded-dataset approach of Chapter 1 and the water mass fraction framework of Chapters 2 and 3 were designed with the intention of extending this work to other glacial fjords. This would enable direct intercomparison and help distinguish processes that are general from those that are fjord-specific.

The fjords of Kalaallit Nunaat are changing, and tracking that change requires records long enough to distinguish a significant trend from system variability. The thirteen year data record from Sermilik Fjord is just beginning to make this possible. Just as important as the length of the record is who builds it and who learns from it: long-term monitoring is most valuable, and most equitable, when Kalaallit people and institutions have involvement in data collection and the questions we seek to answer. Among the most urgent of those questions is how physical fjord dynamics are linked to thriving fjord ecosystems—how might phytoplankton, zooplankton, fish, seals, whales, and birds respond to ever-increasing glacial meltwater, glacial recession, and a globally warming ocean? What comes next will require sustained, comparable observations, interdisciplinary teams working together, and a science culture willing to self-reflect and contextualize science within historical and political realities.

Historically, the local perspectives of Kalaallit people—encompassing their priorities, needs, and goals for their self-determined future—have been marginalized by international scientists working in Kalaallit Nunaat with motivations related to global impacts. As one of those international scientists working in a team dedicated to prioritizing collaboration and conducting more equitable science, this dissertation has shown that research with motivations of global concern can include actions that support Kalaallit Nunaat's science institutions and goals. Though we still have more work to do, these actions included making data from Greenland accessible and open, utilizing Greenlandic research vessels, collaborating with and learning from Greenlandic and Greenland-based scientists, and prioritizing outreach and opportunities for Greenlandic students.

Science is not separate from politics, and the current political relationship between the U.S. and Kalaallit Nunaat has never been more strained and bizarre. My hope and commitment is that scientific partnerships can remain a place where we navigate shared challenges with equity and respect.

I am deeply grateful and indebted to the lands and waters at the core of the research questions presented here, and these lands and waters are uniquely Kalaallit. Kalaallit Nunaat Kalaallit Pigaat. Greenland belongs to Greenlanders.

# Appendix A

# Supplementary Figures

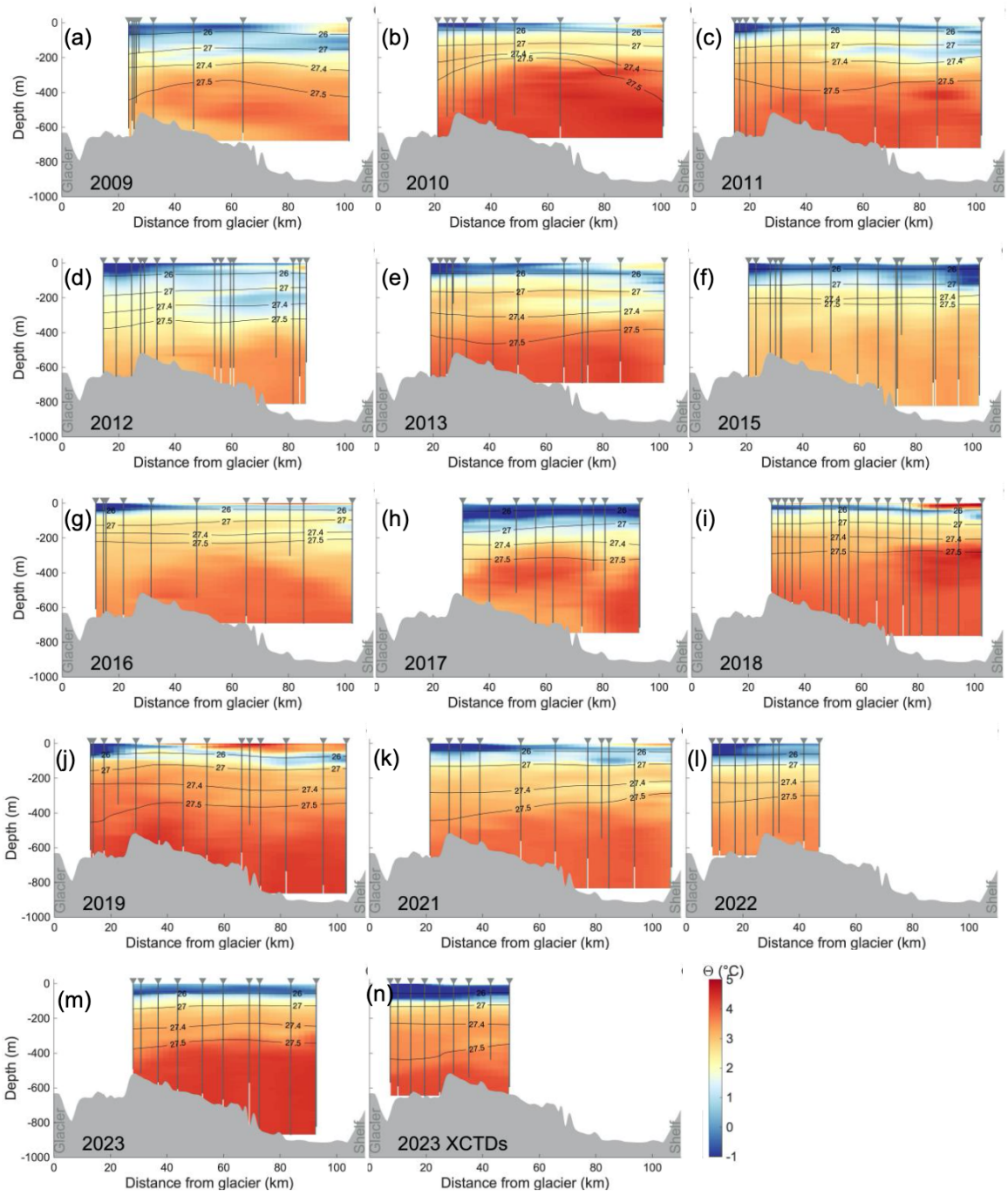


**Figure A.1.** The conservative temperature objectively mapped gridded fields for all years with potential density anomaly isopycnals (black contours). Original CTD and XCTD profile locations in the along-fjord direction are shown by triangle markers with vertical black lines representing the depth extent of each profile. White lines show where the bottom of a profile was filled in to facilitate greater data coverage for mapping. The bathymetry (grey area) is derived from a thalweg line (Figure 1) of BedMachine Greenland v4 data (Morlighem et al., 2017). Distance 0 km is the location of the Helheim terminus in 2019.

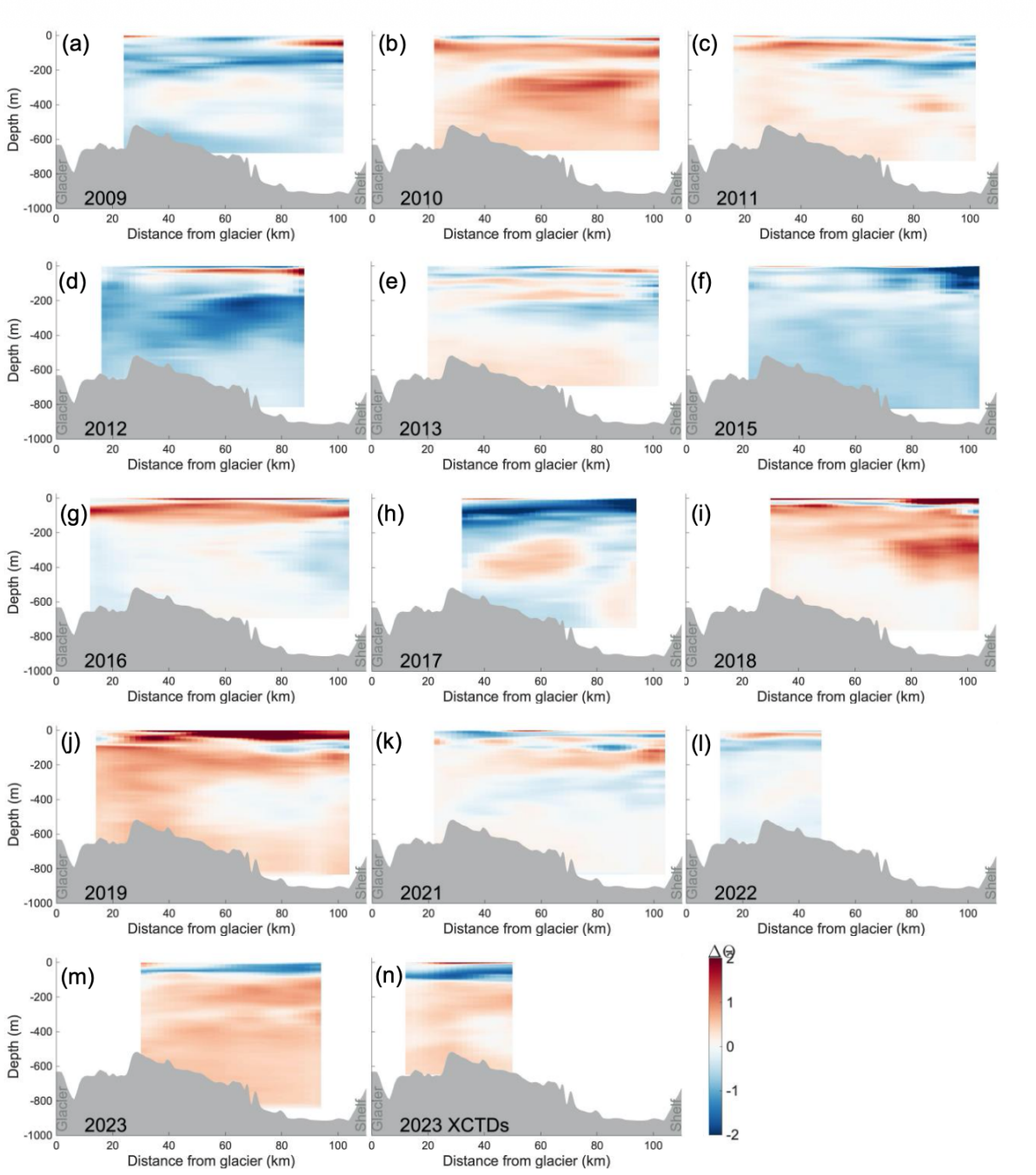


**Figure A.2.** Conservative temperature anomalies from the climatological mean for all yearly grids. Cooler (warmer) colors show values less (greater) than the mean for each grid cell.

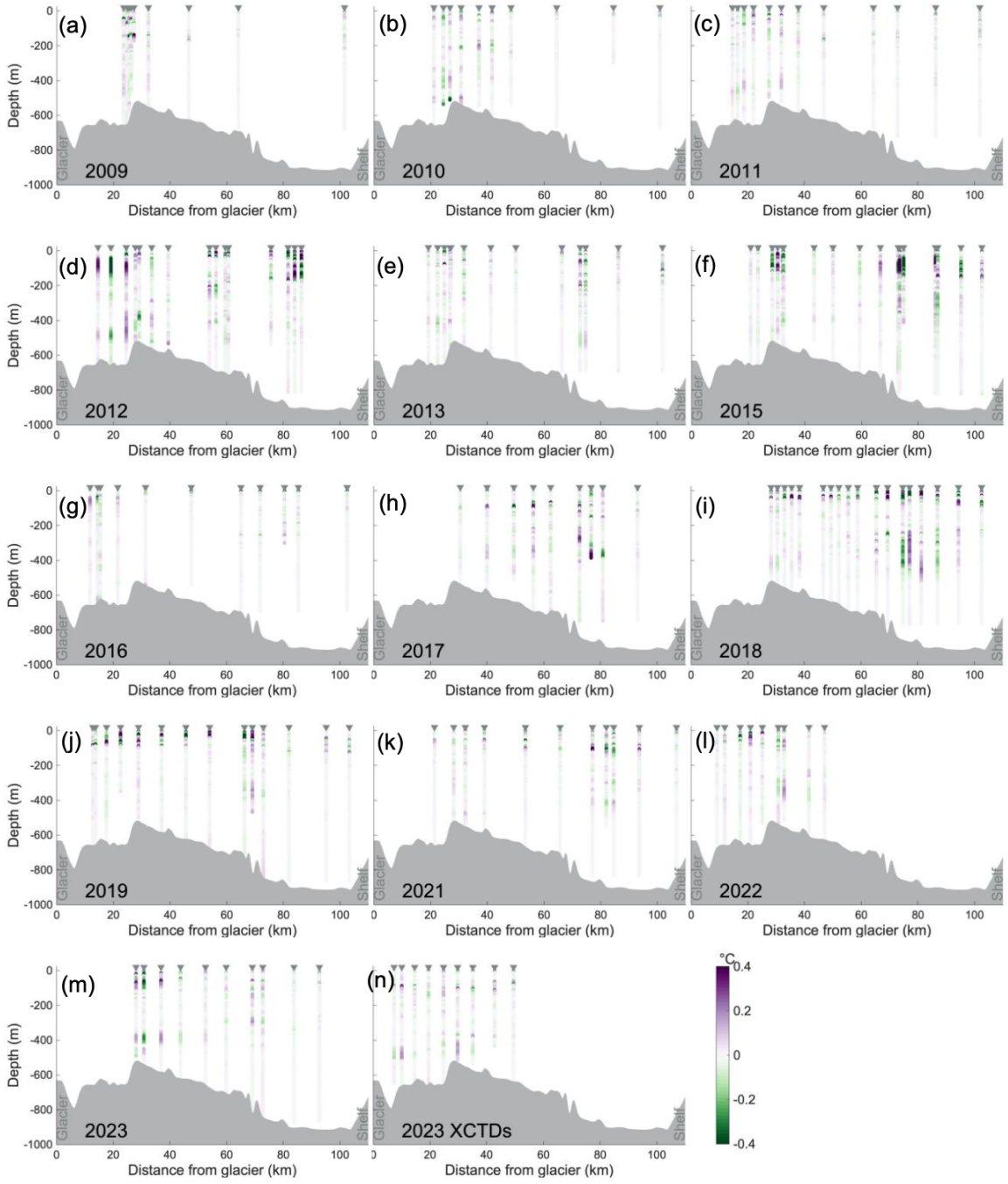


**Figure A.3.** Conservative temperature residuals between the profile data and gridded data interpolated to the same position of every data point. Residuals were calculated as profile data minus gridded data values.

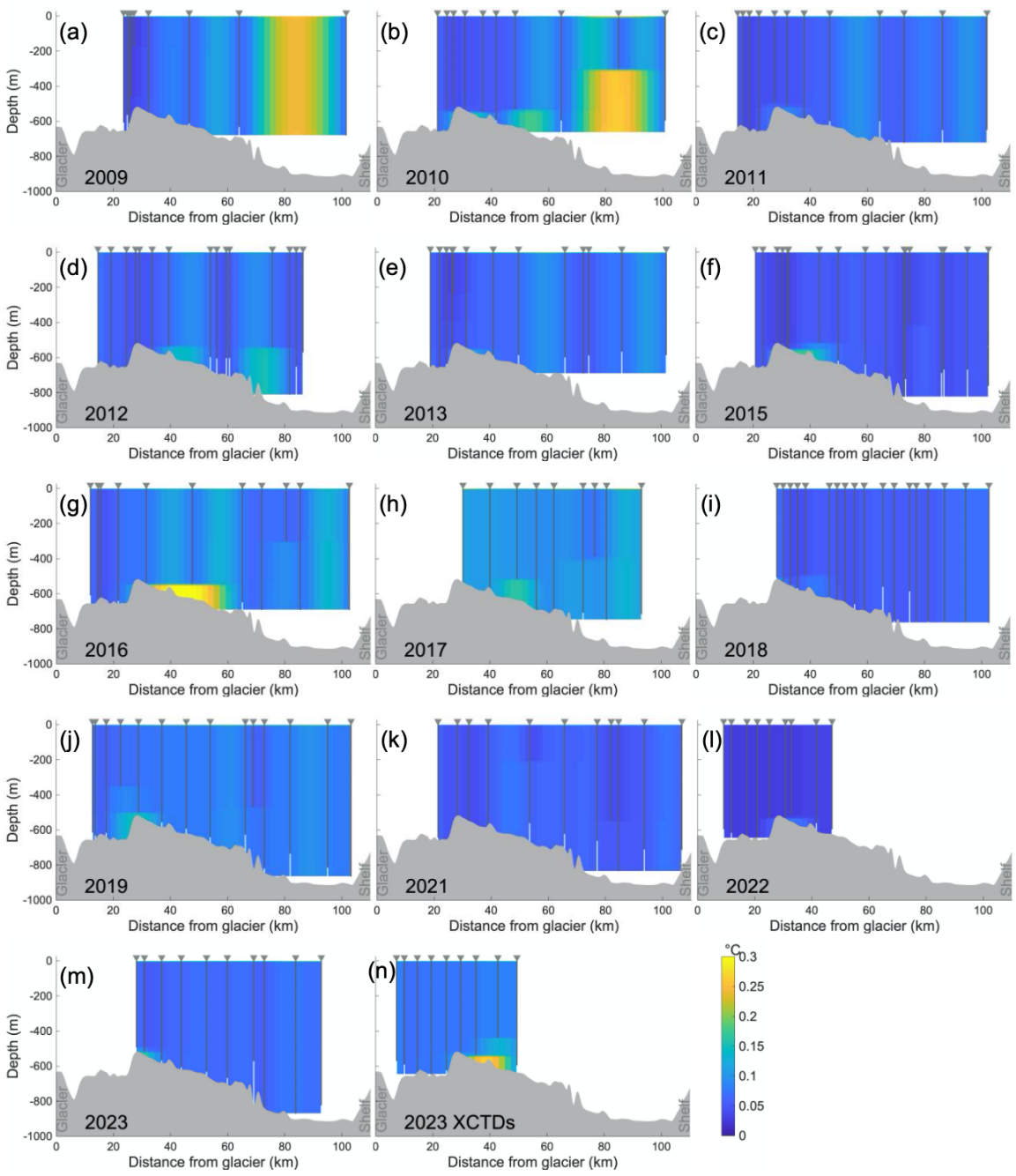


**Figure A.4.** Conservative temperature mapping relative error. Original CTD and XCTD profile locations in the along-fjord direction are shown by triangle markers with vertical black lines representing the depth extent of each profile. White lines show where the bottom of a profile was filled in to facilitate greater data coverage for mapping.

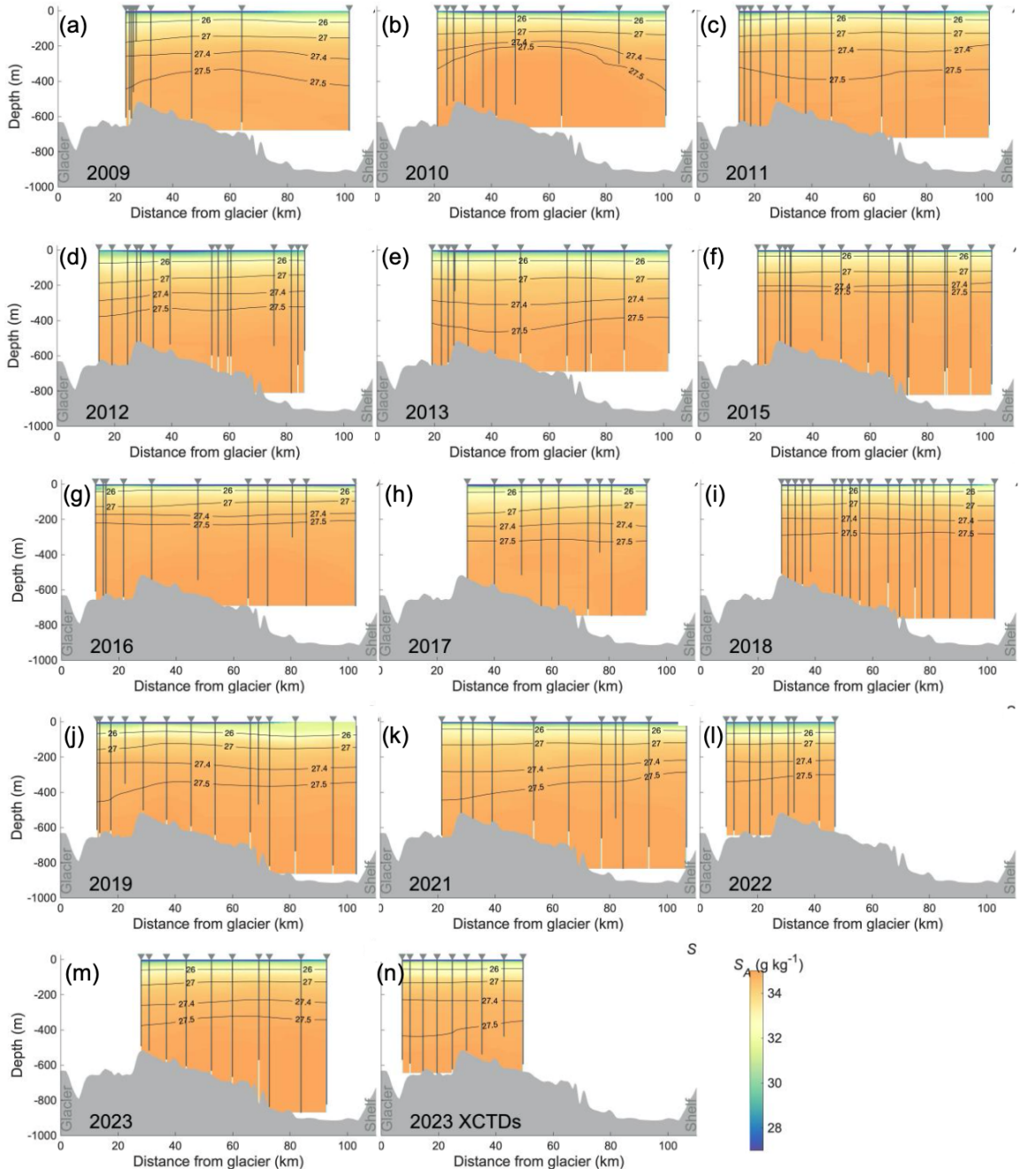


**Figure A.5.** The absolute salinity objectively mapped gridded fields for all years with potential density anomaly isopycnals (black contours). Original CTD and XCTD profile locations in the along-fjord direction are shown by triangle markers with vertical black lines representing the depth extent of each profile. White lines show where the bottom of a profile was filled in to facilitate greater data coverage for mapping. The bathymetry (grey area) is derived from a thalweg line (Figure 1) of BedMachine Greenland v4 data (Morlighem et al., 2017). Distance 0 km is the location of the Helheim terminus in 2019.

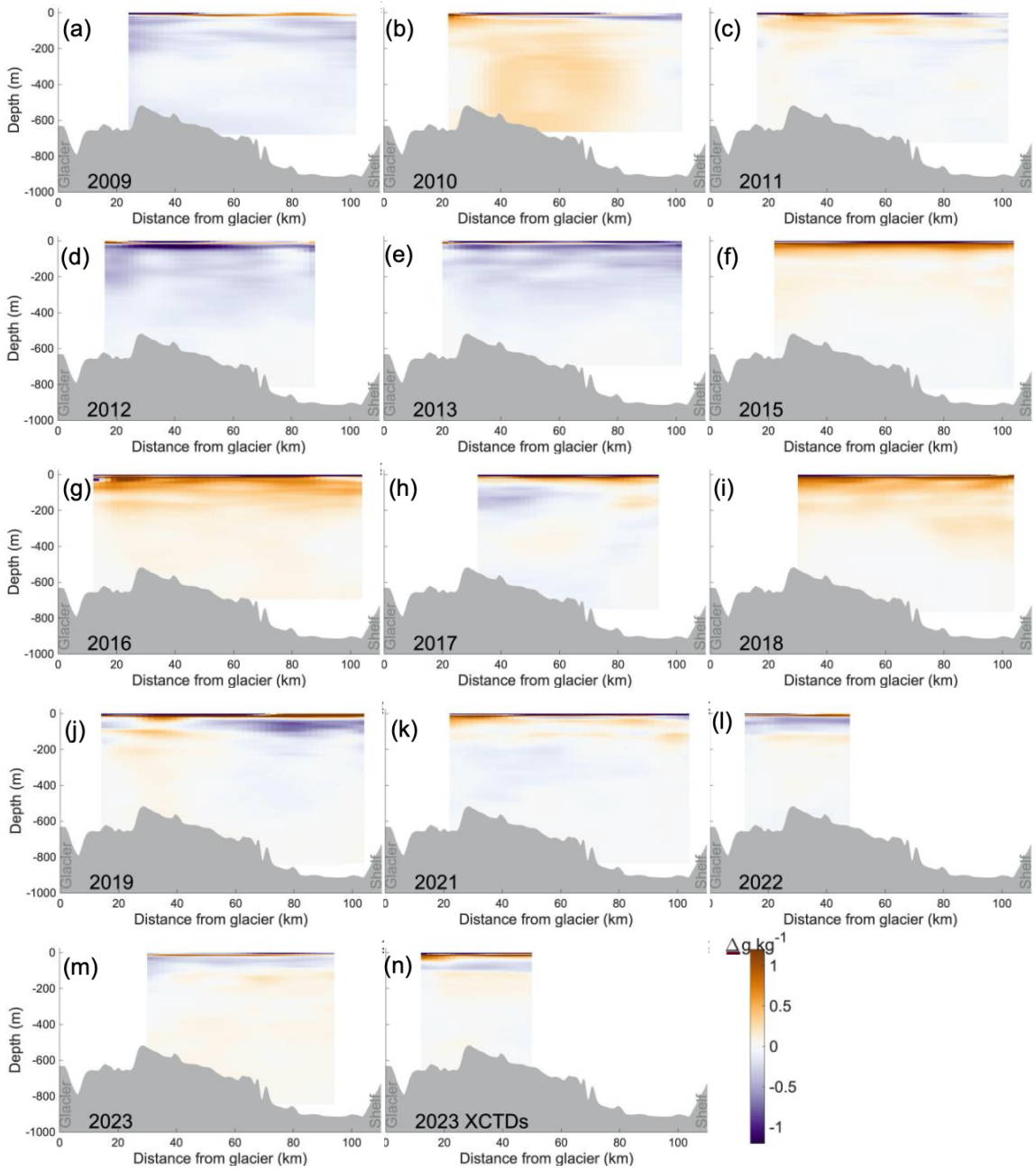


**Figure A.6.** Absolute salinity anomalies from the climatological mean for all yearly grids. Warmer (cooler) colors show values greater (less) than the mean for each grid cell.

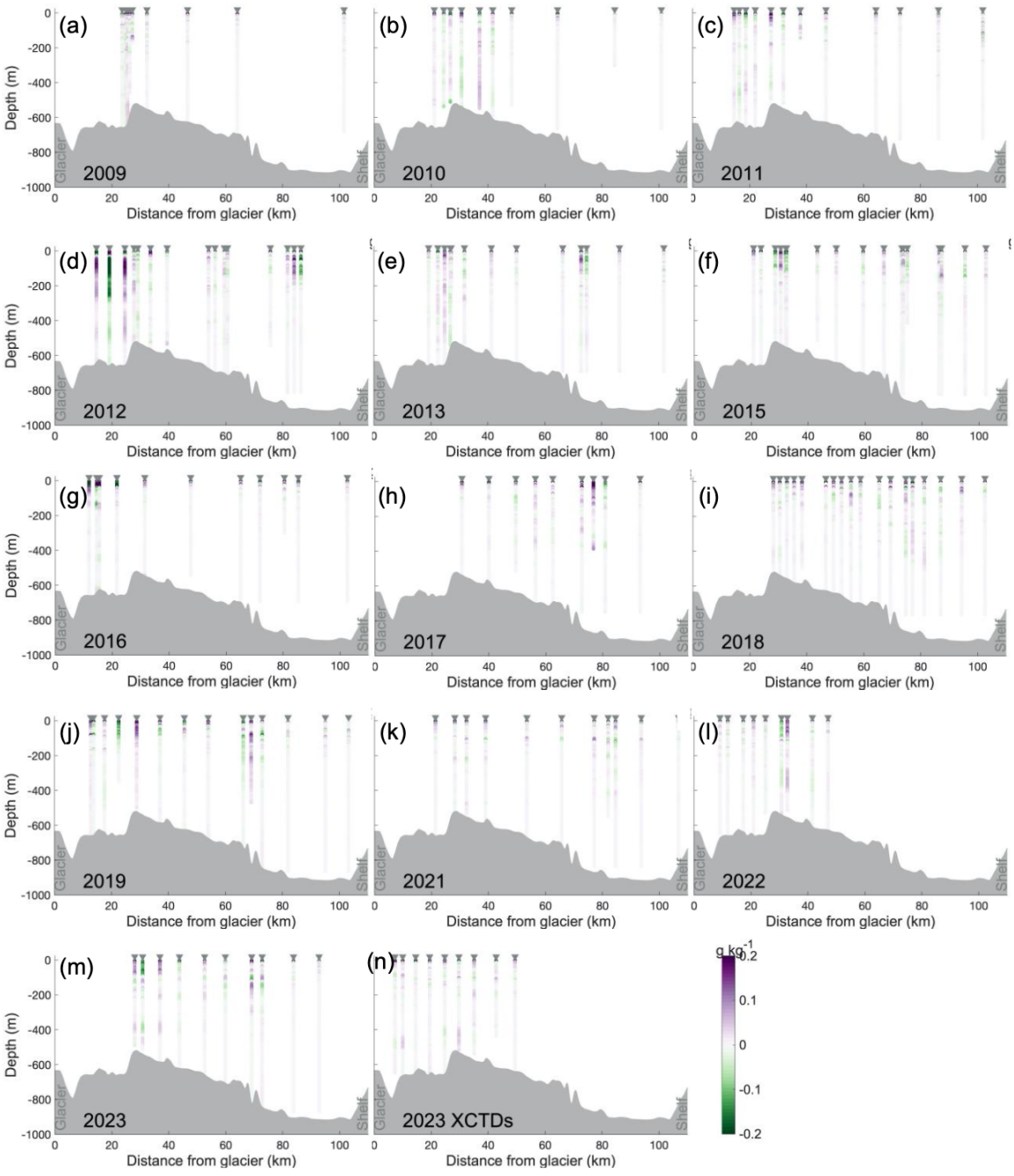


**Figure A.7.** Absolute salinity residuals between the profile data and gridded data interpolated to the same position of every data point. Residuals were calculated as profile data minus gridded data values.

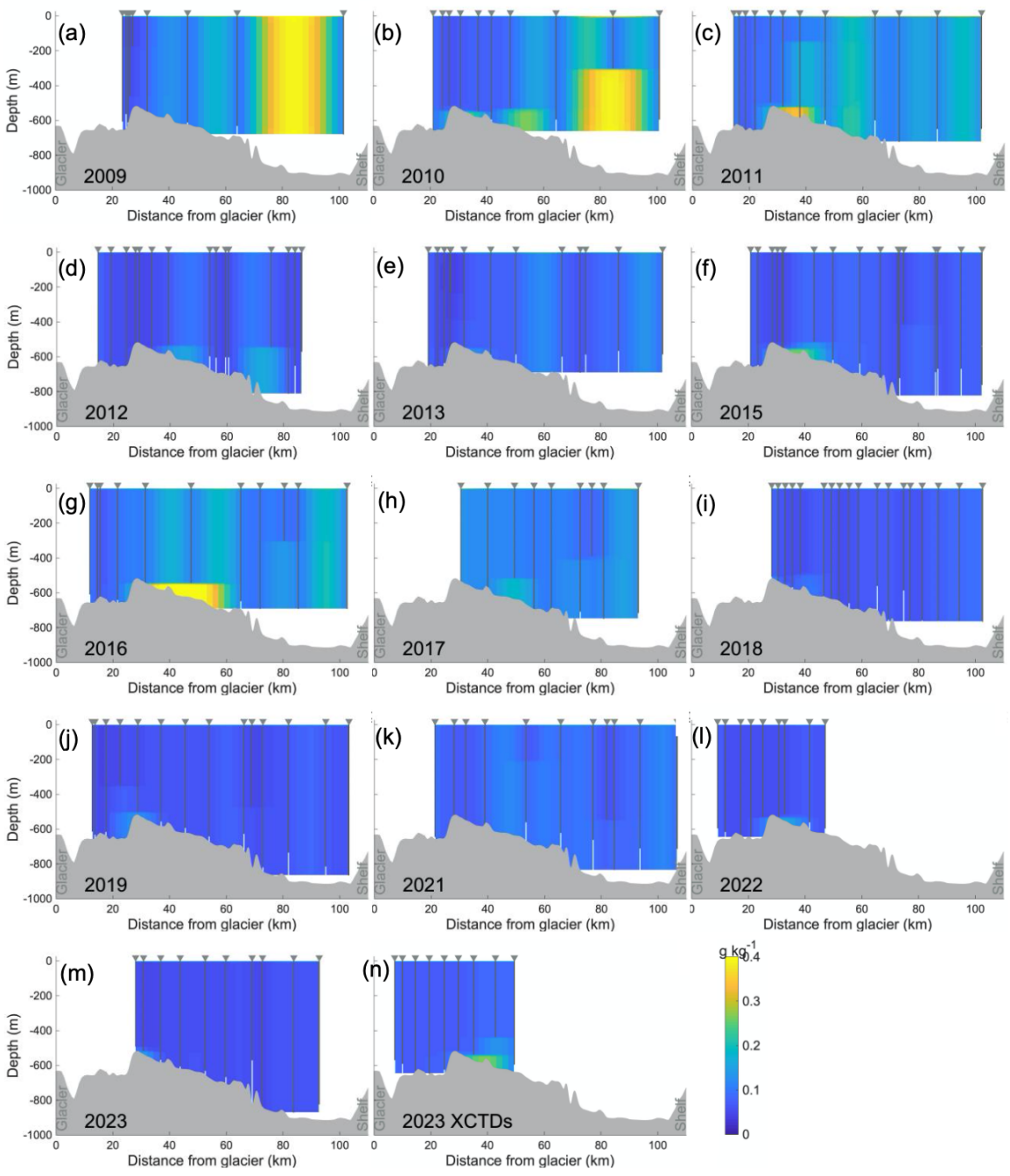


**Figure A.8.** Conservative temperature mapping relative error. Original CTD and XCTD profile locations in the along-fjord direction are shown by triangle markers with vertical black lines representing the depth extent of each profile. White lines show where the bottom of a profile was filled in to facilitate greater data coverage for mapping.

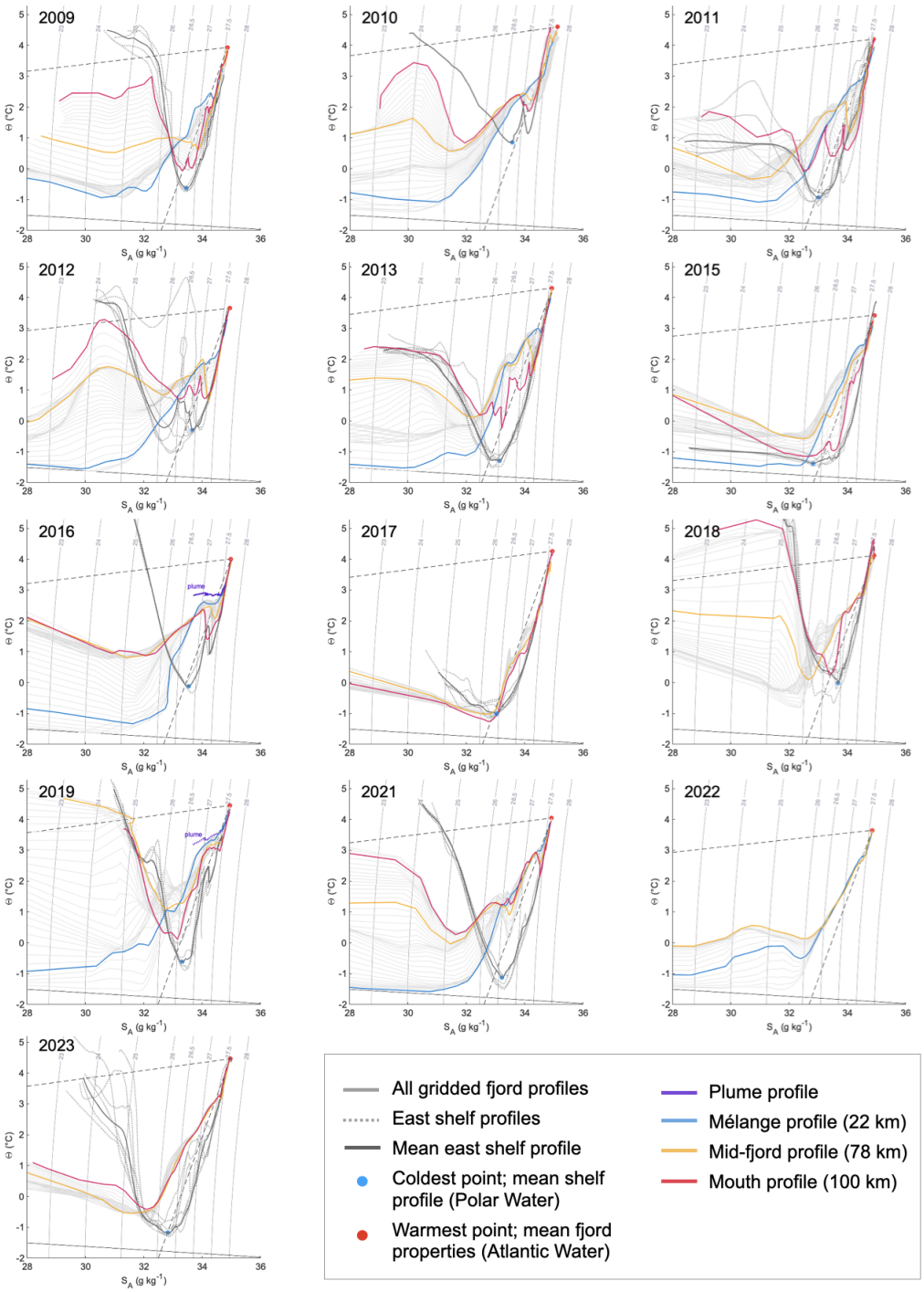


**Figure A.9.** $\Theta - S_A$ plots for each year in the hydrographic gridded dataset for Sermilik Fjord. Where the gridded domain extends to these regions, the plume (purple), mélange (blue), mid-fjord (yellow), and mouth (red) profiles are highlighted. All East shelf profiles are shown (dashed) and the mean shelf profile for each year is represented with a bold grey line. Each plot shows the AW-SGD/runoff mixing line and AW-SMW mixing line and freezing line. Red dot indicates the AW properties used as endmember properties and blue dot indicates the PW properties.

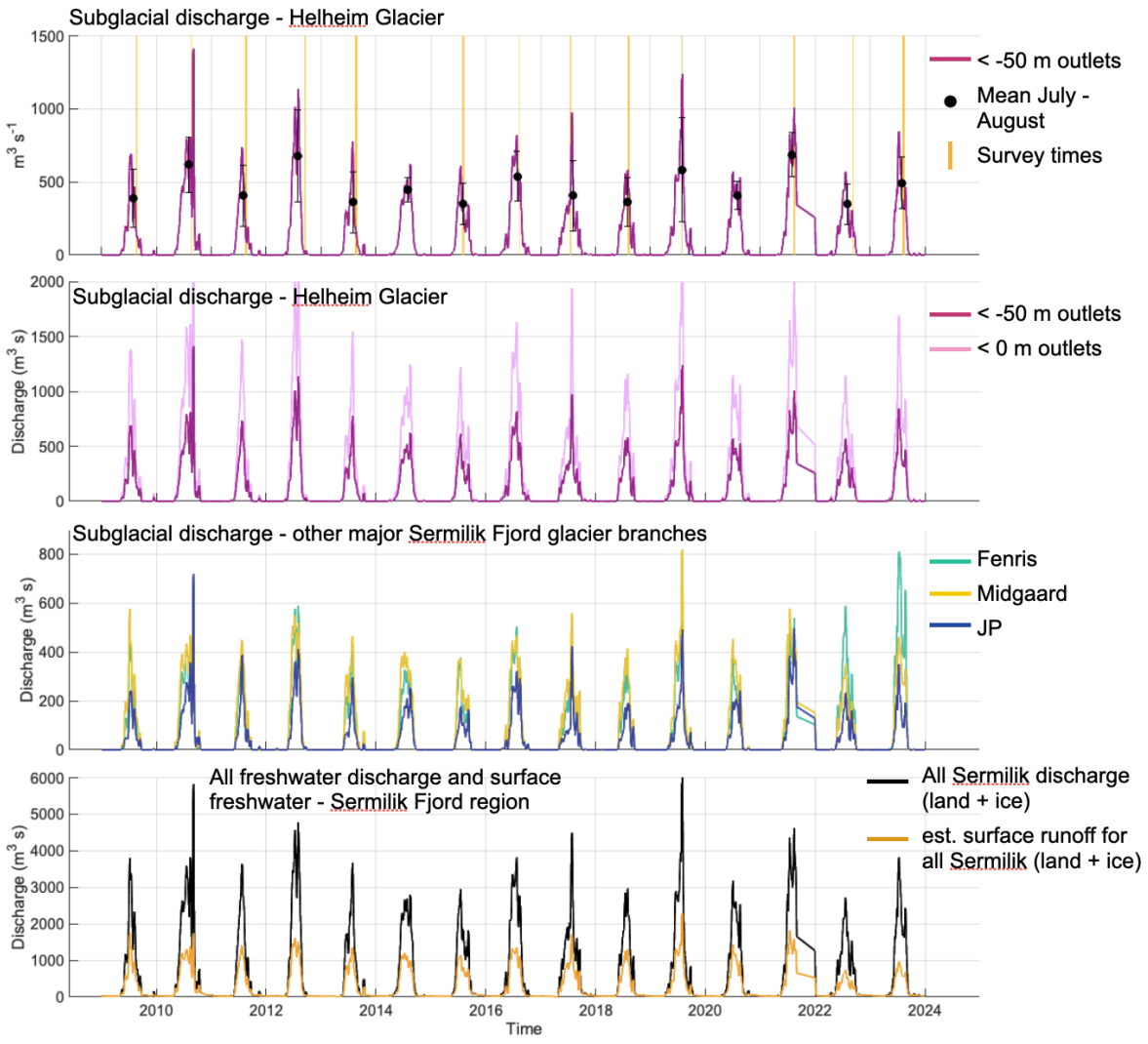


**Figure A.10.** Freshwater runoff discharge partitioned for subglacial discharge outlets for Helheim Glacier alone (a-b), for the other dominant tidewater glaciers in Sermilik Fjord with subglacial discharge (c). All freshwater discharge, including freshwater entered at the surface and depth, for the entire Sermilik Fjord region is compared to surface runoff only (d). The gap between these curves represents all subglacial discharge in Sermilik Fjord.

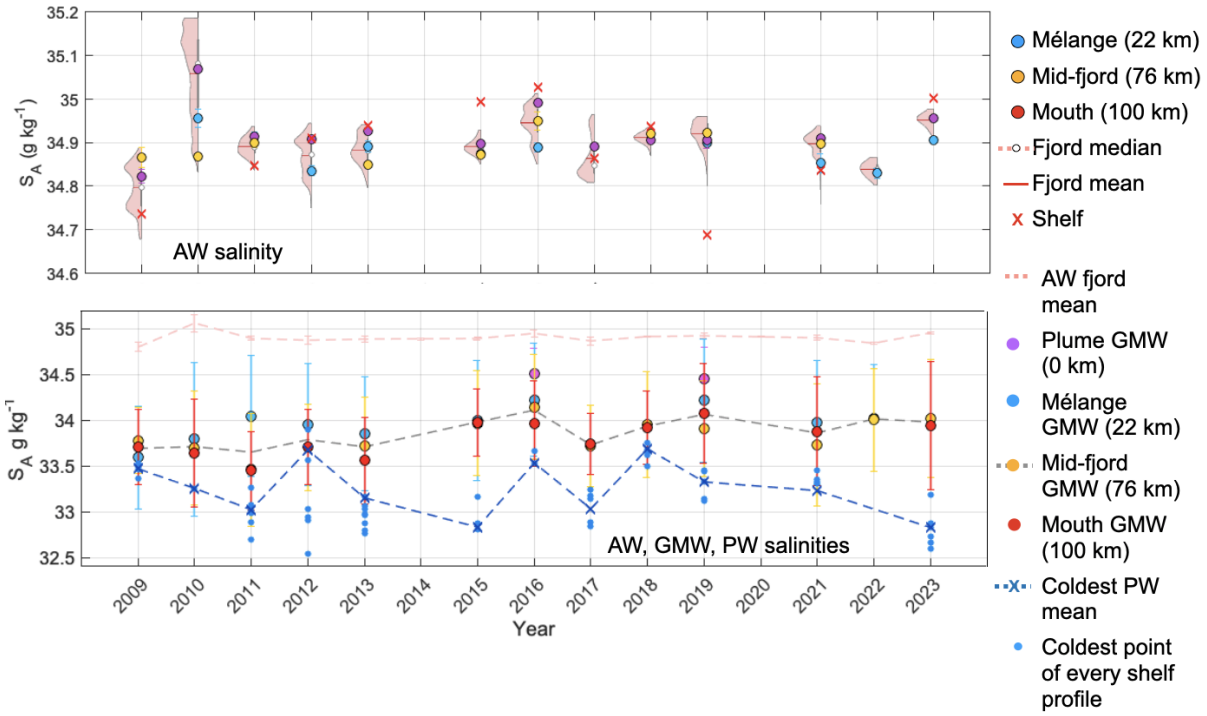


**Figure A.11.** Half-violin plots of AW fjord salinity properties across the full fjord domain for each year. Shaded pink region represents a histogram of salinity properties. Minimum and maximum vertical extent of half-violin plots correspond to minimum and maximum salinity values in the fjord domain for that year. Salinity values in specific fjord regions are shown (dots). Bottom plot compares AW salinity to PW and GMW salinity.

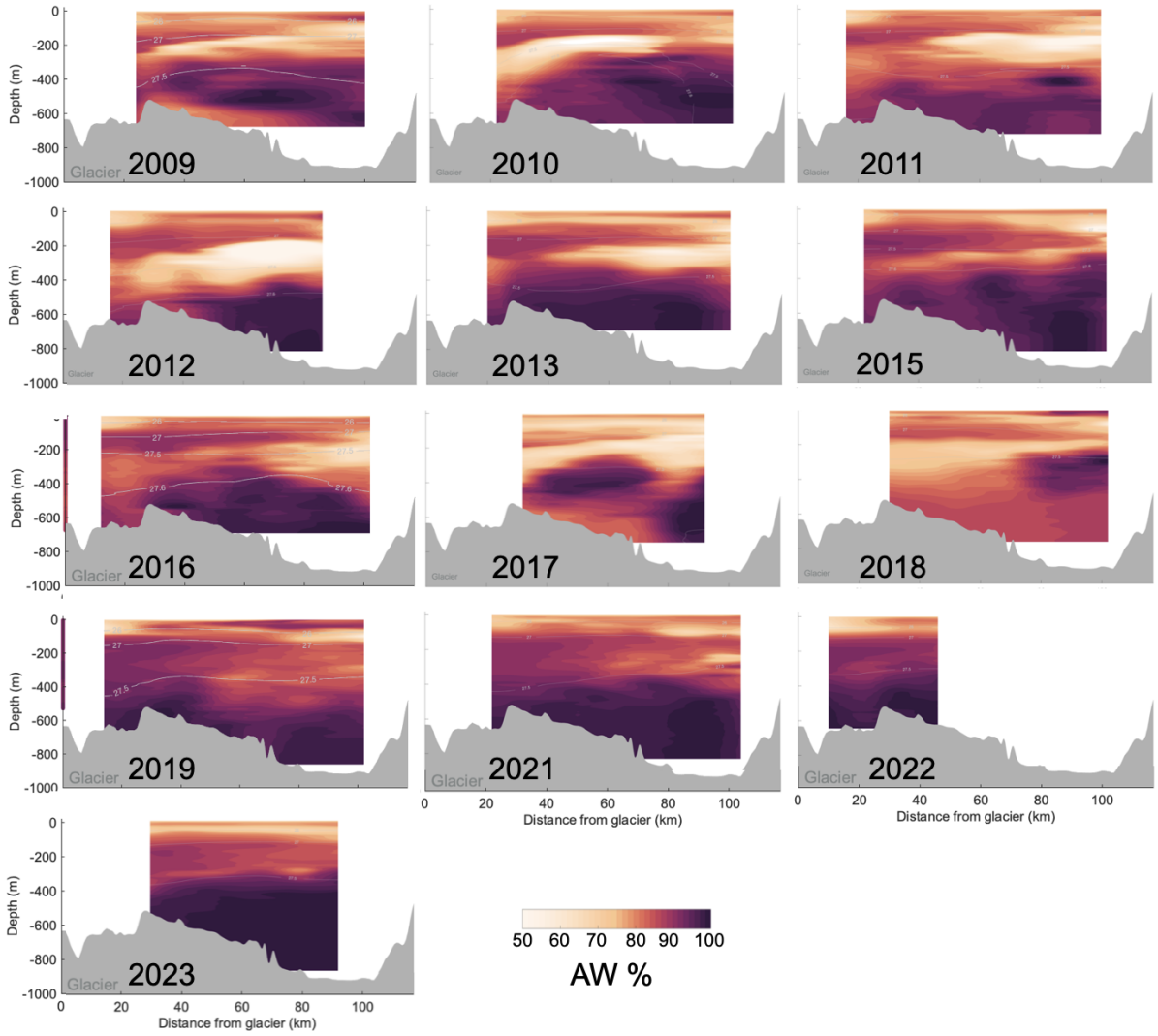


**Figure A.12.** Atlantic Water (AW) fractions (%) as calculated from the RLS method for every grid points of every year in the Sermilik Fjord gridded hydrography dataset. Plume profiles and associated AW fractions are shown in 2016 and 2019. Bathymetry along the Sermilik Fjord thalweg section is represented by the shaded grey area (Morlighem et al., 2017).

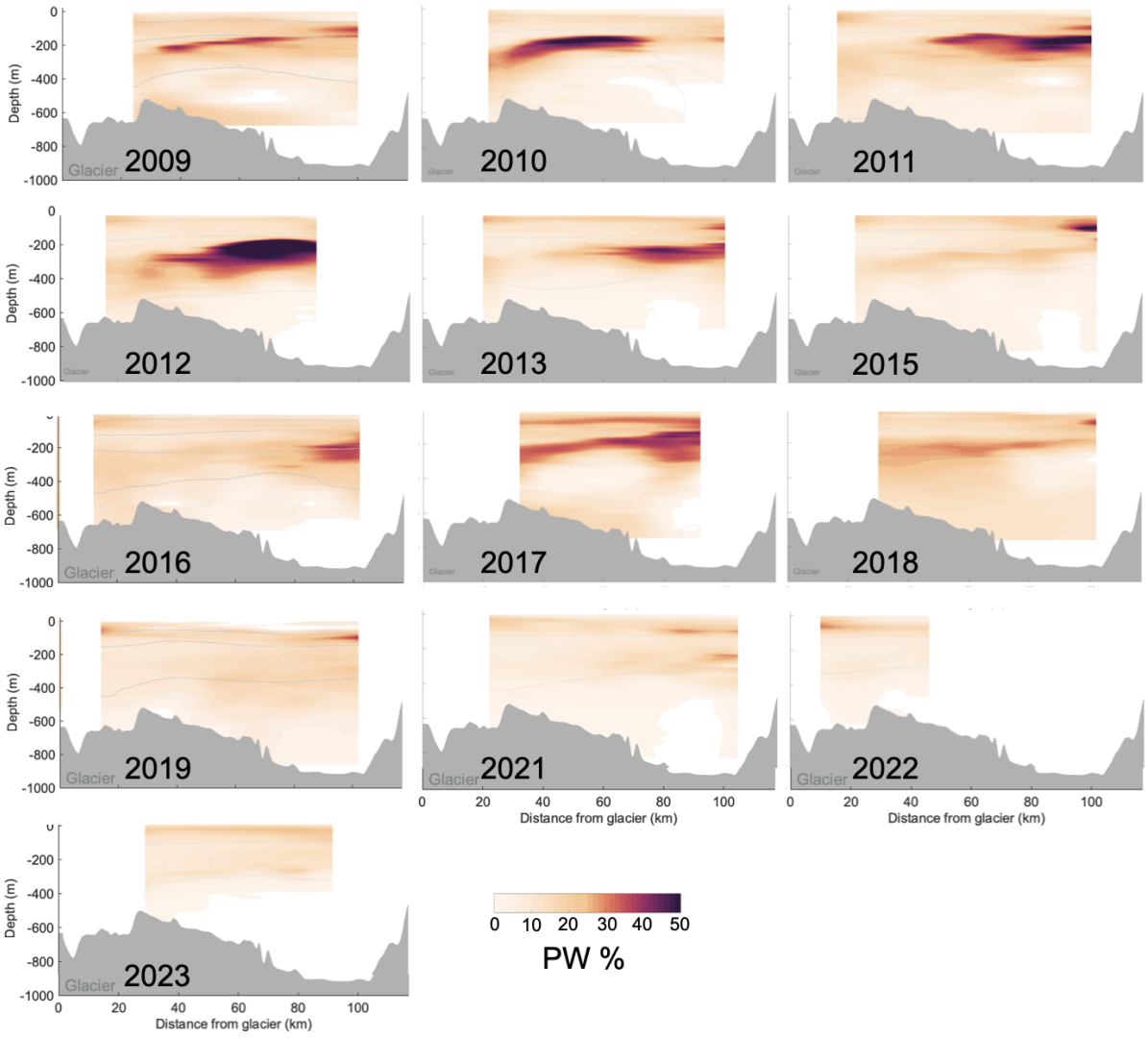


**Figure A.13.** Polar Water (PW) fractions (%) as calculated from the RLS method for every grid points of every year in the Sermilik Fjord gridded hydrography dataset. Note the scale is 0-50% for PW. Plume profiles and associated AW fractions are shown in 2016 and 2019. Bathymetry along the Sermilik Fjord thalweg section is represented by the shaded grey area (Morlighem et al., 2017).

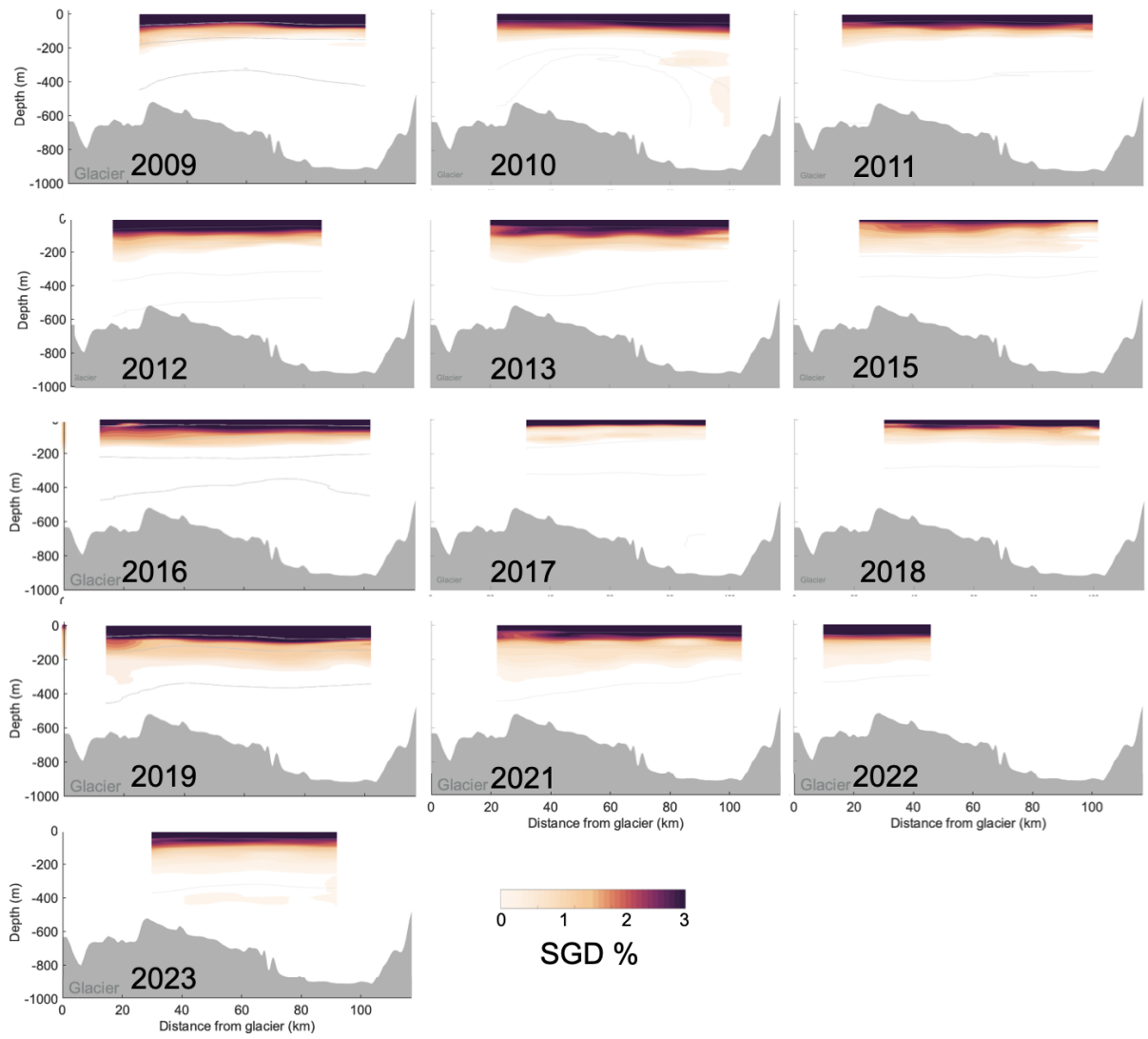


**Figure A.14.** Subglacial discharge (SGD) fractions (%) as calculated from the RLS method for every grid points of every year in the Sermilik Fjord gridded hydrography dataset. Note the scale is 0-3% for SGD. Plume profiles and associated AW fractions are shown in 2016 and 2019. Bathymetry along the Sermilik Fjord thalweg section is represented by the shaded grey area (Morlighem et al., 2017).

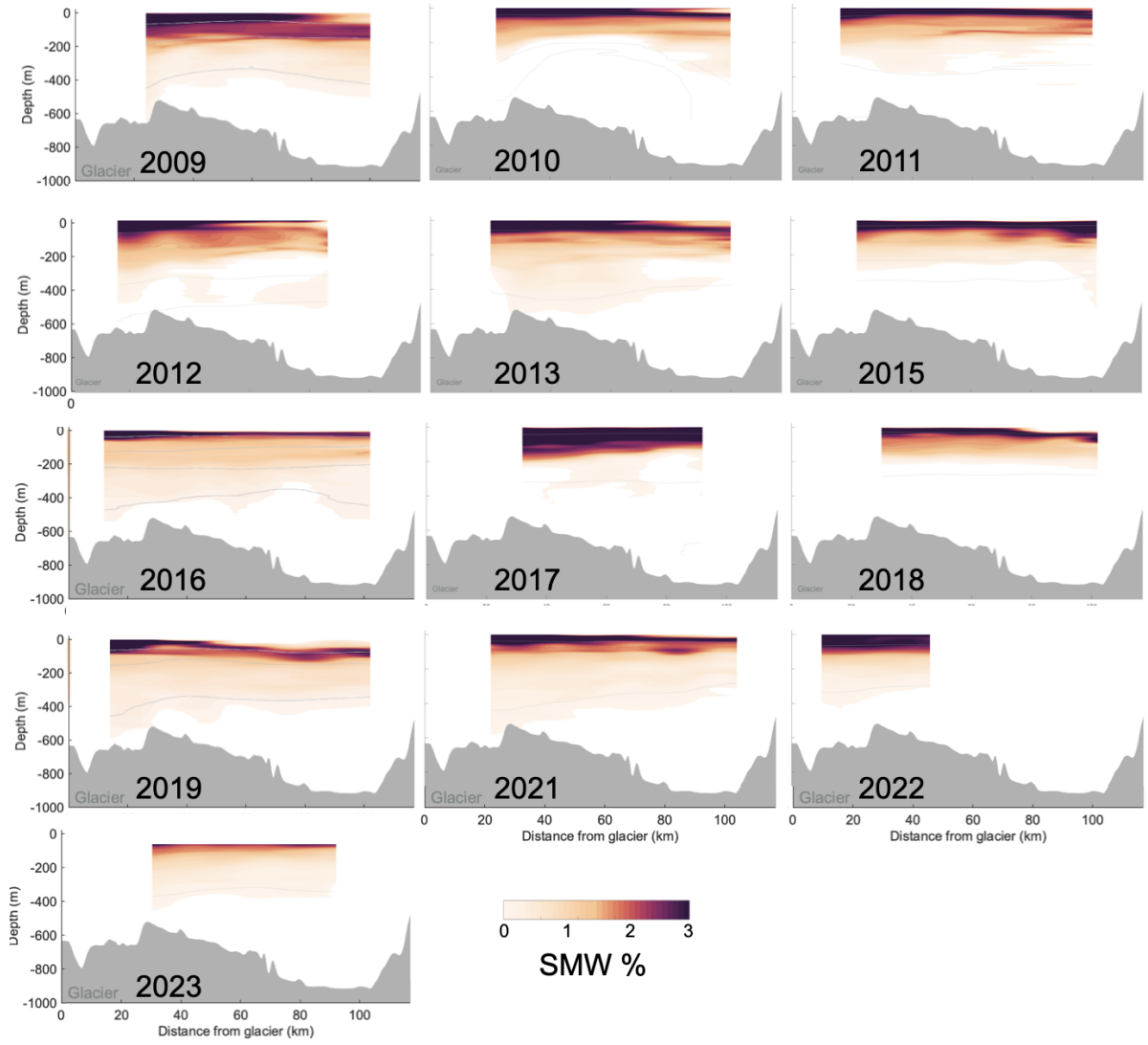


**Figure A.15.** Submarine meltwater (SMW) fractions (%) as calculated from the RLS method for every grid points of every year in the Sermilik Fjord gridded hydrography dataset. Note the scale is 0-3% for SGD. Plume profiles and associated AW fractions are shown in 2016 and 2019. Bathymetry along the Sermilik Fjord thalweg section is represented by the shaded grey area (Morlighem et al., 2017).

# Bibliography


Akshay Agrawal, Robin Verschueren, Steven Diamond, and Stephen Boyd. A rewriting system for convex optimization problems. *Journal of Control and Decision*, 5(1):42–60, 2018.

Melanie Bahnke, Vera Korthuis, Alexie Philemonoff, and Michael Johnson. Letter to the Navigating the New Arctic program, National Science Foundation. Kawerak, Inc., March 2020. URL https://kawerak.org/knowledge-sovereignty-and-the-indigenization-of-knowledge-2/. Letter on knowledge sovereignty and the indigenization of knowledge. Accessed April 2026.

Jonathan L. Bamber, Michael Oppenheimer, Robert E. Kopp, Willy P. Aspinall, and Roger M. Cooke. Ice sheet contributions to future sea-level rise from structured expert judgment. *Proceedings of the National Academy of Sciences*, 116(23):11195–11200, 2019. doi: 10.1073/pnas.1817205116.

Nicholas Beaird, Fiammetta Straneo, and William Jenkins. Spreading of Greenland meltwaters in the ocean revealed by noble gases. *Geophys. Res. Lett.*, 42:7705–7713, 2015. ISSN 1944-8007. doi: 10.1002/2015GL065003.

Nicholas L. Beaird, Fiammetta Straneo, and William Jenkins. Export of Strongly Diluted Greenland Meltwater From a Major Glacial Fjord. *Geophys. Res. Lett.*, 45:4163–4170, May 2018. ISSN 1944-8007. doi: 10.1029/2018GL077000.

Louise C. Biddle, Karen J. Heywood, Jan Kaiser, and Adrian Jenkins. Glacial Meltwater Identification in the Amundsen Sea. *J. Phys. Oceanogr.*, 47:933–954, April 2017. ISSN 0022-3670. doi: 10.1175/JPO-D-16-0221.1.

Louise C. Biddle, Brice Loose, and Karen J. Heywood. Upper Ocean Distribution of Glacial Meltwater in the Amundsen Sea, Antarctica. *J. Geophys. Res.*, 124:6854–6870, 2019. ISSN 2169-9291. doi: 10.1029/2019JC015133.

Christopher M. Bishop. *Pattern Recognition and Machine Learning*. Springer, New York, 2006. ISBN 978-0-387-31073-2.

A. A. Bjørk, L. M. Kruse, and P. B. Michaelsen. Brief communication: Getting Greenland's glaciers right – a new data set of all official Greenlandic glacier names. *The Cryosphere*, 9:

2215–2218, December 2015. ISSN 1994-0416. doi: 10.5194/tc-9-2215-2015.

Niklas Boers. Observation-based early-warning signals for a collapse of the Atlantic Meridional Overturning Circulation. *Nature Climate Change*, 11:680–688, 2021. doi: 10.1038/s41558-021-01097-4.

Francis P. Bretherton, Russ E. Davis, and C.B. Fandry. A technique for objective analysis and design of oceanographic experiments applied to MODE-73. *Deep Sea Res.*, 23:559–582, July 1976. ISSN 00117471. doi: 10.1016/0011-7471(76)90001-2.

Nicolas D. Brunet, Gordon M. Hickey, and Murray M. Humphries. The evolution of local participation and the mode of knowledge production in Arctic research. *Ecology and Society*, 19(2):69, 2014. doi: 10.5751/ES-06641-190269. URL https://www.jstor.org/stable/26269571.

Nicolas D. Brunet et al. The evolution of local engagement and the mode of knowledge production in Arctic research: 2011–2020. *FACETS*, 2024. doi: 10.1139/facets-2024-0114.

L. Caesar, S. Rahmstorf, A. Robinson, G. Feulner, and V. Saba. Observed fingerprint of a weakening Atlantic Ocean overturning circulation. *Nature*, 556:191–196, 2018. doi: 10.1038/s41586-018-0006-5.

Mattias R. Cape, Fiammetta Straneo, Nicholas Beaird, Randelle M. Bundy, and Matthew A. Charette. Nutrient release to oceans from buoyancy-driven upwelling at Greenland tidewater glaciers. *Nat. Geosci.*, 12:34–39, January 2019. ISSN 1752-0894. doi: 10.1038/s41561-018-0268-4.

Dustin Carroll, David A. Sutherland, Emily L. Shroyer, Jonathan D. Nash, Ginny A. Catania, and Leigh A. Stearns. Modeling turbulent subglacial meltwater plumes: Implications for fjord-scale buoyancy-driven circulation. *Journal of Physical Oceanography*, 45(8):2169–2185, 2015. doi: 10.1175/JPO-D-15-0033.1.

Copernicus Climate Change Service. Global climate highlights 2024. Technical report, European Centre for Medium-Range Weather Forecasts (ECMWF), 2025. URL https://climate.copernicus.eu/global-climate-highlights-2024. Accessed April 2026.

T. R. Cowton, D. A. Slater, and M. E. Inall. Subglacial-Discharge Plumes Drive Widespread Subsurface Warming in Northwest Greenland's Fjords. *Geophys. Res. Lett.*, 50:e2023GL103801, 2023. ISSN 1944-8007. doi: 10.1029/2023GL103801.

Lauren E. Culler, S. Lund, J. Nymand, and R. A. Virginia. Facilitating increased engagement between the research communities of Greenland and the U.S. Report, Institute of Arctic Studies, 2018. Published in both English and Greenlandic.

Danish Meteorological Institute. Greenland's west coast posts warmest January on record.

AFP news release, reported via *Phys.org*, February 2026. URL https://phys.org/news/2026-02-greenland-west-coast-warmest-january.html. Accessed April 2026.

Benjamin J. Davison, Tom R. Cowton, Andrew J. Sole, Finlo R. Cottier, and Peter Nienow. Modelling the effect of submarine iceberg melting on glacier-adjacent water properties. *The Cryosphere*, 16:1181–1196, 2022. doi: 10.5194/tc-16-1181-2022.

Erik Daxberger, Agustinus Kristiadi, Alexander Immer, Runa Eschenhagen, Matthias Bauer, and Philipp Hennig. Laplace redux – effortless Bayesian deep learning. In *Advances in Neural Information Processing Systems*, 2021. URL https://arxiv.org/abs/2106.14806.

M. F. de Jong and L. de Steur. Strong winter cooling over the irminger sea in winter 2014–2015, exceptional deep convection, and the emergence of anomalously low sst. *Geophysical Research Letters*, 43(7):7106–7113, 2016. doi: 10.1002/2016GL069596.

Damien Desbruyères, Léon Chafik, and Guillaume Maze. A shift in the ocean circulation has warmed the subpolar North Atlantic Ocean since 2016. *Communications Earth & Environment*, 2:48, 2021. doi: 10.1038/s43247-021-00120-y.

Steven Diamond and Stephen Boyd. CVXPY: A Python-embedded modeling language for convex optimization. *Journal of Machine Learning Research*, 17(83):1–5, 2016.

Tiago S. Dotto, Mauricio M. Mata, Rodrigo Kerr, and Carlos A. E. Garcia. A novel hydrographic gridded data set for the northern Antarctic Peninsula. *Earth Syst. Sci. Data*, 13:671–696, February 2021. ISSN 1866-3508. doi: 10.5194/essd-13-671-2021.

M. L. Druckenmiller, R. L. Thoman, and T. A. Moon. Arctic report card 2025. Technical report, National Oceanic and Atmospheric Administration, 2025. URL https://arctic.noaa.gov/report-card/report-card-2025/. Eds. Druckenmiller, M. L., Thoman, R. L., Moon, T. A.

Matthew L. Druckenmiller. Co-production of knowledge in Arctic research: Reconsidering and reorienting amidst the Navigating the New Arctic initiative. *Oceanography*, 35(3–4):189–191, 2022. doi: 10.5670/oceanog.2022.134. Sidebar.

Ellam Yua, Julie Raymond-Yakoubian, Raychelle Aluaq Daniel, and Carolina Behe. A framework for co-production of knowledge in the context of Arctic research. *Ecology and Society*, 27(1): art34, 2022. doi: 10.5751/ES-12960-270134.

Ellyn M. Enderlin and Ian M. Howat. Submarine melt rate estimates for floating termini of Greenland outlet glaciers (2000–2010). *Journal of Glaciology*, 59(213):67–75, 2013. doi: 10.3189/2013JoG12J049.

Ellyn M. Enderlin, Gordon S. Hamilton, Fiammetta Straneo, and David A. Sutherland. Iceberg meltwater fluxes dominate the freshwater budget in Greenland's iceberg-congested glacial

fjords. *Geophys. Res. Lett.*, 43:11,287–11,294, 2016. ISSN 1944-8007. doi: 10.1002/2016GL070718.

European Space Agency and Copernicus Programme. Sentinel-2 cloudless mosaic of Greenland, 2019, 2019. URL https://sentinel.esa.int. Contains modified Copernicus Sentinel data 2019, accessed via QGreenland v3 (Moon et al., 2023).

Alistair Everett, Tavi Murray, Nick Selmes, David Holland, and Daniel E. Reeve. The impacts of a subglacial discharge plume on calving, submarine melting, and mélange mass loss at Helheim Glacier, south east Greenland. *Journal of Geophysical Research: Earth Surface*, 126 (3):e2020JF005910, 2021. doi: 10.1029/2020JF005910.

Steven Foga. Characterization of ice mélange and its implications toterminus stability at helheim glacier, southeast greenland. Master's thesis, University of Kansas, Lawerence, KS, May 2016. Available at https://core.ac.uk/reader/213418374.

B. Fox-Kemper, H. T. Hewitt, C. Xiao, G. Adalgeirsdottir, S. S. Drijfhout, T. L. Edwards, N. R. Golledge, M. Hemer, R. E. Kopp, G. Krinner, A. Mix, D. Notz, S. Nowicki, I. S. Nurhati, L. Ruiz, J.-B. Schlosser, A. B. A. Slangen, and K. Yu. Ocean, cryosphere and sea level change. In V. Masson-Delmotte, P. Zhai, A. Pirani, S. L. Connors, C. Pean, S. Berger, N. Caud, Y. Chen, L. Goldfarb, M. I. Gomis, M. Huang, K. Leitzell, E. Lonnoy, J. B. R. Matthews, T. K. Maycock, T. Waterfield, O. Yelekci, R. Yu, and B. Zhou, editors, *Climate Change 2021: The Physical Science Basis. Contribution of Working Group I to the Sixth Assessment Report of the Intergovernmental Panel on Climate Change*, pages 1211–1362. Cambridge University Press, 2021. doi: 10.1017/9781009157896.011.

Herman G. Gade. Melting of Ice in Sea Water: A Primitive Model with Application to the Antarctic Ice Shelf and Icebergs. *J. Phys. Oceanogr.*, 9:189–198, January 1979. ISSN 0022-3670. doi: 10.1175/1520-0485(1979)009⟨0189:MOIISW⟩2.0.CO;2.

Herncin E. Garcia and Louis I. Gordon. Oxygen solubility in seawater: Better fitting equations. *Limnology and Oceanography*, 37(6):1307–1312, 1992. doi: 10.4319/lo.1992.37.6.1307.

Maribel I. García-Ibáñez, Fiz F. Pérez, Pascale Lherminier, Patricia Zunino, Herlé Mercier, and Paul Tréguer. Water mass distributions and transports for the 2014 GEOVIDE cruise in the North Atlantic. *Biogeosciences*, 15(7):2075–2090, 2018. doi: 10.5194/bg-15-2075-2018.

C. V. B. Gjelstrup, J. Boje, B. R. MacKenzie, S. Post, K. M. Werner, A. W. Visser, and C. A. Stedmon. The East Greenland Polar Front as a mediator of climate-ocean-ecosystem variability along Southeast Greenland. *Journal of Geophysical Research: Oceans*, 130(10): e2025JC022669, 2025. doi: 10.1029/2025JC022669.

Heather Sauyaq Jean Gordon and Deana Around Him. Conducting research "in a good way": relationships as the foundation of research. *Arctic Science*, 11:1–16, 2025. ISSN 2368-7460.

doi: 10.1139/as-2023-0078. URL https://cdnsciencepub.com/doi/10.1139/as-2023-0078. Open access. Published online 13 January 2025.

Naja Dyrendom Graugaard. Collaborative research methods in the arctic: Experiences from greenland. Routledge, 2020.

Noa Gvèret. Natural and Indigenous sciences: Reflections on an attempt to collaborate. *Regional Environmental Change*, 22:101, 2022. doi: 10.1007/s10113-022-01967-3.

Alexander O. Hager, David A. Sutherland, and Donald A. Slater. Local forcing mechanisms challenge parameterizations of ocean thermal forcing for Greenland tidewater glaciers. *The Cryosphere*, 2024. doi: 10.5194/tc-18-911-2024.

Anne Merrild Hansen and Carina Ren, editors. *Collaborative Research Methods in the Arctic: Experiences from Greenland*. Routledge, London, 2021. doi: 10.4324/9781003085508.

Per Christian Hansen. *Rank-Deficient and Discrete Ill-Posed Problems: Numerical Aspects of Linear Inversion*. SIAM Monographs on Mathematical Modeling and Computation. Society for Industrial and Applied Mathematics, Philadelphia, PA, 1998. ISBN 978-0-89871-403-6. doi: 10.1137/1.9780898719697.

William D. Harcourt, Michael G. Shahin, Leigh A. Stearns, and Siddharth Shankar. Structural weaknesses in ice mélange revealed by high-resolution iceye sar imagery. *Journal of Glaciology*, page 1–32, 2025. doi: 10.1017/jog.2025.10085.

Ben E. Harden, Fiamma Straneo, and David A. Sutherland. Moored observations of synoptic and seasonal variability in the east greenland coastal current. *Journal of Geophysical Research: Oceans*, 119:8838–8857, 2014. doi: 10.1002/2014JC010134.

Donna D. W. Hauser, Alex V. Whiting, Andrew R. Mahoney, John Goodwin, Cyrus Harris, Robert J. Schaeffer, Roswell Schaeffer, Nathan J. M. Laxague, Ajit Subramaniam, Carson R. Witte, Sarah Betcher, Jessica M. Lindsay, and Christopher J. Zappa. Co-production of knowledge reveals loss of Indigenous hunting opportunities in the face of accelerating Arctic climate change. *Environmental Research Letters*, 16(9):095003, 2021. doi: 10.1088/1748-9326/ac1a36.

Mads Peter Heide-Jørgensen, Philippine Chambault, Teunis Jansen, Caroline V. B. Gjelstrup, Aqqalu Rosing-Asvid, Andreas Macrander, Gísli Víkingsson, Xiangdong Zhang, Camilla S. Andresen, and Brian R. MacKenzie. A regime shift in the Southeast Greenland marine ecosystem. *Global Change Biol.*, 29:668, February 2023. doi: 10.1111/gcb.16494.

Lene Holm. *Sila-Inuk: Study of the Impacts of Climate Change in Greenland*, pages 145–160. 02 2010. ISBN 978-90-481-8586-3. doi: 10.1007/978-90-481-8587-0_6.

Mark J. Hopwood, Dustin Carroll, Thorben Dunse, Andy Hodson, Johnna M. Holding, José L. Iriarte, Sofia Ribeiro, Eric P. Achterberg, Carolina Cantoni, Daniel F. Carlson, Melissa Chierici, Jennifer S. Clarke, Stefano Cozzi, Agneta Fransson, Thomas Juul-Pedersen, Mie H. S. Winding, and Lorenz Meire. Review article: How does glacier discharge affect marine biogeochemistry and primary production in the Arctic? *The Cryosphere*, 14:1347–1383, April 2020. ISSN 1994-0424. doi: 10.5194/tc-14-1347-2020.

Ian Howat. MEaSUREs annual Greenland outlet glacier terminus positions from SAR mosaics, version 2 [dataset], 2022. [dataset].

Ian M. Howat, Angelica Negrete, and Bruce E. Smith. The greenland ice mapping project (gimp) land classification and surface elevation data sets. *The Cryosphere*, 8(4):1509–1518, 2014. doi: 10.5194/tc-8-1509-2014.

Kenneth G. Hughes. Pathways, form drag, and turbulence in simulations of an ocean flowing through an ice mélange. *Journal of Geophysical Research: Oceans*, 127(6):e2021JC018228, 2022. doi: 10.1029/2021JC018228.

Flora Huiban, Romain Millan, Kristian Kjellerup Kjeldsen, Camilla S. Andresen, Mads Dømgaard, Amaury Dehecq, Stephen Brunt, Shfaqat Abbas Khan, Jerémie Mouginot, and Anders Anker Bjørk. Regional ice flow piracy following the collapse of midgaard glacier in southeast greenland. *Nature Communications*, 15:9976, 2024. doi: 10.1038/s41467-024-54045-z.

Kayo Ide, Philippe Courtier, Michael Ghil, and Andrew C. Lorenc. Unified Notation for Data Assimilation: Operational, Sequential and Variational. *J. Meteor. Soc. Japan*, 75:181–189, 1997. doi: 10.2151/jmsj1965.75.1B_181.

Interagency Arctic Research Policy Committee (IARPC). Principles for conducting research in the arctic. Technical report, Interagency Arctic Research Policy Committee, 2017.

Inuit Circumpolar Council. Inuit arctic policy. Technical report, Inuit Circumpolar Council, 2010. URL https://iccalaska.org/wp-icc/wp-content/uploads/2016/01/Inuit-Arctic-Policy-June02_FINAL.pdf. Revised and updated edition. Original policy developed 1980s; revision led by Aqqaluk Lynge and Marianne Stenbaek.

Inuit Circumpolar Council. Ethical and equitable engagement: A synthesis report on the inuit circumpolar council's engagement protocols. Technical report, Inuit Circumpolar Council, 2022a.

Inuit Circumpolar Council. Inuit Circumpolar Council Establishes New Standard in International Engagement with the Release of Circumpolar Inuit Protocols for Equitable and Ethical Engagement, June 2022b.

Cana Uluak Itchuaqiyaq, Chris A. Lindgren, and Corina Qaaġraq Kramer. Decolonizing

community-engaged research: Designing CER with cultural humility as a foundational value. *Communication Design Quarterly Review*, 11(3):12–20, December 2023. doi: 10.1145/3592367.3592369. URL https://dl.acm.org/doi/abs/10.1145/3592367.3592369.

Rebecca H. Jackson and Fiammetta Straneo. Heat, Salt, and Freshwater Budgets for a Glacial Fjord in Greenland. *J. Phys. Oceanogr.*, 46:2735–2768, September 2016. ISSN 0022-3670. doi: 10.1175/JPO-D-15-0134.1.

Rebecca H. Jackson, Fiammetta Straneo, and David A. Sutherland. Externally forced fluctuations in ocean temperature at Greenland glaciers in non-summer months. *Nat. Geosci.*, 7:503–508, July 2014. ISSN 1752-0908. doi: 10.1038/ngeo2186.

Rebecca H. Jackson, Steven J. Lentz, and Fiamma Straneo. The Dynamics of Shelf Forcing in Greenlandic Fjords. *J. Phys. Oceanogr.*, 48:2799–2827, November 2018. ISSN 0022-3670. doi: 10.1175/JPO-D-18-0057.1.

Rebecca H. Jackson, Jonathan D. Nash, Christian Kienholz, David A. Sutherland, Jason M. Amundson, Roman J. Motyka, Daniel Winters, Eric Skyllingstad, and Erin C. Pettit. Meltwater intrusions reveal mechanisms for rapid submarine melt at a tidewater glacier. *Geophysical Research Letters*, 47(2):e2019GL085335, 2020. doi: 10.1029/2019GL085335.

Rebecca H. Jackson, Roman J. Motyka, Jason M. Amundson, Nicole Abib, David A. Sutherland, Jonathan D. Nash, and Christian Kienholz. The relationship between submarine melt and subglacial discharge from observations at a tidewater glacier. *Journal of Geophysical Research: Oceans*, 127(10):e2021JC018204, 2022. doi: 10.1029/2021JC018204.

L. Jain et al. Modelling ocean melt of ice mélange at Greenland's marine-terminating glaciers. *The Cryosphere*, 19:6865–6889, 2025. doi: 10.5194/tc-19-6865-2025.

Adrian Jenkins. The Impact of Melting Ice on Ocean Waters. *J. Phys. Oceanogr.*, 29:2370–2381, September 1999. ISSN 0022-3670. doi: 10.1175/1520-0485(1999)029⟨2370:TIOMIO⟩2.0.CO;2.

Adrian Jenkins. Convection-Driven Melting near the Grounding Lines of Ice Shelves and Tidewater Glaciers. *J. Phys. Oceanogr.*, 41:2279–2294, December 2011. ISSN 0022-3670. doi: 10.1175/JPO-D-11-03.1.

Adrian Jenkins and Stan Jacobs. Circulation and melting beneath George VI Ice Shelf, Antarctica. *J. Geophys. Res.*, 113, April 2008. ISSN 2156-2202. doi: 10.1029/2007JC004449.

Thomas Juul-Pedersen, Søren Rysgaard, Paul Batty, John Mortensen, Anja Retzel, Rasmus Nygaard, AnnDorte Burmeister, Ditte Marie Mikkelsen, Mikael Kristian Sejr, Martin E. Blicher, Dorte Krause-Jensen, Peter Bondo Christensen, Aili L. Labansen, Lars M. Rasmussen, Malene Simon, Tenna K. Boye, Peter T. Madsen, and Fernando Ugarte. *NUUK BASIC: The*

*MarineBasis Programme*, pages 39–58. National Environmental Research Institute, Aarhus University, 2009. ISBN 978-87-7073-125-6.

Karita Kajanto, Fiammetta Straneo, and Kerim Nisancioglu. Impact of icebergs on the seasonal submarine melt of Sermeq Kujalleq. *The Cryosphere*, 17(1):371–390, 2023. doi: 10.5194/tc-17-371-2023.

Naoya Kanna, Shin Sugiyama, Yoshihiko Ohashi, Daiki Sakakibara, Yasushi Fukamachi, and Daiki Nomura. Upwelling of Macronutrients and Dissolved Inorganic Carbon by a Subglacial Freshwater Driven Plume in Bowdoin Fjord, Northwestern Greenland. *J. Geophys. Res. Biogeosci.*, 123:1666–1682, 2018. ISSN 2169-8961. doi: 10.1029/2017JG004248.

Naoya Kanna, Shin Sugiyama, Yasushi Fukamachi, Daiki Nomura, and Jun Nishioka. Iron Supply by Subglacial Discharge Into a Fjord Near the Front of a Marine-Terminating Glacier in Northwestern Greenland. *Global Biogeochem. Cycles*, 34:e2020GB006567, 2020. ISSN 1944-9224. doi: 10.1029/2020GB006567.

Johannes Karstensen and Matthias Tomczak. OMP Analysis Package for MATLAB Version 2.0, August 1999. URL https://omp.geomar.de/README.html. available at: https://omp.geomar.de/README.html.

Hyebin Kim, Dukki Han, Sang Rul Park, and Tae-Hoon Kim. Seasonal interplay of water mass mixing and nutrient dynamics in an Arctic fjord: a case study of Kongsfjorden, Svalbard. *Ocean Sci.*, 21:3089–3103, November 2025a. ISSN 1812-0784. doi: 10.5194/os-21-3089-2025.

Jae Hun Kim, Eric Rignot, Hanning Chen, David Holland, and Denise Holland. Grounding zone of Helheim glacier, Greenland, from terrestrial radar interferometry. *Geophysical Research Letters*, 2025b. doi: 10.1029/2024GL112345.

Kylie Kinne, Robert Sanchez, Lia Siegelman, Fiammetta Straneo, and Kenneth Hughes. The Seasonality of Greenland Iceberg Melt and Its Influences on Fjord Properties and Dynamics. *J. Geophys. Res.*, 130:e2025JC022587, 2025. ISSN 2169-9291. doi: 10.1029/2025JC022587.

Kristin L. Laidre, Megan A. Supple, Erik W. Born, Eric V. Regehr, Øystein Wiig, Fernando Ugarte, Jon Aars, Rune Dietz, Christian Sonne, Peter Hegelund, Carl Isaksen, Geir B. Akse, Benjamin Cohen, Harry L. Stern, Twila Moon, Christopher Vollmers, Russ Corbett-Detig, David Paetkau, and Beth Shapiro. Glacial ice supports a distinct and undocumented polar bear subpopulation persisting in late 21st-century sea-ice conditions. *Science*, 376(6599): 1333–1338, 2022. doi: 10.1126/science.abk2793. URL https://www.science.org/doi/abs/10.1126/science.abk2793.

F. W. Landerer et al. Extending the global mass change data record: GRACE follow-on instrument performance, data quality, and early science results. *Geophysical Research Letters*,

47:e2020GL088306, 2020. doi: 10.1029/2020GL088306.

Joshua Lanham, Matthew Mazloff, Alberto C. Naveira Garabato, Martin Siegert, and Ali Mashayek. Seasonal regimes of warm Circumpolar Deep Water intrusion toward Antarctic ice shelves. *Commun. Earth Environ.*, 6:168, March 2025. ISSN 2662-4435. doi: 10.1038/s43247-025-02091-w.

Olga Lauter. Challenges in combining Indigenous and scientific knowledge in the Arctic. *Polar Geography*, 46(1):62–74, 2023. doi: 10.1080/1088937X.2023.2233578.

R. M. Lawrence, A. Shrikumar, E. Le Roy, J. Swift, P. J. Lam, G. A. Cutter, and K. L. Casciotti. Analysis of nutrient and hydrographic patterns on the GEOTRACES Pacific Meridional Section (GP15) using PYOMPA, a new framework for water mass analysis. *Mar. Chem.*, 274: 104598, January 2026. ISSN 0304-4203. doi: 10.1016/j.marchem.2025.104598.

M. R. Lindeman, F. Straneo, H. M. Adams, M. J. S. Nelson, and A. T. Schartup. Low mercury concentrations in a Greenland glacial fjord attributed to oceanic sources. *Commun. Earth Environ.*, 5:320, June 2024. ISSN 2662-4435. doi: 10.1038/s43247-024-01474-9.

M. Susan Lozier, F. Li, S. Bacon, F. Bahr, A. S. Bower, S. A. Cunningham, M. F. de Jong, L. de Steur, B. deYoung, J. Fischer, S. F. Gary, B. J. W. Greenan, N. P. Holliday, A. Houk, L. Houpert, M. E. Inall, W. E. Johns, H. L. Johnson, C. Johnson, J. Karstensen, G. Koman, I. A. Le Bras, X. Lin, N. Mackay, D. P. Marshall, H. Mercier, M. Oltmanns, R. S. Pickart, A. L. Ramsey, D. Rayner, F. Straneo, V. Thierry, D. J. Torres, R. G. Williams, C. Wilson, J. Yang, I. Yashayaev, and J. Zhao. A sea change in our view of overturning in the subpolar North Atlantic. *Science*, 363(6426):516–521, 2019. doi: 10.1126/science.aau6592.

David L. Mackas, Kenneth L. Denman, and Andrew F. Bennett. Least-squares multiple tracer analysis of water mass composition. *Journal of Geophysical Research: Oceans*, 92(C3): 2907–2918, 1987. doi: 10.1029/JC092iC03p02907.

David J. C. MacKay. A practical Bayesian framework for backpropagation networks. *Neural Computation*, 4(3):448–472, 1992. doi: 10.1162/neco.1992.4.3.448.

Kenneth D. Mankoff, Fiammetta Straneo, Claudia Cenedese, Sarah B. Das, Clark G. Richards, and Hanumant Singh. Structure and dynamics of a subglacial discharge plume in a Greenlandic fjord. *J. Geophys. Res.*, 121:8670–8688, 2016. ISSN 2169-9291. doi: 10.1002/2016JC011764.

Kenneth D. Mankoff, Brice Noël, Xavier Fettweis, Andreas P. Ahlstrøm, William Colgan, Ken Kondo, Kirsty Langley, Shin Sugiyama, Dirk van As, and Robert S. Fausto. Greenland liquid water discharge from 1958 through 2019. *Earth Syst. Sci. Data*, 12:2811–2841, November 2020. ISSN 1866-3508. doi: 10.5194/essd-12-2811-2020.

Matthew R. Mazloff, Ariane Verdy, Sarah T. Gille, Kenneth S. Johnson, Bruce D. Cornuelle,

and Jorge Sarmiento. Southern Ocean Acidification Revealed by Biogeochemical-Argo Floats. *J. Geophys. Res.*, 128:e2022JC019530, May 2023. ISSN 2169-9275. doi: 10.1029/2022JC019530.

T.J. McDougall and P.M. Barker. Getting started with TEOS-10 and the Gibbs Seawater (GSW) Oceanographic Toolbox, 2011. ISSN 978-0-646-55621-5. URL https://www.teos-10.org/software.htm.

Lorenz Meire, John Mortensen, Patrick Meire, Thomas Juul-Pedersen, Mikael K. Sejr, Søren Rysgaard, Rasmus Nygaard, Philippe Huybrechts, and Filip J. R. Meysman. Marine-terminating glaciers sustain high productivity in greenland fjords. *Global Change Biology*, 23(12):5344–5357, 2017. doi: https://doi.org/10.1111/gcb.13801. URL https://onlinelibrary.wiley.com/doi/abs/10.1111/gcb.13801.

Lorenz Meire, Maria Lund Paulsen, Patrick Meire, Søren Rysgaard, Mark Hopwood, Alice Stuart-Lee, Koen Sabbe, Willem Stock, and John Mortensen. Glacier retreat alters downstream fjord ecosystem structure and function in Greenland. *Nat. Geosci.*, 2023. doi: 10.1038/s41561-023-01218-y.

Sierra M. Melton, Richard B. Alley, Sridhar Anandakrishnan, Byron R. Parizek, Michael G. Shahin, Leigh A. Stearns, Adam L. Lewinter, and David C. Finnegan. Meltwater drainage and iceberg calving observed in high-spatiotemporal resolution at helheim glacier, greenland. *Journal of Glaciology*, 68(270):812–828, 2022. doi: 10.1017/jog.2021.141.

Yue Meng, Ching-Yao Lai, Riley Culberg, Michael G. Shahin, Leigh A. Stearns, Justin C. Burton, and Kavinda Nissanka. Seasonal changes of mélange thickness coincide with Greenland calving dynamics. *Nature Communications*, 16(1):573, January 2025. ISSN 2041-1723. doi: 10.1038/s41467-024-55241-7. URL https://doi.org/10.1038/s41467-024-55241-7.

Jennifer Mercer, Josephine Nymand, Lauren Culler, Rebecca Lynge, Sten Lund, Bo Gregersen, Brett Makens, Ross Virginia, and Kristian Moore. Bilateral collaboration between the greenland (kalaallit nunaat) and united states research communities – from a vision to everyday practice. *Polar Record*, 58, 12 2022. doi: 10.1017/S0032247422000298.

Maria Monakhova, Abigail York, Malory Peterson, Jack Andrew McCracken Pringle, Shauna BurnSilver, and Tatiana Degai. Co-production of Arctic sea ice knowledge: A systematic review. *Ambio*, 55:1198–1217, 2025. doi: 10.1007/s13280-025-02303-9.

Twila Moon, David Sutherland, Dustin Carroll, Dennis Felikson, Laura Kehrl, and Fiamma Straneo. Subsurface iceberg melt key to Greenland fjord freshwater budget. *Nat. Geosci.*, 11:49–54, January 2018. ISSN 1752-0894. doi: 10.1038/s41561-017-0018-z.

Twila A. Moon, M. Fisher, T. Stafford, and A. Thurber. QGreenland (v3) [dataset], 2023. URL https://qgreenland.org. [dataset].

Twila A. Moon, B. Cohen, Taryn E. Black, K. L. Laidre, H. L. Stern, and Ian Joughin. Characterizing southeast Greenland fjord surface ice and freshwater flux to support biological applications. *The Cryosphere*, 18(10):4845–4872, 2024. doi: 10.5194/tc-18-4845-2024.

M. Morlighem, C. N. Williams, E. Rignot, L. An, J. E. Arndt, J. L. Bamber, G. Catania, N. Chauché, J. A. Dowdeswell, B. Dorschel, I. Fenty, K. Hogan, I. Howat, A. Hubbard, M. Jakobsson, T. M. Jordan, K. K. Kjeldsen, R. Millan, L. Mayer, J. Mouginot, B. P. Y. Noël, C. O'Cofaigh, S. Palmer, S. Rysgaard, H. Seroussi, M. J. Siegert, P. Slabon, F. Straneo, M. R. van den Broeke, W. Weinrebe, M. Wood, and K. B. Zinglersen. Bedmachine v3: Complete bed topography and ocean bathymetry mapping of greenland from multibeam echo sounding combined with mass conservation. *Geophysical Research Letters*, 44(21):11,051–11,061, 2017. doi: https://doi.org/10.1002/2017GL074954. URL https://agupubs.onlinelibrary.wiley.com/doi/abs/10.1002/2017GL074954.

Theresa Jayne Morrison. *From Greenland Fjords to the Labrador Sea: Mechanisms of Heat and Freshwater Transport in Mesoscale Eddy Active Ocean/Sea-ice Simulations*. PhD thesis, UC San Diego, 2022. URL https://escholarship.org/uc/item/4rs975gf.

J. Mortensen, J. Bendtsen, R. J. Motyka, K. Lennert, M. Truffer, M. Fahnestock, and S. Rysgaard. On the seasonal freshwater stratification in the proximity of fast-flowing tidewater outlet glaciers in a sub-Arctic sill fjord. *J. Geophys. Res.*, 118:1382–1395, 2013. ISSN 2169-9291. doi: 10.1002/jgrc.20134.

J. Mortensen, S. Rysgaard, K.E. Arendt, T. Juul-Pedersen, D.H. Søgaard, J. Bendtsen, and L. Meire. Local coastal water masses control heat levels in a west greenland tidewater outlet glacier fjord. *Journal of Geophysical Research: Oceans*, 123(11):8068–8083, November 2018. doi: 10.1029/2018JC014549.

John Mortensen, Søren Rysgaard, Jørgen Bendtsen, Kunuk Lennert, Torsten Kanzow, Henrik Lund, and Lorenz Meire. Subglacial Discharge and Its Down-Fjord Transformation in West Greenland Fjords With an Ice Mélange. *J. Geophys. Res.*, 125:e2020JC016301, 2020. ISSN 2169-9291. doi: 10.1029/2020JC016301.

Jérémie Mouginot, Eric Rignot, Anders A. Bjørk, Michiel van den Broeke, Romain Millan, Mathieu Morlighem, Brice Noël, Bernd Scheuchl, and Michael Wood. Forty-six years of Greenland Ice Sheet mass balance from 1972 to 2018. *Proceedings of the National Academy of Sciences*, 116(19):9239–9244, 2019. doi: 10.1073/pnas.1904242116.

Anna N. Moyer, David A. Sutherland, Peter W. Nienow, and Andrew J. Sole. Seasonal variations in iceberg freshwater flux in Sermilik Fjord, Southeast Greenland from Sentinel-2 imagery. *Geophysical Research Letters*, 46:8903–8912, 2019. doi: 10.1029/2019GL082309.

Morven Muilwijk, Fiamma Straneo, Donald A. Slater, Lars H. Smedsrud, James Holte, Michael Wood, Camilla S. Andresen, and Ben Harden. Export of Ice Sheet Meltwater from Upernavik

Fjord, West Greenland. *J. Phys. Oceanogr.*, 52:363–382, March 2022. ISSN 0022-3670. doi: 10.1175/JPO-D-21-0084.1.

Naalakkersuisut (Government of Greenland). Greenland's national research strategy 2022–2030. Technical report, Naalakkersuisut, Nuuk, Greenland, 2022. URL https://naalakkersuisut.gl.

G. J. Nabuurs, R. Mrabet, A. Abu Hatab, et al. Agriculture, forestry and other land uses (AFOLU). In P. R. Shukla, J. Skea, R. Slade, et al., editors, *Climate Change 2022: Mitigation of Climate Change. Contribution of Working Group III to the Sixth Assessment Report of the Intergovernmental Panel on Climate Change*, pages 747–860. Cambridge University Press, 2022. doi: 10.1017/9781009157926.009.

NASA Jet Propulsion Laboratory. Greenland ice mass loss 2002–2025. NASA Scientific Visualization Studio, 2025. URL https://svs.gsfc.nasa.gov/31156/. Accessed April 2026.

National Science Foundation. Updates to the Navigating the New Arctic (NNA) program. NSF Dear Colleague Letter NSF 23-088, 2023. URL https://www.nsf.gov/pubs/2023/nsf23088/nsf23088.jsp. Accessed April 2026.

Monica Nelson, M. Femke de Jong, Samar Khatiwala, and Matthew R. Mazloff. Delayed recovery of the Irminger interior from cooling in 2015 due to widespread buoyancy loss and suppressed restratification. *Geophysical Research Letters*, 51(2):e2023GL106501, 2024. doi: 10.1029/2023GL106501.

Peter W. Nienow, Andrew J. Sole, Donald A. Slater, and Thomas R. Cowton. Recent advances in our understanding of the role of meltwater in the Greenland Ice Sheet system. *Current Climate Change Reports*, 3:330–344, 2017. doi: 10.1007/s40641-017-0083-9.

Mark Nuttall. Water, ice, and climate change in northwest greenland. *WIREs Water*, 7(3):e1433, 2020. doi: 10.1002/wat2.1433. URL https://wires.onlinelibrary.wiley.com/doi/abs/10.1002/wat2.1433.

Joy M. O'Brien, Nathan Blais, Carmen Butler, Natalie White, Ash Bustead, Collin Figler, McKenna Wells, George Anderson, Anna Yuhas, and Jessica Gilman Ernakovich. Ten "simple" rules for non-Indigenous researchers engaging Indigenous communities in Arctic research. *PLOS Computational Biology*, 20(6):e1012093, 2024. doi: 10.1371/journal.pcbi.1012093. URL https://pmc.ncbi.nlm.nih.gov/articles/PMC11210771/. Open access. Authors contributed equally: O'Brien and Blais (co-first authors); Butler, White, and Bustead (co-third authors). Published 27 June 2024.

Yoshihiko Ohashi, Shigeru Aoki, Yoshimasa Matsumura, Shin Sugiyama, Naoya Kanna, and Daiki Sakakibara. Vertical distribution of water mass properties under the influence of subglacial discharge in Bowdoin Fjord, northwestern Greenland. *Ocean Sci.*, 16:545–564, May 2020. ISSN 1812-0784. doi: 10.5194/os-16-545-2020.

Hilde Oliver, Donald Slater, Dustin Carroll, Michael Wood, Mathieu Morlighem, and Mark J. Hopwood. Greenland Subglacial Discharge as a Driver of Hotspots of Increasing Coastal Chlorophyll Since the Early 2000s. *Geophys. Res. Lett.*, 50:e2022GL102689, 2023. ISSN 1944-8007. doi: 10.1029/2022GL102689.

Mayuko Otsuki and Shin Sugiyama. Community perspectives inform coastal marine ecosystem research in northwestern Greenland. *Polar Science*, 44:101112, 2025. doi: 10.1016/j.polar.2024.101112.

Bridget Ovall, Rebecca H. Jackson, Ginny A. Catania, Elias J. Hunter, Duncan C. Wheeler, and Michael Jakuba. Velocity observations in an upwelling subglacial discharge plume reveal links between entrainment and ice morphology. *Journal of Geophysical Research: Oceans*, 2025. doi: 10.1029/2025JC022902.

Robert Poole and Matthias Tomczak. Optimum multiparameter analysis of the water mass structure in the Atlantic Ocean thermocline. *Deep-Sea Res. I*, 46:1895–1921, November 1999. ISSN 0967-0637. doi: 10.1016/S0967-0637(99)00025-4.

Peter L. Pulsifer, Shari Gearheard, Henry P. Huntington, Mark A. Parsons, Christopher McNeave, and Heidi S. McCann. The role of data management in engaging communities in Arctic research: Overview of the Exchange for Local Observations and Knowledge of the Arctic (ELOKA). *Polar Geography*, 35(3–4):271–290, 2012. doi: 10.1080/1088937X.2012.708364.

Stefan Rahmstorf. Is the Atlantic overturning circulation approaching a tipping point? *Oceanography*, 37(3), 2024. doi: 10.5670/oceanog.2024.228.

E. Randall-Goodwin, M. P. Meredith, A. Jenkins, P. L. Yager, R. M. Sherrell, E. P. Abrahamsen, R. Guerrero, X. Yuan, R. A. Mortlock, K. Gavahan, A.-C. Alderkamp, H. Ducklow, R. Robertson, and S. E. Stammerjohn. Freshwater distributions and water mass structure in the Amundsen Sea Polynya region, Antarctica. *Elementa: Sci. Anthropocene*, 3:000065, August 2015. ISSN 2325-1026. doi: 10.12952/journal.elementa.000065.

Kamilla Rathcke, Mathane Qatsa, Anna Burdenski, and RikkeBecker Jacobsen. Understanding marine biodiversity shifts in southeast greenland with indigenous and local knowledge. *Human Ecology: An Interdisciplinary Journal*, 53(1):29–40, 2025. doi: 10.1007/s10745-025-00570-4.

K. A. Reeve, O. Boebel, T. Kanzow, V. Strass, G. Rohardt, and E. Fahrbach. A gridded data set of upper-ocean hydrographic properties in the Weddell Gyre obtained by objective mapping of Argo float measurements. *Earth Syst. Sci. Data*, 8:15–40, February 2016. ISSN 1866-3516. doi: 10.5194/essd-8-15-2016.

Monika Rhein, Reiner Steinfeldt, Oliver Huhn, Jürgen Sültenfuß, and Tilia Breckenfelder. Greenland Submarine Melt Water Observed in the Labrador and Irminger Sea. *Geophys. Res. Lett.*, 45:10570–10578, 2018. ISSN 1944-8007. doi: 10.1029/2018GL079110.

Eric Rignot, Michele Koppes, and Isabella Velicogna. Rapid submarine melting of the calving faces of West Greenland glaciers. *Nature Geoscience*, 3(3):187–191, 2010. doi: 10.1038/ngeo765.

Dean Roemmich. Optimal Estimation of Hydrographic Station Data and Derived Fields. *J. Phys. Oceanogr.*, 13:1544–1549, August 1983. ISSN 0022-3670. doi: 10.1175/1520-0485(1983)013⟨1544:OEOHSD⟩2.0.CO;2.

Aurora Roth, Fiamma Straneo, James Holte, Margaret Lindeman, and Matthew Mazloff. A dataset for multidisciplinary applications: thirteen years of ocean observations in Sermilik Fjord, Southeast Greenland. *Earth Syst. Sci. Data*, 17:6025–6048, November 2025a. ISSN 1866-3508. doi: 10.5194/essd-17-6025-2025.

Aurora Roth, Fiamma Straneo, James Holte, Mark Lindeman, and Matthew Mazloff. Gridded hydrographic dataset for Sermilik Fjord, Southeast Greenland from 2009–2023, 2025b. URL https://doi.org/10.18739/A28G8FK6D. [data set].

Aurora Roth, Fiamma Straneo, James Holte, Mark Lindeman, and Matthew Mazloff. Sermilik gridded hydrography v1, 2025c. URL https://doi.org/10.5281/zenodo.17563180. [code], last access: 7 November 2025.

Margaret Anamaq Rudolf. Co-production of knowledge in Arctic research: A paradigm shift or another cycle of oppression? In Lara A. Jacobs, editor, *Indigenous Critical Reflections on Traditional Ecological Knowledge*. Oregon State University Press, Corvallis, OR, 2025. ISBN 978-1962645324.

S. Rysgaard, J. Mortensen, M. Haxen, L. C. Gillard, and N. Risgaard-Petersen. Summer Hydrography Conditions at Proglacial Fjord Entrances Along East Greenland. *J. Geophys. Res.*, 129:e2023JC020665, 2024. ISSN 2169-9291. doi: 10.1029/2023JC020665.

Robert Sanchez, Donald Slater, and Fiamma Straneo. Delayed freshwater export from a greenland tidewater glacial fjord. *Journal of Physical Oceanography*, 53:1291–1309, 2023. doi: 10.1175/JPO-D-22-0137.1.

Robert Sanchez, Fiammetta Straneo, Kenneth Hughes, Philip Barbour, and Emily Shroyer. Relative roles of plume and coastal forcing on exchange flow variability of a glacial fjord. *Journal of Geophysical Research: Oceans*, 129(6):e2023JC020492, 2024. doi: 10.1029/2023JC020492. URL https://agupubs.onlinelibrary.wiley.com/doi/abs/10.1029/2023JC020492. e2023JC020492 2023JC020492.

Rodrigo Sanchez, Fiamma Straneo, and Magdalena Andres. Using Acoustic Travel Time to Monitor the Heat Variability of Glacial Fjords. *J. Atmos. Oceanic Technol.*, 38:1535–1550, 2021. doi: 10.1175/JTECH-D-20-0176.1.

Kristin M. Schild, David A. Sutherland, Pedro Elosegui, and Daniel Duncan. Measurements of iceberg melt rates using high-resolution gps and iceberg surface scans. *Geophysical Research Letters*, 48(3):e2020GL089765, 2021. doi: 10.1029/2020GL089765. URL https://agupubs.onlinelibrary.wiley.com/doi/abs/10.1029/2020GL089765. e2020GL089765 2020GL089765.

Sascha Schiøtt, Pelle Tejsner, and Søren Rysgaard. Inuit and local knowledge on the marine ecosystem in ilulissat icefjord, greenland. *Human Ecology*, 50:167–181, 2022. doi: 10.1007/s10745-021-00277-2. URL https://link.springer.com/article/10.1007/s10745-021-00277-2.

Robert W. Schlegel and Jean-Pierre Gattuso. A dataset for investigating socio-ecological changes in Arctic fjords. *Earth Syst. Sci. Data*, 15:3733–3746, August 2023. ISSN 1866-3508. doi: 10.5194/essd-15-3733-2023.

Gavin A. Schmidt, Kenneth D. Mankoff, Jonathan L. Bamber, Dustin Carroll, David M. Chandler, Violaine Coulon, Benjamin J. Davison, Matthew H. England, Paul R. Holland, Nicolas C. Jourdain, Qian Li, Juliana M. Marson, Pierre Mathiot, Clive R. McMahon, Twila A. Moon, Ruth Mottram, Sophie Nowicki, Anna Olivé Abelló, Andrew G. Pauling, Thomas Rackow, and Damien Ringeisen. Datasets and protocols for including anomalous freshwater from melting ice sheets in climate simulations. *Geoscientific Model Development*, 18:8333–8361, 2025. doi: 10.5194/gmd-18-8333-2025.

R. Sciascia, F. Straneo, C. Cenedese, P. Heimbach, M. H. Ribergaard, J. Mortensen, and R. D. Muench. Seasonal variability of submarine melt rate and circulation in an east greenland fjord. *Journal of Geophysical Research: Oceans*, 118(5):2492–2506, 2013. doi: 10.1002/jgrc.20142.

Avanti Shrikumar, Rian Lawrence, and Karen L. Casciotti. PYOMPA version 0.3: Technical note, may 2021. URL https://essopenarchive.org/doi/full/10.1002/essoar.10507053.1. Preprint, not peer reviewed.

P. R. Shukla, J. Skea, R. Slade, A. Al Khourdajie, R. van Diemen, D. McCollum, M. Pathak, S. Some, P. Vyas, R. Fradera, M. Belkacemi, A. Hasija, G. Lisboa, S. Luz, and J. Malley. *Climate Change 2022: Mitigation of Climate Change. Contribution of Working Group III to the Sixth Assessment Report of the Intergovernmental Panel on Climate Change*. Cambridge University Press, Cambridge, UK and New York, NY, USA, 2022. doi: 10.1017/9781009157926.

D. A. Slater and F. Straneo. Submarine melting of glaciers in Greenland amplified by atmospheric warming. *Nat. Geosci.*, 15:794–799, October 2022. ISSN 1752-0908. doi: 10.1038/s41561-022-01035-9.

Donald A. Slater, Dan N. Goldberg, Peter W. Nienow, and Tom R. Cowton. Scalings for Submarine Melting at Tidewater Glaciers from Buoyant Plume Theory. *J. Phys. Oceanogr.*, 46:1839–1855, June 2016. ISSN 0022-3670. doi: 10.1175/JPO-D-15-0132.1.

Donald A. Slater, Dustin Carroll, et al. FjordRPM v1.0: a reduced-physics model for efficient

simulation of glacial fjords. *Geosci. Model Dev.*, 2025a. doi: 10.5194/egusphere-2024-3934. URL https://egusphere.copernicus.org/preprints/2025/egusphere-2024-3934/.

Donald A. Slater et al. FjordRPM v1.0: a reduced-physics model for efficient simulation of glacial fjords. *Geoscientific Model Development*, 18:7475–7495, 2025b. doi: 10.5194/gmd-18-7475-2025.

D. A. Smeed, S. A. Josey, C. Beaulieu, W. E. Johns, B. I. Moat, E. Frajka-Williams, D. Rayner, C. S. Meinen, M. O. Baringer, H. L. Bryden, and G. D. McCarthy. The North Atlantic Ocean is in a state of reduced overturning. *Geophysical Research Letters*, 45:1527–1533, 2018. doi: 10.1002/2017GL076350.

T. Snow, W. Zhang, E. Schreiber, M. Siegfried, W. Abdalati, and T. Scambos. Alongshore winds force warm Atlantic Water toward Helheim Glacier in southeast Greenland. *J. Geophys. Res.*, page e2023JC019953, 2023. ISSN 2169-9291. doi: 10.1029/2023JC019953.

Michael A. Spall, Rebecca H. Jackson, and Fiammetta Straneo. Katabatic Wind-Driven Exchange in Fjords. *J. Geophys. Res.*, 122:8246–8262, October 2017. ISSN 2169-9275. doi: 10.1002/2017JC013026.

Sharon Stein, Cash Ahenakew, Will Valley, Pasang Y. Sherpa, Eva Crowson, Tabitha Robin, Wilson Mendes, and Steve Evans. Toward more ethical engagements between Western and Indigenous sciences. *FACETS*, 2024. doi: 10.1139/facets-2023-0071. Perspective.

B. Stellato, G. Banjac, P. Goulart, A. Bemporad, and S. Boyd. OSQP: An operator splitting solver for quadratic programs. *Mathematical Programming Computation*, 12(4):637–672, 2020. doi: 10.1007/s12532-020-00179-2.

Marianne Stenbaek. Arctic policy—blueprint for an Inuit homeland. *Études Inuit Studies*, 9(2): 5–14, 1985. URL https://www.jstor.org/stable/42869516.

Richard Stone. As the Arctic thaws, Indigenous Alaskans demand a voice in climate change research. *Science*, September 2020. doi: 10.1126/science.abe7149. News article.

Fiamma Straneo and Claudia Cenedese. The Dynamics of Greenland's Glacial Fjords and Their Role in Climate. *Annu. Rev. Mar. Sci.*, 7:89–112, January 2015. ISSN 1941-1405. doi: 10.1146/annurev-marine-010213-135133.

Fiamma Straneo, Dave Sutherland, Leigh Stearns, and Ginny Catania. The Case for a Sustained Greenland Ice Sheet-Ocean Observing System (GrIOOS), 2019.

Fiamma Straneo, Aurora Roth, James Holte, and Mark Lindeman. Sermilik Fjord Hydrography Data Portal. https://arcticdata.io/catalog/portals/sermilik/Overview, 2025. available at: https://arcticdata.io/catalog/portals/sermilik/Overview, last access: 7 November 2025.

Fiammetta Straneo and Patrick Heimbach. North Atlantic warming and the retreat of Greenland's outlet glaciers. *Nature*, 504:36–43, December 2013. ISSN 1476-4687. doi: 10.1038/nature12854.

Fiammetta Straneo, Gordon S. Hamilton, David A. Sutherland, Leigh A. Stearns, Fraser Davidson, Mike O. Hammill, Garry B. Stenson, and Aqqalu Rosing-Asvid. Rapid circulation of warm subtropical waters in a major glacial fjord in East Greenland. *Nat. Geosci.*, 3:182–186, March 2010. ISSN 1752-0908. doi: 10.1038/ngeo764.

Fiammetta Straneo, Ruth Curry, David Sutherland, Gordon Hamilton, Claudia Cenedese, Kjetil Vaage, and Leigh Stearns. Impact of ocean stratification on submarine melting of a major Greenland outlet glacier. *Nature Precedings*, February 2011. ISSN 1756-0357. doi: 10.1038/npre.2011.5670.1.

Fiammetta Straneo, David Sutherland, David Holland, Carl Gladish, Gordon S. Hamilton, Helen L. Johnson, Eric Rignot, Yun Xu, and Michele Koppes. Characteristics of ocean waters reaching Greenland's glaciers. *Ann. Glaciol.*, 53:202–210, January 2012. ISSN 0260-3055. doi: 10.3189/2012AoG60A059.

Fiammetta Straneo, Gordon S. Hamilton, Leigh A. Stearns, and David A. Sutherland. Connecting the greenland ice sheet and the ocean: A case study of helheim glacier and sermilik fjord. *Oceanography*, 29(4):34–45, 2016. URL https://www.jstor.org/stable/24862280. available at: https://www.jstor.org/stable/24862280, last access: 21 April 2023.

Fiammetta Straneo, Donald Slater, Caroline Bouchard, Mattias Cape, Mark Carey, Lorenzo Ciannelli, James Holte, Patricia Matrai, Kristin Laidre, Christopher Little, Lorenz Meire, Helene Seroussi, and Maria Vernet. An Interdisciplinary Perspective on Greenland's Changing Coastal Margins. *Oceanography*, 2022. ISSN 10428275. doi: 10.5670/oceanog.2022.128.

Shin Sugiyama, Atsushi Yamaguchi, Tatsuya Watanabe, Yasumasa Tojo, Naotaka Hayashi, Jean-Baptiste Thiebot, Masafumi Tomiyasu, Kazunari Hasegawa, Yoko Mitani, Mari Ogawa, Koji Tanaka, Keita Sakurai, Koji Matsuno, Nao Kanna, Elena Podolskiy, Rie Kusaka, Yefan Wang, Yoko Imazu, Kazuyuki Watanabe, Keisuke Sato, Syugo Ukai, Shun Yamada, Koichi Kondo, Satoshi Yamasaki, Kenji Tateyama, Koto Sato, Jun Inoue, Takayuki Mori, Tatsuya Fukazawa, Anders Rosing-Asvid, Karin Langley, Amy M. U. Gierisch, Julia Sutherland, and Tsuyoshi Oshima. Rapidly changing glaciers, ocean and coastal environments, and their impact on human society in the Qaanaaq region, northwestern Greenland. *Polar Sci.*, 27:100632, 2020. doi: 10.1016/j.polar.2020.100632.

Shin Sugiyama, Atsushi Yamaguchi, Tatsuya Watanabe, Yasumasa Tojo, Naotaka Hayashi, Jean-Baptiste Thiebot, Masafumi Tomiyasu, Kazunari Hasegawa, Yoko Mitani, Mari Ogawa, Koji Tanaka, Keita Sakurai, Koji Matsuno, Nao Kanna, Elena Podolskiy, Rie Kusaka, Yefan Wang, Yoko Imazu, Kazuyuki Watanabe, Keisuke Sato, Syugo Ukai, Shun Yamada, Koichi Kondo, Satoshi Yamasaki, Kenji Tateyama, Koto Sato, Jun Inoue, Takayuki Mori, Tatsuya

Fukazawa, Anders Rosing-Asvid, Karin Langley, Amy M. U. Gierisch, Julia Sutherland, and Tsuyoshi Oshima. Changes in the coastal environments and their impact on society in the qaanaaq region, northwestern greenland. *Polar Science*, page 101206, 2025. doi: 10.1016/j.polar.2025.101206.

David A. Sutherland and Robert S. Pickart. The East Greenland Coastal Current: Structure, variability, and forcing. *Prog. Oceanogr.*, 78:58–77, 2008. doi: 10.1016/j.pocean.2007.09.006.

David A. Sutherland, George E. Roth, Gordon S. Hamilton, Sebastian H. Mernild, Leigh A. Stearns, and Fiammetta Straneo. Quantifying flow regimes in a Greenland glacial fjord using iceberg drifters. *Geophys. Res. Lett.*, 41:8411–8420, 2014a. ISSN 1944-8007. doi: 10.1002/2014GL062256.

David A. Sutherland, Fiammetta Straneo, and Robert S. Pickart. Characteristics and dynamics of two major Greenland glacial fjords. *J. Geophys. Res.*, 119:3767–3791, 2014b. ISSN 2169-9291. doi: 10.1002/2013JC009786.

David A. Sutherland, Rebecca H. Jackson, Christian Kienholz, Jason M. Amundson, William P. Dryer, David Duncan, Emily F. Eidam, Roman J. Motyka, and Jonathan D. Nash. Direct observations of submarine melt and subsurface geometry at a tidewater glacier. *Science*, 365 (6451):369–374, 2019. doi: 10.1126/science.aax3528.

The IMBIE Team. Mass balance of the Greenland Ice Sheet from 1992 to 2018. *Nature*, 579: 233–239, 2020. doi: 10.1038/s41586-019-1855-2.

Kirsty J. Tinto, Jacqueline Austermann, Robin E. Bell, Margie Turrin, and Greenland Institute of Natural Resources. Greenland Rising/Kalaallit Nunaat qaffappoq: NNA track 2, EAGER: Community Responses to Coastal Change in the Arctic. NSF Navigating the New Arctic, Award #1928146, Lamont-Doherty Earth Observatory, Columbia University, in partnership with the Greenland Institute of Natural Resources, 2019. URL https://www.nsf.gov/awardsearch/showAward?AWD_ID=1928146. Accessed April 2026.

Matthias Tomczak and Daniel G. B. Large. Optimum multiparameter analysis of mixing in the thermocline of the eastern Indian Ocean. *J. Geophys. Res.*, 94:16141, 1989. ISSN 0148-0227. doi: 10.1029/JC094iC11p16141.

Matthias Tomczak, Daniel G. B. Large, and Nathan Nancarrow. Identification of diapycnal mixing through optimum multiparameter analysis: 1. Test of Feasibility and Sensitivity. *J. Geophys. Res.*, 99:25267–25274, 1994. ISSN 2156-2202. doi: 10.1029/94JC01947.

Mâliâraq Vebæk. *Sassuma Arnaanut pulaarneq*. Atuakkiorfik, Nuuk, Kalaallit Nunaat, 1995. ISBN 978-87-92790-58-3. Translated into English as *A Journey to the Mother of the Sea* (1999).

Paul Voosen. Our future in the fjords. *Science*, 366(6462):170–173, 2019. doi: 10.1126/science.366.6462.170.

Anneke L. Vries, Willem Jan van de Berg, Brice Noël, Lorenz Meire, and Michiel R. van den Broeke. Seasonal and interannual variability in freshwater sources for Greenland's fjords. *The Cryosphere*, 19:3897–3914, September 2025. ISSN 1994-0416. doi: 10.5194/tc-19-3897-2025.

Nina Wallerstein and Bonnie Duran.

Peter Washam, Keith W. Nicholls, Andreas Münchow, and Laurie Padman. Summer surface melt thins Petermann Gletscher Ice Shelf by enhancing channelized basal melt. *J. Glaciol.*, 65:662–674, August 2019. ISSN 0022-1430. doi: 10.1017/jog.2019.43.

Meagan E. Wengrove, Erin C. Pettit, Jonathan D. Nash, Rebecca H. Jackson, and Eric D. Skyllingstad. Melting of glacier ice enhanced by bursting air bubbles. *Nature Geoscience*, 16 (10):871–876, 2023. doi: 10.1038/s41561-023-01262-8.

Joshua J. Williams, Noel Gourmelen, Peter Nienow, Charlie Bunce, and Donald Slater. Helheim Glacier Poised for Dramatic Retreat. *Geophys. Res. Lett.*, 48:e2021GL094546, 2021. ISSN 1944-8007. doi: 10.1029/2021GL094546.

Annie P. S. Wong, Gregory C. Johnson, and W. Brechner Owens. Delayed-Mode Calibration of Autonomous CTD Profiling Float Salinity Data by $\theta$–S Climatology. *J. Atmos. Oceanic Technol.*, 20:308–318, February 2003. ISSN 0739-0572. doi: 10.1175/1520-0426(2003)020⟨0308:DMCOAC⟩2.0.CO;2.

M. Wood et al. Feedbacks between fjord circulation, mélange melt, and the subglacial discharge plume at Kangerlussuaq Glacier, East Greenland. *Journal of Geophysical Research: Oceans*, 130, 2025. doi: 10.1029/2024JC021639.

Michael Wood, Eric Rignot, Ian Fenty, Lu An, Anders Bjørk, Michiel van den Broeke, Cilan Cai, Emily Kane, Dimitris Menemenlis, Romain Millan, Mathieu Morlighem, Jeremie Mouginot, Brice Noël, Bernd Scheuchl, Isabella Velicogna, Josh K. Willis, and Hong Zhang. Ocean forcing drives glacier retreat in Greenland. *Science Advances*, 7(1):eaba7282, 2021. doi: 10.1126/sciadv.aba7282.

World Meteorological Organization. State of the global climate 2024. Technical report, World Meteorological Organization, Geneva, Switzerland, 2025. URL https://wmo.int/publication-series/state-of-global-climate-2024. Accessed April 2026.

Carl Wunsch. The North Atlantic general circulation west of 50°W determined by inverse methods. *Rev. Geophys.*, 16:583–620, 1978. ISSN 1944-9208. doi: 10.1029/RG016i004p00583.

Carl Wunsch. *The Ocean Circulation Inverse Problem*. Cambridge University Press, Cambridge, 1996. ISBN 978-0-521-48090-1.

Carl Wunsch. *Discrete Inverse and State Estimation Problems: With Geophysical Fluid Applications*. Cambridge University Press, Cambridge, 2006. ISBN 978-0-521-85424-5. doi: 10.1017/CBO9780511535949.